

NOTE TO USERS

This reproduction is the best copy available.

UMI[®]

CONSOLIDATION OF CLAY-GRANULAR MEDIUM COMPOSITES

By

Hani Ghiabi

May, 2008

Department of Civil Engineering and Applied Mechanics
McGill University, Montreal

A thesis submitted to
McGill University
in partial fulfillment of the requirements of the degree of
Doctor of Philosophy

© Copyright

2008 Hani Ghiabi



Library and Archives
Canada

Published Heritage
Branch

395 Wellington Street
Ottawa ON K1A 0N4
Canada

Bibliothèque et
Archives Canada

Direction du
Patrimoine de l'édition

395, rue Wellington
Ottawa ON K1A 0N4
Canada

Your file *Votre référence*
ISBN: 978-0-494-66709-5
Our file *Notre référence*
ISBN: 978-0-494-66709-5

NOTICE:

The author has granted a non-exclusive license allowing Library and Archives Canada to reproduce, publish, archive, preserve, conserve, communicate to the public by telecommunication or on the Internet, loan, distribute and sell theses worldwide, for commercial or non-commercial purposes, in microform, paper, electronic and/or any other formats.

The author retains copyright ownership and moral rights in this thesis. Neither the thesis nor substantial extracts from it may be printed or otherwise reproduced without the author's permission.

AVIS:

L'auteur a accordé une licence non exclusive permettant à la Bibliothèque et Archives Canada de reproduire, publier, archiver, sauvegarder, conserver, transmettre au public par télécommunication ou par l'Internet, prêter, distribuer et vendre des thèses partout dans le monde, à des fins commerciales ou autres, sur support microforme, papier, électronique et/ou autres formats.

L'auteur conserve la propriété du droit d'auteur et des droits moraux qui protègent cette thèse. Ni la thèse ni des extraits substantiels de celle-ci ne doivent être imprimés ou autrement reproduits sans son autorisation.

In compliance with the Canadian Privacy Act some supporting forms may have been removed from this thesis.

While these forms may be included in the document page count, their removal does not represent any loss of content from the thesis.

Conformément à la loi canadienne sur la protection de la vie privée, quelques formulaires secondaires ont été enlevés de cette thèse.

Bien que ces formulaires aient inclus dans la pagination, il n'y aura aucun contenu manquant.


Canada

To My Parents

ABSTRACT

The thesis deals with the study of soil composites that are constructed by combining regions of soft clay and granular materials in various spatial configurations. The underlying basis for the work stems from the practical application of the results of the research to offshore land reclamation practices. Due to depletion of local coarse-grained soil sources and the high cost of imported granular fill, the use of dredged and excavated marine clay has become the preferred source of materials in reclamation activities. A common reclamation technique involves placing dredged clay lumps directly on top of other layers; these lumpy fills contain large initial inter-lump voids with the result that the fills experience substantial compression purely due to the closure of the void space. A practical solution therefore is to fill the void space with a granular soil to enhance the load-carrying capacity and to minimize the settlements of the reclaimed fills.

In this research a coordinated experimental investigation was undertaken to examine the consolidation behavior of composites fabricated using a number of spherical and disk-shaped clay inclusions placed within an artificial granular medium (ballotini). The results of this experimental research program indicated that the volume fraction, shape, configuration and the constitutive properties of both the clay inclusions and the granular component are all important factors that could affect the mechanical response of the soil composites. A computational scheme, validated using the results of the bench-scale experiments, was used to analyze the response of an idealized composite lumpy fill subjected to self-weight stresses, surcharge and a load applied through a rigid footing. The computational results indicated that the consolidation behavior of the composite lumpy layers can be significantly influenced by the volume proportion, location and configuration of the clay inclusions interspersed within the granular fill. The incorporation of the constitutive behaviors of the soil components, used in reclamation activities, into such a computational analysis could assist engineers in designing reclaimed fills where the least ultimate settlement occurs within the shortest time.

RÉSUMÉ

Cette thèse porte sur l'étude de sols composites construits en combinant des régions d'argile molle et de matières granulaires dans différentes configurations spatiales. L'application pratique des résultats de la recherche sur le réaménagement de terrains marins forme la base de cette étude. La diminution des sources locales de sol à gros grains et le coût élevé des remblais granulaires importés ont rendu l'argile marine draguée et excavée la source préférée de matériaux utilisés pour les réaménagements de terrains. Une des techniques de réaménagements les plus communes implique la déposition de morceaux d'argile dragué directement sur les autres couches. Les remblais à gros morceaux contiennent initialement un nombre élevé de vides entre les morceaux. Lorsque l'espace entre les vides disparaît, les remblais subissent une compression considérable. Ces espaces vides, peuvent par contre être remplis par des sols granulaires, améliorant ainsi la capacité portante et diminuant le tassement des remblais réaménagés. Au cours de cette recherche, une investigation expérimentale a été entreprise pour examiner le comportement de consolidation des composites fabriqués avec un grand nombre d'inclusions d'argile en forme de disques ou de sphères et placées dans un médium granulaire artificiel (ballotini). Les résultats de cette recherche ont clairement indiqués que la fraction volumétrique, la forme, la configuration et les propriétés constitutives des inclusions d'argile et des composantes granulaires sont des facteurs essentiels qui affectent la réponse mécanique des composites de sol. Afin de valider les résultats expérimentaux, un schéma de calcul a été utilisé. Il a servit à analyser la réponse d'un composite idéalisé de remblai à gros morceaux soumis aux charges unitaires de soi-poids, de surcharges et de charges appliqués par la dalle rigide. Les résultats numériques ont indiqué que le comportement de consolidation des couches composites à gros morceaux est considérablement influencé par la proportion volumétrique, le lieu et la configuration des inclusions d'argile parsemés dans le remblai granulaire. L'incorporation des comportements constitutifs des composantes de sols, utilisés dans les activités de réaménagements de terrains, dans de telles analyses computationnelles aidera les ingénieurs qui modélisent des remblais réaménagés dont le tassement ultime est minime et qui se produit pendant une très courte période.

ACKNOWLEDGEMENTS

The author wishes to express his great gratitude to his supervisor, Professor A.P.S. Selvadurai FRSC, *William Scott Professor* and *James McGill Professor*, Department of Civil Engineering and Applied Mechanics at McGill University, for suggesting the topic of research, profound guidance and constant support during author's doctoral program at McGill University. His extensive corrections to this thesis and the research papers resulting from the work are gratefully appreciated.

The author wishes an appreciation to Mr. M. Przykorski and Mr. J. Bartzak, research technicians of the Department of Civil Engineering and Applied Mechanics, McGill University, for their help in designing, manufacturing and assembling the experimental apparatus used in this research. The author would particularly like to thank the graduate students in the *Geomechanics Laboratory* for creating a friendly and stimulating environment in this research laboratory; these include Dr. Ali Shirazi, Dr. Qifeng Yu, Dr. Wenjun Dong, Mr. Tuan Luu, Mr. P.A. Selvadurai and Ms. Maria F. F. de Oliveira.

The author is grateful for the help of Mrs. Sally Selvadurai for her expert and precise editorial corrections. The author would also like to appreciate Mr. Patrick Mattar and Ms. Mei Shi for their assistance in preparing the French abstract.

The research conducted in this thesis was made possible through the financial assistance provided by the *Max Planck Research Prize in the Engineering and Science* and the *NSERC- Discovery Grant* awarded to Professor A.P.S. Selvadurai.

The author would particularly like to thank his sisters for the emotional support and encouragement given him through these years. Above all, the author would like to acknowledge the tremendous sacrifices that his parents made for him during his graduate studies. It is to them that he dedicates this dissertation.

TABLE OF CONTENTS

Abstract.....	i
Résumé.....	ii
Acknowledgements.....	iii
Table of Contents.....	iv
List of Tables.....	viii
List of Figures.....	ix
Statement of Originality and Contributions.....	xiv
List of Publications.....	xv
Chapter 1: Inhomogeneous soil media	
1.1 Introduction.....	1
1.2 Introduction of layered inhomogeneous foundations.....	2
1.2.1 Experimental and theoretical studies of consolidation behavior of layered soil media.....	5
1.2.2 Computational studies of consolidation behavior of layered soil media.....	10
1.3 Introduction of reinforced composite foundations.....	14
1.3.1 Experimental and theoretical analyses of the behavior of reinforced composite foundations	15
1.3.2 Computational analyses of the behavior of reinforced composite foundations	18
1.4 Introduction of land reclamation project	22
1.4.1 The land reclamation methods	24
1.4.2 The study of consolidation behavior of lumpy inhomogeneous fills.....	27
1.5 Objectives and the scope of the thesis	39

Chapter 2: Mechanical behavior of the reconstituted silty clay and the constitutive characterizations

2.1 Introduction.....	41
2.2 Experimental investigations.....	42
2.2.1 Material characteristics.....	42
2.2.2 Measurement of the mechanical properties.....	43
2.3 Experimental results.....	46
2.3.1 Undrained shear strength of the reconstituted silty clay.....	46
2.3.2 Shear strength of the consolidated reconstituted silty clay.....	51
2.3.3 Consolidation properties of the reconstituted silty clay.....	55
2.3.4 The hydraulic conductivity of the silty clay.....	58
2.4 A constitutive model for silty clay.....	60
2.4.1 Generalized stress-strain relations.....	61
2.4.2 Modified Cam clay model for Montreal silty clay.....	65
2.5 Summary remarks.....	69

Chapter 3: Mechanical behavior of ballotini and the constitutive characterizations

3.1 Introduction.....	70
3.2 Experimental investigations.....	70
3.2.1 Material description.....	71
3.2.2 Consolidated drained triaxial compression test.....	72
3.2.3 Isotropic compression test.....	81
3.2.4 Oedometric bench-scale test.....	81

3.2.5 Constant head permeability test.....	89
3.3 A constitutive model for ballotini.....	92
3.3.1 Generalized stress-strain relations.....	92
3.3.2 Stiffness formulation for Drucker-Prager yield surface.....	95
3.3.3 Computational procedure.....	96
3.3.4 Hypoelastic-perfectly plastic model for ballotini.....	99
3.3.5 The prediction of the mechanical response of ballotini.....	105
3.4 Summary remarks.....	108

Chapter 4: Mechanical behavior of a composite containing spherical clay inclusions

4.1 Introduction.....	109
4.2 The test facility and sample preparation	110
4.3 Experimental results.....	113
4.4 Computational modeling of fluid-saturated media.....	115
4.4.1 Constitutive equations.....	115
4.4.2 Finite element formulation of the consolidation problem.....	117
4.4.3 Solution procedure for coupled fluid flow and deformations.....	122
4.4.4 Computational modeling of the composite sample.....	123
4.5 Comparison between numerical predictions and experimental results.....	129
4.6 Summary remarks.....	132

Chapter 5: Mechanical behavior of a soil composite: disk-shaped clay inclusions embedded in a granular region

5.1 Introduction.....	133
-----------------------	-----

5.2 The test facility and sample preparation.....	133
5.3 Experimental results.....	136
5.4 Computational implementations.....	138
5.5 Dependency of the mechanical response on the shape and configuration of the clay inclusions.....	147
5.6 Comparison between numerical predictions and experimental results.....	151
5.7 Summary remarks.....	158
 Chapter 6: Mechanics of a fluid saturated composite porous media subjected to foundation load	
6.1 Introduction.....	159
6.2 Computational modeling of the composite lumpy fills.....	163
6.3 Computational results and discussion.....	171
6.3.1 Composite fills with a composite layer placed at different positions.....	171
6.3.2 Composite fills with different volume proportions of clay.....	174
6.4 Composite fills with densely packed clay lumps.....	187
6.5 Summary remarks.....	192
 Chapter 7: Conclusions and recommendations	
7.1 Summary and Conclusions.....	193
7.2 Recommendations for future work.....	199
 References.....	 202

LIST OF TABLES

Table 2.1	Triaxial unconsolidated undrained test specifications.....	47
Table 2.2	Consolidated undrained triaxial test specifications.....	52
Table 2.3	Physical and mechanical properties of the Montréal silty clay evaluated from consolidation tests.....	55
Table 2.4	Properties of Montreal silty clay derived from oedometer consolidation tests.....	60
Table 3.1	Results for constant head permeameter tests conducted on ballotini samples.....	91
Table 3.2	Model parameters derived for ballotini.....	102

LIST OF FIGURES

Figure 1.1	Varved clay from the New Jersey meadowlands	3
Figure 1.2	Experimental and computational settlement curves for two-layer specimens.....	6
Figure 1.3	Schematic representation of layered clay-sand fill.....	9
Figure 1.4	Comparison between finite element and equivalent anisotropic solutions (a) settlement-time curves, (b) Pore water pressure isochrones.....	12
Figure 1.5	Consolidometer for testing single stone column.....	15
Figure 1.6	Comparison of measured and predicted load-settlement behavior of a loaded single stone column.....	18
Figure 1.7	Finite element mesh for consolidation analysis.....	21
Figure 1.8	(a) Surface settlement and (b) pore pressure variation below the center of the embankment.....	21
Figure 1.9	Schematic profile of reclamation fill constructed from dredged stiff clay using clam-shell.....	26
Figure 1.10	Typical meshes for FEM (a) Plane strain, (b) 3D with external lateral elements, (c) 3D without external lateral elements.....	29
Figure 1.11	Comparison of results obtained from DP model, FE computation and experiment.....	30
Figure 1.12	Schematic setup and instrumentation of the one-dimensional compression test.....	31
Figure 1.13	Different types of composite soils.....	33
Figure 1.14	Comparison of numerical results and centrifuge test.....	36
Figure 1.15	Typical time-settlement curve in different load steps.....	38
Figure 2.1	Grain size distribution chart for Montreal reconstituted silty clay.	42
Figure 2.2	Preparation of triaxial specimen from soft clay.....	45
Figure 2.3	Stress-strain curves from UU triaxial tests (with membrane correction).....	48
Figure 2.4	Results of the fall cone tests on the remolded Montreal clay.....	50
Figure 2.5	Consolidation curves obtained from isotropic compression of the triaxial specimens.....	52

Figure 2.6	K_f -line and Mohr-Coulomb effective stress circles from CU triaxial tests.....	53
Figure 2.7	Empirical correlation between ϕ' and PI from triaxial compression tests.....	54
Figure 2.8	Stress paths obtained from CU triaxial tests.....	54
Figure 2.9	Results of the oedometer consolidation tests.....	56
Figure 2.10	Consolidation curves obtained from conventional oedometer tests.....	57
Figure 2.11	Variation of the coefficient of consolidation with normal stress...	58
Figure 2.12	Yield surface in Modified Cam clay model.....	62
Figure 2.13	Virgin compression line and elastic unloading-reloading line.....	63
Figure 2.14	Comparison between the results of oedometer tests with computational analysis.....	68
Figure 3.1	Grain size distribution curve for ballotini.....	72
Figure 3.2	Sample preparation technique for conducting triaxial compression tests on ballotini.....	73
Figure 3.3	The procedure used in triaxial compression test.....	75
Figure 3.4	Stress-strain curves for ballotini specimens derived from triaxial compression tests: Influence of confining pressure.....	76
Figure 3.5	Stress-strain curves for ballotini specimens derived from triaxial compression tests with unloading-reloading cycles	77
Figure 3.6	Volumetric strain versus vertical strain in triaxial specimens subjected to different confining pressures.....	77
Figure 3.7	K_f -line and stress paths obtained from triaxial compression test	80
Figure 3.8	Results of the isotropic compression test on two samples of ballotini.....	82
Figure 3.9	Experimental setup for Bench-scale test.....	83
Figure 3.10	Loading setup and instrumentations used in the bench-scale test...	85
Figure 3.11	Bench-scale oedometer test results for saturated and dry ballotini samples.....	88
Figure 3.12	Results of oedometer test on ballotini samples tested in drained and dry conditions.....	89
Figure 3.13	Variation of elastic modulus with void ratio for ballotini material	90
Figure 3.14	Flow chart for the implementation of hypoelastic-perfectly plastic model.....	101

Figure 3.15	Finite element model of the triaxial sample.....	103
Figure 3.16	Constitutive representations of the stress-strain responses of the triaxial samples subjected to different confining pressures.....	104
Figure 3.17	Constitutive representation of the variation of void ratio with axial stress in oedometer bench-scale tests.....	105
Figure 3.18	Computational predictions for the compression behavior of ballotini samples subjected to isotropic compression.....	106
Figure 3.19	Computational predictions for the stress-strain responses in triaxial compression tests conducted on ballotini.....	107
Figure 4.1	Preparation of the clay spheres used in fabrication of the composite sample.....	111
Figure 4.2	Fabricated composite specimen.....	112
Figure 4.3	Consolidation of a silty clay sphere subjected to a confining stress.....	113
Figure 4.4	Axial settlement of the composite and homogenous ballotini samples in five successive load steps.....	114
Figure 4.5	Ballotini-clay interface at the termination of the oedometer test...	115
Figure 4.6	Finite element models considered in the problem of consolidation of composite lumpy specimen.....	124
Figure 4.7	Pore fluid pressure change in different locations of composite model (first load step).....	126
Figure 4.8	Variation of contact vertical stress in the composite model (first load step).....	127
Figure 4.9	Stress partitioning in composite sample- end of first load step.....	128
Figure 4.10	Axial deformation of the composite model subjected to oedometric compression test	128
Figure 4.11	Axial compression of the composite sample in five successive load steps.....	129
Figure 4.12	Consolidation curves of the composite sample subjected to the oedometric compression test.....	131
Figure 5.1	Preparation of the silty clay disks.....	134
Figure 5.2	(a) Cross sectional view of the 8-disk composite sample (test-3) (b) Planar cross section (c) the 6-disk composite sample (d) the 4-disk composite sample.....	135
Figure 5.3	Axial settlement of the samples in five successive load steps.....	137

Figure 5.4	Dissecting the soil composite at the termination of the oedometer test.....	138
Figure 5.5	Finite element models considered in the modeling of the consolidation of composite soil specimens.....	140
Figure 5.6	Axial compression of the composite samples in six successive load steps.....	142
Figure 5.7	Pore fluid pressure change in different locations of the soil composites.....	143
Figure 5.8	Variation of contact stress in the eight-disk composite model (fourth load step).....	144
Figure 5.9	Axial deformation of the composite models subjected to an oedometric compression test.....	146
Figure 5.10	Contact stress distributions at the upper surface of the composites (at the termination of the last load step).....	147
Figure 5.11	Computational modeling of the soil composites containing spherical and disk-shaped clay inclusions.....	149
Figure 5.12	Axial deformation of the composite models during six successive load steps.....	150
Figure 5.13	Axial deformation of the composite models subjected to an oedometric compression test.....	150
Figure 5.14	Axial deformation of the composite samples in five successive load steps.....	152
Figure 5.15	Consolidation curves of the four-disk composite sample subjected to an oedometric compression test	155
Figure 5.16	Consolidation curves of the six-disk composite sample subjected to an oedometric compression test.....	156
Figure 5.17	Consolidation curves of the eight-disk composite sample subjected to an oedometric compression test.....	157
Figure 6.1	Typical discretized finite element model ($30 \times 30 \times 5.6m$) used to determine the effect of the boundary interface.....	166
Figure 6.2	Settlement response of the footing for different sizes of the elastic domain.....	166
Figure 6.3	The composite layer with 25% volume fraction of clay.....	167
Figure 6.4	Locations of the composite layers in (a) one-layer-B (b) one-layer-M (c) one-layer-T (d) two-layer (e) three-layer composite fills.....	168
Figure 6.5	Mesh discretizations and boundary conditions in (a) one-layer (BMT) and two-layer (b) three-layer composite models.....	169

Figure 6.6	Surface settlement due to the self-weight and the surcharge pressure.....	172
Figure 6.7	Load-settlement response of a rigid square footing resting on the surface of a granular layer containing a single soil composite layer.....	172
Figure 6.8	Consolidation settlement of a square rigid footing resting on a granular layer containing a single soil composite layer.....	173
Figure 6.9	Surface settlement due to self-weight and the surcharge pressure	174
Figure 6.10	Load-settlement response of the rigid square footing resting on different types of composite soil layer.....	176
Figure 6.11	Excess pore pressure generation at the center of the clay lumps in different composite fills.....	178
Figure 6.12	Mandel-Cryer effect – pore pressure increase at the beginning of the consolidation step.....	180
Figure 6.13	Dissipation of excess pore pressure generated at the center of the clay lumps due to the uniform normal stress of 1500 <i>kPa</i> applied to the rigid footing.....	181
Figure 6.14	Numerical results for the degree of consolidation of composite lumpy fills settles under a square rigid footing.....	182
Figure 6.15	Time-dependent consolidation settlement of a square rigid footing resting on composite lumpy fills.....	183
Figure 6.16	Normal contact stress profile along the diagonal of the square footing.....	184
Figure 6.17	Load-displacement response of the footing for different constitutive models for ballotini.....	186
Figure 6.18	Settlement response of the footing for different flow rules in the constitutive model of ballotini (one-layer-B).....	187
Figure 6.19	The composite layer with 50% volume fraction of clay (dense composite layer).....	188
Figure 6.20	Configurations of the composite fills with densely packed lumps	188
Figure 6.21	Profile of the surface settlement due to the application of self-weight and surcharge load.....	189
Figure 6.22	Load-settlement response of the rigid square footing resting on different types of three-layer lumpy fills.....	190
Figure 6.23	Consolidation settlement of a square rigid footing resting on composite lumpy fills.....	191
Figure 6.24	Degree of consolidation for 3-layer lumpy fills subjected to a footing load.....	191

STATEMENT OF ORIGINALITY AND CONTRIBUTIONS

The work described in this thesis deals with the study of soil composites that are constructed by combining regions of soft clay and granular materials in different volume fractions and various spatial configurations. To the author's knowledge, the experimental investigations and computational analyses conducted in this research are novel and the results obtained for describing the behavior of composite fills, original. This thesis presents results of experiments conducted on a bench-scale version of a soil composite and the experiments necessary to describe the poro-elasto-plastic behavior of the separate phases. These results are used in the computational modeling exercise of the bench scale experiments. The computational approach used to investigate the influence of the mechanical and physical characteristics of the individual phases and their spatial arrangements on the behavior of idealized composite lumpy fills; the results obtained from the computational studies are considered to be novel and highly original.

The results presented in this thesis have significant applications potential in geomechanics, geotechnical engineering and foundation engineering. In practice, the results obtained from this study can assist engineers in design and construction of reclaimed fills with enhanced performance under construction loads. The contributions resulting from the thesis have been published or accepted for publication in leading international journals and refereed conference proceedings in the general area of computational geomechanics, applied mechanics and civil engineering.

The general direction for the scope of the research was proposed by the research supervisor. The author has performed the experimental research reported in the thesis, which includes the monitoring, acquisition and processing of experimental data. The author has performed the computational work reported in the thesis, which included the development of a new UMAT subroutine for examining non-linear elasto-plastic behavior of the granular material used in the ABAQUS Code. The publications resulting from the research were written in collaboration with the research supervisor.

LIST OF PUBLICATIONS

- Selvadurai, A.P.S.; Ghiabi, H. (2008) Consolidation of a soft clay composite: Experimental results and computational estimates, *CMES-Computer Modeling in Engineering and Sciences*, **23(1)**, 53-73.
- Ghiabi, H. and Selvadurai, A. P. S. (2008) The time-dependent mechanical behaviour of a granular medium used in laboratory investigations, *International Journal of Geomechanics*, (accepted).
- Selvadurai, A.P.S. and Ghiabi, H. (2008) Continuum poro-elasto-plasticity of geomaterial composites, *Proceedings of the 3rd Canadian Conference on Nonlinear Solid Mechanics* (E.Croitoro, Ed.), Toronto, Ontario, pp. 335-344.
- Selvadurai, A.P.S. and Ghiabi, H. (2007) Consolidation settlement of a foundation resting on a soil composite layer, *Proceedings of the 50th Canadian Geotechnical Conference*, Ottawa, pp. 1228-1235.
- Selvadurai, A.P.S. and Ghiabi, H. (2007) Oedometric consolidation of a fluid-saturated soil composite, *Proceedings of the 10th International Symposium on Numerical Models in Geomechanics* (G.N. Pande and S. Pietruszczak Eds.), Rhodes, Greece, pp. 289-295.
- Ghiabi, H. and Selvadurai, A.P.S. (2006) Laboratory testing of a soft silty clay, *Soft Soil Engineering, Proceedings of the 4th International Conference* (D.C. Chan and K.T. Law, Eds.), Vancouver, B.C., Taylor and Francis, London, pp. 447-456.
- Selvadurai, A.P.S. and Ghiabi, H. (2006) Consolidation behaviour of a soft clay composite, *Soft Soil Engineering, Proceedings of the 4th International Conference* (D.C. Chan and K.T. Law, Eds.), Vancouver, B.C., Taylor and Francis, London, pp. 437-446.

CHAPTER 1

INHOMOGENEOUS SOIL MEDIA

1.1 Introduction

Although *isotropy* and *homogeneity* are dominant assumptions of geotechnical analyses, there are situations where these assumptions are not accurate representations of geotechnical practice (Gibson, 1974; Selvadurai, 2007). Examples of varved features in clay specimens obtained from Steep Rock Lake, Ontario, were discussed by Eden (1955). The inhomogeneity can be formed naturally during the periodic deposition of eroded material in lacustrine environments and this can lead to formation of geological deposits with anisotropic behavior in both strength and deformability. The paper by Ward et al. (1965) reported a natural inhomogeneity that exists in the deformability characteristics of London Clay. Inhomogeneities can also be deliberately introduced to either enhance the load carrying capacity of soft clays or to accelerate their rate of consolidation. Stone columns and lime-stabilized columns are arrangements where the stiffer inclusion provides the reinforcement for strength and for the reduction of settlements, while the incorporation of geosynthetics and sand layers are there to enhance the rate of consolidation of the construction. Many successful applications of these techniques have been reported in the literature, including interesting combinations of reinforcing zones with in situ soil layers (Barron, 1948; Hansbo, 1979; Goughnour and Bayuk, 1979; Mitchell and Huber, 1985; Barron et al., 2002).

A further class of inhomogeneous soil layers is encountered in land reclamation practices and involves the use of dredged clay lumps to construct reclaimed fills. Currently, land development and reclamation, both offshore and onshore, are indicators of the dynamic development and economic growth of coastal countries that play an important role in world affairs (Glaser et al., 1991; Lui and Tan, 2001).

Herein the mechanical characteristic of the non-homogenous region is studied in three different categories designated as either layered strata, reinforced composite layers, or lumpy reclaimed fills. The ensuing sections briefly summarize the most relevant studies carried out to examine the mechanical characteristics of layered strata and composite reinforced fills. The major emphasis of this review, however, will be on the theoretical, computational, and experimental analyses conducted on lumpy reclaimed fills, which are more relevant to the study presented in this thesis.

1.2 Introduction of layered inhomogeneous foundations

Many fine-grained soil deposits exhibit a finely laminated structure due to seasonal variations in the size of deposited particles. There is no soil layer in nature with complete homogeneity in the different characteristics such as permeability, compressibility and coefficient of consolidation. This observation indicates that the conventional elementary and advanced models of soil consolidation (Terzaghi, 1943; Mikasa, 1965; Davis and Raymond, 1965; Gibson et al., 1967) cannot be implemented with confidence to predict the behavior of naturally occurring inhomogeneous fills. Therefore, the conventional theory of consolidation has been generalized to consider non-homogeneous soil media (Mikasa, 1963; Schiffman and Gibson, 1964). Naturally layered sediments are formed as a result of climatic cycles, such as periodic earth movements, cyclic shifting of tributaries on deltas, periodic volcanism and annual rhythms (Figure 1.1). The thickness of deposits formed during each cycle might vary from less than a millimeter to several meters (Wu, 1976; Mitchell, 1976; Helwick and Bryant, 1977; Quigley et al., 1985). There are many cases, however, where the region can be considered as multi-layered, composed of several accumulated homogeneous layers. Rowe (1972) discussed soil exploration data collected from 35 sites and reported that the majority of boreholes showed occasional fine and coarse lenses with various compressibility and permeability characteristics. Thus the effective field values of these regions used in mathematical solution of the consolidation problems differ from the coefficients of the parent clay; therefore, using consolidation parameters for a homogeneous soil may contribute to serious errors in the estimation of the rate of consolidation.

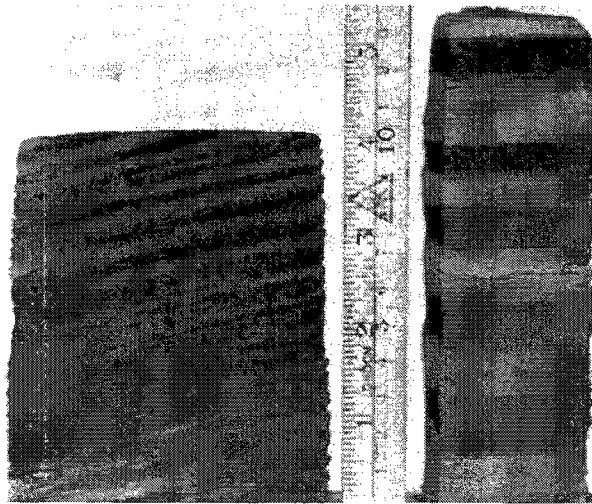


Figure 1.1 Varved clay from the New Jersey meadowlands (Mitchell, 1976)

A further class of layered foundations is clay-sand fills constructed in reclamation projects. Soft clay, which is present in abundance below the seabed, can be used as a fill material in reclamation projects; however, hydraulically placed marine clay would pose problems related to sedimentation and long-term settlement in the fill. A layer of coarse-grained soil sandwiched between clay layers could accelerate the consolidation settlement by providing shorter drainage paths and also improve the strength of the reclaimed area. A field investigation was carried out on a reclaimed area at Pulau Tekong Besar Island where the material was hydraulically pumped into a pond in different layers of clay and sand (Lee et al., 1985, 1987). Field observation indicated that from a sand layer with a thickness of 300 mm hydraulically placed on 1 m soft clay, half of the grains remained on the clay sediments, while the rest penetrated into the underlying clay layer. It was concluded that adequate time should be allowed between the pumping of the clay and initial spreading of sand to allow the clay to settle completely and undergo self-weight consolidation. This duration depends on several factors such as the height of the clay fill, the concentration of the clay slurry, the mode of pumping, and the properties of the clay. To enable engineers to control this phenomenon, the mechanics of penetration of sand grains into the clay layers has been studied. Based on experimental and analytical studies, Lee et al. (1994) indicated that three parameters mainly govern the penetration of sand into the clay slurry, namely, the sand spreading height, the thickness of the sand spread,

and the undrained shear strength of the clay slurry. The analytical model which is based on the motion of a single particle in a non-newtonian fluid showed that the penetration is governed by the balance between the shear resistance and the buoyant weight of the particle, while its impact velocity will only affect the initial entry of the particle. In addition, the analytical results indicated that for the tested clay slurry, the critical water content to trap sand is around 250% which agreed well with experimental and field observations. Furthermore, Tan et al. (1994a,b) reported that, in a clay-sand reclamation scheme, substantial sand loss through penetration into the clay can be significantly reduced with the aid of a low-cost and low-density type jute geotextile laid on the slurry surface. This layer can significantly reduce the amount of grain loss due to penetration in the situation of scarce and expensive sand supply. Several experiments indicated that the key factors that control this phenomenon are the relative sizes of sand particles to jute opening, the intensity of spreading, and the slurry strength.

Another approach in land reclamation is the use of prefabricated band drains in conjunction with granular drain layers; this method is extensively used in Japan due to easy installation and the shortage of good quality sand as drain material (Katayama, 1991). The basic of this method is identical with the clay-sand layer scheme, but in this approach the sandwiched sand layer is connected to the surface by means of band drains in critical regions, such as under runways, to accelerate the consolidation process (Tanaka, 1994).

In some cases the variation of properties in layered foundations is not significant, but there are many occasions in which considering a single mechanical characteristic for the stratified foundation may give rise to incorrect predictions of the overall mechanical responses. In this review, notable efforts carried out to analyze the behavior of layered soil media are separately discussed in sections focusing on experimental- theoretical, and computational studies.

1.2.1 Experimental and theoretical studies of consolidation behavior of layered soil media

There are many cases where the ground is considered as multi-layered, composed of a number of built up homogeneous layers. Moreover, any substrate that has gradual changes in the parameters can be approximated by a multi-layered stratum, which is in many cases easier than using equations applicable to non-homogeneous media. Gray (1945) first considered the consolidation behavior of two contiguous layers of clay possessing different consolidation characteristics. He presented an analytical solution for a special case in which one of the two contiguous layers is relatively incompressible and acts merely to impede the outflow of water from the compressible stratum, as for example the case encountered in a cohesionless silt layer which overlies a stratum of compressible clay. It was indicated that when the upper soil layer has low permeability in comparison with the lower one, the lower layer consolidates as rapidly as the upper permits, while in the top layer the variation is similar to that found in the case of a layer of homogeneous material with free drainage at one surface. Furthermore, the proposed solution was compared with the method expressed by Terzaghi (1940) that considers the averaging coefficient of the layered system to evaluate the overall consolidation behavior. It was indicated that for a given degree of consolidation, the discrepancy in time factor, obtained from these methods, does not appear to exceed 20%; this close agreement is adequate only for practical purposes. Sridharan and Nagaraj (1962) also tried to make an interpretation of equivalent consolidation parameters for two-layer clay samples considering Terzaghi's one-dimensional theory. Based on theoretical calculations, they developed expressions for equivalent coefficient of consolidation and verified these by conducting a set of consolidation tests on two-layer samples with drainage through both surfaces. Their results indicated that the coefficient of consolidation calculated from theoretical equations was in good agreement with experimental results; the maximum difference between calculated and experimental value of the coefficient of consolidation was reported to be less than 9%. Another analytical solution to the layered consolidation problem was presented by Schiffman and Stein (1970) for an n -layer system with a set of boundary conditions and an arbitrary load history. The solution for the excess pore pressure was formally developed by a separation of variables for impeded, impervious

and free draining boundaries; this solution was checked against a wholly numerical results presented by Schiffman and Stein (1969) that showed the maximum relative difference in the order of 10^{-5} .

Takada and Mikasa (1984) examined the consolidation of layered clay specimens reconstituted from Osaka South Port mixed with kaolinite and bentonite powder at different dry weight ratios. Subsequently, 5 cm thick disks were trimmed from the consolidated remolded soils and combined in four different combinations into two-layer 10 cm thick clay blocks and were placed in transparent acrylite cylinders. The specimens were then consolidated to various degrees and the distribution of water content along the depth was quickly measured to obtain the isochrones of volume ratio at each degree of consolidation. The total settlement and the interface displacement were also measured during the tests. In the theoretical part of this study, the finite difference form of finite strain consolidation with variable permeability, volume compressibility and coefficient of consolidation led to the numerically calculated curves which are in satisfactory agreements with the experimental results (Figure 1.2). It was observed that the consolidation compression of the layered soil samples, in which the low permeability clay occupies the upper halves, proceeds slower than other samples.

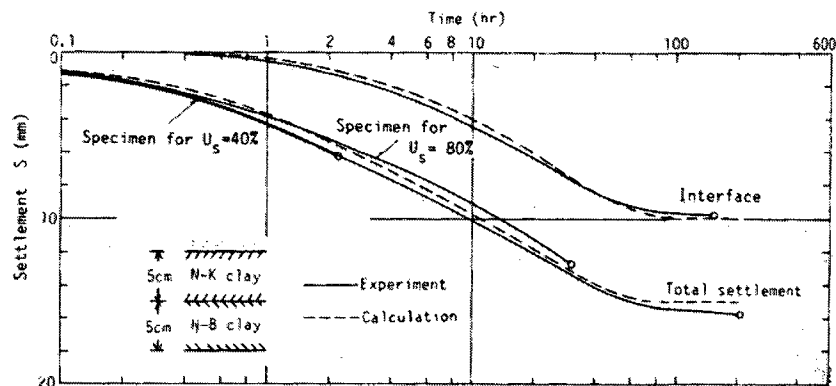


Figure 1.2 Experimental and computational settlement curves for two-layer specimens (after Takada and Mikasa, 1984)

Although some important observations on Gray's approach are worth noting, he developed the solution for only a specific type of boundary condition, which corresponds to the case of drainage on a single side. Moreover, this approach calls for the solution of an auxiliary transcendental equation which is not an easy task. Sadiku (1991) employed

an Heaviside operator, which results in a single differential equation for the pore pressure variation in the composite layered medium. He presented a closed-form expression for the solution by way of a generalized Fourier series for a wide range of practical boundary conditions. The usefulness of this approach lies in its applicability to a wide range of boundary conditions, amenability to computer application and its applicability for solving initial-boundary value problems in composite media. Lee et al. (1992) developed an efficient analytical solution technique together with a computer program for a layered system and carried out an in-depth study on the one-dimensional consolidation behavior of such a system. From different analyses on two, four and six-layer models, they indicated that the coefficient of permeability and volume compressibility of the soil play different roles on the rate of consolidation of the layered system. In other words, the effects of permeability and volume compressibility cannot be replaced by that of the coefficient of consolidation; however, the earlier analytical approaches for evaluating the one-dimensional consolidation process in layered systems were entirely dependent on the coefficient of consolidation. It was also shown that the stiffness of the soil may play a more important role than the permeability of the soil on the rate of consolidation of layered systems. In another study, Bourgeois et al. (1997) proposed an analytical approach, based on a double time scale, that has proved to be successful to find an exact analytical solution for the consolidation of layered soil. They considered a layer constituted from two strata and discussed the situation in which the properties of the strata are extremely different. This solution can be used to test the validity of numerical approaches simulating the vertical compaction of the layered models. Xie et al. (1999) presented another fully explicit analytical solution for the one-dimensional consolidation of two layered soils with partially drained boundaries that can be employed in most practical projects, such as a preloading project on a soft clay ground with partially drained boundaries adjacent to the layer. To facilitate the calculation, a computer program has also been developed for the proposed solution, and the ranges of permeability in which the boundaries can be considered as completely drained or undrained, were estimated. From a simple comparison, it was shown that great differences exist between the results for the one-layer approximation and the accurate analytical solution for a stratified layer with a constant coefficient of consolidation, but

different permeability and compressibility coefficients. This demonstrates that the permeability and compressibility characteristics of a layered soil can separately influence the consolidation behavior of the composite system.

A commonly used procedure for solving the consolidation problem in multi-layered fills is to transform the thickness of the layers in proportion to the square root of their coefficient of consolidation (ASCE, 1994). The layered system is then treated as a single layer with the vertical coefficient of consolidation corresponding to the normalizing layer and the thickness equal to the sum of the transformed thicknesses. Urzua and Christian (2002) made a comparison between this technique and the Gray-Barber analytical solution (Gray, 1945; Barber, 1945) presented for the consolidation of two-layer fills under vertical small strain conditions. The comparison showed that the normalizing technique is valid only if the hydraulic conductivities of the two layers are in proportion to the square root of their coefficients of consolidation; otherwise, the Gray-Barber solution or computational methods are recommended for calculating the consolidation response of layered soil regions.

The classical consolidation theories neglect the nonlinear and irreversible processes that occur in the soil skeleton. Xie et al. (2002) derived an analytical solution for one-dimensional pseudo-nonlinear consolidation (since no unloading effects are considered) of a double-layered soil considering the assumptions made by Davis and Raymond (1965) in which the decrease in permeability is proportional to the decrease in compressibility during the consolidation of a layer and the distribution of initial effective pressure is constant with depth. It was concluded that the discrepancy between the linear and the pseudo-nonlinear consolidation increases with the increase of load level. Several analytical calculations indicated that apart from a boundary drainage condition, the main factors affecting the rate of consolidation of a double-layered soil are the initial coefficients of permeability, the initial coefficients of volume compressibility, the thickness of the clay layers, the construction time, and the ratio of final effective pressure to initial effective pressure.

A further type of layered inhomogeneous soil is the clay-sand fills that can be formed naturally as a result of sedimentation or constructed as an alternative to the conventional

pure sand reclaimed fills (Figure 1.3) (Lee et al., 1985, 1987). Tan et al. (1992) considered the two-dimensional nature of this problem based on fluid transport in the sand drains. According to the analytical analysis, they proposed the drainage efficiency of the system as

$$\hat{\lambda} = \frac{k_s}{k_c} \cdot \frac{H}{L} \cdot \frac{H_s}{L} \quad (1.1)$$

in which k_s and k_c denote the permeability of sand and clay, H is the thickness of each clay layer, H_s is the half-thickness of each sand layer and L is the maximum horizontal drainage distance in the layered system. They also defined the efficiency factor that corresponds to the consolidation behavior of the system in comparison with fully impeded or perfect functioning sand layers, and stated that in different configuration of the layered fills, the efficiency factor depends on drainage efficiency. A high permeability ratio can be attributed to reasonable consolidation behavior (Pulau Tekong project); however, in cases with a lower permeability ratio, the increase in the thickness of the sand drains may results in an acceptable efficiency factor (Changi South Bay Project). Nogami and Li (2002, 2003) presented another formulation based on the transfer matrix approach for a layered clay fill containing multiple thin sand layers. Assuming one-dimensional loading and two-dimensional pore water flow in the layer, it was indicated that for a drainage efficiency, $\hat{\lambda} > 20$, the behavior of units are nearly uncoupled and the excess pore water pressure in the sand layers is remarkably small throughout the consolidation process. Therefore, for multiple clay-sand systems, the optimum drains can be designed in a simple manner by considering a drainage efficiency $\hat{\lambda} \geq 20$.

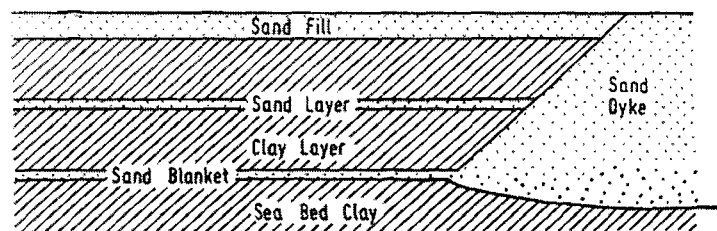


Figure 1.3 Schematic representation of layered clay-sand fill

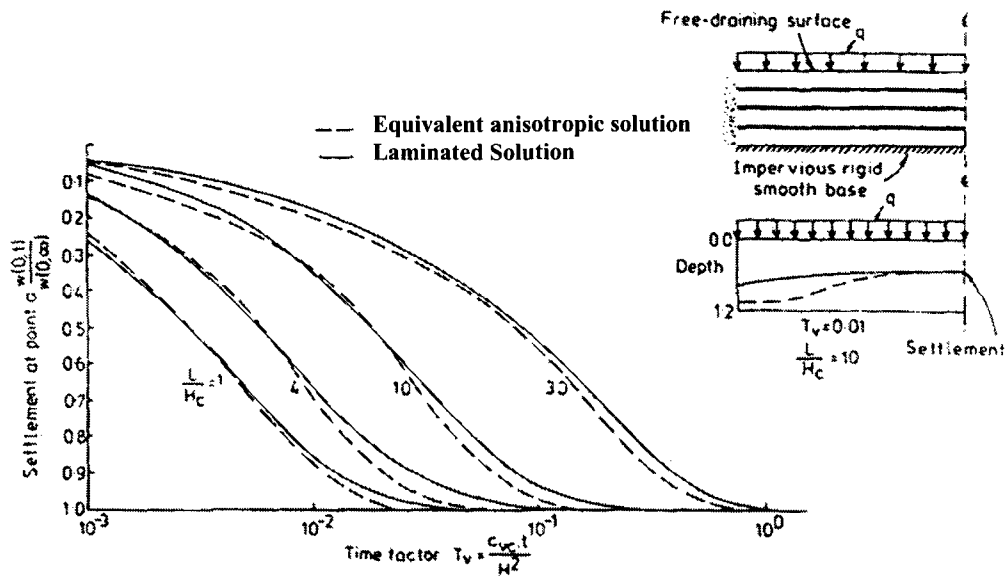
1.2.2 Computational studies of consolidation behavior of layered soil media

A foundation is often underlain by two or more clay layers, in contact with each other and each with different consolidation characteristics. Yang and Huang (1970) solved the governing differential equations subjected to initial conditions, the boundary conditions, and the continuity equation by the finite difference method using implicit formulas. It was shown that for a two-layer soil region, the degree of consolidation of each layer depends on four dimensionless parameters; the time factors, the thickness ratio, the consolidation coefficient ratio and the permeability ratio. They presented the consolidation curves for the two-layer region, assuming equal consolidation and permeability ratios for the case of drainage on a single side. These curves can also be employed for the two-sided drainage case using a trial process; an impervious plane was located by trial and error considering identical degrees of consolidation on each side of the plane. The same procedure was applied to three layers of clay with drainage provided on both sides, and the same close agreement between the theoretical and estimated consolidation response was obtained. The finite element method was also implemented by Saxena et al. (1976) and Desai and Saxena (1977) to predict the behavior of varved soil media with a wide variation in material properties and anisotropies. The model included a two-layered foundation loaded during the construction of three buildings in New Jersey. The results indicated that the finite element solution yielded trends of consolidation settlement similar to those observed in the field; therefore, the method is capable of predicting the field response by accounting for different factors such as anisotropy, rate of loading, and arbitrary geometry in the problems. In the study by Cheung and Tham (1983), Biot's consolidation problem was solved using a finite layer method based on quasi-variational as well as the least squares approach. They considered a simple finite layer model to idealize the consolidation of a layered soil medium; the layer was assumed to be of infinite extent in the two horizontal directions, whereas the displacements and stresses at certain points far from the loading were neglected. It was concluded that the quasi-variational approach, in which only the displacement and pore

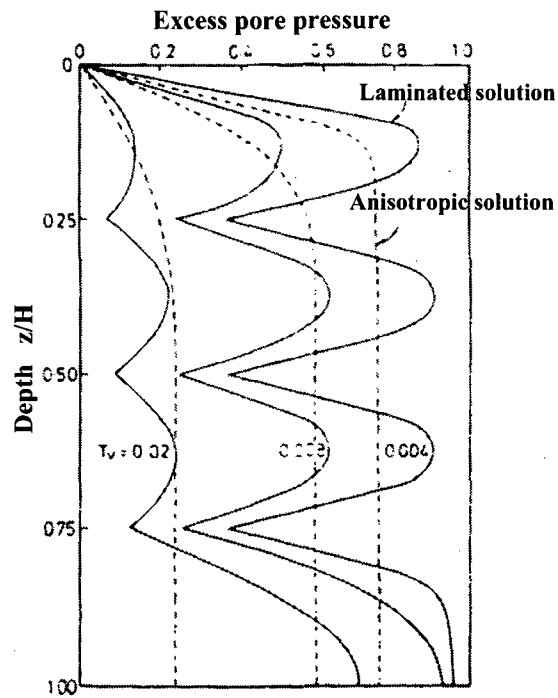
pressure parameter are involved, is preferable to the least squares method since it provides stress continuity along the layer boundaries.

Booker and Small (1987) presented a method to obtain the consolidation process of a layered soil subjected to different types of footing loadings. The solution involves applying a Fourier or Hankel transform along with the Laplace transformation. The advantage of reducing the dimensions of the problem results in great savings in computer storage and data preparation time over methods such as the finite element method and enables solutions to be obtained on microcomputers. In order to verify this theory, the computed results were compared to a solution obtained from a finite layer 'forward marching' analysis. It was shown, although the solutions agree very closely at small time values, at the largest time, some differences in the two solutions exist.

Another approach arose from the realization that laminated soils have a preferred drainage pattern, and led to the technique of treating the deposit as a homogeneous, but anisotropic material with different coefficients of consolidation in the vertical and horizontal directions. Abid and Pyrah (1990) considered two possible alternatives for modeling laminated clays using the finite element method. In the first method, two-dimensional elements were used to model the highly impermeable layers; this method did not satisfy two of the main discretization requirements, which are 'aspect ratio' and the appropriate change in 'size of adjacent elements'. The second method utilized one-dimensional two-noded line elements to model the highly permeable layers; this method has the advantage of satisfying the general characteristics required for the spatial mesh discretization, and efficiency in terms of computational time and storage capacity. Comparisons were made between the proposed laminated finite element solutions and equivalent approximate anisotropic solutions based on the work of Horne (1965). It was shown that a large differential surface settlement was predicted when using the equivalent anisotropic solution, whereas a more uniform settlement was obtained by the defined finite element technique (Figure 1.4a). In addition, the rate at which the maximum value of the pore water pressure dissipates was slower than that predicted by the anisotropic solution; however, the most significant difference was noticed between the solutions obtained for pore water pressure distribution (Figure 1.4b).



(a)



(b)

Figure 1.4 Comparison between finite element and equivalent anisotropic solutions (a) settlement-time curves, (b) Pore water pressure isochrones (after Abid and Pyrah, 1990)

Chiou and Chi (1993, 1994) adopted the uncoupled boundary element and successive stiffness methods for the numerical modeling of the Biot consolidation of an isotropic fluid-saturated porous medium. The computations attempted to examine the settlement induced by surface loading and subsidence due to pumping. The results indicated that the amount of settlement was mainly influenced by the properties of the soil layer. Moreover, the conditions at the top and bottom boundaries affected the rate of consolidation, whereas the final settlement was not influenced by these conditions. In a further study, Pyrah (1996) showed that considering a constant coefficient of consolidation in a layered soil with inhomogeneity in compressibility and permeability can lead to some misleading results. He considered two theoretical approaches for predicting the amount of settlement and pore water pressure in layered soils. The first approach was based on a standard average degree of consolidation curve, in which it was assumed that the degree of settlement is the same as the average degree of consolidation based on the distribution of pore water pressure with depth. Using this approach, the predicted pore water pressure and the rate of consolidation were independent of the arrangement of the layers and the non-homogeneous characteristic of the medium. In the second theoretical approach, which is based on isochrones from the standard solution, the settlement is directly evaluated from the change in effective stress at each point in the soil layer. While this approach takes into account the different compressibility of the layers, no consideration was given to the difference in their permeabilities or its effect on the dissipation of pore pressure and the resulting time-dependent settlements. It was stated that the correct solution can be obtained only if solid-fluid continuity is taken into account throughout the whole soil deposit, including layer boundaries; this condition, which was ignored in the previous approaches, requires that the pore pressure and flow rates at the interface of the adjacent layers are the same. Therefore, a finite element method and a diffusion approach were implemented where the assemblage matrices were formulated in terms of permeability and compressibility rather than the single coefficient of consolidation. The computational results indicated that, for case in which the low permeability soil overlays the soil layer with higher compressibility, the total settlement of the layered region was delayed. Conversely when the more compressible soil lies next to the free-draining top boundary, most of the settlement occurred relatively rapidly. Zhu and Yin (1999) also

presented a general one-dimensional finite element procedure with an emphasis on the implementation of a highly non-linear elastic visco-plastic model for layered clays. The proposed procedure is efficient for the consolidation modeling using a non-linear elastic visco-plastic model and other nonlinear models. As the computations showed, the creep parameters have a significant influence on the compression and pore pressure dissipation of the layered model.

1.3 Introduction of reinforced composite foundations

In many construction activities, loads have to be supported by soft ground. Therefore, different techniques have been used for the improvement of the soft soil layers due to limitation imposed by settlement and bearing capacity considerations. One of the most economic and commonly used methods is the installation of a stiffer material, such as gravel, in the form of closely spaced reinforcing piles. This scheme improves the mechanical performance in the field by accelerating the rate of consolidation and increasing the shear strength of soft clay deposits.

The construction of the stone-columns is usually carried out using replacement or displacement methods. In the former, which is usually implemented in an area with a high ground water level, native soil is replaced by stone-columns in a regular pattern using a vibratory probe (vibroflot) accompanied by a water jet. In the displacement method, native soil is displaced laterally by a vibratory probe using compressed air. There are other installation methods that are less common in practice (Thorburn, 1968; Greenwood, 1970; Baumann and Bauer, 1974; Hughes et al., 1975, Balaam and Poulos, 1983; Munfakh et al., 1987). In this review, major efforts carried out in terms of experimental-theoretical and computational studies of this type of composite fills are discussed separately.

1.3.1 Experimental and theoretical analyses of the behavior of reinforced composite foundations

Many attempts have been made to analyze the stone-column reinforced foundation by considering the composite ground as a unit cell with a stone-column at the center. This approximation may give reasonable results if the influences of the boundary conditions are negligible and also the loads are applied parallel to the vertical direction. However, in the case of nonlinear behavior of the in situ soil this method may not be appropriate. Hughes and Withers (1974) conducted a series of experiments at Cambridge, using radiographic techniques to determine the actual behavior of a single column of sand placed in a uniform normally consolidated kaolin clay (Figure 1.5). The tests were stress controlled and sufficient time was allowed between successive increments of load for full dissipation of the pore pressures. The experimental results indicated that only the clay within a cylinder with a diameter of about two and half times that of the sand column is significantly affected by the loading; in other words, the columns could act independently

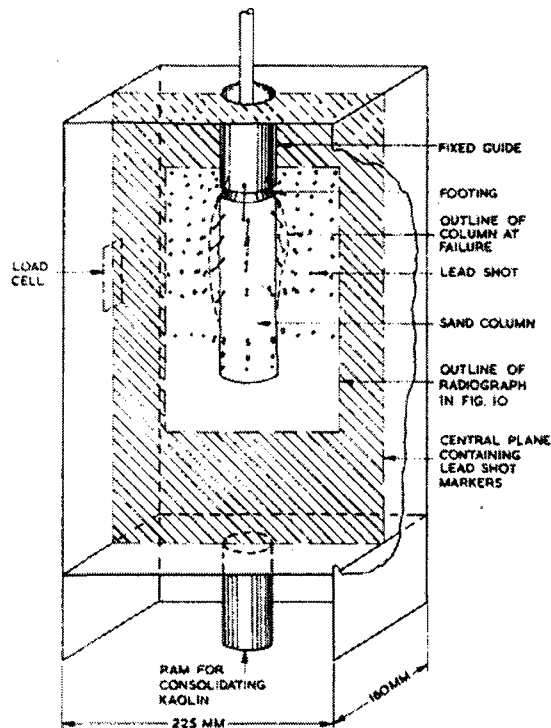


Figure 1.5 Consolidometer for testing single stone column (after Hughes and Withers, 1974)

if placed more than two and half diameters apart. It was also concluded from the test results that the ultimate strength of an isolated column loaded by its top is governed primarily by the maximum lateral reaction of the soil around the bulging zone. This observation was used to derive an expression for the limiting stress; the bulge was idealized as a cylindrical expansion into the clay and the elasto-plastic behavior was considered for the clay material. The comparison of experimental and theoretical approaches showed satisfactory agreements that support the use of the theoretical equations in practical situation.

Other theoretical solutions for the consolidation behavior of the reinforced composite were proposed after Hughes and Withers (1974). Aboshi et al. (1979) considered the effect of drainage and stress distribution on the consolidation behavior of the reinforced regions and proposed a theoretical equation for estimation of the settlement. Later work by Goughnour and Bayuk (1979) simulated the time settlement of the stone-columns by considering the concept of the unit cell with the equal strain assumption in both regions. In this approach the stress-strain behavior of the column was idealized by that of an elasto-plastic material and the major and minor principal stress increments in the in situ soil were related by some constant.

There are also some theoretical techniques developed to estimate the average degree of consolidation in the unit composite cell by taking into account only the effect of fast drainage in the system. Barron (1948) studied the two extreme cases of "free strain" and "equal strain" and showed that the average consolidation response obtained in these cases are nearly the same. Another theoretical solution was proposed by Kjellman (1948) for the ideal case of a circular soil cylinder with impervious boundaries except for the outlets of a central circular drain. Hansbo and his coworkers modified this solution by considering that, in reality, the discharge capacity of the drain is limited; moreover, the installation process may distort the soil in the vicinity of the drain (Hansbo, 1981; Hansbo et al., 1981). Therefore, they developed another solution in which the effects of well resistance and the zone of smear were considered. It was shown that well resistance would reduce the average degree of consolidation by about 10% to 30% for different diameters of sand drain. Therefore it was suggested that the filter surrounding the vertical channels should be fine enough to prevent fine material from passing into the drain and

reducing the discharge capacity of the system. In later work, Balaam and Booker (1981) presented an analytical solution for the settlement of the unit composite cell using the theory of elasticity. In order to reduce the complexity of the analysis, they supposed that each column and its surrounding area respond in virtually the same fashion as those adjacent to it. Moreover, the analysis domain was approximated by a circle of effective diameter, the perimeter of which is shear free and undergoes no radial movement. The comparison between analytical and finite element solutions showed a discrepancy of approximately 0.5% in vertical displacement and contact stresses and a discrepancy of 1.6% in horizontal surface displacement at the column-clay interface, which indicates a reasonable agreement between two methods. This study showed that Barron's (1948) solution predicts a slower rate of consolidation in practical cases where the stiffness ratio ($E_{\text{column}} / E_{\text{clay}}$) is greater than unity. This discrepancy arises since Barron's solution does not take into account the relative stiffness of the column and clay materials, whereas for a given spacing of the columns, as the stiffness ratio increases the columns take a greater proportion of the applied load and, therefore, the rate of consolidation increases. In a further interaction analysis presented by Balaam and Booker (1985), the yielding in the stone column material was taken into account; in this method it was assumed that the response of the in situ clay is elastic and that the column material is elastic-perfectly plastic, satisfying the Mohr-Coulomb yield criterion. The results from the interaction method were in good agreement with those derived from finite element analyses. The analyses showed that different parameters can affect the settlement response of the stabilized clay deposit; the dilatancy of the column is among the important parameters in the prediction of the load-settlement response, and assuming a non-dilatant constitutive behavior for the material that forms the stone columns may result in a conservative conclusion. They also presented the results of this parametric study in the form of correction factors, which enable an expedient manual prediction to be made from the purely elastic solutions.

1.3.2 Computational analyses of the behavior of reinforced composite foundations

The computational methods are applicable to a variety of boundary value problems dealing with complicated domains while the analytical methods and model tests are restricted by simplified boundary conditions and domains. From the computational point of view, the performance of the reinforced foundations was first studied by Mitchell and Huber (1985) using finite element methods. In that study, the nonlinear finite element technique was employed to predict the performance of reinforced soft ground. The finite element analysis was accomplished using an axisymmetric computer program, developed by J. M. Duncan at the University of California at Berkeley, that considers the nonlinear stress-dependent properties for the materials. Since an axisymmetric analysis cannot model a system of several stone columns surrounding a central column, cylindrical rings of elements containing stone column material properties were included in the model. The layering of the soil types within the sediments was modeled by alternating horizontal layers of cohesive and cohesionless soils. The computational results were compared with measured field load-settlement data obtained from vertical load tests performed on 28 individual stone columns, within a group of columns, and the ability of the method to model the actual behavior of the composite reinforced foundations was evaluated (Figure 1.6). It was indicated that the settlements calculated by the finite element analysis

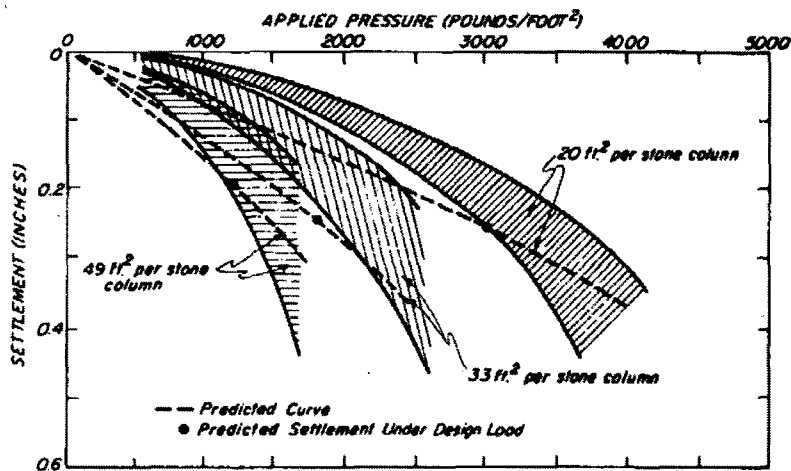


Figure 1.6 Comparison of measured and predicted load-settlement behavior of a loaded single stone column (Mitchell and Huber, 1985)

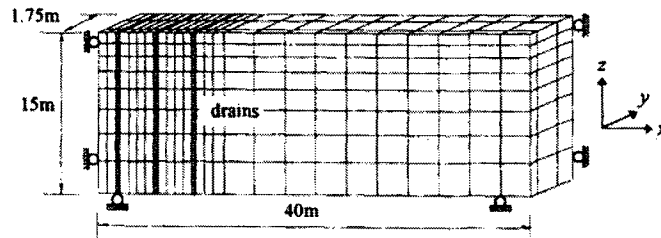
generally overestimated the actual load test settlements; however, the agreement was reasonably acceptable. A further conclusion from this study was that several other more simplified methods, including the Reduced Stress Method (Aboshi et al., 1979; Priebe, 1976; Mitchell, 1981), Elasticity Theory Method (Poulos, 1972), and Experienced-Based Methods (Greenwood and Kirsch, 1983; Barksdale and Bachus, 1983) gave values that agreed reasonably well with both finite element predictions and the field measurements.

Another numerical approach was presented by Schweiger and Pande (1986) on the behavior of stone column-supported foundations. In the formulation of the equivalent material model it was assumed that the influence of the stiff columns is uniformly and homogeneously distributed over the reinforced region. This assumption was justified since column spacing was of an order of magnitude smaller than the dimension of the foundation. In addition, according to the small size of the columns compared to the foundation size, modeling the real problem may need very refined meshing that can significantly increase the cost of the computational modeling. In the formulation, it was assumed that the stone column and the surrounding soil undergoes the same total strains and no slip occurs at the clay column interface, and the stresses on the column-clay interface were considered to be continuous, which was achieved by introducing a pseudo-yield criterion. The computational results were compared with analytical estimations obtained by Balaam and Booker (1985) for the unit cell. From the reasonably good agreements, it was concluded that the proposed approach may have advantages for problems where the assumption of the unit cell are not justified or both the columns and the surrounding soil have to be treated as elasto-plastic materials. However, the assumption of identical radial stresses in the column and soil along with different vertical and shear stresses may violate the equilibrium at the local level. Canetta and Nova (1989) presented another homogenization method in which the stiffness of the homogenized material was derived by imposing both equilibrium and strain compatibility conditions at the interface between the soil and column material. In this method, it was assumed that the second-order work done in the equivalent material is equal to the sum of the work done in the soil and column material. This homogenization model was used to analyze the behavior of a rigid circular foundation over a reinforced region; the axisymmetric

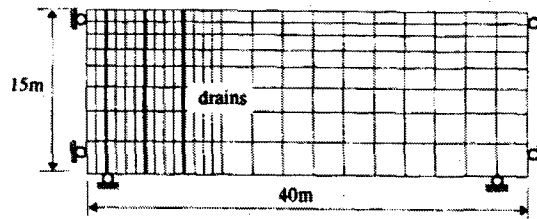
parametric study proposed a quasi-linear inverse relationship between the computed settlements and the radius of the treated zone.

Later work by Cheung et al. (1991) studied the performance of the sand drains by implementing two-dimensional and three-dimensional finite element formulations developed for this type of analysis. In three-dimensional analyses, the circular drains were replaced by square ones of the same cross sectional area, while in two-dimensional analyses the vertical sand drain system was converted into a parallel sand wall system. It was of real practical and theoretical interest to investigate the difference between the results of the foregoing procedures to ascertain whether two-dimensional analyses can be adopted for practical use. However, different computational results obtained from two-dimensional analyses were compared with those from three-dimensional ones; the difference in pore water pressure was significant in both magnitude and distribution, whereas the differences in settlement among various cases were smaller and more reasonable than for the pore pressure. The main reason for this discrepancy in pore pressure was the conversion method in which just reaching 50% of the consolidation was considered as the conversion bench mark. In contrast to two-dimensional analysis, the important characteristics of the composite-improved regions can easily be taken into consideration in three-dimensional computations without any artificial conversion, and the composite ground can be perfectly modeled. Thus, it was noted that when a two-dimensional computer code is available, the two-dimensional computation can be adopted using the best conversion method recommended in this study. Kim and Lee (1997) considered another two-dimensional equivalent model to study the consolidation behavior of the drainage-installed soft regions using the finite element method. In this study, the two-dimensional equivalent permeability was obtained considering 50% and 90% degrees of consolidation and at the same time, equal discharge rates in both the in situ case and the two-dimensional plane strain representation of the problem. Furthermore, the equivalent width of vertical wall drain was adjusted, considering an identical stiffness of the drain in both in situ and plane strain models. In order to validate the proposed equivalent model, two-dimensional and three-dimensional consolidation analyses were performed using the ABAQUS computer program (ABAQUS/Standard, 2005) (Figure 1.7). It was indicated that the average settlement obtained from two-dimensional analysis was highly underestimated, when the drain width was modeled

equal to the actual diameter of the drains. However, the analyses on models with equivalent drain width resulted in reasonable predictions in both pore pressure variation and settlement (Figure 1.8). Thus, the consolidation behavior of drainage-installed soft deposits can be predicted using the proposed two-dimensional equivalent model, which has an equivalent permeability and an adjusted width of the drainage columns.



(a) Finite element mesh for 3-D consolidation analysis



(b) Finite element mesh for 2-D consolidation analysis

Figure 1.7 Finite element mesh for consolidation analysis
(After Kim and Lee, 1997)

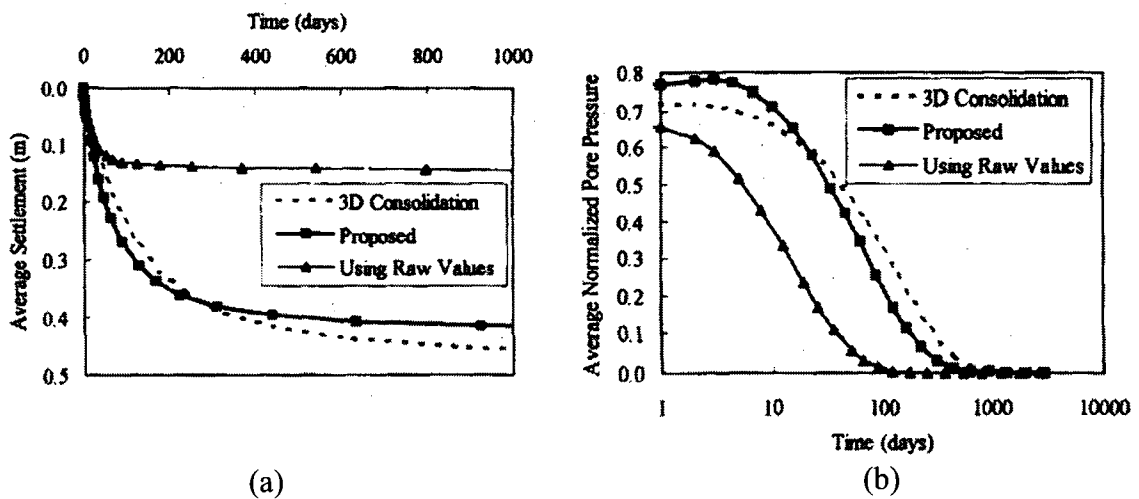


Figure 1.8 (a) Surface settlement and (b) pore pressure variation below the center of the embankment (after Kim and Lee, 1997)

In another approach, Lee and Pande (1998) modified the homogenization technique that has been applied to the shear localization and rock joint analysis (Pande et al., 1993) to be applicable for the analysis of stone-column reinforced foundations. The homogenization was carried out using the averaging rule based on area or volume fraction of the constituents and the equilibrium and kinematic conditions were formulated considering the bonding interface between the in situ soil and stone columns. To validate this approach, a circular steel footing resting on a stone-column reinforced foundation was axisymmetrically modeled using a finite element approach and the settlement behavior of the region was compared with the experimental results. The predicted load-settlement curve, obtained using the homogenization technique, showed good agreement with that of the experimental results. The visualized contour plots of the stress components also indicated that the equilibrium conditions between the in situ soil and stone-columns were satisfied throughout the elastic as well as the elasto-plastic range of material behavior.

1.4 Introduction of land reclamation project

Initial efforts in land reclamation, which began in the early part of twentieth century, involved relatively unplanned projects, including draining swamplands for port construction. After the Second World War the driving forces for new land reclamation were industrial growth and port expansion. The more recent reclamation activities, which commenced in the 1980s, were initiated to maintain and extend the status of the coastal territories as world economic and commercial centers (Du-Plat-Taylor, 1931; Wong, 1985; Sasaki et al., 1987; Glaser et al., 1991)

Currently, land development and reclamation activities are indicators of the dynamic development and economic growth of small coastal territories particularly in South-East Asia that play an important role in world economic affairs. The land reclamation projects have been undertaken in different countries to modify the coastline and extend it seaward; the reclaimed lands are used to expand the residential areas and recreational facilities for the growing population as well as expanding commercial and industrial activities by improving transportation infrastructures including roads, expressways, port and airport facilities. Furthermore, major land reclamation projects are taking place in

some countries to create additional coastline to serve the tourist industry (Shintani, 1991; Lui and Tan, 2001; Anon, 2004).

Large-scale land reclamation projects have been undertaken in various parts of South-East Asia; as an example, since separation from Malaysia in 1965, Singapore has added 120 square kilometers of land, an area which is larger than city of Paris. Surrounded by water, the Singaporean government believes that the country must continue to grow physically, which leads to expansion of commercial and industrial activities. Changi Airport is among several infrastructures built on reclaimed lands, located about 20 *km* north-east of Singapore centre. This aviation hub creates job for over 13,000 people and inputs US\$3.1 billion into the economy of Singapore. In 2005, this airport handled a record of 32.4 million passengers, making it the 26th busiest airport in the world and the sixth in Asia. However, a new terminal will be opened in 2008 to expand the airport capacity to 64 million passengers (Anon, 1985; So, 1986; Pui, 1987; Moh, 1988; Arulrajah et al., 2004).

Other than scarcity of land in many countries, tourism has recently become further objective for land reclamation. This industry is vital for many countries due to the income generated from the consumption of goods and services by tourists, the taxes levied on businesses in the tourism industry, and the opportunity for employment in the service industries associated with tourism. These service industries include transportation services, accommodation such as hotels, restaurants, bars, entertainment venues, and other hospitality industry services and resorts. Dubai, unlike the other gulf states, has practically no oil reserves and has therefore set its sights on the tourism industry, aiming to increase the number of tourists from the current 4.5 million per year to twice that in a period of five years. These tourists are primarily looking for accommodation close to water; however, Dubai's coastline is only 30 *km* long which cannot meet the demands for expansion of the tourist facilities. Therefore a plan was developed to construct four offshore islands, shaped to generate the greatest possible length of shoreline. Three islands are being shaped like palm trees, while the fourth will comprise 264 smaller islands together forming a map of the world. The entire reclamation work involves placing 320 million cubic meters of soil, which is equivalent to building a wall two

meters wide and four meters high around the equator (Anon, 2005a,b; Reina, 2006; Griffith, 2006).

1.4.1 The land reclamation methods

Early land reclamation activities in Southeast Asia, dating back to the beginning of the twentieth century, used materials extracted from the hills and inland borrow-pit area. These materials are now scarce; therefore sea sand and dredged marine soils have become the preferred source of materials used in reclamation activities. Even these options are not without problems: several reclamation sites are surrounded by only soft clay deposits, or the seabed is located in deep water where excavation from sea sand sources is not practically feasible. In such cases, granular fill materials dredged from the seabed at borrow sources located in neighboring countries are used. The most common type of dredging plants used in these projects are cutter suction hopper dredgers, trailer suction hopper dredgers and bottom opening hopper barges that dredge and transfer the excavated fill materials to the reclamation sites. Thus, in reclamation projects, the cost and amount of imported sand and the distance between the borrow sources and reclamation sites are important factors of economy for the project (Sladen and Hewitt, 1989; Li and Jeng, 1997; Lee et al., 1999; Chang et al., 2006).

Over the past decades, land reclamation has modified the coastline of territories, extending it seawards. There are, however, limiting constraints as to how far the coastline can be modified through land reclamation works. One main constriction is the increase of the cost of projects as the reclamation sites move towards deeper water. Furthermore, in many countries there is a competing need to maintain the sea lanes in order to construct larger ports that can serve the commercial and industrial activities. However, the most significant concern of the contractor companies is providing sufficient granular fill, which is the basic and only construction material that has been used during the past decades. This problem has been raised as a result of the depletion of inland resources and also the banning of export of sand by donor countries due to environmental considerations. Singapore, as a leading country in reclamation work, has expanded its maritime borders by nearly 20 percent as a result of land reclamations carried out in

different parts of this island; however, this city-state is completely dependent on its neighboring countries for sand imports used for construction and land reclamation activities. Malaysia banned the export of sand to Singapore in 1997, and since then, Singapore has annually spent 120 to 160 million dollars importing sand from Indonesia. However, in February 2007, the government of Indonesia also banned the export of sand to its neighbor believing that the land reclamation projects lead to environmental damages and changes in the maritime borders of the countries. Therefore, Singapore's government started importing sand from more distant countries; this resulted in more than 100% price increase with an ensuing higher overall construction cost. Furthermore, although this solution could serve the immediate needs of the construction sector not to interrupt the projects, the government has begun looking for alternative resources in order to move away from such high dependency on sand import for reclamation work.

Although the sand resources are now limited in many coastal regions, large quantities of dredged soft clay can be obtained from the construction and maintenance of navigation channels and seaports as well as inland construction activities. These excavated clay lumps used to be dumped in deeper regions of the sea; however, several objections have been raised about this procedure for environmental reasons. One of the significant problems posed during investigations revealed that the water at the dumping grounds becomes turbid and dredged masses often contain heavy metals that may affect the environmental conditions at the dump areas (Hartlen and Ingers, 1981; Wang et al., 1997). The use of these soft soils to construct the reclaimed fills is therefore regarded as a plausible solution for disposing of the excavated soil and for providing a local fill material for land reclamation works (Tan et al., 2000; Leung et al., 2001). The fills constructed from dredged clay can have different properties depending on the method of transporting the excavated soil. The *hydraulic filling* is the conventional reclamation procedure, where the dredged clay lumps, with dimensions of the order of 10 mm to 300 mm, are suspended in a semi-fluid clay slurry for transportation and subsequently deposited at the reclamation site (Choa, 1994; Nogami et al., 2004). Casagrande (1949) reported the use of hydraulically dredged clay lumps as reclamation material for construction of the Logan Airport in Boston. The same method was also used for the

construction of a man-made island (The Lacuster terminal) in Lake Maracaibo by pumping in sedimentary overconsolidated clay (Whitman, 1970).

Another method implemented in reclamation activities is the *lumpy filling* method, which has been employed in several reclamation projects, mainly in Singapore, since the 1980's (Leung et al., 1996, 2001; Wong, 1997; Nogami et al., 2004). Using advanced facilities such as bottom-opening barges and huge clam-shells, there is always the tendency to accelerate the reclamation activities and, at the same time, increase the efficiency of the projects. The New Container Terminal in Singapore can be addressed as one of the reclaimed land areas recently constructed from large dredged stiff lumps extracted from the seabed (Figure 1.9).

The results of several field investigations reported from different land reclamation projects indicate that constructing the reclaimed fills from large lumps is easier since the use of the hydraulic filling method involves double handling. The dredged clay first has to be mixed to a higher water content to facilitate pumping, while during the soil improvement, the water content of the slurry should be reduced. Besides, the net solid volume achieved from the slurry pumping process is very small. However, the use of stiff clay lumps instead of the hydraulic pumping scheme may lead to certain problems resulting from large void spaces that exist within the reclaimed fills (Bo et al., 2001; Leung et al., 2001). In this review, notable efforts carried out to analyze the behavior of lumpy fills will be briefly discussed.

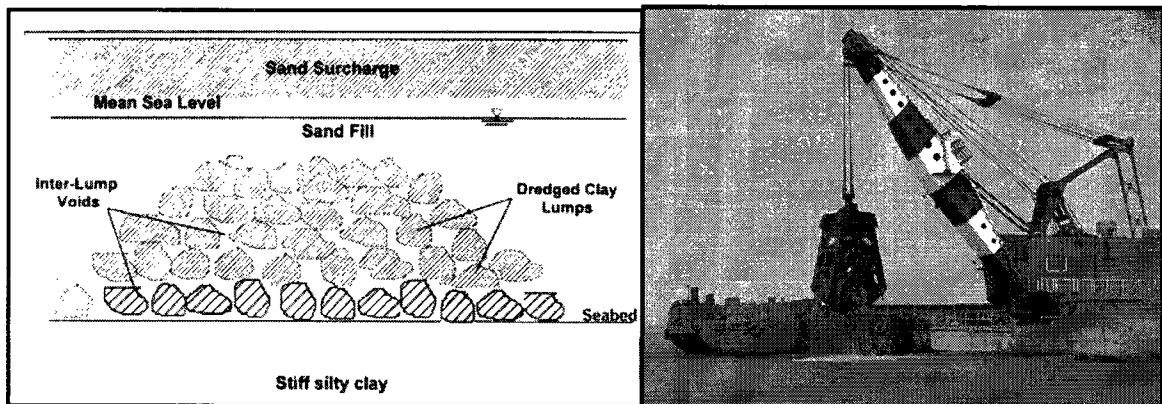


Figure 1.9 Schematic profile of reclamation fill constructed from dredged stiff clay using clam-shell (after Leung et al., 2001)

1.4.2 The study of consolidation behavior of lumpy inhomogeneous fills

In land reclamation projects, the clay lumps removed from the seabed have a softened exterior while their inner cores remain relatively stiff for a long period. When these lumps are dumped, the profile of the fill can be expected to be highly variable due to the presence of *inter-lump* voids. Hartlen and Ingers (1981) reported that reclamation of Halmstad Harbor, situated in south-western Sweden, employed both reclamation methods to construct the fill; the bottom 3 m of the fill consisted of barge-dumped clay lumps of about 1 m³ deposited between two break-waters by bottom opening barges, underlain by a 3.4 m layer formed hydraulically with clay lumps excavated with a cutter suction dredger. The material leaving the dredger pipe consisted of well-rounded lumps of varying sizes, with diameters up to 300 mm. A test embankment was then built, 14 months after the completion of the filling, and the vertical and horizontal movements of the constructed layers were measured using different types of displacement transducers. The results indicated that the larger part of both the vertical and horizontal movements took place in the barge-dumped part of the fill; this happened as a result of the nature of blocks with their sharp edges and interspersed voids which had not been completely filled by the suspended material. The hydraulically placed fill, consisting of well rounded lumps and voids filled with suspended material, was able to withstand the applied stresses due to its relatively uniformity.

The consolidation characteristics of reclamation fills made up of clay lumps are complex, since the *inter-lump* voids also close up during the consolidation of the lumps; the conventional consolidation theories are therefore not applicable for analyzing the consolidation behavior of lumpy fills. Wang et al. (1997) proposed a solution for the consolidation problem associated with spatial co-ordinates using the Laplace transformation method; however, for such a complicated structure, direct calculation will take a long time and makes the solution procedure more complicated. Therefore, a homogenization method was implemented to find an effective medium that has the same macro-response and involves microstructural effects. In this approach, the conventional Terzaghi-Rendulic consolidation theory, which involves the microstructural effect, was considered and the homogenized consolidation coefficients for a multi-layer medium

were determined. The proposed method is applied to back analyze the centrifuge model tests on dredged lumpy materials conducted by Leung et al. (1996). In this analysis, the lumpy fill pores were divided into *inter-lump* and *intra-lump* pores, and the consolidation coefficient reaches its lowest value at the complete closure of the *inter-lump* voids, while the peak value occurs at the beginning of the loading. It was seen that the clay lumps deform completely or collapse; therefore, even a large deformation theory is not applicable when this deformation is mixed with the conventional consolidation processes. However, in the long term, after the closure of the *inter-lump* voids, the process follows the conventional consolidation theory as the deformations are small and the consolidation coefficient is stable. The prediction from the proposed homogenization method was in good agreement with the experimental data except for the initial settlement. At the beginning of the loading, the microstructure of a lumpy fill has a considerable deformation that results in a reduction of permeability and the coefficient of consolidation. Thus, the conventional consolidation theory with a revised consolidation coefficient can only be applied after the initial compression, when the microstructure shows a more stable deformation.

A study by Callari and Federico (2000) presented a double porosity model for the consolidation behavior of structured clay and compared the analytical results with experimental evaluations and the results obtained from finite element analyses. In double porosity approach, the highly fissured porous medium was modelled as a continuous medium with two different void systems, in which the first system of pores represents the net of fissures besides the pores within the intact material fragments. The equivalent elastic parameters of the model were evaluated from the average final settlement and the average effective stresses obtained from finite element computations. The results indicated, as expected, that in double porosity media consolidation occurs faster than in single porosity media. Moreover, in double porosity model, the layer thickness has less influence on the rate of consolidation in comparison with single porosity media, as a result of the role of fissured regions. In finite element computations, a stratum of highly fissured material was represented through a regular arrangement of staggered porous square elements (two-dimensional) or cubic blocks (three-dimensional) separated by an ordered net of fissures with linear elastic behavior (Figure 1.10). The computations

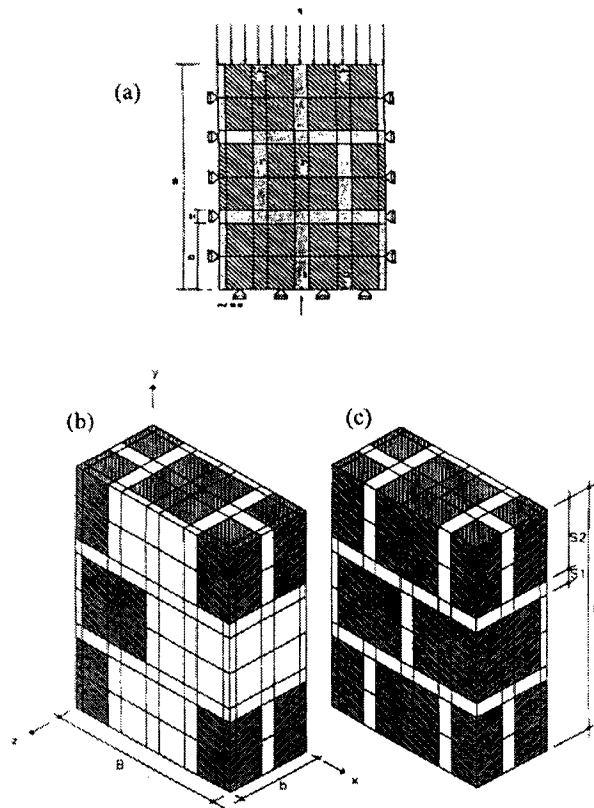
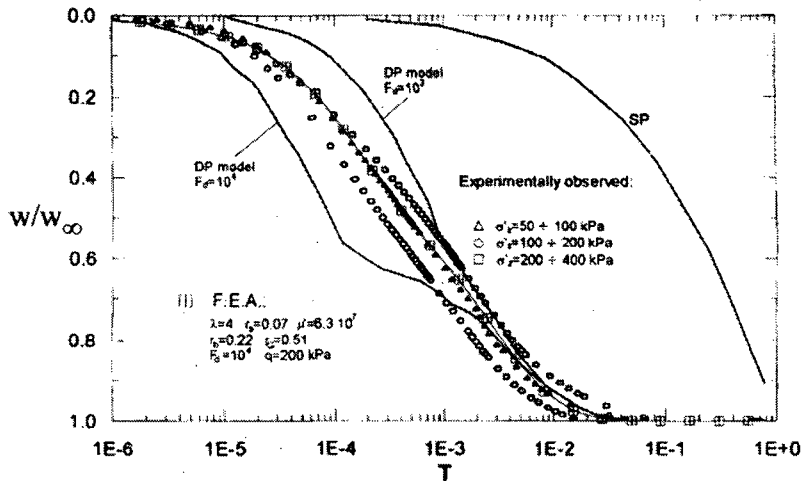


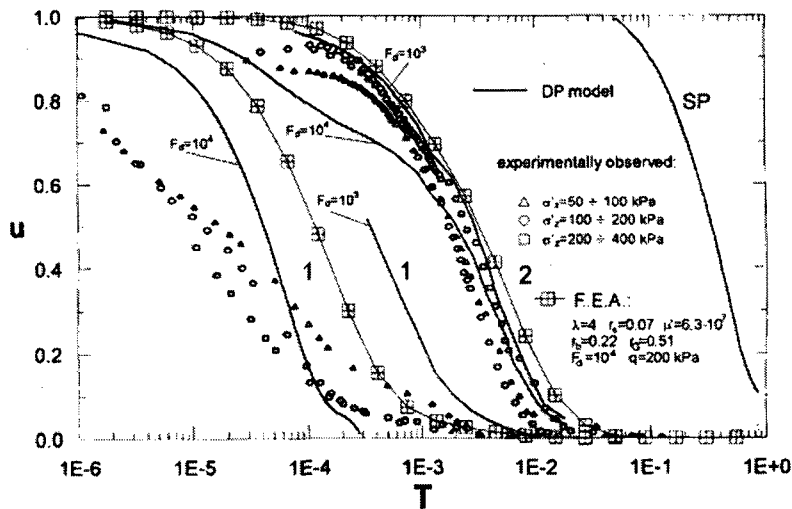
Figure 1.10 Typical meshes for FEM (a) Plane strain, (b) 3D with external lateral elements, (c) 3D without external lateral elements (after Callari and Federico, 2000)

indicated that a significant decrease of pore pressure in the intact lumps can be observed only after nearly total dissipation of excess pore pressure in the fissures. Also, in the three-dimensional case, the pore pressure dissipation and the settlement evolution are faster than in plane strain conditions, as a consequence of the increased path ways available for pore pressure dissipation. For purposes of validation, the results obtained from the computational model were compared with those obtained from the double porosity model: the comparison indicated that the analytical model could predict reasonably well the consolidation of structured media provided appropriate values of the physico-mechanical parameters are assigned. Furthermore, the results of the proposed analytical and computational methods were validated with an experimental study conducted on structured clay consisting of an assembly of small cubical clay blocks (6 cm sized), each covered by a thin geotextile layer. The blocks were placed in four layers, within a large-scale Rowe's cell (diameter 49 cm, height 25 cm) equipped to measure the

fluid pressure at the base, at different points corresponding to the geotextile and clayey blocks. The comparison showed that the theoretical double porosity results for pore pressure dissipation and settlement evolution agreed well with the experimental and computational results (Figure 1.11). However, experimental data agrees more closely with the results of finite element computations, due to better modeling of the fluid exchange between the two porous systems.



(a) The results of normalized settlement curves



(b) Non-dimensional pore pressure inside (u_2) and in between the lumps (u_1)

Figure 1.11 Comparison of results obtained from DP model, FE computation and experiment (after Callari and Federico, 2000)

Work by Leung et al. (2001) evaluated the load-settlement response and the movement of the lumps in one-dimensional compression, obtained from tests on lumpy specimens made up of dredged stiff clay lumps. The apparatus consisted of a loading frame and a cylindrical Perspex container with an internal diameter of 235 mm and a wall thickness of 6.5 mm (Figure 1.12). Spherical lumps of 50 mm diameter were taken from the recompressed clay using a cylindrical scoop, and placed by hand in hexagonal face packing in layers in the container. In this experiment, five vertical load steps of 25 kPa, 50 kPa, 100 kPa, 200 kPa, and 300 kPa were applied sequentially. In the first loading step, a large immediate settlement of approximately 100 mm was recorded (axial strain of 39%), while during other loading steps, the magnitude of the immediate settlement was significantly reduced and a consolidation response similar to that of a homogeneous sample was observed. This behavior indicated that much of the *inter-lump* voids had been reduced during the preloading step. The observations also indicated that the upper spheres had moved down substantially, while relatively little movement was noted for the

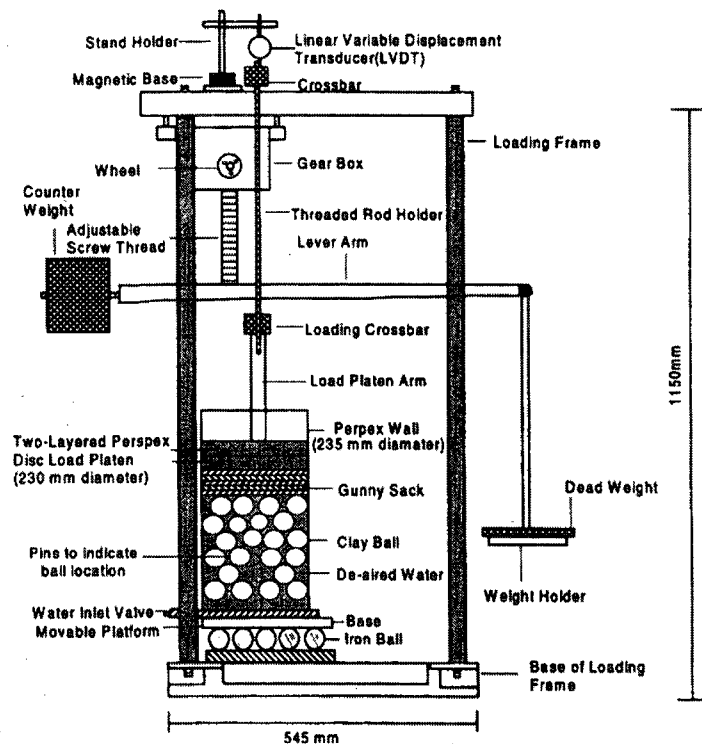


Figure 1.12 Schematic setup and instrumentation of the one-dimensional compression test (after Leung et al., 2001)

lower spheres; however, the lower spheres deformed significantly more, when compared with the upper clay inclusions, and this is attributed to the higher stresses experienced in the lower layer. Centrifuge model tests were also conducted to simulate prototype stresses more realistically, while the duration of the consolidation process was expedited. To determine the effect of lump shape, spherical, cubical and irregular shaped lumpy samples were brought to 100 g to achieve an equilibrium condition under self-weight. The samples were immediately spun down to 1 g and an 80 mm thick sand surcharge was placed on top of the lumpy fill. The model was again brought to 100 g in which the equivalent prototype sand surcharge pressure was estimated at 120 kPa. It was noted that the fill made up of spherical lumps experienced less settlement strain compared to either cubical or irregular shaped lumpy fills; this is attributed to the fact that spherical lumps have a more stable open structure that effectively forms a densely packed structure within the lumpy fill. It was also found that the final void ratio after both self-weight and surcharge consolidation was almost identical. This illustrated that due to the self-weight of the fill, many of the *inter-lump* voids have closed up, which is in agreement with observations reported in the Halmstad Harbor field study (Hartlen and Ingers, 1981). Further observations showed that the rate of consolidation is considerably faster for the lumpy fill as compared to homogeneous clay, whereas the difference in the consolidation rate reduces with an increase in loading pressure as the voids are reduced. It was, therefore, recommended that in engineering reclamation projects with a fill made of stiff clay lumps, preloading needs to be applied in order to eliminate the large soil settlement before any construction takes place in the reclaimed regions.

Wang et al. (2002a) proposed a simplified homogenization approach for soil composites typically composed of soft clay reinforced by stiff soil columns or stiff soil layers that contain soft clay lumps (Figure 1.13). They assumed that the stress in each phase of a composite model is homogeneous and the stresses in the matrix and the reinforcement phases are distributed according to some proportion. Thus, the stress localization tensor for a two-phase material was obtained as

$$C = \begin{cases} \frac{b_s}{(b_s - 1)f + 1} I & \text{(in f-phase)} \\ \frac{1}{(b_s - 1)f + 1} I & \text{(in m-phase)} \end{cases} \quad (1.2)$$

in which f denotes the ratio of reinforcement volume (f-phase) to the whole volume of composite model, and b_s is the stress ratio defined as the ratio of stress increment in reinforcement stiff phase to that in soft soil (m-phase). This tensor was used to predict some characteristic parameters such as Young's modulus and strength parameters in alloys and soil mixtures. Comparison showed good agreements between the results of the proposed method and experimental data; however, when the material has more than two phases and its microstructure has definite orientations, this method has its limitation and the rigorous procedure of the homogenization method was recommended for such cases.

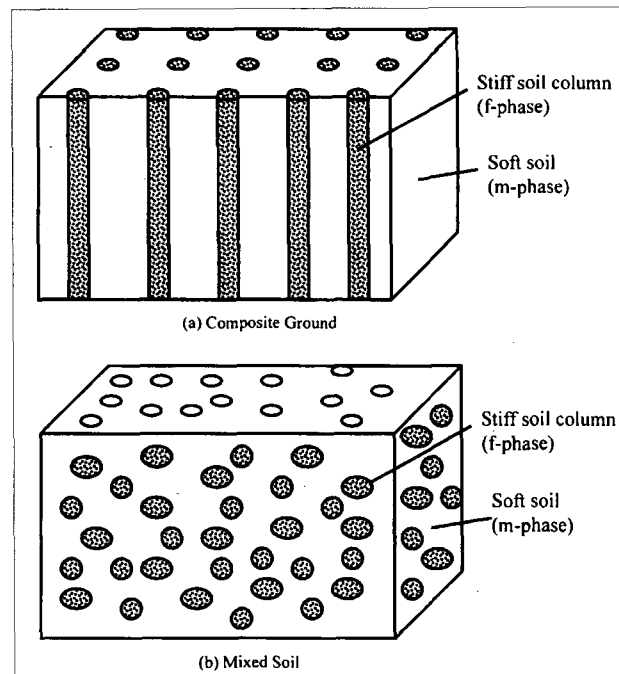


Figure 1.13 Different types of composite soils (after Wang et al., 2002a)

Later work by Nogami et al. (2001) implemented a double porosity consolidation model, first used in the petroleum industry to deal with flow in a fractured porous medium, to analyze the consolidation of lumpy reclaimed fills. In the approach adopted by Nogami et al. (2001), the effect of self-weight consolidation was not considered; however, in

reclamation works self-weight consolidation is important since deposition of the fill with dredged and excavated materials will take several years before a sand fill is placed on top. Yang et al. (2002) presented an analytical solution to an idealized problem for the case where the linear elastic soil with constant permeability undergoes consolidation under self-weight and a surcharge load. After clay lumps have been deposited, two different mechanisms will contribute to the settlement: expulsion of fluid from the *inter-lump* voids, as well as the progress of the consolidation process within the clay lumps. The exact analytical solution was derived to highlight the essential features in the consolidation of lumpy clay fills under self-weight and surcharge pressure. It was shown that when the difference between the pressure in the *intra-lump* and *inter-lump* voids increases, a higher volume of fluid is transferred between the two phases of the material. To evaluate this further, a parametric study of the effect of *inter-lump* and *intra-lump* permeability was carried out: It concluded that the permeability of *inter-lump* voids not only has an immediate impact on the dissipation of pore pressure in the *inter-lump* voids, but also, through its effect on the transfer term, can directly influence the dissipation of the *intra-lump* pore pressure. Thus, in such a system the permeability of the *inter-lump* system plays a key role in the consolidation behavior of the soil composites constructed with clay lumps.

Mesh-dependent methods such as the boundary element method (BEM) and finite element method (FEM) are powerful tools to solve problems involving coupled fields; however, both methods are mesh-based schemes that require a pre-defined connectivity between all the elements. In other words, mesh generation has been one of the most significant challenges in mesh-based methods that can take most of the computational time and effort (Jin et al., 1989; Weatherill, 1996). To avoid mesh generation, considerable efforts have been devoted to the development of mesh-less methods. It eliminates the element concept for constructing approximation functions for field variables and only uses a set of nodes to discretize the problem domain. There is no fixed connectivity among nodes and hence it can remove or at least alleviate the difficulty of meshing or re-meshing the problem domain by simply adding or deleting nodes. Most of the mesh-less methods developed to analyze consolidation problems are based on moving least squares approximations and their interpolation shape functions are polynomials

associated with nodal values by weighted least squares approximations (Modaressi and Aubert, 1996; Murakami et al., 2001). The basic idea of the point interpolation method is to provide a method through a data point so that the enforcement of the essential boundary conditions may be simplified. The basis used in the point interpolation method is polynomials and the order of polynomials is dependent on the number of nodes that contribute to the approximation. The main shortcoming of this method is that singular matrices may occur if the arrangement of a set of scattered nodes is not consistent with the order of basis. In order to overcome this difficulty, a point interpolation mesh-less method based on radial basis functions was proposed by Wang and Liu (2002). As the most attractive characteristic of the radial point interpolation method, the well-performed shape functions can be constructed by adopting the radial and polynomial basis function together; the partial derivatives of these shape functions are easily obtained, thus improving computational efficiency. Wang et al. (2002b) applied this method to solve Biot's consolidation equations and obtained satisfying results. Subsequently, Nogami et al. (2004) developed a numerical method for the consolidation analysis of lumpy clay fillings, adopting the double porosity model and the mesh-less method based on the radial point interpolation approach. The consolidation equations for lumpy clay fills were derived using the double porosity model; these equations were discretized with the radial point interpolation method, specially formulated with the interpolation functions of mutually different orders for the displacement and pore water pressure. The rate of fluid exchange between the matrix and *inter-lump* voids was assumed to be proportional to their pressure difference at interface with a fluid exchange factor that is a function of the permeability, shape and porosity of each medium. In order to improve the possible numerical problems caused by the inconsistency in the accuracy between the displacement and pore water pressure, a one-order higher interpolation function was specially used for the displacement over that for the pore water pressure. Nogami et al. (2004) considered a one-dimensional problem in which nodes were arranged in regular and irregular distribution; comparisons confirmed that the current numerical approach is not sensitive to the mode of node distribution. The computational approach developed was compared with numerical methods (finite element and transfer matrix methods), which had been previously formulated for the consolidation of fissured clay, and good

agreements were observed among the results computed by these methods. The method developed was also examined using results of centrifuge test conducted at the National University of Singapore (Wong, 1997); comparisons made on excess pore pressure and normalized settlement implied that the double porosity model can predict the consolidation behavior of lumpy clay fillings reasonably well, provided that proper material properties are given (Figure 1.14). Numerical experiments were also carried out to examine the effect of different factors on the consolidation of the lumpy fills. The results indicated that a longer consolidation time is required for smaller permeability ratios (permeability of *inter-lump* region to the permeability of the matrix); this may be

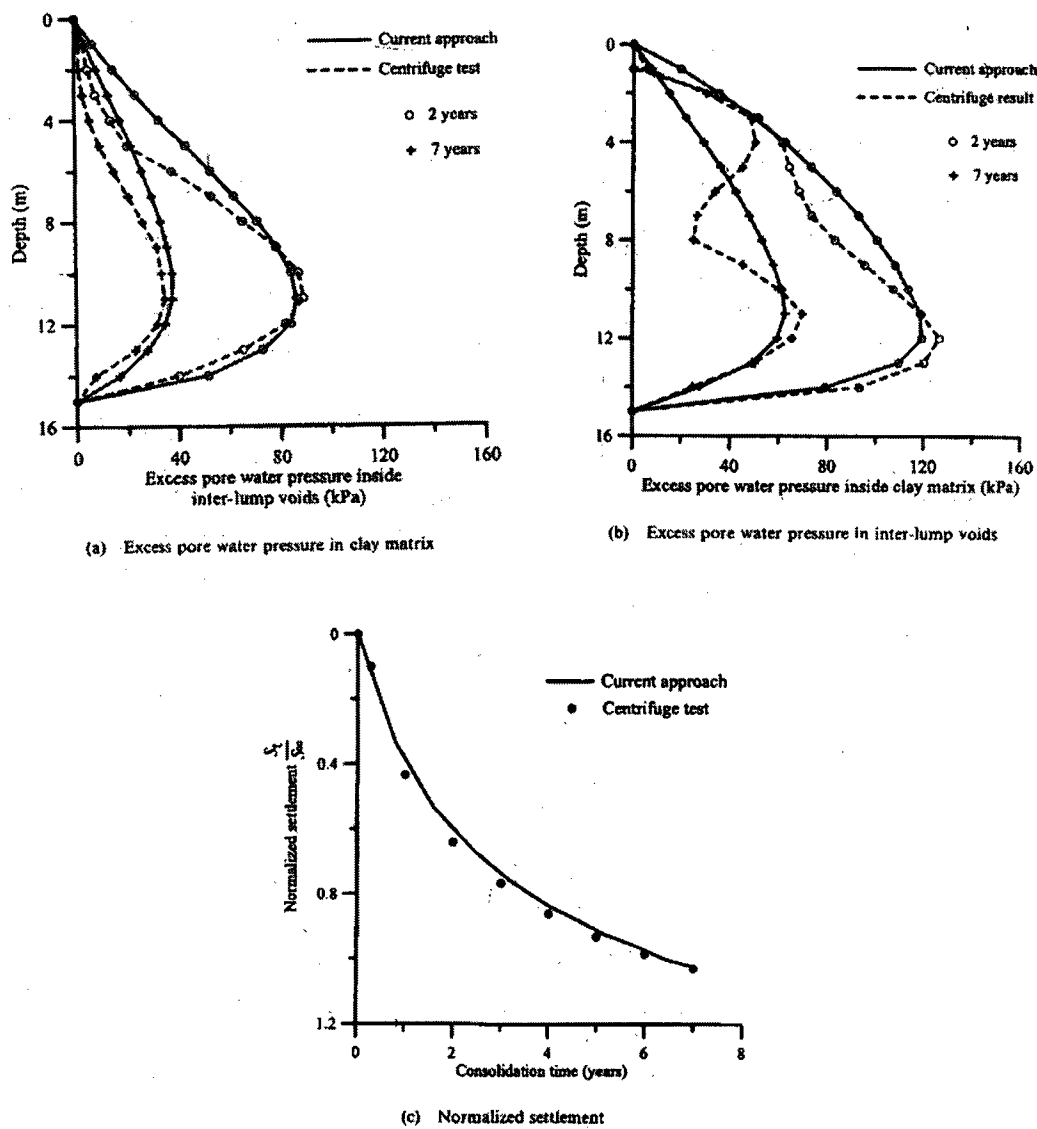


Figure 1.14 Comparison of numerical results and centrifuge test (after Nogami et al., 2004)

attributed to the fact that a higher fluid exchange rate between the matrix and *inter-lump* voids results in a more rapid dissipation of pore pressure in the clay lumps and thus faster settlement of the fills. Karthikeyan et al. (2004) reported the results of an extensive site investigation carried out at a 12-year old man-made island. In the reclamation of Punggol Timor Island in Singapore, large dredged clay lumps of up to about 8 m^3 were excavated using a clam-shell grab to construct an 8 m thick lumpy fill layer. During transportation and dumping, the original big lumps may have been broken into lumps of various sizes ranging from 0.5 m to 2.0 m . A sand layer of 10 m thick was subsequently placed as a top fill and also as a surcharge to accelerate consolidation of the lumpy fill layer. The goals of this site investigation were to determine the size of the *inter-lump* voids at the end of the consolidation process in the fill and also to evaluate the strength and deformation characteristics of such reclaimed ground. The results obtained from Nuclear Density-Cone Penetration Tests (ND-CPT) showed frequent changes in wet density and cone friction ratio below 11.5 m , which indicated the presence of a layer of sand-clay mixture that was formed by penetration of the sand into the large initial *inter-lump* voids. This is possible because, initially, the *inter-lump* voids are open and large enough for sand particles to penetrate. The CPT profiles also showed three distinct soil layers present in the reclaimed fill; sand at the top, an intermediate sand-clay mix and then a lumpy fill layer. The thickness of this intermediate mix zone was found to be between 3 m and 5 m . Further investigations showed that the compression of lumps due to surcharge causes yielding at the edges, and adjacent lumps move towards one another; this process squeezes the disintegrated material within the initial *inter-lump* voids and appears to have filled the initial *inter-lump* voids completely. Therefore, visual observations made on a large number of cross-sections of soil samples indicated that the original large *inter-lump* voids were reduced to the size of *intra-lump* voids and cannot be seen by the naked eye.

Later work by Yang and Tan (2005) implemented the double porosity formulation in finite element analysis, taking into account a non-linear void ratio vs. permeability and effective stress relationships to ensure a more realistic prediction of the one-dimensional behavior of the lumpy fill. This is necessary since, in reality, the coefficient of the permeability in the *inter-lump* system will change significantly during consolidation, and this has an important influence on the process of consolidation. The finite element

program was first shown to be able to predict results that matched the analytical solutions developed by Yang et al. (2002). To check the applicability of the proposed model, it was then used to analyze results from the two one-dimensional consolidation tests on lumpy clay samples; one with water in the *inter-lump* voids, and the other with slurry in the *inter-lump* voids. The results presented showed that the model can predict well the measured settlement and pore pressures in the *inter-lump* and *intra-lump* systems of both experiments.

Another laboratory study was carried out by Robinson et al. (2005) on lumpy fills made up of cubical clay lumps with sizes ranging from 12.5 mm to 50 mm. The lumpy fills were fabricated in containers with different internal diameters (100 mm, 150 mm and 235 mm). It was shown that for consolidation pressures less than 50 kPa, the shape of the time-settlement curves in the logarithmic plot were concave upward, which is in contrast with homogenous clay samples, that corresponds to Terzaghi's model (Figure 1.15). Therefore, considering the two void systems that exist in the lumpy fills, it was concluded that a double porosity model should be adopted to investigate the behavior of these layers. Furthermore, the variation of pore pressure inside and between the lumps, recorded by miniature pressure transducers, showed that during the load increase, the pore pressure inside the lumps reached a maximum value greater than the applied pressure increment due to processes such as the Mandel-Cryer effect (Mandel, 1953;

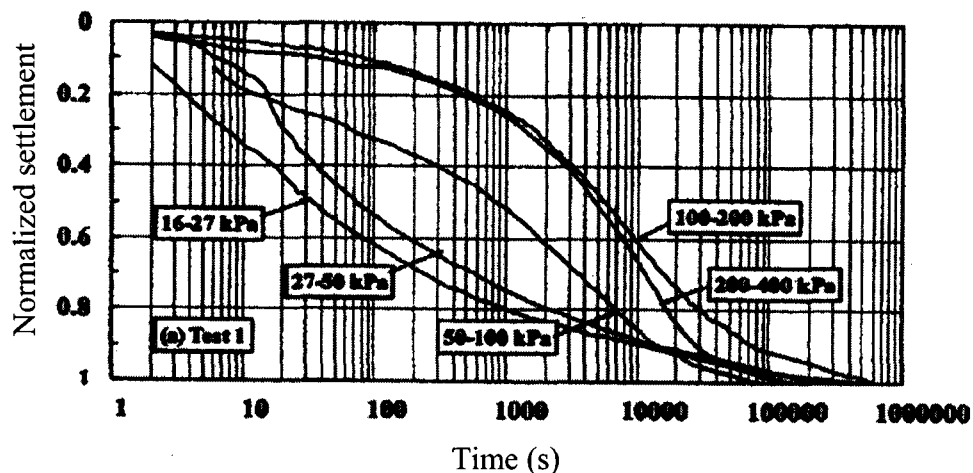


Figure 1.15 Typical time-settlement curve in different load steps (after Robinson et al., 2005)

Cryer, 1963; Selvadurai and Shirazi, 2004). At higher stress levels, the similarity in the magnitude of pore pressures recorded inside the *inter-lump* voids and the clay lumps also indicated that the *inter-lump* voids were practically closed and the sample could be considered as a homogeneous clay specimen.

1.5 Objectives and the scope of the thesis

Early reclamation activities used granular soils obtained either from inland-pit areas or dredged from the seabeds; however, several restrictions imposed on these practices during the past decades have limited the use of such operations. The main restriction is the scarcity of sand resources in many coastal regions; therefore sand needs to be transported from distant borrow sources, which leads to higher costs for the land reclamation projects. Since the 1980's, the dumping of the clay lumps extracted from the seabed has been regarded as a plausible method for the construction of the reclaimed fills. However, there are some features of lumpy reclaimed fills that restrict the use of these as built-up layers. Reclamation lumpy fills experience substantial compression purely due to the reduction of the *inter-lump* void space, quite apart from the consolidation of the clay lumps themselves, which would be regarded as unacceptable if the fill is directly used to support foundations. As a practical method to resolve this problem, the constructed fills are usually subjected to surcharge loads that accelerate the closure of the *inter-lump* voids. Based on several experimental studies and in situ investigations cited earlier in this chapter, the closure of *inter-lump* voids generally occurs under low stress levels, and after this stage, the reclaimed fills behave as a homogeneous layer. As a result, the rate of the consolidation process decreases with the closure of the *inter-lump* voids; therefore, a longer time period is required to reach a certain degree of consolidation settlement that is necessary for construction to commence.

This study presents a practical method in the construction of lumpy clay fills in which the void space between the lumps is filled with a granular material. The mechanical behavior of a coarse-grained soil makes the filler material appropriate for this purpose:

- Due to the cohesionless nature of the granular soil, when this material is placed or deposited on a constructed lumpy layer, it can fill the *inter-lump* voids that exist within the lumpy fills.
- The lumpy fill, the voids of which are filled with coarse-grained filler, will not show any excessive settlement due to the closure of *inter-lump* voids.
- The granular filler possesses a higher stiffness compared to excavated clay from offshore location, thereby enhancing the load-carrying capacity and minimizing the settlement of the composite layer.
- Due to the high hydraulic conductivity of the filler material, the rate of consolidation of the composite increases; this rate depends only on the size of the clay lumps rather than the thickness of the lumpy layer. In such a system the permeability of the filler soil plays a key role in the consolidation behavior of the composite fill.

The research reported in this thesis is a coordinated effort to examine the mechanical characteristics of the composite soil media constructed using clay lumps in conjunction with an interspersed granular fill. In particular, the constitutive models are developed for two fine-grained and coarse-grained materials through a series of triaxial and oedometer compression tests. The poroelasto-plastic model for the saturated clay and an elasto-plastic model for the granular material are incorporated in the highly documented and validated finite element code ABAQUS/Standard (2005) to predict the consolidation responses of composite specimens tested in a bench-scale oedometer compression apparatus. The influence of volume proportion and packing configuration of the clay lumps on the response of a large-scale composite fill of finite thickness subjected to self-weight, surcharge pressure, and loaded by a rigid footing was assessed.

CHAPTER 2

MECHANICAL BEHAVIOR OF THE RECONSTITUTED SILTY CLAY AND THE CONSTITUTIVE CHARACTERIZATIONS

2.1 Introduction

In this chapter, the mechanical behavior of a soft clay is analyzed using different experimental techniques. In the context of this study, the term soft clay specifies a saturated cohesive soil with a consistency close to that of its liquid limit and with little or no sensitivity. Such clays can occur either naturally or be reconstituted for laboratory studies; clays of this type are usually associated with soft unconsolidated sediments and dredged material recovered from marine environments. The testing of soft clays needs to address the problematic nature of its consistency, which limits the application of conventional sample retrieval and preparation procedures associated with laboratory testing. The experimental investigations conducted in this study include unconsolidated-undrained (UU) and consolidated-undrained (CU) triaxial tests, the fall cone tests and the conventional oedometer tests performed to examine the stiffness and strength properties of the material under different consistencies and stress states. Furthermore, the hydraulic conductivity, defined as the capacity of the soil to transmit water flow, was estimated from the rate of consolidation estimated in the one-dimensional oedometer test. The results of the experiments are used to develop a constitutive model for the reconstituted soil. This study develops a model that can adequately represent the stiffness characteristics and yielding behavior of the specimens as observed in the experimental investigations.

2.2 Experimental investigations

2.2.1 Material characteristics

The clay used in the experimental research was obtained from an excavation site located on Sherbrooke East Street, Montréal. The clay, which is typical of the weathered Champlain Sea clay located in this region, was recovered from a depth of approximately 4 m and the natural water content was at about its plastic limit of 15%. At this depth the clay has undergone extensive weathering and leaching of the salts originally associated with its deposition in a marine environment (Eden and Crawford, 1957; Crawford, 1968). The excavated clay was allowed to dry for a period of 3 months and the dried clay was finely ground using a soil grinder. A particle size analysis, including a sieve analysis and hydrometer analysis, conducted on the reconstituted clay showed that the fine-grained soil contained 40% clay fraction (<0.002 mm), 52% silt and 8% sand and could be classified as a silty clay soil of low plasticity (USDA, 1975; AASHTO, 1996; Day, 1999) (Figure 2.1). The silty clay occasionally contained gravel particles ranging from 2 mm to 5 mm, which were removed by sieving the ground soil. The specific gravity of the silty clay was estimated at $G_s=2.63$ and the Atterberg limits of the reconstituted clay,

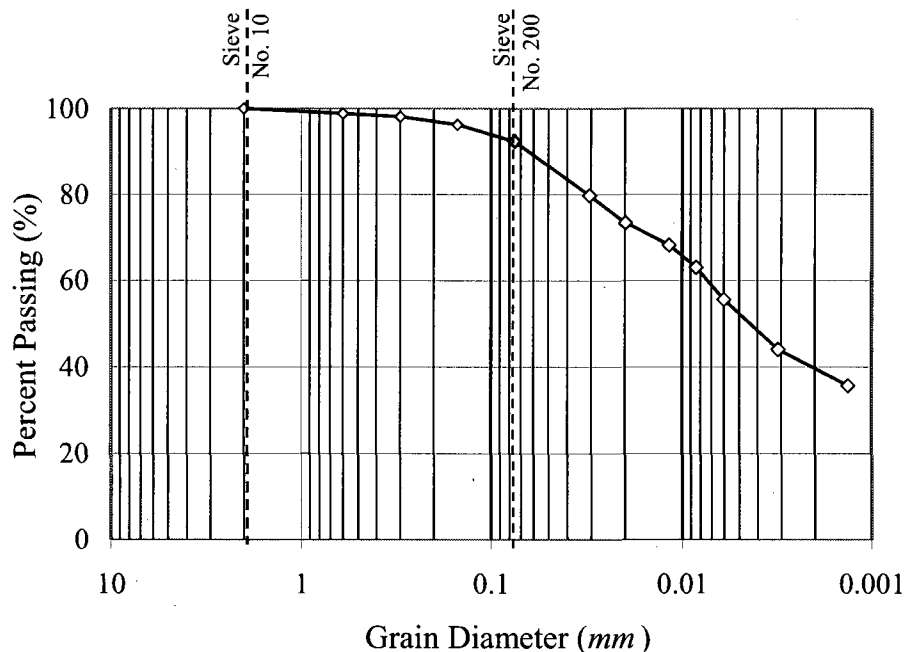


Figure 2.1 Grain size distribution chart for Montreal reconstituted silty clay

measured using the ASTM D4318 procedures, were as follows: liquid limit=25%, plastic limit=15%. The activity of the clay was also estimated at 0.25, corresponding to the group of inactive clays that include leached post-glacial or estuarine clay deposits (Skempton and Northey, 1952; Skempton, 1953).

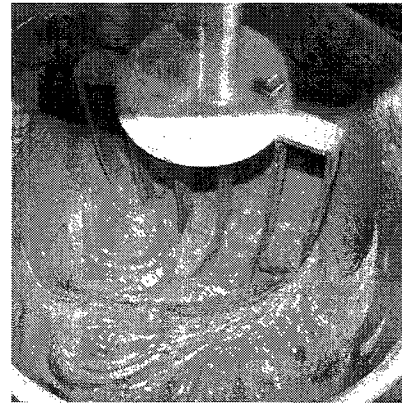
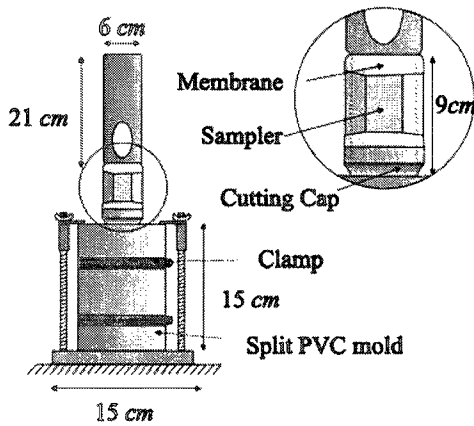
2.2.2 Measurement of the mechanical properties

When intact and relatively undisturbed samples can be retrieved and prepared, various tests can be performed to determine the constitutive properties of geomaterials. The consistency of the soft clay used in this investigation presents an added complication to the routine testing of the clay using conventional tests. At a moisture content close to the liquid limit, the reconstituted soft clay is unable to support its self weight and maintain a cylindrical shape. The approach adopted therefore was to prepare a sample for the different tests, including triaxial, cone penetration and oedometer tests, from a slurry prepared at a moisture content close to the liquid limit of the clay.

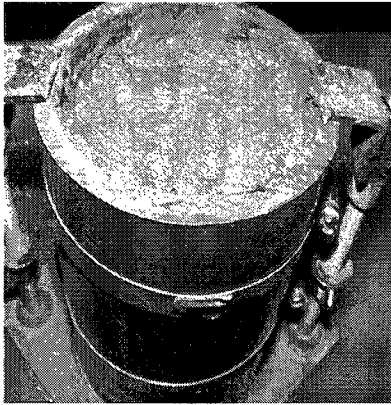
There are various methods for retrieving samples for use in laboratory experiments. The Sub-sampling is a preparation technique proposed by True (1971) involves inserting a small corer with the same dimension as the specimen into the large primary sampler. The sample is then extruded into the triaxial test membrane and mounted in the cell. This method is likely to introduce greater sampling disturbance to the specimen than those introduced during the initial sample recovery. In another sample preparation technique, reported by Sanchez et al. (1979) and Sanchez and Sagaseta (1981), the specimen was prepared from a slurry mixed at a water content approximately twice the liquid limit of the clay. The slurry was allowed to consolidate in a split mold oedometer (diameter 38.1 mm and height 165.1 mm) under an axial stress of 24.5 kPa. Upon consolidation the split mold was removed and the sample was cut to a height of 76.2 mm and used for UU testing. In a more elaborate sample preparation procedure presented by Baldi et al. (1988), the sample was extruded vertically into a trimming ring with the excess material trimmed ahead of the ring; here, the clay sample directly entered the membrane which was stretched in the mold connected to the trimming ring; similar sample preparation

techniques were described by Hanzawa et al. (1980) and Berre (1985). Goldscheider and Scherzinger (1991) conducted one-dimensional consolidation tests and undrained triaxial compression tests to determine the mechanical properties of lacustrine soft clay from the city of Constance, Germany. In their studies, samples of 109 mm diameter were obtained from boreholes using thin, smooth-walled steel tubes inserted into a sampler with a slender cutting ring. They then used the technique suggested by Berre (1985) to prepare the sample for triaxial testing. Another laboratory method for sample preparation was presented by Katagiri and Imai (1994) in which the soil slurry with a high water content (100% to 2000%) was poured into an acrylic pipe with an internal diameter of 75 mm and length 100 mm. After the sedimentation process, a preconsolidation pressure of 49 kPa was applied to the sample for 48 hours using a piston inserted inside the preconsolidation pipe. Triaxial specimens with dimensions of 5 cm both in diameter and height, were then trimmed from the preconsolidated sample. Another sample preparation technique involved continuously extruding of soil from a tube, trimming and feeding the soil into the split-tube containing a stretched membrane. Sheahan and DeGroot (1997) used this technique to design a trimming device for triaxial specimens. Later work by Yin (2002) presented a technique where a thin-walled PVC tube with an internal diameter of 50 mm was pushed into a reconsolidated soft Hong Kong marine deposit to obtain specimens for triaxial testing.

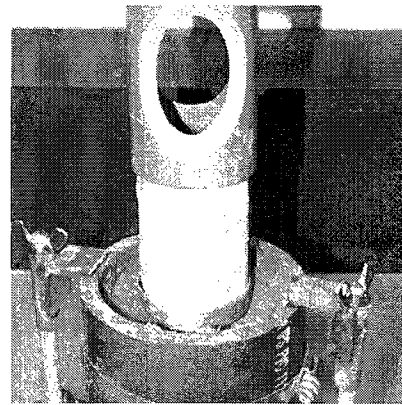
An assessment of the advantages and disadvantages of the various sampling methods described in the literature led to the development of the sample preparation and sample recovery procedure that was used in the current experimental research (Figure 2.2). The ground dry clay was mixed with distilled water using a paddle-rotary mixer to achieve a moisture content close to its liquid limit of 25% (Figure 2.2b). During mixing, water was gradually added to the clay paste and the consistency of the paste was estimated using the Casagrande liquid limit apparatus. Using samples taken from different batches, it was observed that the water content of the paste varied between 23% and 25%. The clay paste was then kept in sealed containers for 3 weeks to allow for attainment of moisture equilibrium.



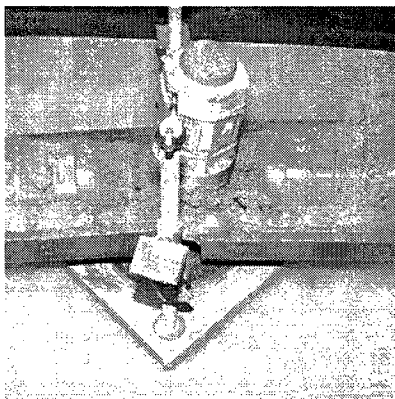
(b)



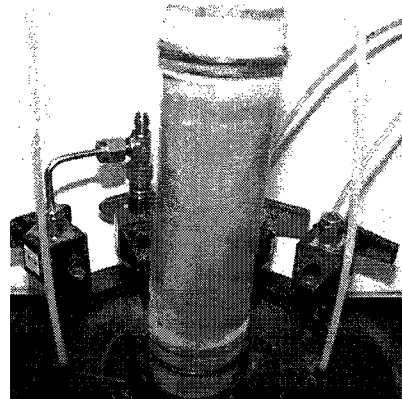
(c)



(d)



(e)



(f)

Figure 2.2 Preparation of triaxial specimen from soft clay (a) Sample preparation technique, (b) Paddle-rotary mixer, (c) Compacting clay in split mold, (d) Retrieving the clay sample, (e) Sample extraction, (f) Mounting the specimen on the triaxial base

To prepare a triaxial specimen, the clay paste was first compacted in 3 layers inside a PVC split mold using a 625 g plunger (20 impacts per layer) to minimize trapped air inside the clay sample (Figure 2.2c). The split mold, with internal diameter of 9 cm and 15.5 mm height, was held together by two steel ring clamps and placed on the base of a Proctor mold. A membrane was then stretched over the split sampler with an internal diameter of 35.5 mm and the cutting edge was attached to one end. Another PVC tube was employed to gradually push the sampler into the compacted clay and the entry of the clay to the sampler was observed through openings of the PVC tube (Figure 2.2d). When the clay soil completely filled the sampler, the clamps were removed and the PVC mold was opened to retrieve the sampler (Figure 2.2e). After trimming the ends of the sample, the sampler containing the specimen was mounted on the base of the sample assembly of the triaxial apparatus and the membrane was attached to the caps by four O-rings at both the top and the bottom. The same method was employed to prepare specimens for oedometer and fall cone tests; the consolidation ring and the base container of the fall cone test were pushed into the clay material compacted inside the PVC split mold. The retrieved materials were then trimmed to prepare the specimens that would be used in the experimental research.

2.3 Experimental results

2.3.1 Undrained shear strength of the reconstituted silty clay

In geotechnical practice, for stability analysis of fine-grained soils, it is necessary to determine the undrained shear strength of the soil. Many methods for the determination of undrained shear strength, both in the field and the laboratory, have been proposed in the literature; this parameter can be measured by means of in situ tests, such as the vane test (Law, 1979; Eden and Law, 1980; Kietkajornkul and Vasinvarthana, 1989; Khan and Garga, 1991; Chung et al., 2007) and SPT test (Yilmaz and Erzin, 2004; Sivrikaya and Togrol, 2006) screw plate tests (Selvadurai and Nicholas, 1979; Selvadurai et al., 1980) or in the laboratory by conducting UU triaxial tests (Matsuo and Shogaki, 1988; Long and Menkiti, 2007) and fall cone tests (Houlsby, 1982; Zreik et al., 1995; Kumar and

Wood, 1999) on undisturbed or remolded specimens. In this study, UU triaxial tests were first performed to evaluate the undrained shear strength of the reconstituted silty clay. The accuracy of the strength estimates was then verified using the results of the laboratory fall cone test.

Results of unconsolidated undrained triaxial tests

The UU triaxial tests were conducted at different confining pressures on four samples of the clay that were compacted and extracted using the procedures described previously. Prior to application of the deviator stresses, the specimens were subjected to a back pressure of 300 *kPa*, which was maintained for 4 hours to ensure complete saturation of the sample. The degree of saturation was established indirectly through measurement of the pore water pressures and by calculating the value of Skempton's *B* parameter; results indicated that the clay samples were in an almost saturated condition (Table 2.1).

The stress-strain curves shown in Figure 2.3 illustrate consistently repeatable results. The higher peak value deviator stress in the first test is most likely due to the lower water content (24.2%) of the specimen; this observation indicates the importance of the degree of saturation on the undrained strength of a soft clay soil. A further observation is that the stress-strain response shows little or no softening behavior, which is indicative of the mechanical behavior of a normally consolidated remolded clay.

Table 2.1 Triaxial unconsolidated undrained test specifications

Test no.	Water Content (%)	Diameter (cm)	Height (cm)	Back Pressure (kPa)	Effective Confining Pressure (kPa)	Estimation of <i>B</i> value		
						Confining Pressure Increase (kPa)	Pore Pressure Increase (kPa)	<i>B</i> Value
1	24.2	3.50	6.9	300	50	70	69.3	0.99
2	25.4	3.55	6.9	300	100	70	69.7	0.99
3	25.8	3.55	6.9	300	100	70	69.1	0.99
4	25.6	3.40	6.9	300	150	70	69.5	0.99

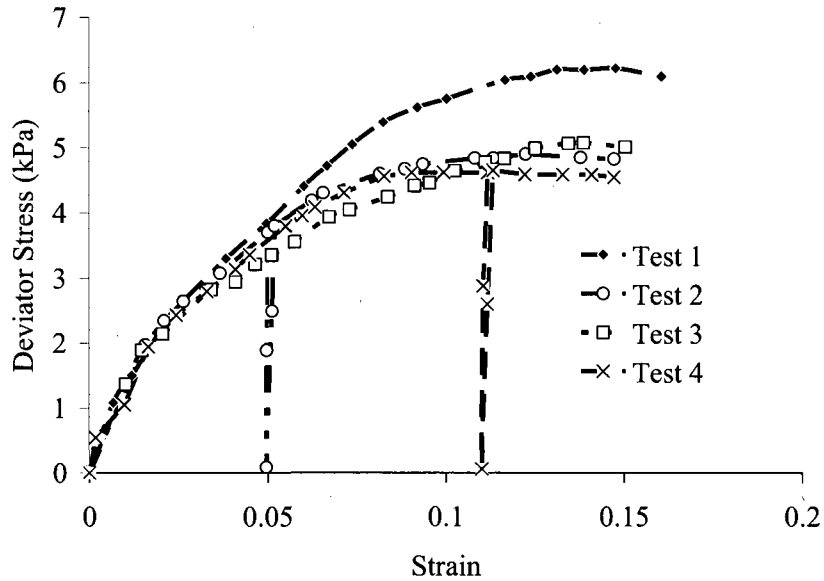


Figure 2.3 Stress-strain curves from UU triaxial tests (with membrane correction)

Membrane correction- When performing triaxial tests on soils that are constituted at or above the liquid limit of the soil, the measured strength can be influenced by the membrane that is used to retain the soil and for transmitting the cell pressures to the soil sample. The importance of the membrane stiffness on the estimation of the strength and deformability characteristics of soft soils was first recognized by Henkel and Gilbert (1952). In their study, these authors assumed that the rubber membrane and the test specimen will deform as a unit with a restraining shell action around the sample. They also suggested a procedure that would take into account the influence of buckling of the rubber membrane during sample compression. In a related study, Kuerbis and Yoginder (1990) developed a procedure that accounts for membrane effects by considering changes in the membrane thickness during straining. A correction factor that can be applied to the deviator stress to account for membrane stiffness effects is given in ASTM D4767-88 as:

$$\Delta(\sigma_1 - \sigma_3) = \frac{4E_m t_m \varepsilon_1}{D_c} \quad (2.1)$$

where $\Delta(\sigma_1 - \sigma_3)$ is the reduction that should be applied to the measured deviator stress $(\sigma_1 - \sigma_3)$; E_m is Young's modulus of the membrane material; t_m is the wall thickness of the membrane; D_c is the diameter of the soil sample after consolidation and ε_1 is the axial strain.

Results of Fall Cone Tests

Low shear strengths encountered in soft clays make the constitutive characterizations of these materials sensitive to the test methodology. The preparation of samples from soft clay for triaxial testing is prone to sample disturbance, both during extraction of the sample and its assembly for triaxial testing. In addition, the constraining action of the membrane and the frictional/adhesion effects between the membrane and the soft clay sample can influence the results derived from the triaxial tests. For this reason, it is necessary to independently verify the accuracy of the strength estimates derived from the triaxial tests. In a laboratory context, the estimation of strength can be approached either by using a laboratory vane test or a laboratory fall cone test. In this research program, a fall cone test was used to validate the results for the strength properties determined from the UU triaxial tests conducted on the soft clay (British Standards Institution-1377, 1990; CAN/BNQ-2501-092, 1986). The test performed in this study involves the release of a cone with an apex angle of 30° through the activation of an electrical switch for a specified time period ($5 \pm 0.5 \text{ sec}$). The penetration of the cone during this procedure is accurately measured and correlated with the undrained shear strength of the material at various moisture contents. Fall cone tests were first used by Hansbo (1957) for the measurement of the undrained shear strength c_u of saturated clays. The relationship proposed for estimating the undrained shear strength is as follows:

$$c_u = \frac{k_\alpha Q}{h^2} \quad (2.2)$$

where Q is the weight of the cone; k_α is a cone factor for a cone of angle α and h is the cone penetration. Various expressions have been proposed for the parameter k_α ; Hansbo (1957) suggested a cone factor of 0.82 for a cone with an apex angle of 30° . Karlsson (1961) proposed cone factor values between 0.70 and 0.86, and revised the estimates to a specific value $k_{30} \approx 0.80$ (Karlsson, 1977). Research conducted by Wood (1985) proposed a range of values for a 30° cone, with an average value of 0.85. In the current research study, the value of k_{30} was obtained using results from Brown and

Huxley (1996); this value was estimated at approximately 0.33 at a moisture content close to the plastic limit and 0.76 for moisture content close to the liquid limit.

The results of fall cone tests (Figure 2.4) were used to validate the undrained shear strength obtained from UU triaxial tests. Using Hansbo's equation, the undrained shear strength of the clay was estimated to be 2.63 *kPa* for a moisture content near 26%. The results indicate a good agreement with the shear strength obtained from UU triaxial experiment. The results of the fall cone test can also be used to estimate the liquid limit of the soft clay. The British Standards Institution guide BSI (1990) defines the liquid limit as the moisture content at which the cone with an apex angle of 30° and mass of 80 g penetrates into the soil for 20 mm in (5+0.5) seconds. In the tests conducted for the current research, the liquid limit is estimated at 29% whereas the conventional Casagrande tests gave a value of approximately 25%. The difference in the estimates can be attributed to the different modes of testing and to the empiricism associated with the tests. The results obtained by Belviso et al. (1985), Sampson and Netterberg (1985) and Wasti (1987) from studies conducted using the British fall cone device and a Casagrande device with a hard base indicated that the fall cone testing procedure leads to a liquid limit that is 4.2% to 4.9% higher than that obtained from the Casagrande device.

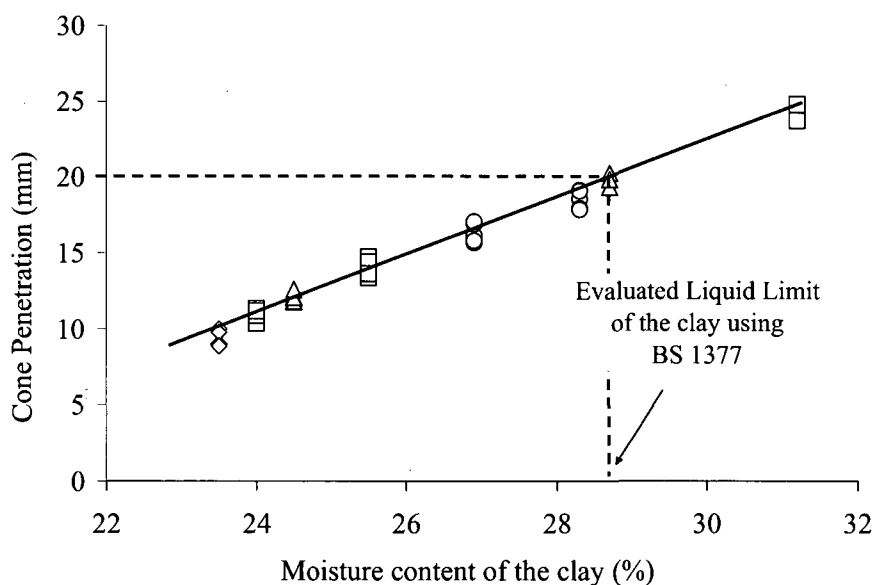


Figure 2.4 Results of the fall cone tests on the remolded Montreal clay

2.3.2 Shear strength of the consolidated reconstituted silty clay

The consolidated drained tests are usually restricted to granular soils with high hydraulic conductivity. For a true drained test, the pore water pressures should be maintained either at zero value or without any increase during the application of deviator stress. In order to satisfy this requirement in fine-grained soils the rate of application of the strains should be carefully controlled (Bishop and Henkel, 1962; Newson et al., 1997). Therefore, consolidated undrained (CU) tests *with pore pressure measurement* are the preferred alternative for determining of the strength characteristics of fine-grained soils with low hydraulic conductivity (Yamaguchi et al., 1985; Aoki et al., 1996). This procedure was adopted in the triaxial testing of the reconstituted silty clay.

After mounting the prepared triaxial samples in the triaxial apparatus, the specimens were brought to a fully saturated condition; this was accomplished by applying a back pressure of 300 *kPa* to the samples for a duration of 8 *hours*. Other conditions associated with each test are presented in Table 2.2. After saturation, the specimens were isotropically consolidated in the triaxial chamber. In each test, the confining pressure was increased in two equal increments and the volume change was determined by measuring the volume of water leaving the sample. In the second stage, the confining pressure was applied after the termination of the primary consolidation process in the first load step. The time for completion of the primary consolidation process was estimated to be between 6 and 8 *hours* (Figure 2.5). During the consolidation phase, the strength of the saturated samples increased due to the reduction of the void ratio. The initial moisture content of the specimens was approximately at the liquid limit ($\approx 25\%$) and it reduced to approximately 19% under the application of 50 *kPa* of confining pressure (Table 2.2); however, by further increasing the confining pressure, the moisture content of the specimens was approaching its plastic limit due to the consolidation process. Furthermore, the value of the pore pressure parameter, the *B* value, was determined prior to the application of the deviator stresses. The parameter was determined by subjecting the sample to a confining pressure increment of 70 *kPa* while the drainage valves were kept closed. The experimentally determined value of Skempton's *B* parameter indicates the near-full saturation of the triaxial specimens.

Table 2.2 Consolidated undrained triaxial test specifications

Test no.	Effective Confining Pressure (kPa)	Back Pressure (kPa)	Isotropic Consolidation Pressures (kPa)	Initial water content %	Initial wet unit weight (kN/m^3)	Water content after consolidation %	B value
1	50	300	25-50	23.2	19.8	19.3	0.98
2	100	305	50-100	24.9	19.9	18.9	0.99
3	100	305	50-100	25.0	19.8	18.6	0.99
4	150	305	75-150	25.3	19.8	18.0	0.99
5	200	305	100-200	25.0	20.1	17.2	0.98
6	200	305	100-200	25.0	19.8	17.1	0.99

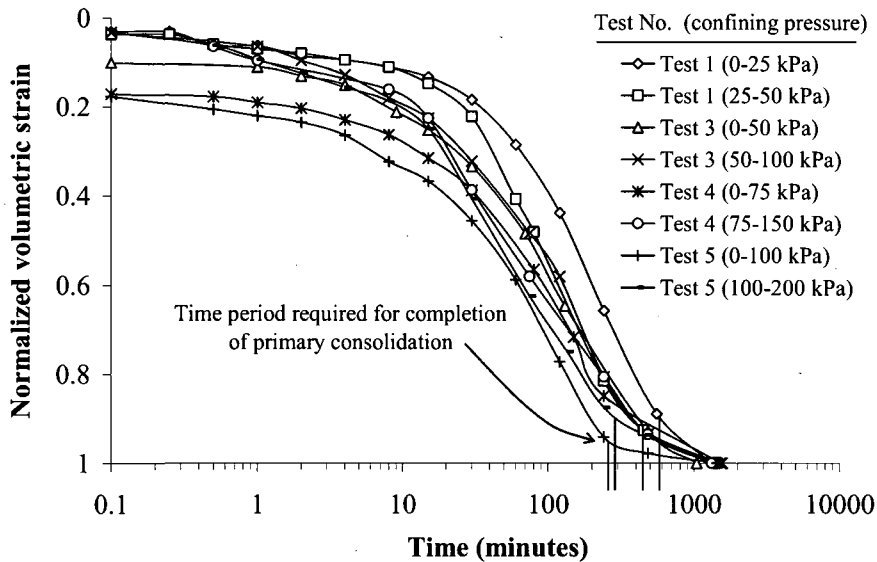


Figure 2.5 Consolidation curves obtained from isotropic compression of the triaxial specimens

The results of the CU test with pore pressure measurement were used to determine the effective shear strength parameters c' and ϕ' (Figure 2.6). Holtz and Kovacs (1981) presented typical values of effective shear strength for cohesive soils and indicated that for natural clays, the value of ϕ' reduces as the plasticity index increases. They presented an empirical correlation between effective friction angle and the plasticity index for normally consolidated undisturbed clays (Figure 2.7). For the Montréal silty clay, which

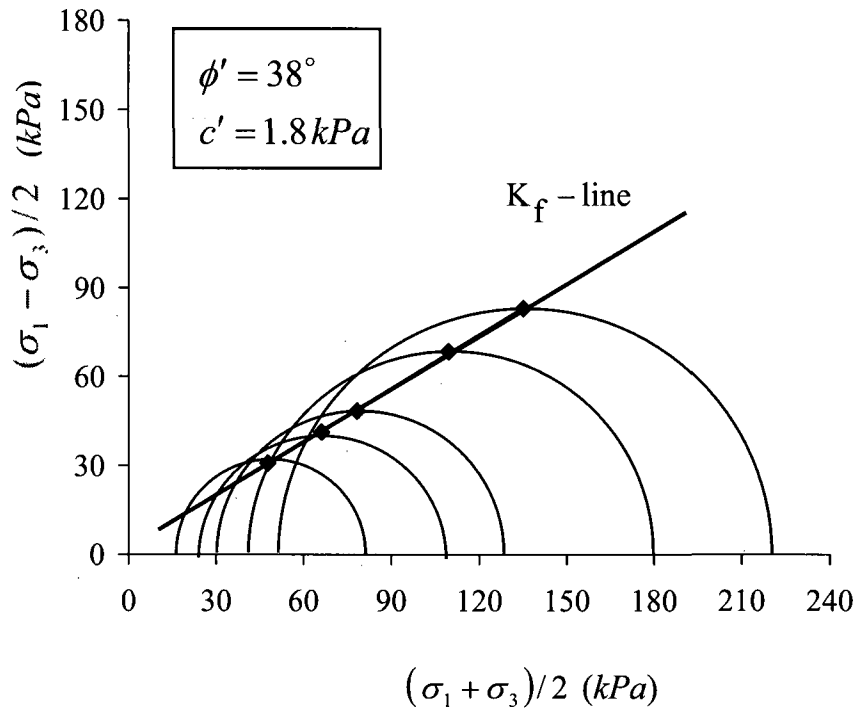


Figure 2.6 K_f -line and Mohr-Coulomb effective stress circles from CU triaxial tests

has a plasticity index of 10%, the value of ϕ' could be in the range of 30° to 38° . This value seems to agree with other results obtained from experimental studies on low plasticity soils with a high portion of fine particles in the range of silt (Borgesson, 1981; Brandon et al., 2006). Figure 2.8 shows that in CU triaxial tests all the effective stress paths deviate to the left, indicating behavior that is consistent with normally consolidated behavior of clay. The deviation of the effective stress paths results from the generation of positive pore pressure during the shearing process.

Following the method indicated in section 2.3.1, the membrane correction was also applied in the procedure used to determine the strength parameters based on effective stresses. Calculations showed that in the CU test series, 4% to 10% of the deviator stress at failure was carried by the membrane, whereas in the UU tests this increased to approximately 50% of the total deviator stress. This observation clearly indicates the importance of the *membrane stiffness* in influencing the stress-strain behavior obtained from undrained tests on a soft clay at or near the liquid limit.

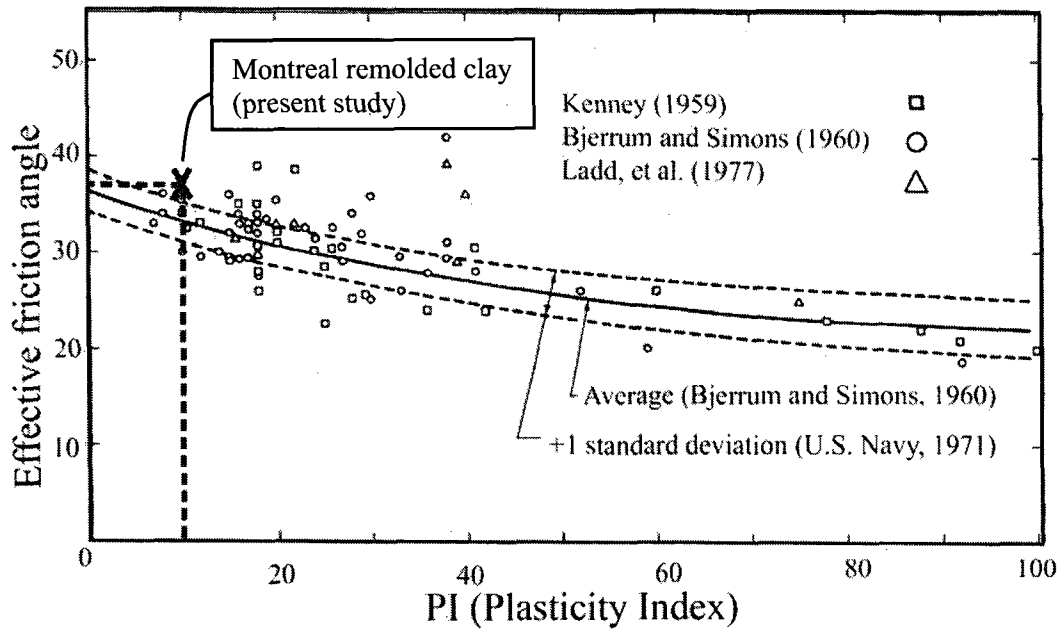


Figure 2.7 Empirical correlation between ϕ' and PI from triaxial compression tests (after Holtz and Kovacs, 1981)

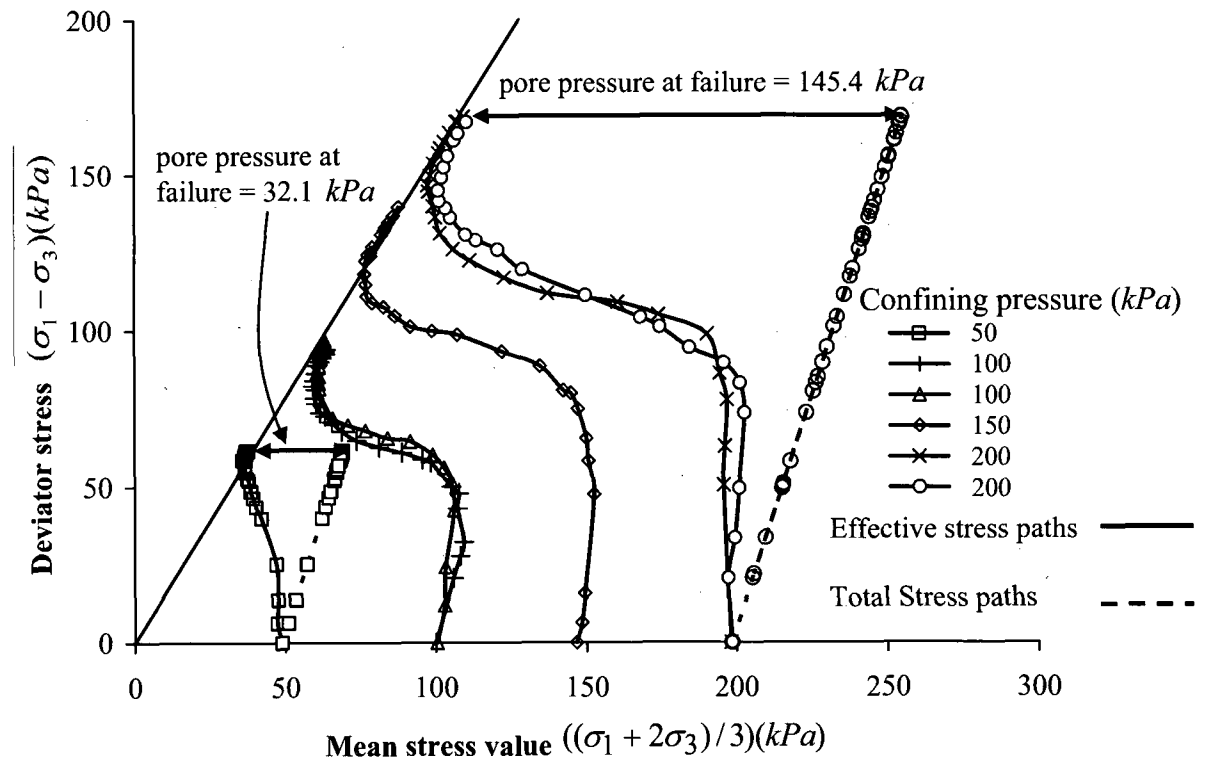


Figure 2.8 Stress paths obtained from CU triaxial tests

2.3.3 Consolidation properties of the reconstituted silty clay

The assessment of the consolidation settlement of soft clays is important for geotechnical engineering activities involving such soil deposits, whether they occur naturally or are created by dredge and fill operations. In this research program, one-dimensional consolidation tests were performed to determine the consolidation characteristics of the reconstituted Montréal silty clay. The specimens were prepared using a method identical to that used in the preparation of the specimens for triaxial testing. The soil, with a moisture content near its liquid limit, was compacted in a split proctor mold in three layers using a plunger. A stack of three rings was then inserted into the compacted clay and the material contained in the central ring was trimmed to form the sample for the oedometer consolidation test. The samples had an internal diameter of 6.6 cm and a height of 1.9 cm. The axial stress on the samples was increased from 12 kPa to approximately 508 kPa during the loading process. The evaluation of the physical properties of the material indicated that the samples were in a saturated state. Other information relevant to the test is presented in Table 2.3.

Figure 2.9 illustrates a close agreement between the consolidation curves obtained from the two tests. The value of the virgin compression index C_c and the recompression index C_r can be obtained from the experimental consolidation curves that show good repeatability. Furthermore, the swelling index C_s can be calculated from the experimental data obtained from the unloading cycle performed in both tests (Table 2.3).

Table 2.3 Physical and mechanical properties of the Montréal silty clay evaluated from consolidation tests

Test no.	1	2
Initial wet density (gr/cm^3)	2.05	2.04
Initial moisture content (%)	24.0	24.1
Initial degree of saturation (%)	100	100
Initial Void ratio	0.63	0.63
Compression Index C_c	0.14	0.13
Recompression Index C_r	-	0.0296
Swelling Index C_s	0.025	0.024

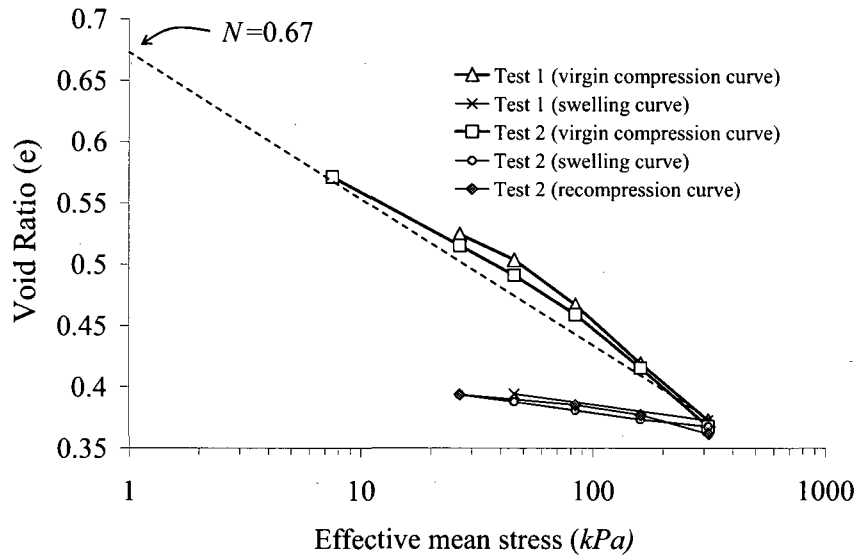


Figure 2.9 Results of the oedometer consolidation tests

There are several empirical relations proposed in the literature for the estimation of compression and swelling indices. Terzaghi and Peck (1948) modified the relationship between C_c and the liquid limit LL proposed by Skempton (1944) for normally consolidated remolded clay. The modified equation is of the form

$$C_c = 0.009(LL - 10) \quad (2.3)$$

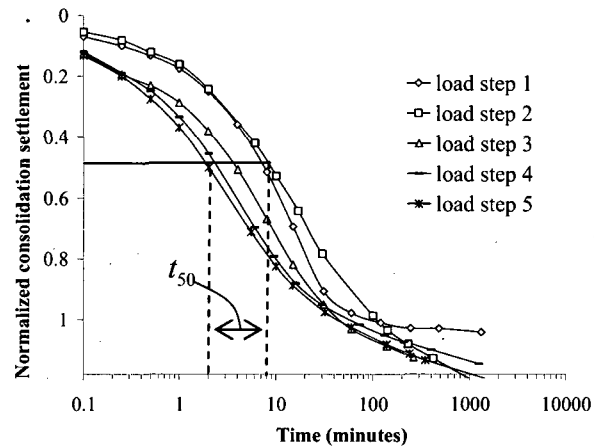
Considering a liquid limit of 25% for the reconstituted Montréal clay, the compression index C_c is estimated at 0.135. Nagaraj and Murthy (1985) also suggested another form of relationship obtained from consolidation curves of several normally consolidated fine-grained soil samples with different liquid limit values. The equations of the best-fit lines of all points in the working stress range give the following relationships for estimating compression and swelling indices from the liquid limit and the specific gravity G_s of the clay:

$$C_c = 0.2343 \left(\frac{LL}{100} \right) G_s \quad (2.4)$$

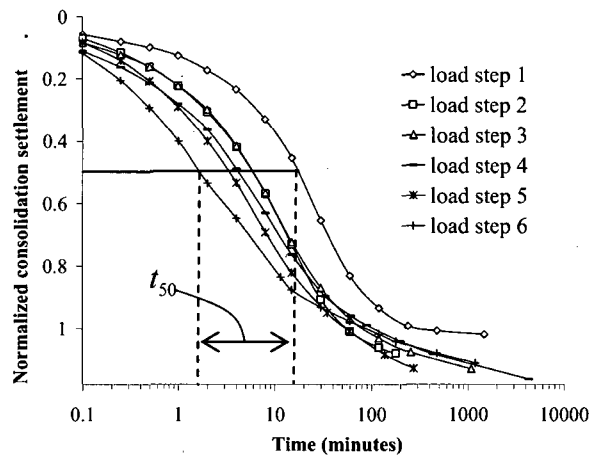
$$C_s = 0.0463 \left(\frac{LL}{100} \right) G_s \quad (2.5)$$

Using the measured specific gravity of silty clay $G_s = 2.63$, the compression and swelling indices are estimated from these empirical relationships at approximately 0.15 and 0.03, respectively. This comparison indicates a reasonable agreement between the experimental results and empirical estimates.

There are two common methods that have been developed to illustrate the time-dependent consolidation settlement of the clay specimens; the first method is based on the “log of time” plot (Casagrande and Fadum, 1940) whereas the second one is constructed based on the “square root of time” plot (Taylor, 1942, 1948). For the two consolidation tests conducted in this study, the consolidation settlement in each load step is plotted against logarithm of time to construct the consolidation curves (Figure 2.10). These



(a)



(b)

Figure 2.10 Consolidation curves obtained from conventional oedometer tests (a) Test 1, (b) Test 2

curves can be used to estimate different properties of the tested soil, including the coefficient of consolidation c_v and the hydraulic conductivity k . The coefficient of consolidation of the clay was determined using Terzaghi's construction (Day, 2001). In this method, the coefficient of consolidation was calculated from the estimated time required for 50% of the consolidation settlement to occur in each load step. The estimated value of c_v shown in Figure 2.11 indicates the dependency of this value on the vertical effective stress σ'_v applied in each load step. Some degree of variation of c_v with σ'_v can be observed in the tests; however, the trends in the experimental data are similar and value of c_v is within the range $0.01 \text{ cm}^2/\text{min}$ to $0.08 \text{ cm}^2/\text{min}$ for vertical stress ranging from 12 kPa to 508 kPa .

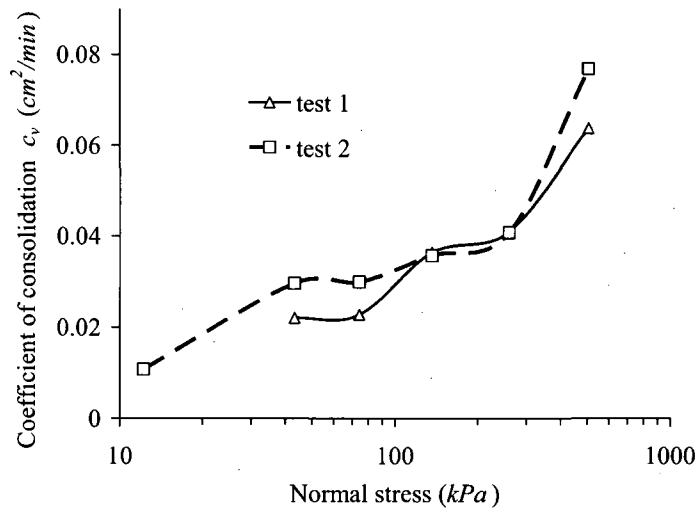


Figure 2.11 Variation of the coefficient of consolidation with normal stress

2.3.4 The hydraulic conductivity of the silty clay

The one-dimensional theory of consolidation of fine-grained soil subjected to uniform loading, based on the assumptions made by Terzaghi (1943), leads to a partial differential equation governing the time- and space-dependent variation in the pore water pressure $u(z, t)$ of the form (see Selvadurai, 2000)

$$\frac{\partial u}{\partial t} = c_v \frac{\partial^2 u}{\partial z^2} \quad (2.6)$$

where c_v is the coefficient of consolidation defined as $c_v = k / \gamma_w m_v$ in which k is the hydraulic conductivity, m_v is the coefficient of volume compressibility, γ_w is the unit weight of water. Solving this partial differential equation for the one-dimensional consolidation for a finite region, we can define a “Degree of Consolidation” U as follows:

$$U(t) = \frac{\delta(t)}{\delta(\infty)} = f\left(\frac{c_v t}{h^2}\right) \quad (2.7)$$

where $\delta(t)$ is the one-dimensional compression at any time t , $\delta(\infty)$ is the ultimate compression as $t \rightarrow \infty$ and h is the length of the longest drainage path of the region. The expression $c_v t / h^2$ is a dimensionless value which can be replaced by a time factor T_v . The solution of the one dimensional consolidation expression gives rise to a relationship between U and T_v which was derived by Terzaghi (1923, 1943). Since pore water pressure follows the diffusion equation, the mathematical analyses indicate that the degree of consolidation U will approach 100% only as time tends to infinity. An empirical method proposed by Casagrande (Head, 1994) is commonly used to find the hydraulic conductivity of the tested soil from the results of the oedometer test. In this approach the magnitude of settlement is plotted against the log of time in each load step. The coefficient of volume compressibility m_v can be also estimated from the variation of the void ratio using the following equation:

$$m_v = \frac{a_v}{1 + e_1} \quad (2.8)$$

in which e_1 is the void ratio at the start of each increment and a_v is the coefficient of compressibility estimated using the following equation

$$a_v = -\frac{e_2 - e_1}{dp^*} \quad (2.9)$$

where p^* is the external axial stress applied to the sample and e_2 is the void ratio at the termination of each load step. When the coefficient of consolidation c_v and the

coefficient of volume compressibility m_v , have been determined, the hydraulic conductivity k can be calculated. The magnitude of the hydraulic conductivity derived from the results of two oedometer consolidation tests is shown in Table 2.4. Considering the presented method for calculating the hydraulic conductivity, the value is estimated to be between $1.3 \times 10^{-8} \text{ cm/sec}$ and $7.2 \times 10^{-8} \text{ cm/sec}$. This is a reasonable range for the hydraulic conductivity of a fine-grained soil that contains a significant volume portion of silt and clay (Head, 1994; Day, 2001).

Table 2.4 Properties of Montreal silty clay derived from oedometer consolidation tests

Test no.	Load step	Normal Pressure (kPa)	Coefficient of volume compressibility, m_v $\left(\frac{m^2}{MN}\right)$	Coefficient of consolidation, c_v $\times 10^{-2} \left(\frac{cm^2}{min}\right)$	Hydraulic conductivity, k $\times 10^{-8} \left(\frac{cm}{sec}\right)$
Test 1	1	43	1.57	2.2	5.7
	2	74	0.43	2.3	1.6
	3	136	0.38	3.6	2.3
	4	260	0.25	4.1	1.7
	5	508	0.12	6.4	1.3
Test 2	1	12	4.09	1.1	7.2
	2	43	1.14	3.0	5.5
	3	74	0.55	3.0	2.7
	4	136	0.34	3.6	2.0
	5	260	0.20	4.1	1.4
	6	508	0.12	7.7	1.5

2.4 A constitutive model for silty clay

The mechanical behavior of fine-grained soil can be characterized using different constitutive models presented in the literature (Lee et al. 2001; Chan and Law, 2006). The incremental elasto-plastic model is a class of constitutive models formulated based on essential constitutive components. These include (i) a limiting surface, or a yield surface, discriminating between admissible and inadmissible states of stress, (ii) a plastic

potential which will provide the orientation of the increment of the plastic deformation vector in the stress space, and (iii) a hardening rule specifying the continuous yielding of the material. During the deformation process, the yield surface can move in the stress state as well as change its shape (Kutter and Sathialingam, 1992; Fodil et al., 1997; Wedage et al., 1998). A group of conventional plasticity models used in soil engineering has been developed based on the critical state concept (Schofield and Wroth, 1968; Desai and Siriwardane, 1984; Davis and Selvadurai, 2002). This theory implies that when a soil sample is sheared, it passes through progressive states of yielding before reaching a state of collapse. Therefore, this continuous yielding occurs until the material reaches a critical void ratio, after which the void ratio remains constant. In other words, in the critical state, the arrangement of the particles is such that no volume change takes place during shearing.

The first critical state models for describing the behavior of soft soils such as clay were formulated by researchers at Cambridge University (Schofield and Wroth, 1968; Roscoe and Burland, 1968). Both *Cam clay* and *Modified Cam clay* models use a minimum number of parameters, that can be obtained from standard laboratory tests, to describe important aspects of soil behavior including strength, compression and dilatancy and the critical states. Several studies indicated that these models can be implemented successfully in predicting the mechanical response of normally consolidated cohesive soils subjected to static loading (Britto and Gunn, 1987; Muir Wood, 1990; Potts and Zdravkovic, 1999). Therefore, the *Modified Cam clay* constitutive model was utilized to characterize the mechanical responses of the Montreal reconstituted silty clay.

2.4.1 Generalized stress-strain relations

In an attempt to study the behavior of normally consolidated clays, Roscoe and coworkers (Roscoe et al., 1958, 1963; Schofield and Wroth, 1968) analyzed several tests conducted on samples of saturated clay. They showed that, in the ultimate states, the stress paths reached a straight line on the *deviator stress-mean normal stress* plot. The

deviator stress q and mean normal stress p formulated for the axisymmetric triaxial conditions, $\sigma_2 = \sigma_3$ and $\varepsilon_2 = \varepsilon_3$, are defined as

$$p = \frac{\sigma_1 + 2\sigma_3}{3} \quad (2.10)$$

$$q = \sigma_1 - \sigma_3 \quad (2.11)$$

The results of the drained triaxial tests conducted on the same soil have also shown that the ultimate states lie on the same line observed in the undrained behavior. The slope of the critical state line on the $q-p$ plot is denoted by M , which is a constitutive parameter (Figure 2.12). The consideration of the critical state line is similar to the concept of fixed failure envelopes in conventional models such as the von Mises and Mohr-Coulomb. In contrast to the conventional plasticity models, additional yield surfaces are introduced to account for continued yielding of soils. Thus additional closed yield surfaces that expand during the deformation can be employed to complete the failure envelope. In the Cam clay model, the slope of the critical state line can be obtained from conventional triaxial tests, while deformation behavior of the material is characterized using the results of consolidation tests. The projection of the isotropic compression line (ICL) on the $e - \ln p$ plane is shown in Figure 2.13, which is a straight line. Furthermore, the unloading path will not follow the loading path due to the

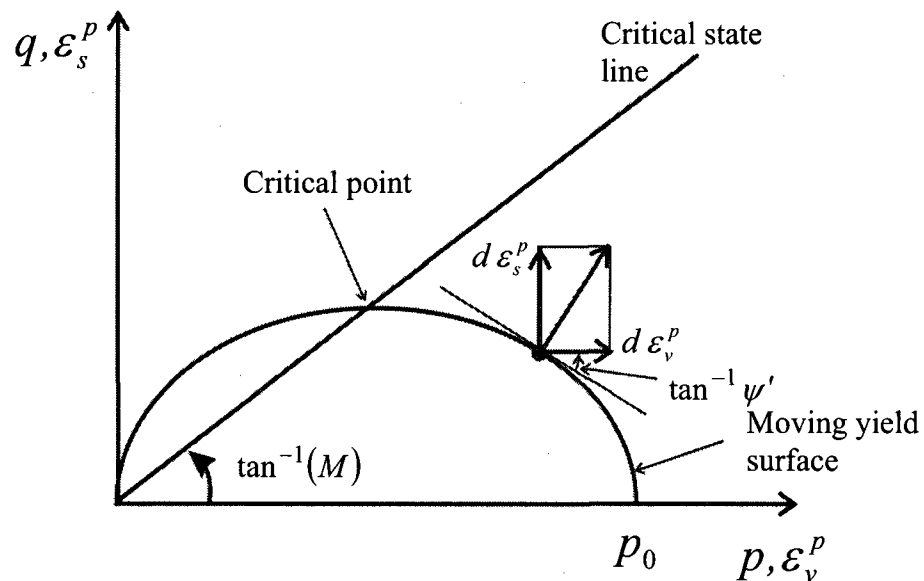


Figure 2.12 Yield surface in Modified Cam clay model

irreversible elasto-plastic behavior of the soil. As shown in Figure 2.13, the slope of the loading path is denoted by λ , and the slope of unloading path (which is assumed to coincide with the reloading path) is denoted by κ . Considering points A and B located on the isotropic consolidation line and point C that lies on the unloading-reloading path, the change of the void ratio e is expressed by

$$e = e_A - e_B = \lambda(\ln p_B - \ln p_A) \quad (2.12)$$

$$e = e_C - e_B = \kappa(\ln p_C - \ln p_B) \quad (2.13)$$

Thus the incremental void ratio de and the elastic component of the incremental void ratio de^e can be written as

$$de = -\lambda \frac{dp}{p} \quad (2.14)$$

$$de^e = -\kappa \frac{dp}{p} \quad (2.15)$$

Hence

$$de^p = de - de^e = -(\lambda - \kappa) \frac{dp}{p} \quad (2.16)$$

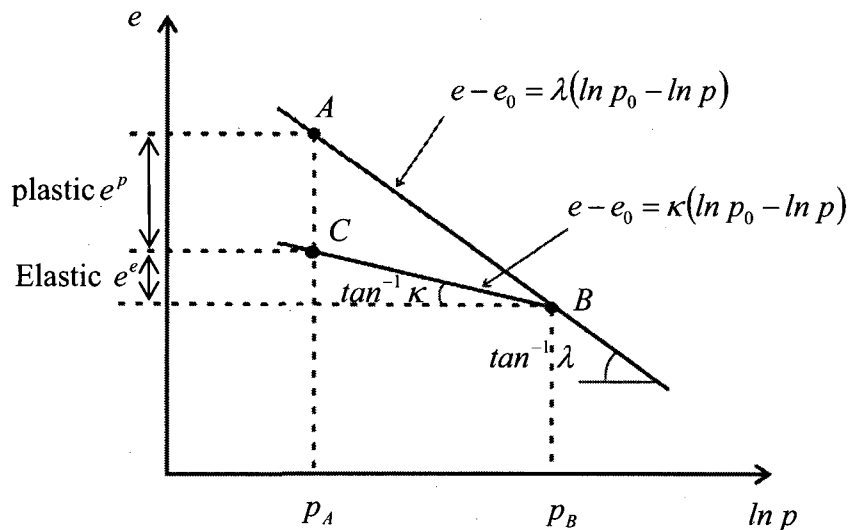


Figure 2.13 Virgin compression line and elastic unloading-reloading line

where de^p is the plastic component of the incremental void ratio. To define the expressions of the Cam clay model, the stress ratio is defined as

$$\eta = \frac{q}{p} \quad (2.17)$$

Therefore,

$$dq = pd\eta + \eta dp \quad (2.18)$$

Assuming that the slope of the yield surface projected on $p-q$ plane be ψ' (Figure 2.12)

$$\frac{dq}{dp} = -\psi' \quad (2.19)$$

Substitution of Eq. (2.19) in to Eq. (2.18) yields

$$\frac{dp}{p} + \frac{d\eta}{\eta + \psi'} = 0 \quad (2.20)$$

Therefore any yield locus passing through a known point can be obtained by integrating Eq. (2.20); that is

$$\ln p - \ln p_0 + \int_0^\eta \frac{d\eta}{\eta + \psi'} = 0 \quad (2.21)$$

Eq. (2.21) represents a yield curve passing through $(p_0, 0)$; here p_0 is the value of p when $\eta = 0$. Eq. (2.21) is the general equation of all yield loci corresponding to all elastic limit curves on the state boundary surface while the variable p_0 has a constant value for any individual yield locus. Expressed in differential form all yield loci are therefore represented by

$$\frac{dp_0}{p_0} - \frac{dp}{p} - \frac{d\eta}{\psi' + \eta} = 0 \quad (2.22)$$

The change of the stress state from one yield locus to another varies the hardening parameter. Substituting Eq. (2.22) in Eq. (2.16), the plastic component of the incremental void ratio can be written as

$$de^p = -(\lambda - \kappa) \left(\frac{dp}{p} + \frac{d\eta}{\psi' + \eta} \right) \quad (2.23)$$

Thus, the plastic volumetric strain, de_v^p , can be expressed as

$$d\varepsilon_v^p = \frac{de^p}{1+e} = \frac{(\lambda - \kappa)}{1+e} \left(\frac{dp}{p} + \frac{d\eta}{\psi' + \eta} \right) \quad (2.24)$$

The ratio ψ' can be obtained by considering the energy dissipated while undergoing deformation on the state boundary surface. Here any assumption of the magnitude of the dissipated energy dW results in the development of a different hypothesis. In the *Modified Cam clay* model, the dissipated energy is assumed to be

$$dW = pd\varepsilon_v^p + qd\varepsilon_s^p = p\sqrt{(d\varepsilon_v^p)^2 + M^2(d\varepsilon_s^p)^2} \quad (2.25)$$

where $d\varepsilon_v^p$ and $d\varepsilon_s^p$ are the volumetric and shear plastic strains, respectively. This leads to

$$\frac{d\varepsilon_s^p}{d\varepsilon_v^p} = \frac{2\eta}{M^2 - \eta^2} = \frac{1}{\psi'} \quad (2.26)$$

Substituting ψ' in Eq. (2.21) and integrating the expression gives rise to the elliptical yield locus for the *Modified Cam clay* model. That is,

$$M^2 p^2 - M^2 p_0 p + q^2 = 0 \quad (2.27)$$

The following expressions can be obtained for incremental quantities of strain by substituting the value of ψ' in Eqs. (2.24) and (2.26):

$$d\varepsilon_v^p = \frac{(\lambda - \kappa)}{1+e} \left(\frac{dp}{p} + \frac{2\eta d\eta}{M^2 + \eta^2} \right) \quad (2.28)$$

$$d\varepsilon_s^p = \frac{\lambda}{1+e} \left[\frac{dp}{p} + \left(1 - \frac{\kappa}{\lambda} \right) \frac{2\eta d\eta}{M^2 + \eta^2} \right] \quad (2.29)$$

$$d\varepsilon_s^p = \frac{(\lambda - \kappa)}{1+e} \left(\frac{dp}{p} + \frac{2\eta d\eta}{M^2 + \eta^2} \right) \frac{2\eta}{M^2 - \eta^2} \quad (2.30)$$

2.4.2 Modified Cam clay model for Montreal silty clay

The experimental results presented in section 2.3 were used to determine the parameters for the critical state model. The parameter M is the slope of the critical state line on a $q - p$ plot that can be determined from the stress paths obtained in the CU triaxial tests.

This parameter can also be measured from the effective friction angle ϕ' of the Mohr-

Coulomb yield criterion, measured in the triaxial compression test, using the following equation:

$$M = \frac{6 \sin \phi'}{3 - \sin \phi'} \quad (2.31)$$

Thus, the value of M for the silty clay tested was estimated to be 1.55. Moreover, the values of λ and κ can be related to the compression index C_c and swelling index C_s . The compression index C_c is defined as the slope of the virgin loading line on $e - \log_{10} p$ plot while the swelling index C_s is defined as the slope of the unloading-reloading curves on the same plot. In this study, the compression and swelling indices are defined from the results of one-dimensional consolidation tests, which is a special case of a constant q/p test. Therefore, the values of λ and κ can be computed as

$$\lambda = \frac{C_c}{\ln 10} = \frac{C_c}{2.303} \quad (2.32)$$

$$\kappa = \frac{C_s}{\ln 10} = \frac{C_s}{2.303} \quad (2.33)$$

Substituting the magnitudes of the compression and swelling indices in the preceding expressions, the values of λ and κ are computed to be 0.0564 and 0.0104, respectively. In addition to the slope, another parameter is needed to specify the location of the virgin consolidation line in e vs. $\ln p$ plot. The virgin consolidation line is therefore defined as

$$e = N - \lambda \ln p \quad (2.34)$$

in which N is the void ratio of the virgin consolidation line at unit mean effective stress, and is dependent on the units considered in the analysis. From the compression curves of $e - \ln p$ plot obtained from the oedometer tests (Figure 2.9) this value is estimated to be 0.67.

The material parameters determined in this research were used in the computational modeling of the problem to simulate the response of the consolidation specimens subjected to different stress levels. The consolidation specimen was modeled as an axisymmetric problem (Figure 2.14) using the general-purpose finite element code, ABAQUS/Standard (2005). The main purpose of this computational modeling was to verify the value of the hydraulic conductivity calculated using the Casagrande

construction. A uniform pressure was applied to the rigid plate attached to the top surface of the soil sample with a stiffer constituent material compared to the soil ($E = 2 \times 10^5 \text{ MPa}, \nu = 0.3$). In this analysis, the soil region was discretized into 594 eight-noded biquadratic axisymmetric elements with quadrilateral displacement and bilinear pore pressure variation, formulated on the basis of the use of a reduced integration scheme. Each node in this element has three degrees of freedom corresponding to the displacement in the radial and vertical directions and the magnitude of the pore pressure. The boundary condition applied to the soil region is an oedometer-type constraint while free drainage conditions were considered for the upper and lower boundaries of the model.

The computational analysis, conducted with different hydraulic conductivities of the material and the time-dependent deformation of the specimen, was compared with the experimental results. The comparison of results showed that the experimental settlement curves lie between the numerically predicted curves corresponding to a hydraulic conductivity, k , of 10^{-8} cm/sec and $5 \times 10^{-8} \text{ cm/sec}$ (Figure 2.14). It is shown that by increasing the normal effective stress in successive load steps, the settlement curves obtained from the experiments approach the numerically predicted curves with lower value of hydraulic conductivity. This phenomenon can be attributed to the decrease in the hydraulic conductivity in the fine-grained soil due to the decrease in the void ratio resulting from compression of the soil specimen.

2.5 Summary remarks

The accurate modeling of the mechanical response of fine-grained soils is required to predict the behavior of various geotechnical constructions, such as natural slopes, pavement structures and foundations. The reconstituted Montreal silty-clay is a cohesive soil that can represent the soft load-bearing strata that can be encountered as soft sediments in marine environments or in barge-dumped reclaimed lands. Certain naturally occurring soft marine clay could display similar characteristics.

Due to the low strength of the material, experimental results derived from conventional triaxial testing suffer from errors resulting from sample preparation and assembly and sensitivity of the data acquisition systems. In this study, therefore, a strength-based fall cone test was adopted to verify the undrained shear strength determined from UU triaxial testing. Furthermore, it was shown that the progress of consolidation can improve the strength characteristics of fine-grained soils and reduce further deformation of the soft deposits under construction loads. The experimental results of CU triaxial tests showed an increase in the shear strength of the samples subjected to higher effective confining stresses. This phenomenon, which was also seen in the results of oedometer tests, rationalizes the need for preloading soft foundations in order to reduce excessive deformation during the application of construction loads.

The results of experiments conducted on Montreal reconstituted silty clay were used to develop a plausible constitutive model, that is based on critical state concepts, which incorporate both the stiffness and strength characteristics of the material. After determining the parameters of the *Modified Cam clay* model, the constitutive model was then used in computations to duplicate the results of conventional oedometer tests conducted in connection with research. The computation also attempts to predict the rate of consolidation obtained from one-dimensional oedometer tests. It is shown that the computational analyses give a satisfactory prediction of the rate of consolidation, considering the range of hydraulic conductivities estimated from the Casagrande construction. Therefore, the capabilities of this model in correlating the mechanical responses of the tested material permit the use of the constitutive model in the study of various composite media encountered in geotechnical endeavors.

CHAPTER 3

MECHANICAL BEHAVIOR OF BALLOTINI AND THE CONSTITUTIVE CHARACTERIZATIONS

3.1 Introduction

The constitutive modeling of cohesionless soils such as sands and gravels has been a topic of interest for geotechnical engineers over the past several decades. There are numerous experimental and theoretical studies that have contributed significantly to the understanding of the important factors that control the mechanical response of granular soil media. In this chapter, the mechanical behavior of an ideal granular material, consisting of glass spheres of uniform size (ballotini A3), is examined experimentally. The experimental investigations include the consolidated drained (CD) triaxial, isotropic compression and oedometric bench-scale tests performed to examine the stiffness and strength properties of the material in different stress states. Furthermore, constant head hydraulic conductivity tests were also conducted to determine the hydraulic properties. The results of the experimental investigations are used to develop a constitutive model for the ballotini that can adequately represent the mechanical behavior in terms of its stiffness and yield behavior.

3.2 Experimental investigations

The mechanical properties of the ballotini were examined through a series of tests involving different states of stress (e.g. CD triaxial, isotropic and oedometric compression tests). The stiffness characteristic of a granular material is an important factor in predicting the stress-strain response of the material prior to yield. This behavior can be represented by different constitutive relations proposed in the literature, such as elastic, hyperelastic, or hypoelastic models (Yamamuro and Kaliakin, 2005; Lade, 2005;

Collins, 2005; Hill and Selvadurai, 2005). The understanding of the shear strength of geomaterials is essential in geotechnical engineering practice, since a sufficient factor of safety needs to be provided to prevent the occurrence of failure. Failure in geomaterials that are characterized as granular can occur by various modes depending upon the density of the material, inter-particle friction, particle shape and the nature of the applied loading (e.g. static vs. dynamic)(Li et al., 2005).

In this research, CD triaxial tests were conducted to examine the behavior of the ballotini under different stress states. Two bench-scale confined uniaxial compression tests were also carried out on loosely placed ballotini ($D_r \approx 0.52$) to determine the stiffness properties of ballotini at low stress states. A subset of experimental results obtained from CD triaxial and bench-scale uniaxial compression tests were used to develop a constitutive model capable of predicting the mechanical response of the tested material. After validating the model with other experimental results obtained from isotropic compression test and triaxial compression test with unloading-reloading cycles, it will be implemented in the computational studies of the composite samples consisting of ballotini and reconstituted lumps of silty clay.

3.2.1 Material description

Ballotini, an artificial particulate medium consisting of glass beads, is used in a wide range of industrial applications, such as cleaning, shot-peening and the finishing process for metal surfaces in a variety of industries, including aerospace, automotive and electronics. In this research program, the ballotini used was Type A3 with a specific gravity estimated at $G_s = 2.5$, manufactured by Potters Industries Inc. (La Prairie, Quebec). In the material specification Table provided by the supplier, the grain size of ballotini Type A3 is reported to be in the range of $600 \mu m$ (sieve no. 30) to $850 \mu m$ (sieve no. 20), whereas grain size analysis conducted on supplied material indicated that 83% of this granular material ranged from $600 \mu m$ to $850 \mu m$, while approximately 17% had a particle size between $300 \mu m$ (sieve no. 50) and $600 \mu m$ (Figure 3.1).

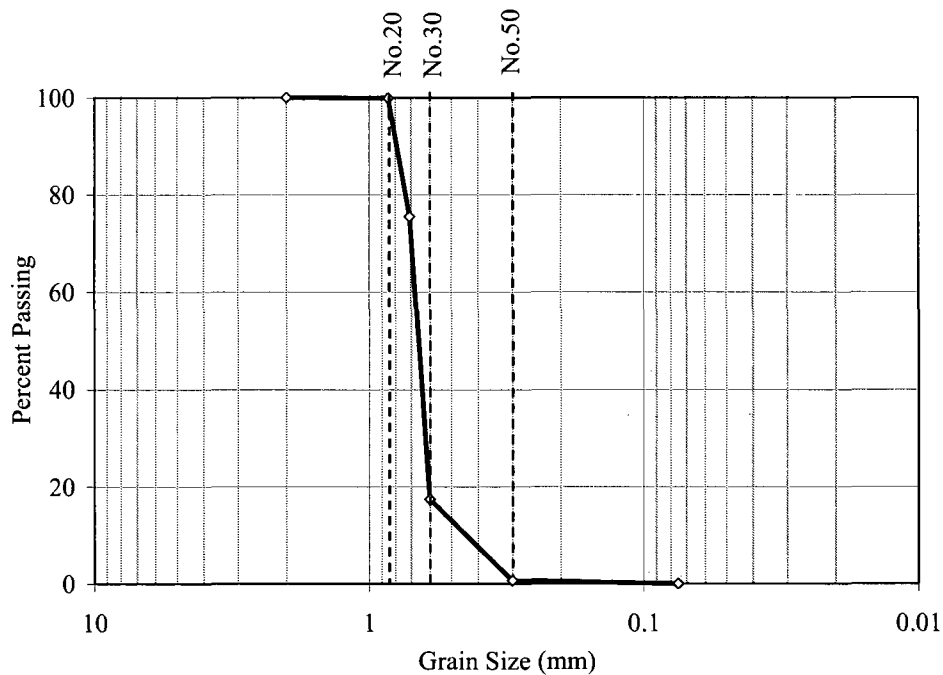


Figure 3.1 Grain size distribution curve for ballotini

3.2.2 Consolidated drained triaxial compression test

The first test conducted on the particulate material was the conventional triaxial test used extensively in the laboratory testing of soil specimens. In the case of granular material this test is more difficult to perform than the direct shear test; however, it has several advantages over direct shear tests, such as controlling the drainage condition in the test (Bishop and Henkel, 1962; Murthy, 2003). To perform triaxial tests on coarse-grained samples, a specimen preparation technique proposed by Holtz and Kovacs (1981) and Bardet (1997) was used. In the preparation of the triaxial specimens, a rubber membrane with the diameter of 70 mm and the thickness of 0.4 mm is placed inside an assembled split mold, with the same internal diameter as the membrane, and the two ends of the membrane were folded back on the rims of the mold. A porous stone and a filter paper were then placed on the base platen of the triaxial setup (Figure 3.2a). After placing the split mold on the porous stone, rubber membrane was attached to the base platen of the triaxial base using two O-rings (Figure 3.2b). The ballotini was poured inside the stretched membrane in four layers of approximate equal depth (Figure 3.2c); each layer

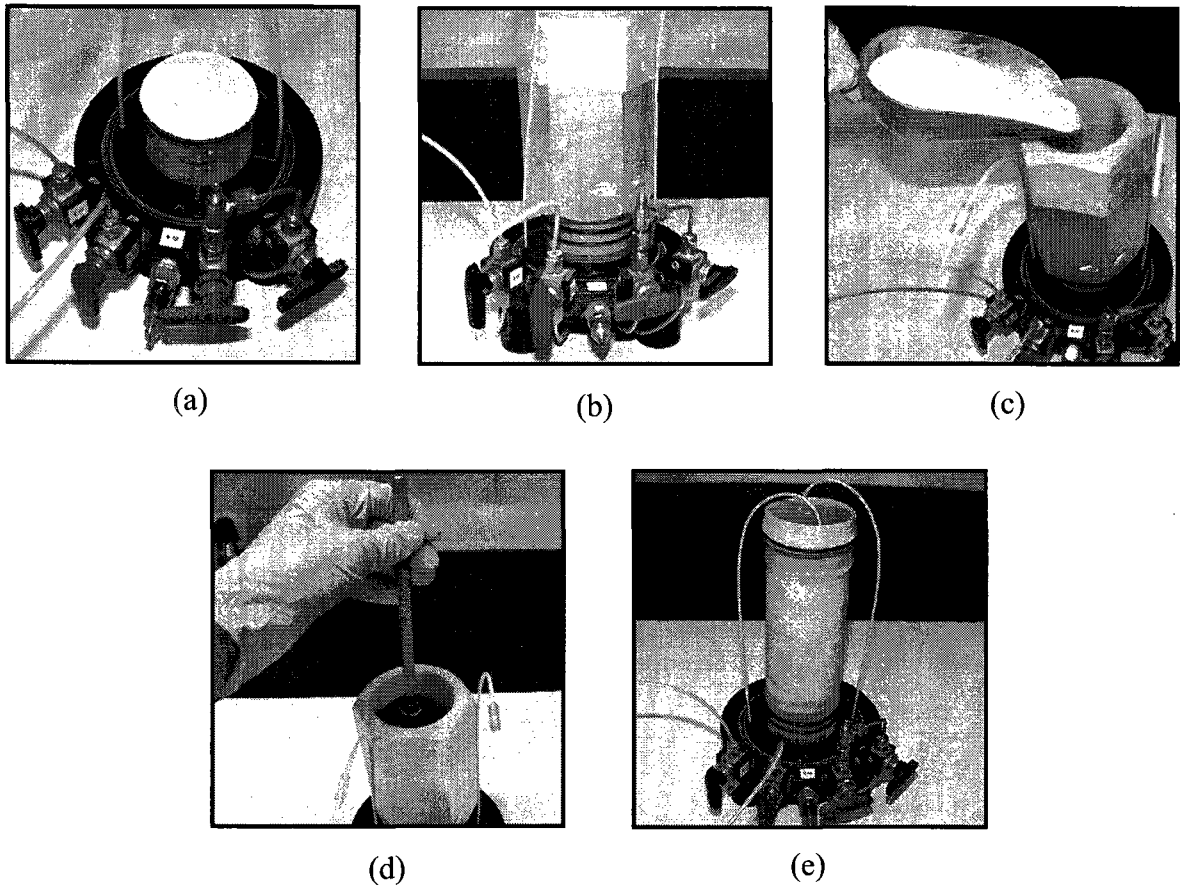


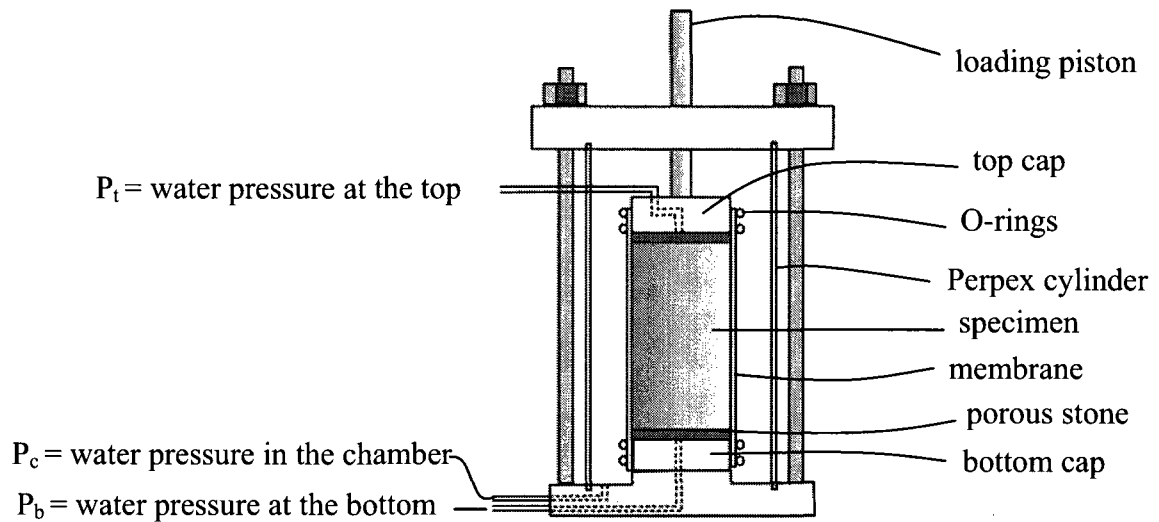
Figure 3.2 Sample preparation technique for conducting triaxial compression tests on ballotini

was slightly compacted by 20 impacts applied using a plunger with a mass of 625 g (Figure 3.2d). The mass of the dish containing ballotini was measured before and after placement of the ballotini, to determine the initial density of the specimens. After filling the membrane to the desired height ($\approx 13.5\text{ cm}$), the filter paper, porous stone and the top cap were placed on the specimen and the membrane was rolled over the top cap and fastened with two O-rings. In the next step, the split mold was removed and the initial height and diameter of the specimens were measured (Figure 3.2e). The initial dry density of the ballotini samples was estimated in the range of 1.54 g/cm^3 ($D_r = 0.51$) to 1.56 g/cm^3 ($D_r = 0.55$).

In CD triaxial tests, the specimens must be fully saturated before applying the confining pressures and subsequent application of deviatoric stresses. Therefore, after placing the specimen in the triaxial chamber and filling the chamber with water, a chamber pressure equal to 30 kPa was applied to the samples. In the saturation phase, the upward flow of

interstitial water must be slow enough to prevent the sample from expanding or compacting while it is saturated. Therefore, in order to saturate the samples, a back pressure of 20 kPa was applied to the burette connected to the bottom of the sample; at the same time, the burette connected to the top cap was maintained under zero pressure. The deaired water inside the saturation burette was pushed through the ballotini sample until air bubbles ceased to appear in the saturation line. After complete saturation, the back pressure was increased to 30 kPa , equal to the initial cell pressure. Skempton's pore pressure coefficient B measured for each test was at least 0.98; indicating an acceptable saturation level for the specimens to be sheared in a CD triaxial test. After saturation, the samples were subjected to an increase in the confining pressure. For isotropic consolidation, the back pressure was maintained while the cell pressure was increased, until the *difference between the cell pressure and back pressure became equal to the desired confining pressure*. In this experiment, the samples were subjected to a confining pressure that varied between 100 kPa and 500 kPa , which was selected based on the estimated stress states that would be encountered in the bench-scale oedometric tests. During the application of confining pressure, the volume change of the samples was measured from the amount of fluid expelled from the saturated samples. The procedure described for conducting CD triaxial test on ballotini is shown in Figure 3.3.

In the drained triaxial tests, the strain rate suggested for shearing the coarse-grained samples is about 0.5% of axial strain per minute (see e.g. Bardet, 1997); thus, a displacement rate equal to 0.5 mm/min was chosen for the CD triaxial testing of ballotini. At this rate, no excess pore fluid pressure was expected to be generated; this fact was verified by recording the pore pressure with pressure transducers connected to the top and bottom of the samples. It was observed that the pore pressure remained equal to the back pressure during the entire shearing process. The shearing portion of the triaxial test was considered to be complete once the maximum deviator stress was reached. Two additional tests were also conducted with the unloading-reloading cycles performed after the failure of the ballotini specimens to assess the irreversible deformations that followed the failure of the material.



	Saturation phase	Equilibrium condition	B -value measurement	Application of axial load
P_t (kPa)	0	30	30	30
P_c (kPa)	30	30	50	30+confining pressure
P_b (kPa)	20	30	30	30

Figure 3.3 The procedure used in triaxial compression test

Stiffness characteristics- The stiffness properties of the ballotini can be determined from the results of the triaxial tests; therefore, the consolidated drained triaxial tests were carried out on the specimens subjected to different confining pressures σ_3 . In order to fully determine the compressibility behavior of ballotini, each test specimen was first compressed isotropically under different chamber pressures, which resulted in a range of void ratios in the tested samples. By increasing the vertical stress in a strain-controlled loading frame, the specimens were subjected to shearing until the peak value of the deviator stress, corresponding to failure, was obtained. However, the stiffness of the specimens in different physical states, indicated by density and stress state, can be estimated from the slope of the triaxial stress-strain curves before reaching the failure loads. When the value of Young's modulus is required, it is usually estimated from the axial strain obtained at a deviator stress equal to 1/2 or 1/3 of the peak deviator stress.

Figure 3.4 indicates that the stiffness of the material increases when it is sheared under higher confining pressure. Further triaxial compression tests were also conducted with unloading-reloading cycles applied after failure to estimate unloading-reloading stiffness of the material. These tests were conducted on the samples subjected to the confining pressures of 400 *kPa* and 500 *kPa*. The stress-strain curves for the triaxial compression tests that included unloading-reloading cycles, are shown in Figure 3.5. The results indicate the development of irreversible deformation in the stress-strain response of the samples during the unloading-reloading phase.

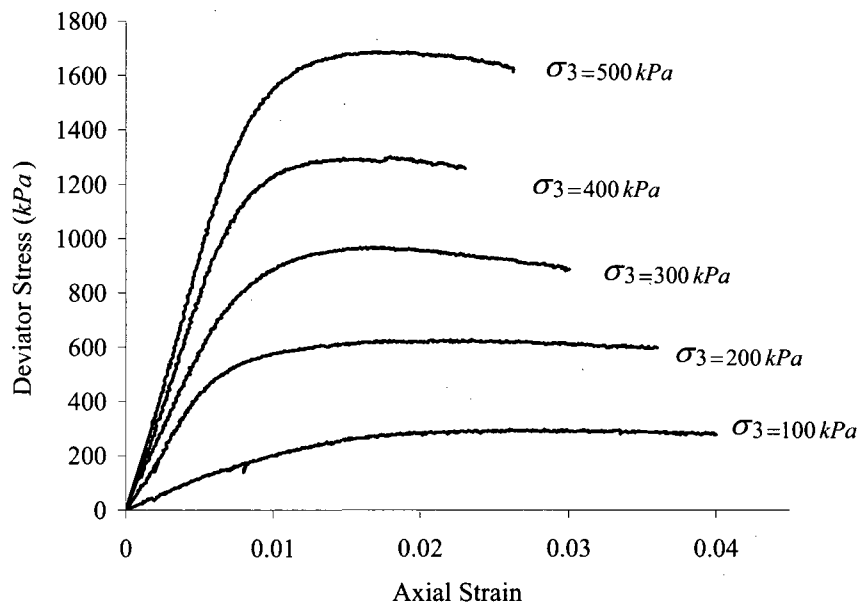


Figure 3.4 Stress-strain curves for ballotini specimens derived from triaxial compression tests: Influence of confining pressure

Poisson's ratio ν is another parameter that can generally be estimated from the ratio of the lateral strain to axial strain during the CD triaxial compression test. The volumetric strain of the triaxial specimens, determined from the volume of deaired water that is expelled from the samples, can also be used to determine the Poisson's ratio. During the early range of strains, for which concepts from the theory of elasticity can be used, the Poisson's ratio can be obtained from the strains that occur in the samples. From the variation of the volumetric strain with axial strain shown in Figure 3.6, the Poisson's ratio of ballotini is estimated at approximately 0.3.

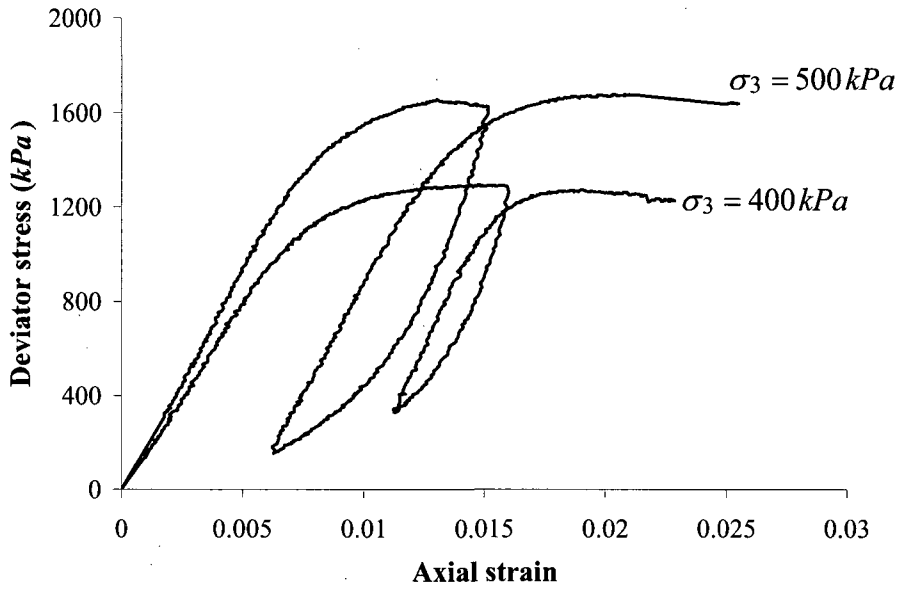


Figure 3.5 Stress-strain curves for ballotini specimens derived from triaxial compression tests with unloading-reloading cycles

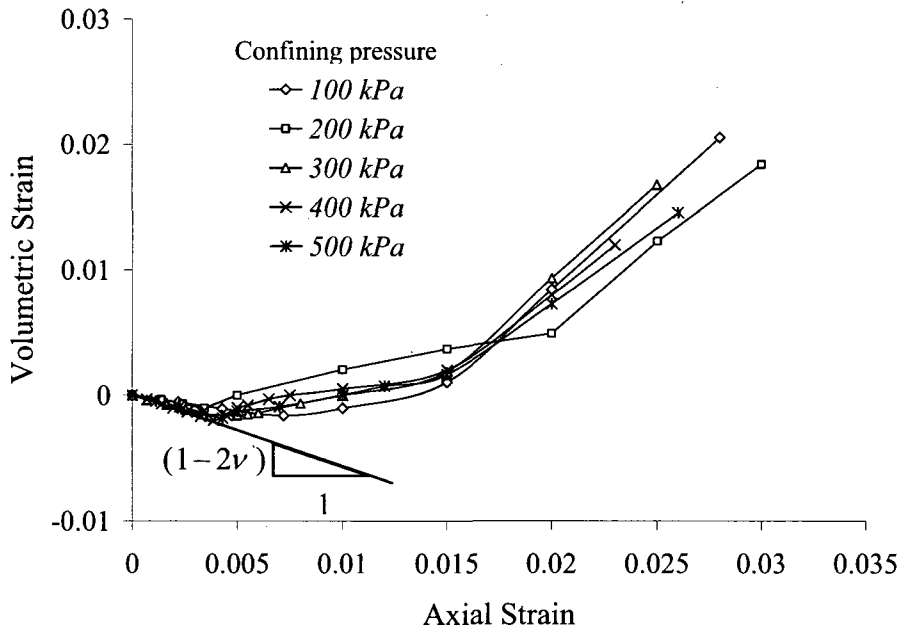


Figure 3.6 Volumetric strain versus vertical strain in triaxial specimens subjected to different confining pressures

Shear dilatancy- Another important aspect of granular material behavior is shear dilatancy, defined as the change in volume associated with the shear distortion of an element in the material. This phenomenon is more observable for specimens that are densely compacted or subjected to high confining pressures. The dilatancy angle ψ is a parameter used to describe the volume change behavior of a granular material. Vermeer and de Borst (1984) indicated that for granular soils the dilatancy angle is significantly smaller than the friction angle. Based on energy concepts, they proposed the following equation for assessing the dilatancy angle in its general form:

$$\sin \psi_{\max} = \left[\frac{d\varepsilon_v}{(d\varepsilon_v - 2d\varepsilon_1)} \right]_{\max} \quad (3.1)$$

where ε_v is volumetric strain, and ε_1 is axial strain. Bolton (1986) showed that both the effective stress and the soil density have an influence on the dilative behavior and strength characteristics of a dilatant soil. He proposed a theoretical solution of the maximum dilation angle in plane strain condition in the form:

$$\sin \psi_{\max} = \left[-\frac{(d\varepsilon_1 + d\varepsilon_3)}{(d\varepsilon_1 - d\varepsilon_3)} \right]_{\max} \quad (3.2)$$

where ε_1 is axial strain, and ε_3 is lateral strain. Furthermore, assuming the uniform lateral strain in a standard triaxial compression test, a theoretical expression was presented by Tatsuoka (1987) between the maximum dilation angle and the strains occurring in the triaxial specimen:

$$\sin \psi_{\max} = \left[-\frac{(d\varepsilon_1/2 + d\varepsilon_3)}{(d\varepsilon_1/2 - d\varepsilon_3)} \right]_{\max} \quad (3.3)$$

He proposed this relationship by comparing the $d\varepsilon_v/d\varepsilon_1$ obtained from plane strain and triaxial compression tests on Toyoura sand covering a wide range of relative densities and confining pressures (Fukushima and Tatsuoka, 1984; Lam and Tatsuoka, 1986). He showed that considering Eq.(3.3) for triaxial compression tests give similar results for ψ_{\max} compared to that obtained from plane strain tests using Eq.(3.2). This expression was considered when estimating the dilatancy angle of the ballotini from the volume

change of the specimens sheared in the CD triaxial tests. Figure 3.6 indicates that the specimens, subjected to different confining pressures, initially exhibited compressive behavior followed by a dilation response when the deviator stress approached the peak value. The variation of volumetric strain at peak strength suggests a dilation angle in the range 5° to 8°. Furthermore, a higher rate of volumetric dilation was observed when the samples were subjected to higher axial strain. For axial strains above 2%, therefore, the dilation angle is estimated to be in the range 20° to 24° for different confining pressures.

Shear strength- Cohesionless soils develop their shear strength as a result of friction and interlocking resistance between the individual soil particles. Therefore, the granular soils can exhibit stiffness and strength under confining pressures that are compressive. The most common laboratory tests used to determine the shear strength of granular soil are the direct shear and triaxial tests. The complete state of stress is assumed to be known at all stages during the triaxial test, whereas only the stresses at failure are known in the direct shear test. In this study, the strength of the ballotini was determined by conducting CD triaxial tests. Two different definitions are presented in the literature based on the (i) *total stress* and (ii) *effective stress* concepts, to define failure derived from the results of triaxial tests. Since no excess pore pressure is generated in the CD triaxial test, both definitions give rise to identical values of shear strength in the specimens. The shear strength of the soil is therefore considered to be the maximum difference of the principal stresses applied to the specimen. Since the minor principal stress, σ_3 , is maintained constant during the triaxial compression test, the maximum deviator principal stress corresponds to the maximum major principal stress, σ_1 , sustained by the soil specimen.

The results of the CD triaxial test can be used to determine the shear strength parameters of the Mohr-Coulomb failure criterion. For this purpose, the K_f -line was drawn in the $p - q$ plot through the peak points of the Mohr's circle corresponding to the failure state (Figure 3.7). In this study, p and q are defined as follows:

$$p = \frac{\sigma_1 + \sigma_3}{2} \quad (3.4)$$

$$q = \frac{\sigma_1 - \sigma_3}{2} \quad (3.5)$$

where σ_1 is the axial stress and σ_3 is the confining stress applied to the sample. The path of the peak point of the Mohr's circle, referred to as the stress path, is shown on the $p-q$ plot for each test (Figure 3.7). The cohesion c and the friction angle ϕ of the material are usually computed from the slope α and the intercept of the K_f -line drawn in the $p-q$ plot using a linear regression. Since granular soils possess no cohesion, the K_f -line is plotted taking the origin of the $p-q$ plot as a data point. Using the K_f -line, the friction angle of the material is estimated at 38° from the slope of the K_f -line using the following relationship:

$$\sin \phi = \tan \alpha \quad (3.6)$$

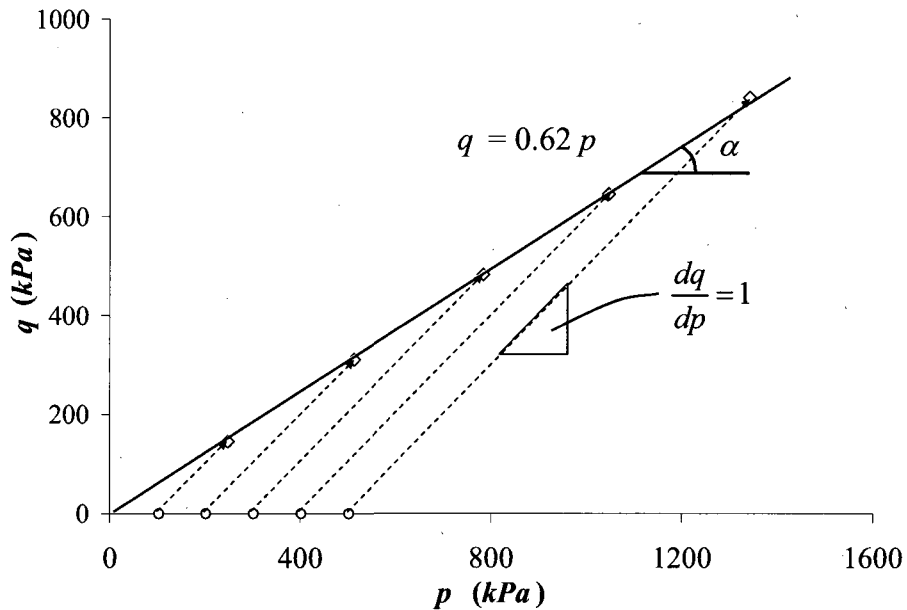


Figure 3.7 K_f -line and stress paths obtained from triaxial compression test

3.2.3 Isotropic compression test

In this test, the procedure used for sample preparation is identical to that described for the triaxial test. After mounting the cylindrical specimens in the triaxial setup, an upward flow was induced to saturate the samples. The specimens were then subjected to a cell pressure that was increased in different load steps while the drainage valves were kept open. The volumetric compression and expansion of the saturated specimens can be obtained from the volume of the pore fluid extruded from or entered into the samples. In this test, two loading-unloading cycles were conducted on the triaxial specimens prepared with different initial void ratios; in the first cycle, the chamber pressure was increased to 500 *kPa* and 600 *kPa* (pressure increments of 100 *kPa*) in Test-1 and Test-2, respectively (Figure 3.8). The loading and unloading of the samples in this cycle were conducted in approximately 30 seconds in which the volume change of the specimens was recorded at different confining pressures. In the second cycle, the chamber pressure was maintained after each increase in chamber pressure for a period of approximately 5 minutes in both loading and unloading parts. It was observed that the specimens exhibited further time-dependent compression in the second cycle; therefore, higher irreversible compressions were observed in the samples. The results provided information on the volume or bulk behavior of the material, generally presented in terms of confining pressure versus void ratio. The results of the isotropic compression tests were not considered to identify the parameters of the constitutive model. Thus, these experimental results will be used to validate the constitutive model developed for the material.

3.2.4 Oedometric bench-scale test

In order to investigate the stiffness properties of the ballotini, two oedometric compression tests were carried out in a bench-scale apparatus containing the ballotini samples. The bench-scale experimental setup, which was mainly designed for testing the composite soil specimens, was utilized to test homogenous ballotini samples (Figure 3.9). This setup consisted of a consolidation cell, a loading frame and a data acquisition system. The oedometric cell was made of 316L stainless steel and had wall thickness of

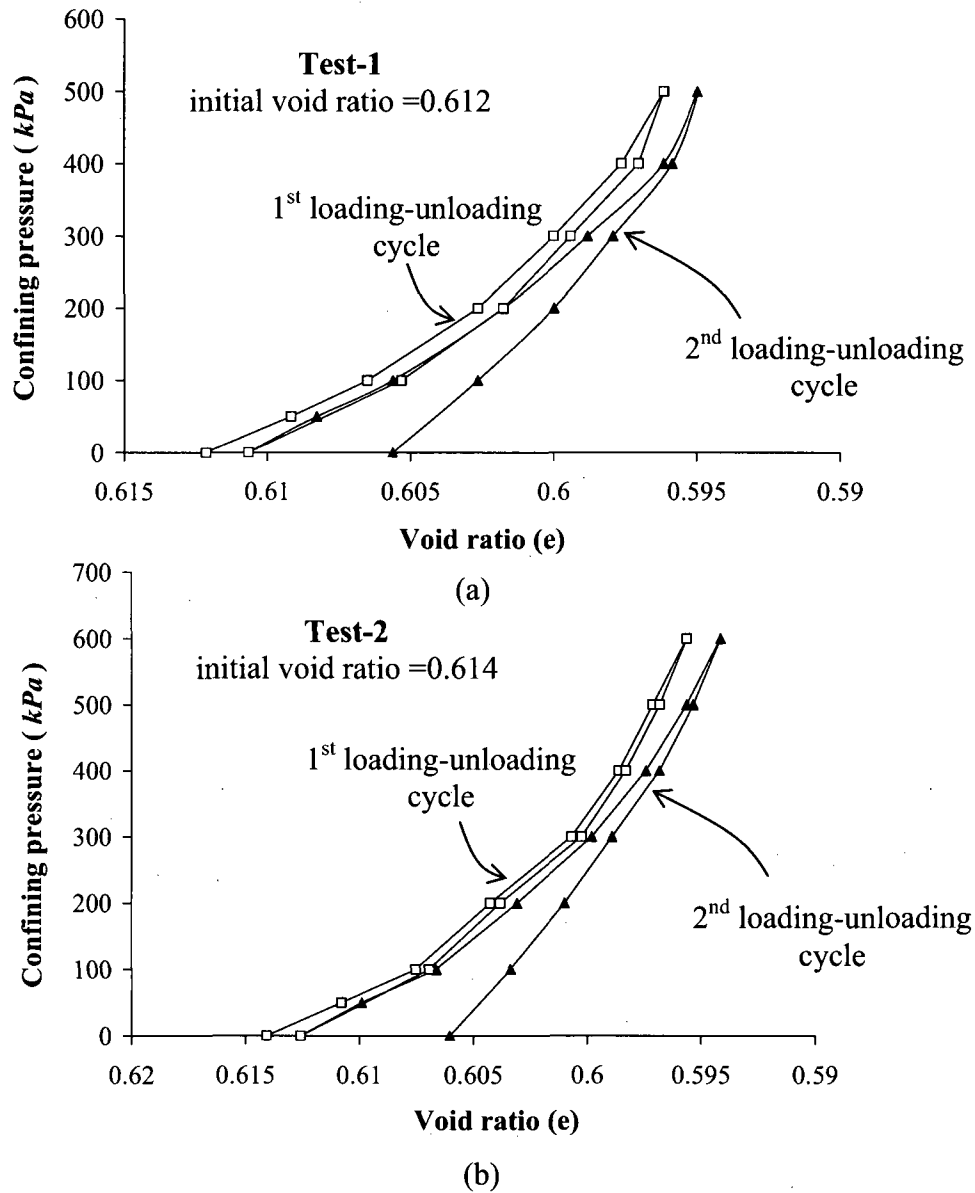


Figure 3.8 Results of the isotropic compression test on two samples of ballotini

44 mm. The cylindrical region inside the cell had a diameter of 152 mm and a height of 305 mm with a highly polished inner surface.

The loading frame, built of hollow square section steel tubing (3.5 in \times 3.5 in \times 5/16 in), included a base with a consolidation cell and jacking system. The main frame was connected to the base beams using four bolts by which the setup could be adjusted to a level position. In this setup, the axial stress was established by a static load applied to the end of the lever arm. The dead load was created by the weight of the rack, the lever arm

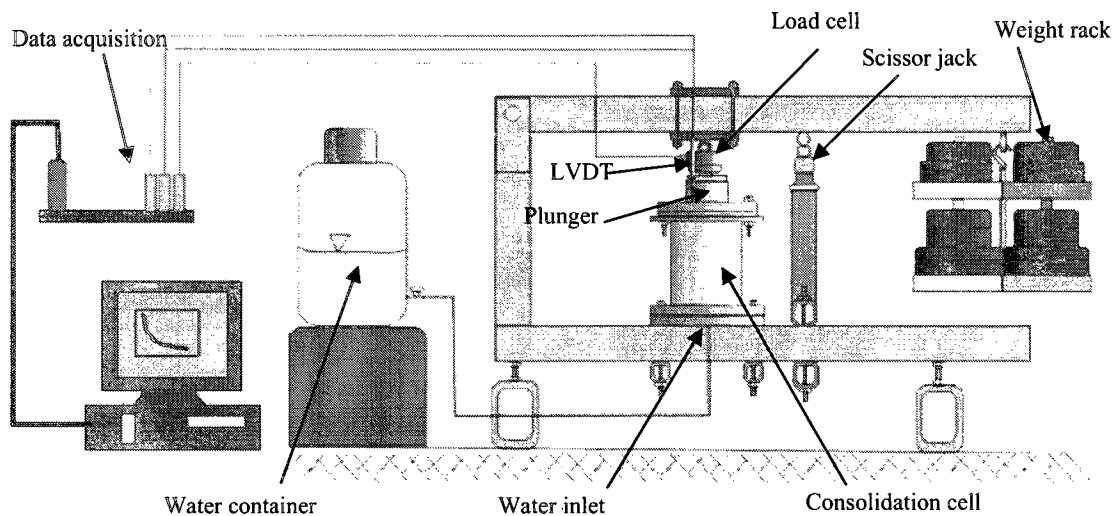
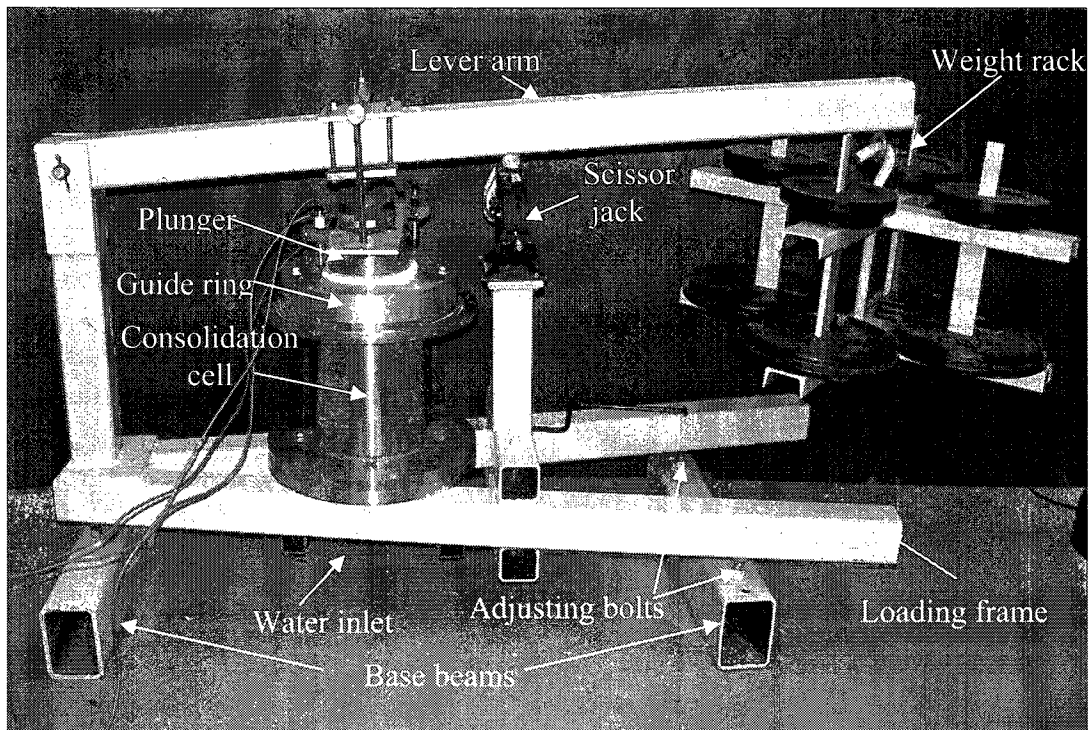


Figure 3.9 Experimental setup for Bench-scale test

and the weight plates placed on it; the load was transferred by a lever arm with a load ratio of 2.8, to the top of the plunger through a steel sphere of 38.1 mm diameter. A load cell was also used to record the axial load applied to the plunger. Figure 3.10 shows two stiffening plates of thickness 12.7 mm attached to the bottom and the top of the lever arm at locations in contact with the steel sphere and aluminium bar to avoid localized loading of the steel section. An aluminium guide ring was attached to the consolidation cell to

align the plunger through the cell and to prevent contact between the plunger and internal surface of the consolidation cell. To facilitate the vertical movement of the plunger, a Teflon ring was mounted on the inner part of the guide ring to minimize frictional effects of load transfer. A weight rack was also designed to hold weight plates of 11.3 kg (25 lbs) and 9.1 kg (20 lbs) mass with a maximum capacity of 272 kg (600 lbs). For gradual application of the vertical load to the sample, a scissor jack (load capacity 1.5 tons and maximum travel 26 cm) was mounted on the frame to hold the lever arm while adding the weight plates at each load increment. The jack was attached to the steel frame between the cell and the weight rack, 80 cm away from the hinged end of the lever arm (Figure 3.9). A rectangular plate was also attached to the top of the plunger; and two steel rods and an aluminium bar were used to connect this plate to the lever arm (Figure 3.10). With this arrangement, the load could be gradually applied to the samples when the lever arm was lowered during each load step.

The instrumentation used in the experimental setup for the oedometric compression test included a load cell located on the top of the plunger and two LVDTs connected to the rectangular plate to measure the uniaxial compression of the sample (Figure 3.10). The load cell used in this experiment had a capacity of 44.48 kN (10 kips) with an accuracy equal to $\pm 0.04\%$. Two LVDTs, with a displacement range of 2.5 cm, were attached to opposite sides of the plunger to record the vertical compression of the specimen. The 10 Volt excitation voltage required for the transducers was supplied from the rack of the signal conditioner module (ISO-RACK8), which can be connected to eight signal conditioning blocks. In these tests, three signal conditioner blocks (PCI-5B38) with an accuracy of $\pm 0.08\%$ span and a gain of 50 converted the transmitted signals to high-level analog voltage outputs after a filtering and amplification process. These output voltages were then recovered via a desktop computer through a USB-based DAQ module (PMD-1606FS). Due to the higher rate of axial displacement during the initial stages of the load increments, all readings were taken every second during the first hour of each load step. The data acquisition rate was then reduced to one reading per minute for the remainder of the load step, where a lower rate of axial compression was observed.

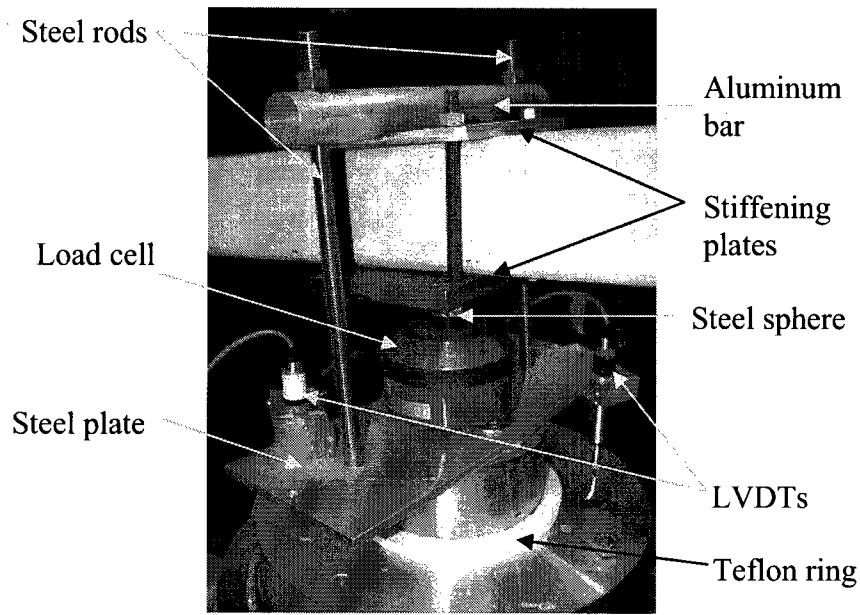


Figure 3.10 Loading setup and instrumentations used in the bench-scale test

The specimens with the approximate height of 168 mm were fabricated by placing the ballotini in the oedometric cell in four layers; each layer was poured after slightly tapping and flattening the surface of the previous layer. The mass of the ballotini placed in the consolidation cell was used to calculate the physical properties of the samples. In the first experiment, the ballotini sample was saturated prior to loading whereas in the second test the sample was maintained in a dry condition; the comparison of the results obtained from these tests highlights the influence of the moisture/saturation on the strain-stress behavior of the ballotini samples. In the test conducted on the saturated sample, water was allowed to flow into the cell through the bottom inlet connected to a water container prior to the application of the load. An initial hydraulic gradient close to unity was used in the saturation stage, and the water level was maintained at the upper surface of the specimen for a period of one day. Furthermore, adequate drainage was ensured by placing geotextile layers (F-300, Texel inc.) at the upper and lower surfaces of the specimens. In a study on the influence of stress level on the physical properties of non-woven Polyester geotextiles, Palmeira and Gardoni (2002) indicated that geotextile layers can be compressed to approximately 0.35 of the initial thickness under the normal pressure of

1000 *kPa*. Furthermore, a significant part of the compression of the geotextile (80% to 90% of this compression) takes place at normal stresses up to 100 *kPa*. Thus it is assumed that a significant portion of the compression of the geotextile layers, with initial thickness of 1.2 *mm*, occurred during the application of the priming stress, while the compression of the geotextile layers during the application of the five main loading increments was considered to be negligible. This fact was also verified by comparing the compression response of the saturated sample with that of a dry specimen, in which no geotextile was placed at the top and bottom of the sample. After completion of the saturation phase and during the loading time, the water level in the container was kept at the same level as the top of the sample. In addition, a free drainage condition was also provided for the top of the specimen through vertical vent through the plunger.

The deformations experienced by an element of a granular material are largely the result of relative motions among the many particles that make up the element. These deformations depend on the physical nature (gradation, grain shape, etc.) and the physical state (relative density, stress state, etc.) of the particulate material. The local strains that occur at the contacts between the particles may be significantly larger than the overall strain defined in engineering practice. There are two main mechanisms that contribute to the deformation of the soil media: distortion and crushing of the particles, and relative sliding or rolling of the soil grains (Rowe, 1962; Pestana and Whittle, 1995; Fedá, 2002; Alramahi and Alshibli, 2006). Several studies therefore have suggested three different phases in the stress-strain behavior of coarse-grained materials: The first phase corresponds to the locking phenomenon in which the loose arrays within the soil medium collapse; therefore, a stiffer material is achieved due to a more tightly packed arrangement of the particles. By subjecting the samples to higher stress levels, another type of deformation is induced, which is attributed to the fracturing of individual particles. The occurrence of this phenomenon can be investigated through microscopic examination or grain size analyses before and after testing. In the next phase, the fractured particles constitute a tighter packing of the new and remaining particles. Therefore, stiffer material is reconstituted due to the denser arrangement and lower average contact force between the grains.

In geotechnical practice, the stress levels are usually less than those needed to reach the particle crushing stage. Considering the results of confined compression tests, Lambe and Whitman (1969) suggested that the fracturing process in granular particulates became important only when the stresses exceed approximately 3.5 *MPa*. Lade et al. (1996) also observed that in the triaxial test, sand specimens subjected to the confining pressures above 12 *MPa* showed increasing amounts of particle crushing. In a recent study, Nakata et al. (2001) indicated that sand subjected to uniaxial compression exhibited significant crushing under axial stress of up to 100 *MPa*. Fedá (2002) also presented the results of the oedometer test conducted on rounded silica gel specimens; he indicated that a sudden grain crushing occurs in the stress interval of 3.5 *MPa* to 4.5 *MPa*, resulting in sudden compression of the samples. Considering stress levels presented in previous studies for the initiation of grain crushing, the fracturing of the particles may become important in special construction projects, such as foundations of earth dams or in the case of rock-fill structures with large particles.

In the bench-scale oedometer tests conducted on ballotini, the specimens were subjected to a maximum vertical stress equal to 493 *kPa*, and in the triaxial testing, the highest confining pressure applied to the sample was 500 *kPa*. These pressure ranges were selected based on the stress level experienced by material in the bench-scale tests of composite samples or for a general problem, such as a footing resting on composite subsoil. Therefore, it is concluded that the stress-strain responses observed in this experimental research were mainly attributed to the locking phenomenon rather than the crushing of particles. This assumption was justified by performing grain size analyses on the tested ballotini and the observed particle degradation.

Using the bench-scale setup described in section 3.2.2, two stress-controlled oedometer tests on both saturated and dry samples of ballotini were carried out. In the initial load step, a uniform vertical pressure of approximately 81 *kPa* was applied to the specimens. This pressure resulted from the weight of the plunger, lever arm, weight rack, load cell, and the accessory rods and plates used in the loading setup. The void ratio of the specimens, after placing the plunger on the samples, was estimated at 0.612. The LVDTs are then installed to record the axial deformations that occurred in the subsequent loading stages. The vertical pressure on the samples was raised successively to 149, 219, 273,

383, and 493 kPa in five loading steps, by adding weight plates on the weight rack. Since a small amount of the axial displacement occurs in the long-term because of the time-dependent compression of the material, the vertical pressure was maintained for approximately 24 hours, and the ultimate deformation was determined at the end of this period.

Most of the reported results obtained from triaxial and uniaxial compression tests, mainly on glass beads and sands, indicated that for a good approximation the relation between the void ratio and logarithm of stress can be assumed to be linear for stresses not causing particle crushing (Been et al., 1991; Uygur and Doven, 2006). In Figure 3.11, which depicts the results of the uniaxial compression test on ballotini, a linear relationship was obtained between the void ratio and logarithm of vertical stress applied to the saturated and dry specimens. The axial settlement of the specimens during the five consecutive loading steps is shown in Figure 3.12. It is observed that the dry specimen shows time-dependent compression response similar to that observed in saturated samples, indicating that the rapid dissipation of pore pressure has no appreciable influence on the time-dependent compression response of the saturated samples, and that the apparent creep of the material is due to particle re-arrangement under load.

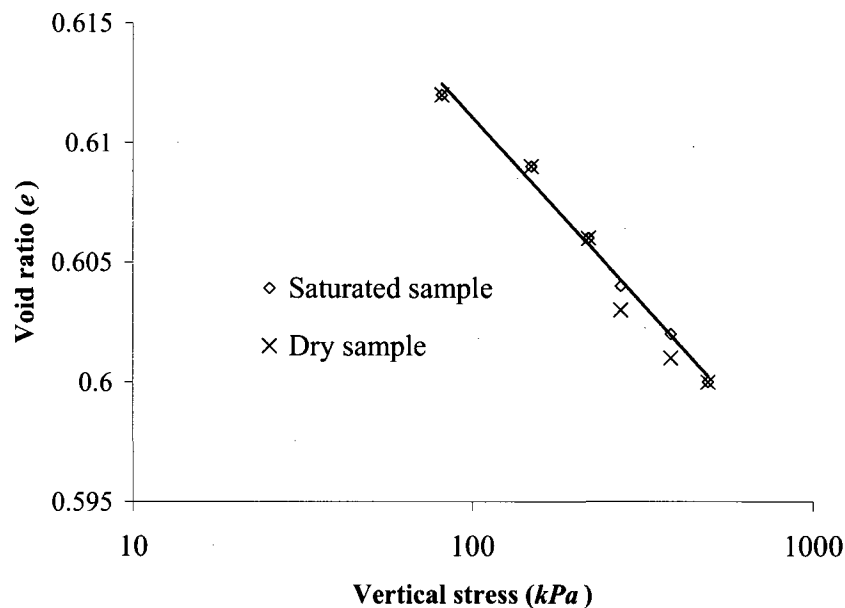


Figure 3.11 Bench-scale oedometer test results for saturated and dry ballotini samples

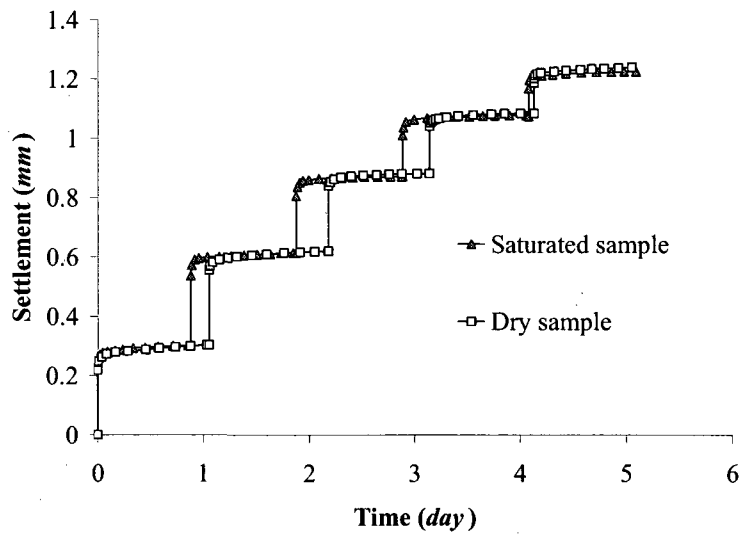


Figure 3.12 Results of oedometer test on ballotini samples tested in drained and dry conditions

Various studies carried out on granular soils indicated that the stiffness of the material depends on the stress state or the physical state of the particulate soil. Figure 3.13 shows the variation of the elastic modulus E with the void ratio obtained from the results of bench-scale uniaxial and triaxial compression tests conducted on ballotini samples. The material shows an approximately constant stiffness property in the loose state corresponding to a void ratio greater than 0.605 ($D_r < 0.54$). The elastic modulus of ballotini increases when the material is compressed to a void ratio lower than 0.605, largely due to the interlocking effect that occurs in granular media.

3.2.5 Constant head permeability test

Permeability can be defined as the ability of a saturated soil to transfer a flow of water or other fluids. The hydraulic conductivity is a measure of the permeability of soils, which can be determined in the laboratory using different types of tests, such as the constant head or falling head permeability; it also can be estimated from field tests that include

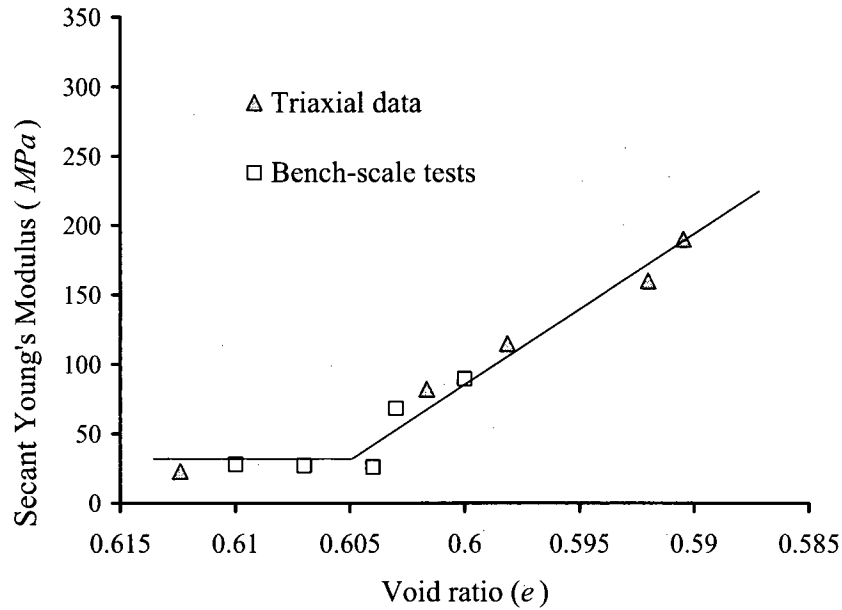


Figure 3.13 Variation of elastic modulus, E_{50} , with void ratio for ballotini material

well casing or pumping tests. Based on laboratory and field experiences, Holtz and Kovacs (1981) provided a chart which indicates the type of permeameter apparatus that is best suited for measuring the hydraulic conductivity of a range of soils. They suggested that for a well-drained soil with a hydraulic conductivity greater than 10^{-4} cm/s , the constant head permeameter is an appropriate device for determining the hydraulic conductivity.

In the constant head permeameter test, a saturated soil is subjected to a hydraulic gradient that is maintained constant during the test. Considering Darcy's law, the hydraulic conductivity k can be calculated from the constant head permeameter as follows:

$$k = \frac{QL}{\Delta h At} \quad (3.7)$$

where Q is the volume of water that flows out of the soil specimen, A is the cross-sectional area, t is the time duration, L is the length of the soil specimen and Δh is the total head loss across the sample. The constant head permeameter test, which is often used for sandy soil, can be implemented for ballotini with a particle size distribution

within the same range as sand grains. In this experimental investigation, considering the concepts of the constant head test, the hydraulic conductivity of the ballotini was measured using the triaxial setup. The cylindrical specimens were prepared with the approximate dimensions of 13 *cm* in height and 7.2 *cm* in diameter. This sample size satisfies the limitation that the specimen diameter should be at least ten times larger than the size of the largest particle to achieve a constraint required for a representative volume element. If the filter papers placed at the top and bottom of the sample has lower hydraulic conductivity, it could significantly influence the estimation of the hydraulic conductivity; therefore, no filter paper was used in the tests. Deaired water was used in the test to eliminate air bubbles that could impede the flow of water through the specimen. A confining pressure of 30 *kPa* was applied to the saturated specimens to ensure proper contact between the specimen and surrounding membrane. In this experiment, the samples were subjected to four different hydraulic gradients ranging between 2.5 and 23.4 and the time required for 100 *ml* of water to pass through the samples was recorded. At each hydraulic gradient, the average time for three experiments was determined. This value was used in the calculations. Table 3.1 shows the values of hydraulic conductivity estimated for different hydraulic gradients. For a hydraulic gradient of 23.4, the hydraulic conductivity was estimated to be 1.2×10^{-3} *cm/s* whereas this value decreased approximately to 1.6×10^{-3} *cm/s* for lower hydraulic gradients. Therefore, considering the low hydraulic gradient encountered in the compression tests, the average value of the last three measurements ($k = 1.6 \times 10^{-3}$ *cm/s*) was used as a representative value of the hydraulic conductivity of ballotini.

Table 3.1 Results for constant head permeameter tests conducted on ballotini samples

Test number	Hydraulic gradient	Hydraulic conductivity (<i>cm/s</i>)
1	23.4	1.24×10^{-3}
2	8.7	1.57×10^{-3}
3	4.8	1.69×10^{-3}
4	2.5	1.54×10^{-3}

3.3 A constitutive model for ballotini

In this study, a subroutine was developed for an elastic-perfectly plastic constitutive model with a Drucker-Prager failure criterion to be used in ABAQUS/Standard. The non-associativity of the flow rule is characterized by an additional parameter, the dilatancy angle, lying within a range from zero to the angle of internal friction of the material. After validation of the model with typical problems, the subroutine was modified to incorporate the hypoelastic behavior as a common characteristic of granular soils. At the end of this chapter, the stiffness and strength properties of the material, obtained from different testing methods (triaxial compression and bench-scale oedometric compression), are incorporated into the developed constitutive model to duplicate and also predict (triaxial and isotropic compression tests) the mechanical behavior of the material through computational analyses. Further examples of procedures given in the ensuing section can be found in the texts by Desai and Siriwardane (1984), Britto and Gunn (1987), Chen and Mizuno (1990), Potts and Zdravkovic (1999) and Davis and Selvadurai (2002).

3.3.1 Generalized stress-strain relations

In this section, the derivation of the stress-strain relations for an ideal plastic material with non-associative flow rule will be discussed. It is assumed that the yield function f is fixed in the principal stress space without movement or expansion during the plastic deformation. The plastic deformation in the material is governed by the potential function g . The incremental plastic strains are given by the relation

$$d\varepsilon_{ij}^p = \chi \frac{\partial g}{\partial \sigma_{ij}} \quad (3.8)$$

where $d\varepsilon_{ij}^p$ is the plastic strain increment, σ_{ij} is the stress tensor and χ is the positive scalar of proportionality. From the incremental Hooke's law and the flow rule equation, the complete stress-strain relationship for an elastic-perfectly plastic material can be written as:

$$d\varepsilon_{ij} = d\varepsilon_{ij}^e + d\varepsilon_{ij}^p = \frac{dI_1}{9K} \delta_{ij} + \frac{ds_{ij}}{2G} + \chi \frac{dg}{d\sigma_{ij}} \quad (3.9)$$

where the superscripts “*e*” and “*p*” refer to the elastic and plastic components of the incremental strain, I_1 is the first invariant of the stress tensor, and G and K are respectively the shear and bulk moduli. Solving Eq. (3.9) for increments of stress deviator tensor s_{ij} , the stress increment tensor can be determined as:

$$d\sigma_{ij} = ds_{ij} + \frac{1}{3} dI_1 \delta_{ij} = 2G d\varepsilon_{ij} - 2G\chi \frac{dg}{d\sigma_{ij}} + \left(\frac{1}{3} - \frac{2G}{9K} \right) dI_1 \delta_{ij} \quad (3.10)$$

The consistency condition for an ideal plastic material can be derived by observing the fact that the yield function is fixed in the stress space: ie

$$df = \frac{\partial f}{\partial \sigma_{ij}} d\sigma_{ij} = 0 \quad (3.11)$$

Substituting Eq. (3.10) into the consistency condition (3.11) gives

$$2G \frac{\partial f}{\partial \sigma_{ij}} d\varepsilon_{ij} - 2G\chi \frac{\partial f}{\partial \sigma_{ij}} \frac{\partial g}{\partial \sigma_{ij}} + \left(\frac{1}{3} - \frac{2G}{9K} \right) dI_1 \frac{\partial f}{\partial \sigma_{ij}} \delta_{ij} = 0 \quad (3.12)$$

The following equation can be derived from Eq. (3.9):

$$dI_1 = 3K(d\varepsilon_{kk} - \chi \frac{\partial g}{\partial \sigma_{ij}} \delta_{ij}) \quad (3.13)$$

Substituting Eq. (3.13) into Eq. (3.12), the proportionality factor χ can be obtained as:

$$\chi = \frac{\frac{\partial f}{\partial \sigma_{ij}} d\varepsilon_{ij} + \frac{3K - 2G}{6G} d\varepsilon_{kk} \frac{\partial f}{\partial \sigma_{ij}} \delta_{ij}}{\frac{\partial g}{\partial \sigma_{mn}} \frac{\partial f}{\partial \sigma_{mn}} + \frac{3K - 2G}{6G} \left(\frac{\partial f}{\partial \sigma_{mn}} \delta^{mn} \right) \left(\frac{\partial g}{\partial \sigma_{mn}} \delta^{mn} \right)} \quad (3.14)$$

Therefore, the factor χ can be determined once the yield function f , the plastic potential function g , and strain increment $d\varepsilon_{ij}$ are known. When dI_1 in Eq. (3.13) is used, the stress increment can be presented as:

$$d\sigma_{ij} = 2Gde_{ij} + Kd\varepsilon_{kk}\delta_{ij} - \chi \left[\left(K - \frac{2}{3}G \right) \frac{\partial g}{\partial \sigma_{mn}} \delta_{mn} \delta_{ij} + 2G \frac{\partial g}{\partial \sigma_{ij}} \right] \quad (3.15)$$

The yield function and plastic potential function defined for geotechnical materials are generally expressed in terms of invariants of stress, I_1 , and stress deviator tensors, J_2 and J_3 , in the form:

$$f(\sigma_{ij}) = f(I_1, J_2, J_3) \quad (3.16a)$$

$$g(\sigma_{ij}) = f(I_1, J_2, J_3) \quad (3.16b)$$

Since

$$\frac{\partial I_1}{\partial \sigma_{ij}} = \delta_{ij} \quad (3.17a)$$

$$\frac{\partial J_2}{\partial \sigma_{ij}} = s_{ij} \quad (3.17b)$$

$$\frac{\partial J_3}{\partial \sigma_{ij}} = t_{ij} = s_{ik}s_{kj} - \frac{2}{3}J_2\delta_{ij} \quad (3.17c)$$

the following relation is obtained:

$$\frac{\partial f}{\partial \sigma_{ij}} = \frac{\partial f}{\partial I_1} \delta_{ij} + \frac{\partial f}{\partial J_2} s_{ij} + \frac{\partial f}{\partial J_3} t_{ij} \quad (3.18a)$$

$$\frac{\partial g}{\partial \sigma_{ij}} = \frac{\partial g}{\partial I_1} \delta_{ij} + \frac{\partial g}{\partial J_2} s_{ij} + \frac{\partial g}{\partial J_3} t_{ij} \quad (3.18b)$$

Substitution of Eq. (3.18) into Eq. (3.15) results in:

$$d\sigma_{ij} = 2Gde_{ij} + Kd\varepsilon_{kk}\delta_{ij} - \chi \left[3K \frac{\partial g}{\partial I_1} \delta_{ij} + 2G \left(\frac{\partial g}{\partial J_2} s_{ij} + \frac{\partial g}{\partial J_3} t_{ij} \right) \right] \quad (3.19)$$

where χ is defined as

$$\chi = \frac{1}{H} \left[3K \frac{\partial f}{\partial I_1} d\varepsilon_{kk} + 2G \left(\frac{\partial f}{\partial J_2} s_{kl} + \frac{\partial f}{\partial J_3} t_{kl} \right) d\varepsilon_{kl} \right] \quad (3.20)$$

in which

$$\begin{aligned}
H = & 9K \left(\frac{\partial f}{\partial I_1} \right) \left(\frac{\partial g}{\partial I_1} \right) + 4GJ_2 \left(\frac{\partial f}{\partial J_2} \right) \left(\frac{\partial g}{\partial J_2} \right) + 6GJ_3 \left(\frac{\partial f}{\partial J_2} \frac{\partial g}{\partial J_3} + \frac{\partial g}{\partial J_2} \frac{\partial f}{\partial J_3} \right) \\
& + 2G \left(s_{ik}s_{kj}s_{il}s_{lj} - \frac{4}{3}J_2^2 \right) \left(\frac{\partial f}{\partial J_3} \right) \left(\frac{\partial g}{\partial J_3} \right)
\end{aligned} \tag{3.21}$$

3.3.2 Stiffness formulation for Drucker-Prager yield surface

For direct use in a finite-element displacement formulation, Eq. (3.19) can be converted to the tensorial form as:

$$d\sigma_{ij} = C_{ijkl}^{ep} d\varepsilon_{kl} \tag{3.22}$$

where C_{ijkl}^{ep} is referred to as the elasto-plastic stiffness tensor which can be defined as

$$C_{ijkl}^{ep} = 2G\delta_{ik}\delta_{jl} + \left(K - \frac{2}{3}G \right) \delta_{ij}\delta_{kl} - \frac{1}{H} H_{ij}^* H_{kl} \tag{3.23}$$

in which

$$H = 9KAL + 2BG(2MJ_2 + 3NJ_3) + 2CG \left(3MJ_3 + Ns_{ik}s_{kj}s_{il}s_{lj} - \frac{4}{3}NJ_2^2 \right) \tag{3.24a}$$

$$H_{ij} = 3KA\delta_{ij} + 2G(Bs_{ij} + Ct_{ij}) \tag{3.24b}$$

$$H_{ij}^* = 3KL\delta_{ij} + 2G(Ms_{ij} + Nt_{ij}) \tag{3.24c}$$

The parameters used in Eq. (3.24) can be obtained from the following relations:

$$A = \frac{\partial f}{\partial I_1}, \quad B = \frac{\partial f}{\partial J_2}, \quad \text{and} \quad C = \frac{\partial f}{\partial J_3} \tag{3.25a}$$

$$L = \frac{\partial g}{\partial I_1}, \quad M = \frac{\partial g}{\partial J_2}, \quad \text{and} \quad N = \frac{\partial g}{\partial J_3} \tag{3.25b}$$

For the Drucker-Prager yield criterion, the yield function and the plastic potential function are defined as:

$$f(\sigma_{ij}) = \sqrt{J_2} + \alpha_1 I_1 - \beta \quad (3.26)$$

$$g(\sigma_{ij}) = \sqrt{J_2} + \alpha_2 I_1 \quad (3.27)$$

Therefore, the coefficients of the constitutive model used in Eq. (3.24) can be derived as:

$$A = \alpha_1, \quad B = \frac{1}{2\sqrt{J_2}} \quad \text{and} \quad C = 0 \quad (3.28a)$$

$$L = \alpha_2, \quad M = \frac{1}{2\sqrt{J_2}} \quad \text{and} \quad N = 0 \quad (3.28b)$$

3.3.3 Computational procedure

Nonlinear problems are generally analyzed using incremental techniques in which a series of piecewise linear problems are solved in each increment after updating the constitutive tensor. In the current study, a procedure that includes incremental and iterative techniques is used to determine the stress state after each strain increment.

In elastic-perfectly plastic models, the material behaves elastically until the state of stress reaches the yield surface. Thus, for any incremental strain at any Gaussian integration point, the increment of stress is computed by using an elastic constitutive relationship as long as the state of stress remains within the yield surface: i.e.

$$f(\{\sigma_0\} + \{\Delta\sigma\}) < 0 \quad (3.29)$$

where $\{\sigma_0\}$ is the state of stress prior to the increment and $\{\Delta\sigma\}$ is the stress increment that results from the incremental strain $\{\Delta\epsilon\}$. For certain strain increments, the state of stress, numerically computed considering the elastic response, can go outside the yield surface; that is $f(\sigma) > 0$. For this case, the material behaves elastically until it reaches the yield criterion, after which it deforms elasto-plastically and the incremental stress can be computed as:

$$\{\Delta\sigma\} = S[C^e]\{\Delta\epsilon\} + (1-S)[C^{ep}]\{\Delta\epsilon\} = \{\Delta\sigma_1\} + \{\Delta\sigma_2\} \quad (3.30)$$

where S is the scaling factor corresponding to the fraction of strain increment that brings the state of stress to the yield surface, $[C^e]$ and $[C^{ep}]$ are the elastic and elasto-plastic stiffness tensors, respectively.

Derivation of scaling factor needed to reach the yield surface

For strain increments for which the transition from elastic to plastic states occurs, a procedure has to be implemented to determine the fraction of strain increment that brings the state of stress, at each integration point, to the yield surface. In this case, the load increment is subdivided into two parts, a fully elastic portion and an elastic-plastic portion, which governs the behavior after the yield surface has been reached. Zienkiewicz et al. (1969) presented a method in which a stress factor r is determined using a linear interpolation and acknowledging the fact that the fractional stress $r\{\Delta\sigma\}$ brings the stress point to the yield surface. That is:

$$f(\{\sigma_0\} + r\{\Delta\sigma\}) = 0 \quad (3.31)$$

Since Zienkiewicz et al. (1969) considered elastic behavior prior to reaching the yield surface, the stress factor r is also the fraction of the strain increment that brings the state of stress to the yield surface, which implies that, $S = r$. In a further study, Nayak and Zienkiewicz (1972) presented another method to calculate this value using higher-order interpolation, which can be used in the case of nonlinear yield functions. Siriwardane and Desai (1983) also used this method to derive a scaling factor for Drucker-Prager and the critical state models; however, this method results in an inaccurate value of S when nonlinearity is considered either for the yield function or for the elastic part of the constitutive model (e.g. nonlinear hypoelastic model).

In this research, a further method was developed to find the scaling factor for the hypoelastic-plastic constitutive model. This method appears to be more efficient in the computations than the linear interpolation method previously discussed. The scheme involved dividing the strain increment into subincrements within the UMAT material subroutine, in the ABAQUS/ Standard finite element code, when the stress increment was calculated for each integration point. Due to the hypoelastic response considered in the constitutive model, the stiffness tensor constantly changes during the loading process;

therefore, the stress increment and the new stiffness tensor are calculated in each subincrement. After updating the stress tensor in each subincrement, the state of the stress was investigated to determine its position in relation to the yield surface. The transition from elastic to plastic states occurs when, in one subincrement, the calculated stress state reaches a point beyond the elastic domain. In this case, the hypoelastic calculation is interrupted and the hypoelastic-plastic stiffness tensor is used to determine the stress increment using the remaining portion of strain increment. In the method presented in this study, dividing the strain increments into 1000 subincrements is equivalent to the calculation of a scaling factor with an accuracy of ± 0.001 , which is considered sufficiently accurate for the computational purposes.

The stress increment after reaching the yield criterion

The computation of $\{\Delta\sigma_2\}$ given in Eq. (3.30) requires an integration process since $[C^{ep}]$ changes with the state of stress. This can be done by dividing the strain interval $(1-S)\{\Delta\epsilon\}$ into a number of subincrements and calculating the stress increment as:

$$\{\Delta\sigma_2\} = \sum_1^n \frac{(1-S)}{n} [C^{ep}] \{\Delta\epsilon\} \quad (3.32)$$

where n is the number of subincrements considered in the plastic portion of the strain increment. The accuracy of the computation in the hypoelastic-plastic part depends upon the size of the strain subincrements; i.e., the computed stress may lie outside the yield surface due to the changes in hypoelasto-plastic stiffness tensor $[C^{ep}]$. A special procedure is used to bring the stress state back to the yield surface, along the direction that is normal to this surface. When the state of stress is outside the yield surface, the value of the yield function is a positive value; let this value be f_1 . Therefore, a change in the yield function can be expressed as:

$$df = \frac{\partial f}{\partial \sigma_{ij}} d\sigma_{ij} \quad (3.33)$$

where $\frac{\partial f}{\partial \sigma_{ij}}$ is the gradient of the yield surface. Since the stress state calculated in the first approximation is outside the yield surface, it can be substituted in the tensorial form of Eq. (3.33) to give

$$0 - f_1 = -f_1 = \left\{ \frac{\partial f}{\partial \sigma} \right\}^T \{ d\sigma \} \quad (3.34)$$

Therefore, the change of stress increment required to bring the state of stress back to the yield surface can be evaluated as follows:

$$\{ d\sigma \} = \frac{-f_1 \left\{ \frac{\partial f}{\partial \sigma} \right\}}{\left\{ \frac{\partial f}{\partial \sigma} \right\}^T \left\{ \frac{\partial f}{\partial \sigma} \right\}} \quad (3.35)$$

Since the gradient is calculated based on the state of stress outside the yield surface, it may not be exactly normal to the yield surface. Therefore, the first iteration may not bring the stress point back to the yield surface. Hence, a further iteration may be needed to bring the stress point within a prescribed tolerance. The tolerance is usually defined as a function of β , in which β is the parameter of the Drucker-Prager yield function defined in Eq. (3.26). There are other computational schemes that achieve this return mapping procedure and recent studies are given by Simo and Hughes (1998), Borja and Lee (1990), Borja (1991) and Wang et al. (2004).

3.3.4 Hypoelastic-perfectly plastic model for ballotini

The mechanical behavior of geomaterials has been investigated in different experimental efforts; it has been shown that the constitutive properties of soils can be the function of the state of the material as expressed by stress and strain states. Hypoelasticity is a constitutive model in which the increment of stress can be expressed as a function of stress, strain and the increment of strain. A special form of the hypoelastic model can be written as:

$$d\sigma_{ij} = f(\varepsilon_{kl}, d\varepsilon_{kl}) \quad (3.36)$$

Therefore, in indicial notation, the hypoelastic constitutive law can be written as:

$$d\sigma_{ij} = C_{ijkl}^{he} d\varepsilon_{kl} \quad (3.37)$$

where C_{ijkl}^{he} is the hypoelastic stiffness tensor, which is a function of the strain tensor or invariants of the strain tensor. To incorporate the hypoelastic model within a plasticity formula, different modifications had to be applied to the computational procedure. The first modification involved the subincremental procedure for calculating the elastic deformation when the stress state lies within the yield surface. Hence, the hypoelastic stiffness tensor $[C^{he}]$ was updated in each subincrement based on the constitutive relations presented for the stiffness parameters. After the stress state reached the yield surface, further stress increments could be calculated considering the hypoelasto-plastic stiffness tensor $[C^{hep}]$. In each subincrement, the state of stress, determined from the new stiffness tensor and strain increment, was scaled back to the yield surface using the procedure described in the previous section. When hypoelastic behavior is considered for the material, this tensor was recalculated in each subincrement based on the state of stress and strain, which can alter the constitutive characteristic of the material. The computational flow chart for the implementation of the hypoelastic-perfectly plastic model is shown in Figure 3.14.

Table 3.2 gives the parameters of the hypoelastic-perfectly plastic constitutive model used in the computations. The hypoelastic-perfectly plastic model presented in this study for ballotini contains six parameters. The elastic parameters are Young's modulus E and Poisson's ratio ν . The results of oedometer compression and triaxial compression tests shown in Figure 3.8 were used to define the elastic modulus E as a bi-linear function of the void ratio e . In each subincrement, the void ratio is calculated from the volumetric strain and the initial void ratio e_0 defined as a model parameter. Further parameters presented in this model are α_1 and β used to define the Drucker-Prager yield surface. These parameters can be expressed in terms of internal friction angle ϕ and cohesion of the material c obtained from triaxial compression tests as follows:

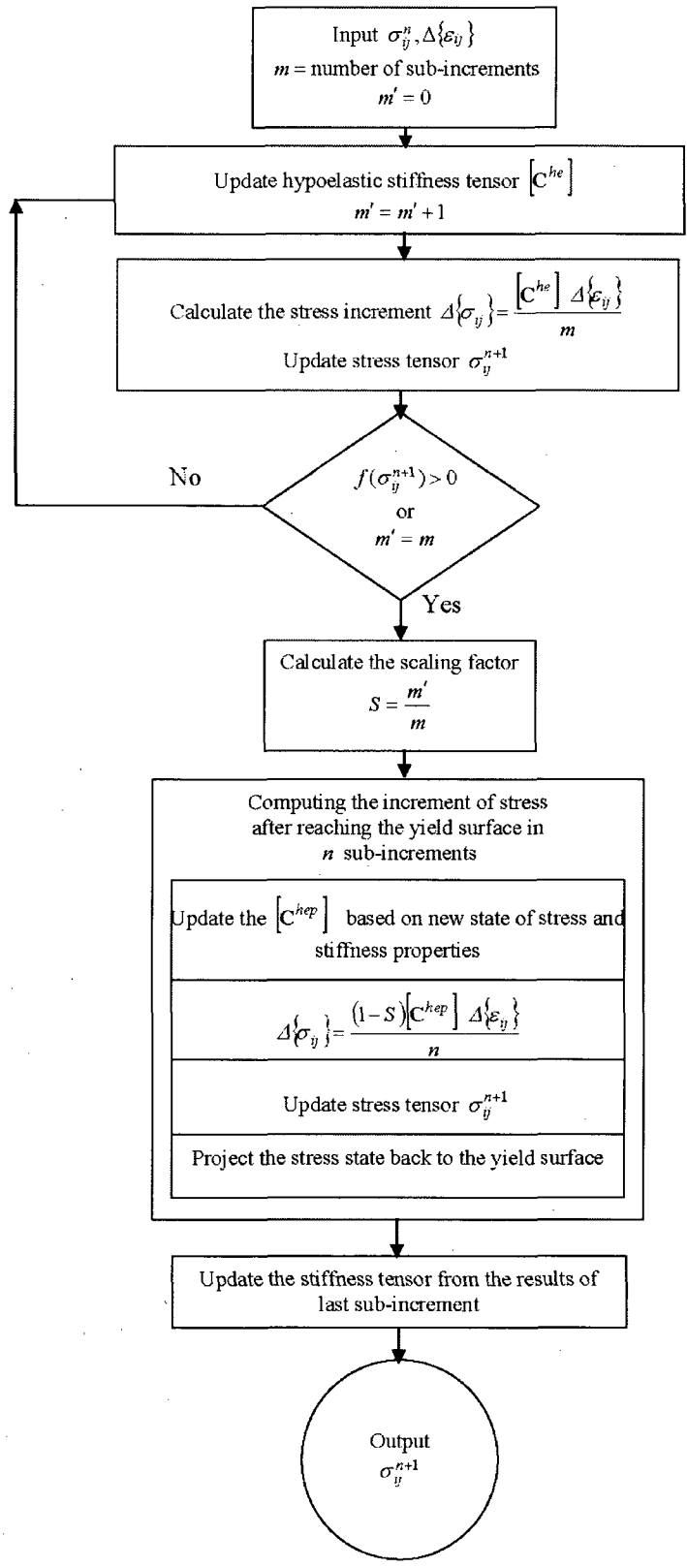


Figure 3.14 Flow chart for the implementation of hypoelastic-perfectly plastic model

Table 3.2 Model parameters derived for ballotini

parameters	value	
Elastic modulus E (kPa)	$e > 0.605$	27000
	$e < 0.605$	$(6.24-10.25 e) \times 10^6$
Initial void ratio e_0	different in each test	
Poisson's ratio ν	0.3	
Yield function parameters Eq. (3.26)	α_1	0.298
	β	0
Plastic function parameter Eq. (3.27)	α_2	0.034

$$\alpha_1 = \frac{2 \sin \phi}{\sqrt{3}(3 - \sin \phi)} \quad (3.38)$$

$$\beta = \frac{6c \cos \phi}{\sqrt{3}(3 - \sin \phi)} \quad (3.39)$$

The dilation angle ψ obtained from the results of the triaxial compression test can be used to determine α_2 , [used in Eq. (3.27)] that defines the plastic potential function: Considering the result given by Christian and Desai (1977):

$$\alpha_2 = \frac{2 \sin \psi}{\sqrt{3}(3 - \sin \psi)} \quad (3.40)$$

The material parameters determined from the test data can now be used to duplicate the experimental response of the material subjected to different stress states. To simulate the material response in the triaxial compression test, the triaxial specimen was modeled using the ABAQUS/Standard (2005) program. In this computational simulation, due to the symmetry of the problem, one fourth of the top portion of the axisymmetric domain was modeled by 240, 20-node quadratic brick elements (Figure 3.15). The reason for conducting the three-dimensional modeling is that the general purpose UMAT material subroutine in ABAQUS was coded on the basis of a three-dimensional formulation.

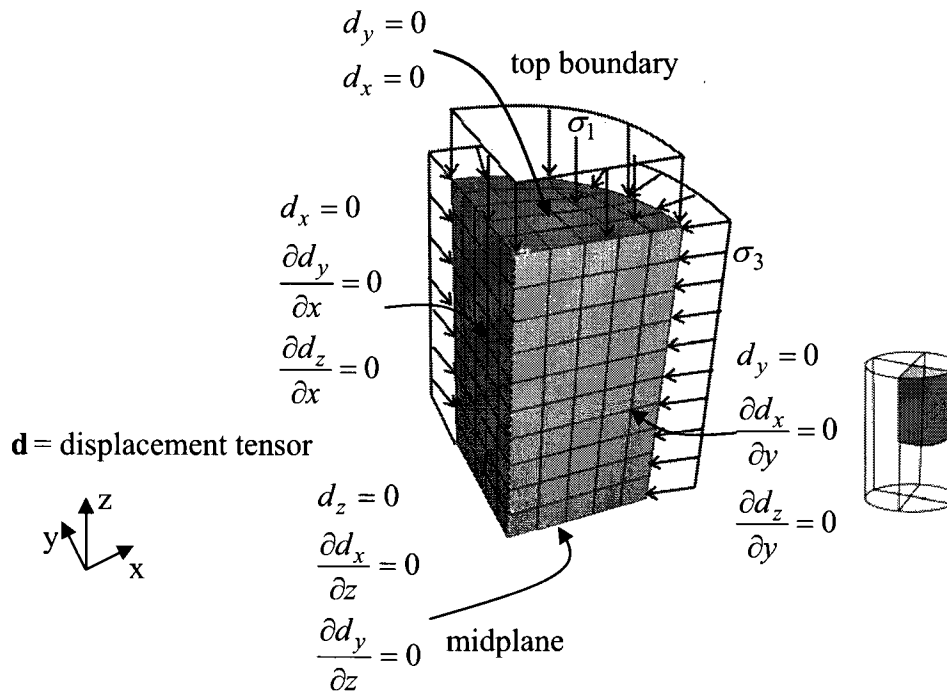


Figure 3.15 Finite element model of the triaxial sample

From the results of triaxial compression tests, only the secant modulus, E_{50} , obtained from the initial part of the stress-strain curves was taken into account; however, the isotropic compression of the samples during the application of confining pressure was not considered in the derivation of the expression for the elastic stiffness. Therefore, the computational simulation of the triaxial tests, that includes both isotropic compression and shearing phases, cannot be considered as a pure duplication of the experimental responses. The computations simulated the drained condition, considering boundary conditions applicable to the triaxial specimen. To simulate the tests conducted at different stress states, the initial void ratio of the sample was set to the value calculated during the sample preparation. After applying the confining pressures, the model was subjected to additional stresses by moving the top boundary downward while this boundary was restrained from moving laterally. Figure 3.16 shows the comparison between the results of the computational modeling and the corresponding test data. The computations had to be capable of simulating the initial mechanical response, prior to failure, and the strength characteristics of the material corresponding to the state of failure. The failure stress, which was assumed to be the attainment of the peak deviator stress, compared well with

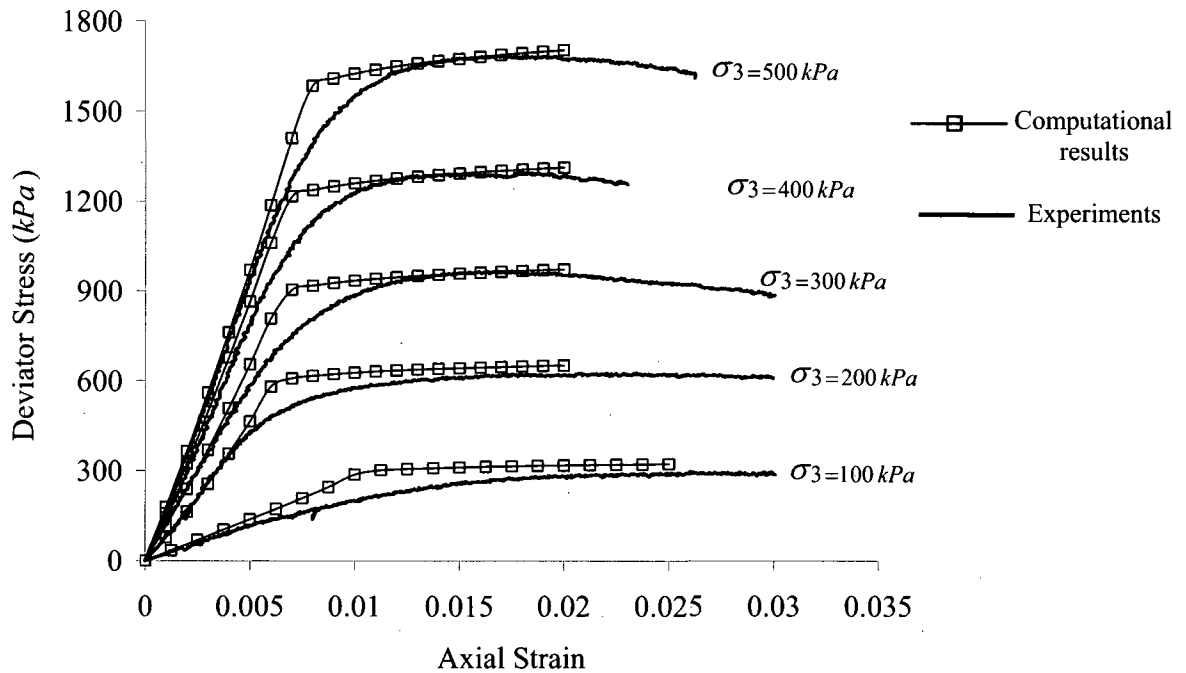


Figure 3.16 Constitutive representations of the stress-strain responses of the triaxial samples subjected to different confining pressures

that obtained from experimental investigations. Furthermore, reasonable correlation was observed for the stiffness characteristics of the material before failure, corresponding to the initial slope of the stress-strain curves. Therefore, the representations correlate well with the experimental data obtained for triaxial tests conducted at different confining pressures.

Further experimental results used to identify the elastic stiffness expression were obtained from oedometer bench-scale tests conducted on both saturated and dry specimens. To simulate the bench-scale test, a cylindrical model was subjected to oedometric compression. Figure 3.17 shows the variation of the void ratio with the axial load obtained from the computational simulation compared with the corresponding test data. The exercise yields satisfactory correlation between experimental results and computational simulations.

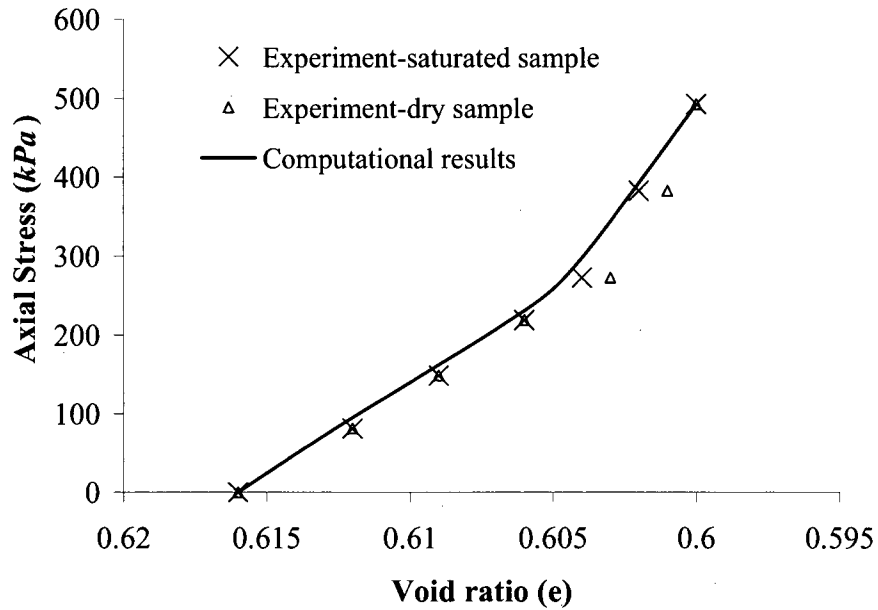


Figure 3.17 Constitutive representation of the variation of void ratio with axial stress in oedometer bench-scale tests

3.3.5 The prediction of the mechanical response of ballotini

A constitutive model that accounts for nonlinear elastic behavior and plastic behavior has been developed for modeling the mechanical response of ballotini. Since the experimental data obtained from isotropic compression tests were not considered in parameter identification, these results can be used to validate the constitutive model developed for ballotini. The predictive capability of the nonlinear formulation used for the elastic response of the material can be examined through comparison of experimental results obtained from isotropic compression tests with computational results.

The sample in the isotropic compression test was simulated by a single element subjected to uniform pressure applied to all the boundaries. Figure 3.18 shows the variation of the void ratio with confining pressure predicted in the computations for two specimens with different initial void ratios. The comparison between the computational results and corresponding test data indicates satisfactory predictions that validate the nonlinear expression defined for the elastic behavior of ballotini. In the computational analyses, the

volumetric strain induced in the model was only due to the elastic deformation of the model, since in the isotropic compression test, the loading path corresponds to the diagonal of the principal stress space and it cannot reach the Drucker-Prager yield function defined for ballotini. Therefore, computations gave identical curves for the loading and unloading cycles in isotropic compression tests. In other words, the developed constitutive model cannot predict the plastic compression observed in two loading-unloading cycles of the isotropic compression tests (Figure 3.8).

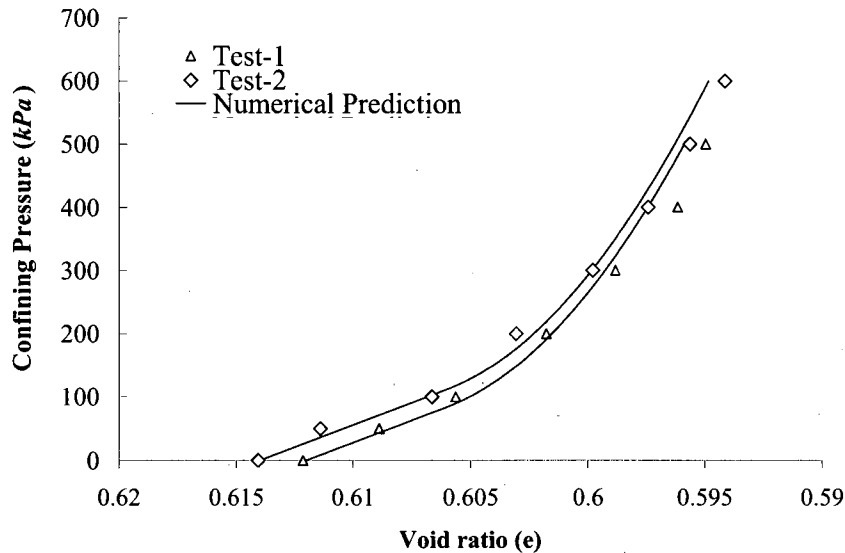


Figure 3.18 Computational predictions for the compression behavior of ballotini samples subjected to isotropic compression

In the previous section, the results of a series of triaxial tests were used to develop a plausible constitutive model that incorporates both stiffness and strength characteristics of the material. Considering the dilation behavior of the ballotini observed in the triaxial tests, the direction of the plastic strain vectors is defined through a non-associated flow rule that uses a plastic potential function, to which the incremental plastic strain vector is orthogonal. The parameters of the constitutive model, identified using a part of the experimental results, were used to predict the mechanical response of the further triaxial tests conducted on the ballotini specimens. The tests conducted at 400 kPa and 500 kPa confining pressures included the unloading-reloading cycles carried out after reaching the peak deviator stress. The computations attempted to predict the response of the material

during isotropic compression, loading, unloading and reloading phases. The same finite element model and boundary conditions shown in Figure 3.15 were used in this analysis. Figure 3.19 depicts the stress-strain response predicted using computational modeling compared with the experimental results; it is shown that the computations gave reasonable estimations for the peak strength of the samples. Furthermore, the computations show a satisfactory prediction of the stress-strain response at the unloading-reloading stage, while it slightly underestimates the irreversible axial deformation of the sample subjected to 400 *kPa* confining pressure. Therefore, the comparisons between the computed and experimental results indicate that the computations provide a satisfactory prediction of the trends in the stress-strain response during different stages of the triaxial compression test.

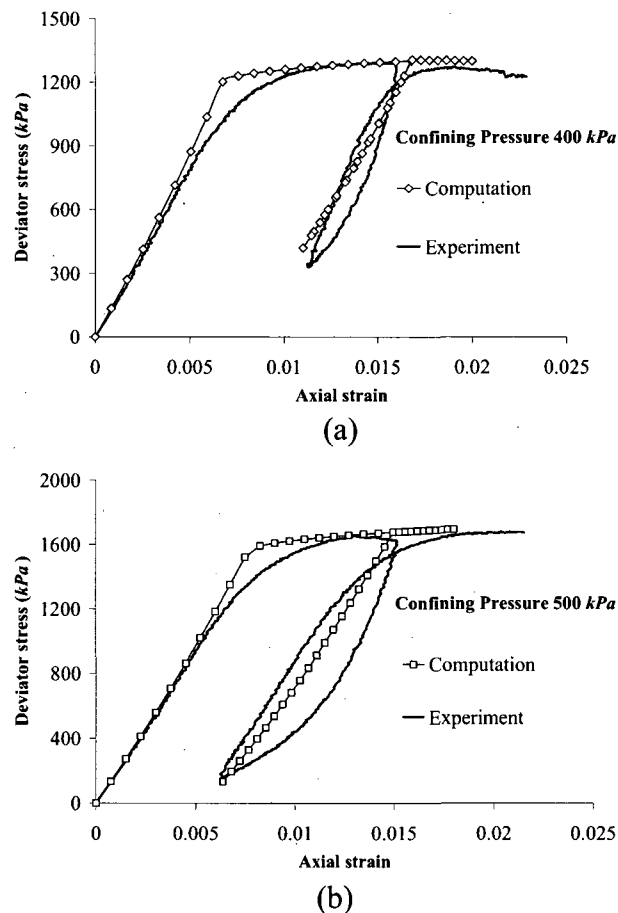


Figure 3.19 Computational predictions for the stress-strain responses in triaxial compression tests conducted on ballotini

3.4 Summary remarks

The accurate modeling of the mechanical response of granular soils is required to predict the behavior of various soil structures, such as natural slopes, earth dams, pavement structures and foundations. Ballotini is an artificial particulate material with a uniform grain size distribution that can, in experimental investigation, represent a coarse-grained soil. The results of the experiments, conducted in connection with this research, indicate that in the loose condition the ballotini exhibits low stiffness properties, whereas the stiffness of the material increases at higher densities; this is mainly attributed to the compression of the material due to the sliding and rolling of the particles. Furthermore, the irreversible deformation of the material in the triaxial tests was investigated by conducting an unloading cycle after the failure of the specimens. The development of a constitutive model for characterizing the nonlinear elastic and irreversible plastic behavior observed in the experiments was approached through the consideration of an elastic-perfectly plastic model that was modified to account for the nonlinear elastic behavior of the material.

In this chapter, the results of a series of triaxial and oedometer compression tests were used to identify the parameters for a plausible constitutive model that incorporates both nonlinear elastic and plastic responses of ballotini. A UMAT material subroutine that can be used in advanced computations by incorporating the nonlinear elastic-perfectly plastic concept and considering the non-associative flow rule that governs the evolution of plastic deformations was developed. The parameter identification was first conducted using a subset of the experimental data. The remaining data set was used to validate the proposed constitutive model. The calibration exercise yielded satisfactory correlations between the predictions and experiments in the range of stresses considered in the tests. Therefore, the capabilities of the model in correlating the mechanical responses of the material permit the use of this constitutive model in the study of composite media containing this material.

CHAPTER 4

MECHANICAL BEHAVIOR OF A COMPOSITE CONTAINING SPHERICAL CLAY INCLUSIONS

4.1 Introduction

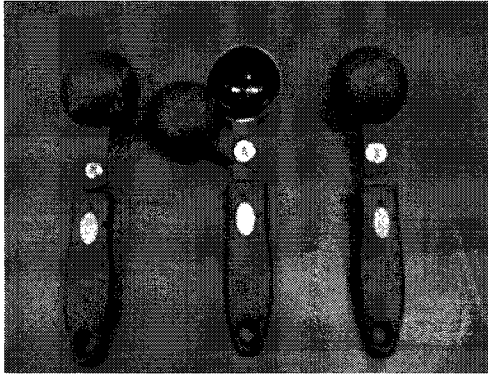
In land reclamation projects, the clay lumps dredged from the seabed using a clam-shell dredge are deposited as fill material to construct the built-up reclaimed regions. Since such clay lumps are placed in an uncompacted manner, there are large voids present in the reclaimed fills. A problem of major concern to geotechnical application of the construction technique relates to void closure associated with either self-weight compaction of the reclaimed land or the settlement resulting from void closure. The results of the field investigation conducted on the reclaimed fills consisting of barge dumped clay lumps (lumpy fills) showed that significant portion of vertical and horizontal movements take place due to the nature of the fill, which consisted of large blocks of clay with interspersed large voids that had not been completely filled by the suspended material (Hartlen and Ingers, 1981; Karthikeyan et al., 2004). The load-settlement response of the lumpy fills investigated in one-dimensional compression tests also indicated that lumpy fills experienced significant settlement compared to homogeneous clay, due to the closing-up of inter-lump voids (Leung et al., 2001; Robinson et al., 2005). A recommended procedure for reducing large settlements in reclaimed fills is to subject the fills to preloading to induce large settlement prior to performing any construction activity. Another improvement technique proposed in this study is to use a granular soil to fill the inter-lump voids during placement of the clay lumps. This coarse-gained filler soil can improve the mechanical characteristics of the fills, under self-weight and structural loads, by reducing the initial settlement induced due to the closure of inter-lump voids. Furthermore, in a composite fill, the presence of the filler material increases the rate of consolidation compared to a homogeneous clay fill whose inter-lump voids close up during the initial stages of the loading.

The idealized composite lumpy fill considered in this study is a coarse-grained medium interspersed with spherical clay inclusions. This chapter describes the experimental program to examine the oedometric mechanical behavior of a composite specimen fabricated with number of silty clay spheres placed within a granular ballotini region and tested in the bench-scale setup described in Chapter 3. The research also describes a computational study that incorporates the constitutive models, developed in Chapters 2 and 3 for silty clay and ballotini, to predict the behavior of the tested oedometric sample. This problem serves as a useful tool for assessing the influence of fine-grained inclusions on the mechanical response and stress distribution that occurs within the composite sample. The experiments also provide useful test data that can be compared with the numerical results to establish the predictive capabilities of the methodology adopted for the computational modeling.

4.2 The test facility and sample preparation

The bench-scale oedometric compression test facility described in 3.2.4 was designed to apply an axial static load to the composite sample fabricated within the cylindrical oedometer cell. The experiments were conducted on a composite sample fabricated using a number of clay spheres placed within the ballotini region. A reconstituted silty clay soil, with a moisture content near its liquid limit ($LL = 25\%$), was used in the preparation of the clay spheres. To prepare the spheres, the clay paste was placed in two hemispherical plastic molds, with an internal diameter of 3.7 cm , using a spatula (Figure 4.1 a,b) and the two silty clay hemispheres were joined by clamping the two halves of the molds (Figure 4.1 c). The specimens and the mold were then placed in a seal bag and kept inside a cold room with an approximate temperature of $-10\text{ }^{\circ}\text{C}$ for one day. After this period, the frozen spheres were extracted from the molds using a heat gun (Figure 4.1d). The consistency of the frozen spheres was estimated by measuring the moisture content of four frozen spheres, which ranged between 24.4% and 25.1%.

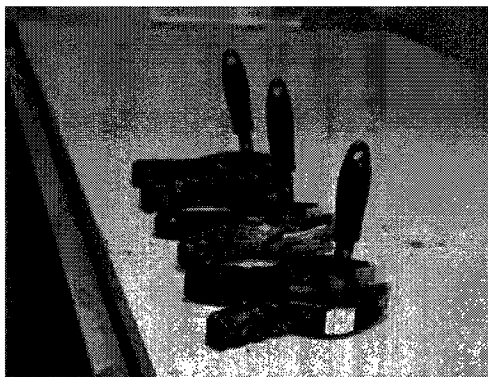
The composite sample was fabricated in a stainless steel cylindrical cell with an internal diameter of 15.2 cm . This sample consisted of 36 clay spheres interspersed in granular ballotini in 4 identical layers with an approximate height of 4.2 cm (Figure 4.2). A



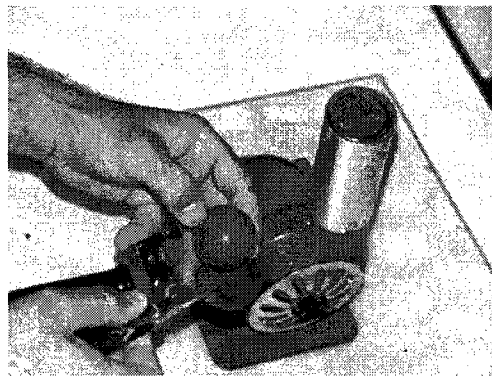
(a)



(b)



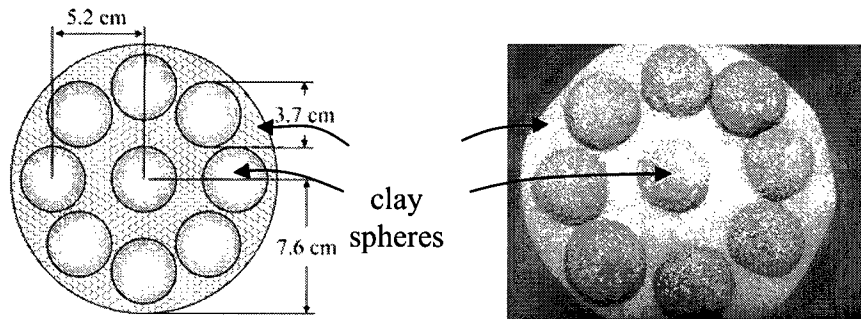
(c)



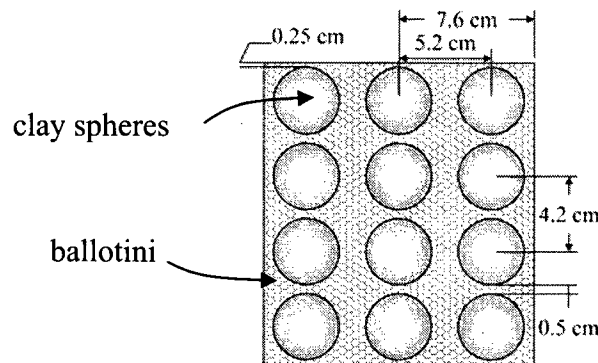
(d)

Figure 4.1 Preparation of the clay spheres used in fabrication of the composite sample

cardboard template was used to place the frozen spheres in a symmetric configuration. The total height of the composite specimen was 16.8 cm and the volume proportion of clay ($V_{\text{clay}}/V_{\text{total}}$) was 31%. The sample was saturated with deaired water, and the water level in the consolidation cell was maintained at the upper level of the sample for a period of 2 days prior to the application of the load. Computations indicate that a frozen clay sphere will thaw completely within 3 minutes ; the volumetric heat capacity and thermal conductivity of the frozen clay are taken as $2.7 \times 10^6\text{ J/m}^3(^{\circ}\text{C})$ and $0.6\text{ W/mK} (^{\circ}\text{C})$, respectively (see, e.g., Selvadurai et al., 1999). During the application of the load, proper drainage was ensured by incorporating two layers of geotextile at the upper and lower surface of the samples, which were connected to the draining vent at the top and the water container at the bottom.



(a) Plane of the fabricated composite specimen



(b) Schematic side view of the fabricated composite specimen

Figure 4.2 Fabricated composite specimen

To initiate oedometric consolidation of the soil composite, the bench-scale loading frame detailed in Chapter 3 was used. This setup is capable of applying axial uniform stresses of up to 493 kPa corresponding to a 273 kg dead weight placed on the weight rack. The initial stress on the sample resulting from the weight of the lever arm, plunger, weight rack and other accessory parts connected to the lever arm was approximately 81 kPa . The axial stress on the sample was increased in five loading steps to 149 , 219 , 273 , 383 and 493 kPa by adding weights to the loading rack. The axial load applied to the sample was measured using a load cell with a peak capacity of 44.5 kN (10 kips). To minimize the development of dynamic effects in the loading process, the load was gradually increased using a scissor jack installed in the loading frame.

The problem of the consolidation of a clay sphere was investigated by Cryer (1963). In this study, a sphere subjected to a confining stress of 20 kPa was modeled in ABAQUS/Standard (Figure 4.3). The *Modified Cam clay* constitutive model with the parameters obtained in Chapter 2 for Montreal reconstituted silty clay was used in the

computational modeling. The hydraulic conductivity of the silty clay was taken as $2 \times 10^{-8} \text{ cm/s}$ and $2 \times 10^{-7} \text{ cm/s}$ corresponding to the range of hydraulic conductivities estimated at different stress states (Table 2.4). The variation of the pore pressure generated at the center of the sphere is shown in Figure 4.3. The results indicate that for both values of hydraulic conductivity, no excess pore pressure was computed at location A after a period of one day. Therefore, at each load step, the axial stress was maintained for a period of approximately one day to allow for dissipation of excess pore water pressure generated within the composite sample and mainly within the clay spheres.

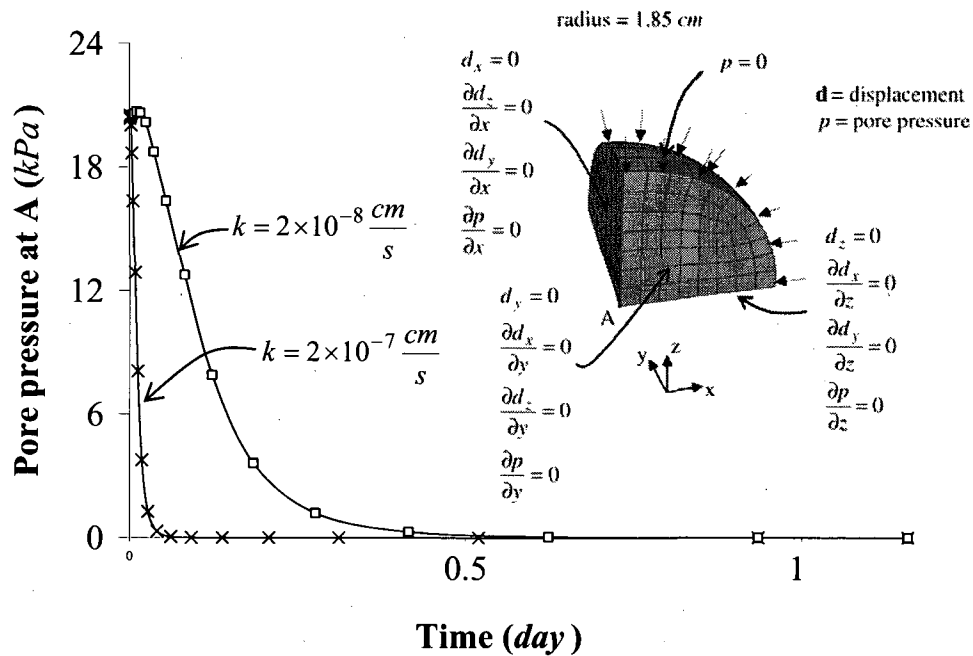


Figure 4.3 Consolidation of a silty clay sphere subjected to a confining stress

4.3 Experimental results

The axial deformation of the composite specimen forms important test data that can be used in the calibration of the computational predictions. During each load step, the axial stress on the sample was increased, and the axial deformation of the sample was continuously recorded through two LVDT transducers connected to a data acquisition system. Figure 4.4 shows the time-dependent settlement response of the composite

sample compared with that of a homogeneous ballotini specimen. The results indicate that the presence of clay inclusions within the ballotini gave rise to a greater axial deformation of the composite; the axial settlement of the composite sample during five consecutive load steps was approximately 1.56 mm, which is about 27% higher than that which occurred in the homogeneous ballotini specimen.

During the application of stress on composite fills containing soft clay inclusions enclosed by a granular region, a mixture interface can develop at the boundary of the two materials as a result of penetration of the particulate phase into the soft clay lumps. The influence of such interfaces on the overall consolidation responses have recently been arrived by Selvadurai (2008). In this study, the development of this mixture interface was investigated by dissecting the composite samples at the termination of the tests. The oedometer sample was drained and dried by connecting an air pump to the draining vent fabricated in the plunger. The flow of the air was maintained for 2 days to ensure that the sample was completely dry and the dried ballotini would be easily extracted from the consolidation cell using a vacuum pump, leaving the surfaces of the clay spheres exposed. A visual inspection indicated that there was no measurable penetration of the ballotini grains into the clay inclusions at the stress levels associated with this experiment, although a layer of ballotini beads had adhered to the surface of the clay spheres; these could be easily removed from the clay surface (Figure 4.5).

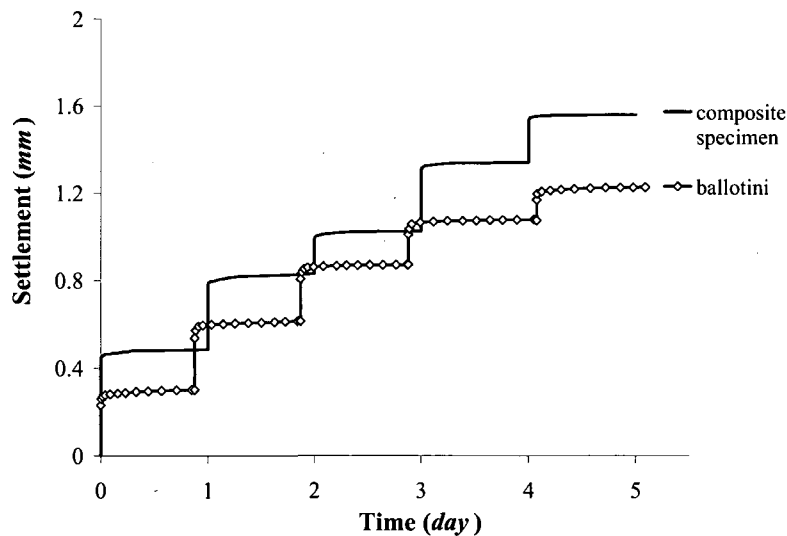


Figure 4.4 Axial settlement of the composite and homogenous ballotini samples in five successive load steps

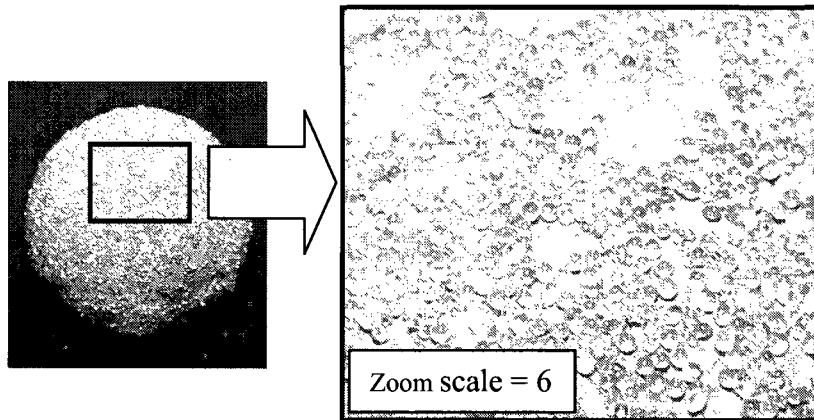


Figure 4.5 Ballotini-clay interface at the termination of the oedometer test

4.4 Computational modeling of fluid-saturated media

Many geotechnical engineering problems include time-dependent mechanical responses of soil media associated with the expulsion of the pore fluid pressure, which depends on hydraulic properties of the material and the associated boundary conditions. To account for this behavior it is necessary to couple the equations governing mass conservation, the flow of pore fluid through the soil skeleton, the constitutive equations governing the mechanical behavior of the soil skeleton and the equations of equilibrium. Such theories are called coupled formulations, as it essentially couples the pore fluid flow and stress-strain behavior encountered in a porous region. This section briefly describes the constitutive equations and coupled formulation used in the finite element analysis. Further details of developments in fluid saturated poro-elastic, poro-elastoplastic media are given by Coussy (1995), Selvadurai (1996a, 2007), Lewis and Schrefler (1998) and Auriault et al. (2002).

4.4.1 Constitutive equations

Under the assumption of small-strain theory, the equation of equilibrium for quasi-static conditions can be written as

$$\nabla[\boldsymbol{\sigma}] + \rho\{\mathbf{g}\} = 0 \quad (4.1)$$

where $[\sigma]$ is the 3×3 total stress tensor and ρ is the average density of the multiphase system defined as

$$\rho = (1 - n)\rho^s + n\rho^w \quad (4.2)$$

where ρ^s and ρ^w are, respectively, densities of the solid phase and water, n is the porosity and $\{\mathbf{g}\}$ is an acceleration vector usually related to the gravitational effects.

A continuity equation is also required for the liquid phase, equating the rate of increase in liquid mass stored at a point to the rate of mass of liquid flowing into the point within the time increment. Due to the fully saturated condition of the domains modeled in this study, the continuity equation is defined for a fully saturated medium as

$$\nabla \cdot \{\mathbf{v}\} - Q = \frac{\partial \varepsilon_v}{\partial t} \quad \text{or} \quad \frac{\partial v_x}{\partial x} + \frac{\partial v_y}{\partial y} + \frac{\partial v_z}{\partial z} - Q = \frac{\partial \varepsilon_v}{\partial t} \quad (4.3)$$

where v_x , v_y and v_z are the components of the superficial velocity of the pore fluid in the coordinate directions, ε_v is the volumetric strain, and Q represents any sources or sinks. The liquid flow is also described by introducing the generalized Darcy's law:

$$\{\mathbf{v}\} = -[\mathbf{k}]\{\nabla h\} \quad \text{or} \quad \begin{Bmatrix} v_x \\ v_y \\ v_z \end{Bmatrix} = - \begin{bmatrix} k_{xx} & k_{xy} & k_{xz} \\ k_{xy} & k_{yy} & k_{yz} \\ k_{xz} & k_{yz} & k_{zz} \end{bmatrix} \begin{Bmatrix} \frac{\partial h}{\partial x} \\ \frac{\partial h}{\partial y} \\ \frac{\partial h}{\partial z} \end{Bmatrix} \quad (4.4)$$

where h is the hydraulic head defined as

$$h = \frac{P_f}{\gamma_f} + (xi_{Gx} + yi_{Gy} + zi_{Gz}) \quad (4.5)$$

Vector $\{\mathbf{i}_G\} = \{i_{Gx} \ i_{Gy} \ i_{Gz}\}^T$ is the unit vector parallel, but in the opposite direction to gravity; and k_{ij} are the components of the symmetric hydraulic conductivity matrix of the soil $[\mathbf{k}]$. In the case of isotropy in the hydraulic conductivity of the material, $k_{xx} = k_{yy} = k_{zz} = k$ and $k_{xy} = k_{xz} = k_{yz} = 0$.

The constitutive relationship of the skeleton is the additional equation that has to be considered in the analysis of the porous medium. When the material behavior is defined in terms of total stress, the constitutive tensor $[\mathbf{D}]$ can be obtained relatively straightforwardly; however, defining the material characteristics in terms of effective stress, which is the preferred approach in soil mechanics, gives rise to additional complications. If the soil region behaves in a way other than either fully drained or undrained conditions, account must be taken of the time dependency of the changes in pore fluid pressure and effective stress. Considering the porous medium as a multiphase material and adopting an effective stress principle to describe its behavior, the total stress tensor in pseudovector form $\{\boldsymbol{\sigma}\}$ acting at a point is assumed to be made up of an average pressure in the pore fluid p_f , called the pore fluid pressure, an average pressure in the gas phase p_a , and an effective stress tensor $\{\boldsymbol{\sigma}'\}$ defined by

$$\{\boldsymbol{\sigma}'\} = \{\boldsymbol{\sigma}\} + (\xi p_f + (1 - \xi)p_a)\mathbf{I} \quad (4.6)$$

For the components of the stress tensor it is assumed that the tensile stress is positive. The value of ξ depends on the degree of saturation; it is equal to 1.0 when the medium is fully saturated and between 0.0 and 1.0 in an unsaturated condition. It can be assumed that the constitutive response of the porous medium consists of simple bulk elasticity relationships for the liquid and for the soil grains, together with a constitutive model for the soil skeleton; however, many geotechnical analyses deal with soils in a saturated condition with incompressible characteristics considered for the pore fluid and soil grains. Using the principle of effective stress, the constitutive equation becomes:

$$\{\Delta\boldsymbol{\sigma}\} = [\mathbf{D}']\{\Delta\boldsymbol{\varepsilon}\} + \{\Delta\boldsymbol{\sigma}_f\} \quad (4.7)$$

where $[\mathbf{D}']$ is the effective constitutive matrix, $\{\Delta\boldsymbol{\varepsilon}\}$ is the incremental strain tensor, and $\{\Delta\boldsymbol{\sigma}_f\}^T = \{\Delta p_f, \Delta p_f, \Delta p_f, 0, 0, 0\}$ where Δp_f is the change in pore fluid pressure.

4.4.2 Finite element formulation of the consolidation problem

The general purpose finite element program ABAQUS/Standard (2005) was used to perform numerical simulations of the mechanical behavior of composite models

composed of two different materials. ABAQUS is a versatile finite element code that can computationally examine problems ranging from relatively simple linear constitutive models to the most challenging nonlinear simulations. This program includes an extensive library of elements that can model almost any domain. It also contains several constitutive models that can simulate the behavior of most typical engineering material including hyperelastic rubber-like materials, composites, reinforced concrete, and geomaterials such as soils and rock. Furthermore, ABAQUS provides users with the capability of characterizing a range of constitutive properties of materials through a user-defined material subroutine (UMAT). This powerful finite element software package can simulate the behavior of the porous media by conducting coupled diffusion-deformation analysis. For further details, the reader is referred to the ABAQUS/Standard (2005) manuals.

ABAQUS/Standard provides capabilities for particular cases of fluid flow through a porous medium associated with the presence of a relatively incompressible liquid within the pore space; the medium can be considered as wholly or partially saturated with this liquid phase. When the medium is only partially saturated the remainder of the voids are filled with another fluid. An example of such a scenario could be the partially saturated soil medium in which the pores between the soil grains are filled with water and air. In the finite element approach, the porous medium is modeled by attaching elements to the solid phase and it is assumed that the nodal displacements and the nodal pore fluid pressures are the primary unknowns. The incremental displacement and pore fluid pressure can be subsequently expressed in terms of nodal values using the following equations:

$$\{\Delta \mathbf{d}\} = [\mathbf{N}] \{\Delta \mathbf{d}\}_n \quad (4.8)$$

$$\Delta p_f = [\mathbf{N}_p] \{\Delta \mathbf{p}_f\}_n \quad (4.9)$$

where $\{\Delta \mathbf{d}\}$ is the displacement tensor, while $\{\Delta \mathbf{d}\}_n$ and $\{\Delta \mathbf{p}_f\}_n$ contain the list of nodal displacements and fluid pressures for a single element, respectively. In (4.8) and (4.9), $[\mathbf{N}]$ and $[\mathbf{N}_p]$ are displacement and pore fluid pressure interpolation functions, which are often assumed to be identical.

Equilibrium condition can be expressed by considering the principle of minimum potential energy. This principle states that the static equilibrium position of a loaded linear elastic body is the one which minimizes the total potential energy. The total potential energy of a body can be defined as

$$\text{Total potential energy}(E) = \text{Strain energy}(W) - \text{Work done by the applied loads}(L) \quad (4.10)$$

The principle of minimum potential energy states that for equilibrium,

$$\delta\Delta E = \delta\Delta W - \delta\Delta L = 0 \quad (4.11)$$

where ΔE is the incremental total potential energy, ΔL is the incremental work done by applied loads and ΔW is the incremental strain energy defined as

$$\Delta W = \frac{1}{2} \int_V \{\Delta\boldsymbol{\varepsilon}\}^T \{\Delta\boldsymbol{\sigma}\} dV \quad (4.12)$$

Using Equation (4.7), this can be written in the following form:

$$\Delta W = \frac{1}{2} \int_V \left[\{\Delta\boldsymbol{\varepsilon}\}^T [\mathbf{D}'] \{\Delta\boldsymbol{\varepsilon}\} + \{\Delta\boldsymbol{\sigma}_f\} \{\Delta\boldsymbol{\varepsilon}\} \right] dV \quad (4.13)$$

Noting that the second term in the equation is equivalent to $\Delta p_f \cdot \Delta \varepsilon_v$, gives

$$\Delta W = \frac{1}{2} \int_V \left[\{\Delta\boldsymbol{\varepsilon}\}^T [\mathbf{D}'] \{\Delta\boldsymbol{\varepsilon}\} + \Delta p_f \cdot \Delta \varepsilon_v \right] dV \quad (4.14)$$

The work done by the incremental applied load ΔL can be divided into contributions from body forces, \mathbf{F} , and surface tractions, \mathbf{T} , and can be expressed as

$$\Delta L = \int_V \{\Delta\mathbf{d}\}^T \{\Delta\mathbf{F}\} dV + \int_S \{\Delta\mathbf{d}\}^T \{\Delta\mathbf{T}\} dS \quad (4.15)$$

Substituting Equations (4.14) and (4.15) into Equation (4.11), the total potential energy of the body becomes

$$\Delta E = \frac{1}{2} \int_V \left[\{\Delta\boldsymbol{\varepsilon}\}^T [\mathbf{D}'] \{\Delta\boldsymbol{\varepsilon}\} + \Delta p_f \cdot \Delta \varepsilon_v \right] dV - \int_V \{\Delta\mathbf{d}\}^T \{\Delta\mathbf{F}\} dV + \int_S \{\Delta\mathbf{d}\}^T \{\Delta\mathbf{T}\} dS \quad (4.16)$$

The essence of the finite element method is now to discretize the domain into elements. Therefore, the total potential energy is replaced by the sum of the potential energy of the separate elements:

$$\Delta E = \sum_{i=1}^N \Delta E_i \quad (4.17)$$

where N is the number of the elements. Furthermore, the variation of the displacement and pore fluid pressure can be expressed in terms of nodal values using Equations (4.8) and (4.9). Equation (4.16) then becomes

$$\Delta E = \sum_{i=1}^N \left(\frac{1}{2} \int_V \left(\{\Delta \mathbf{d}\}_n^T [\mathbf{B}]^T [\mathbf{D}'] [\mathbf{B}] \{\Delta \mathbf{d}\}_n + \{\Delta \mathbf{d}\}_n^T \{\mathbf{m}\} [\mathbf{B}]^T [\mathbf{N}_p] \{\Delta \mathbf{p}_f\}_n - 2 \{\Delta \mathbf{d}\}_n^T [\mathbf{N}]^T \{\Delta \mathbf{F}\} \right) dV - \int_S \{\Delta \mathbf{d}\}_n^T [\mathbf{N}] \{\Delta \mathbf{T}\} dS \right) \quad (4.18)$$

where the volume integral is now taken over the volume of an element and the surface integral is over the portion of the element boundary for which the surface traction is specified. The principal unknowns are the incremental nodal displacements $\{\Delta \mathbf{d}\}_n$ and pore fluid pressure $\{\Delta \mathbf{p}_f\}_n$ over the whole mesh. Minimizing the potential energy with respect to these incremental nodal displacements gives

$$\delta \Delta E = \sum_{i=1}^N \left\{ \{\Delta \mathbf{d}\}_n^T \right\}_i \left[\begin{array}{l} \int_V [\mathbf{B}]^T [\mathbf{D}'] [\mathbf{B}] dV \{\Delta \mathbf{d}\}_n + \int_V \{\mathbf{m}\} [\mathbf{B}]^T [\mathbf{N}_p] dV \{\Delta \mathbf{p}_f\}_n \\ - \int_V [\mathbf{N}]^T \{\Delta \mathbf{F}\} dV - \int_S [\mathbf{N}]^T \{\Delta \mathbf{T}\} dS \end{array} \right] = 0 \quad (4.19)$$

which is equivalent to a set of equations of the form

$$[\mathbf{K}]^G \{\Delta \mathbf{d}\}_n^G + [\mathbf{L}]^G \{\Delta \mathbf{p}_f\}_n^G = \{\Delta \mathbf{R}\}^G \quad (4.20)$$

where:

$$[\mathbf{K}]^G = \sum_{i=1}^N [\mathbf{K}]_i^E = \sum_{i=1}^N \left(\int_V [\mathbf{B}]^T [\mathbf{D}'] [\mathbf{B}] dV \right)_i \quad (4.21)$$

$$[\mathbf{L}]^G = \sum_{i=1}^N [\mathbf{L}]_i^E = \sum_{i=1}^N \left(\int_V \{\mathbf{m}\} \{\mathbf{B}\}^T [\mathbf{N}_p] dV \right)_i \quad (4.22)$$

$$\{\Delta \mathbf{R}\}^G = \sum_{i=1}^N \{\Delta \mathbf{R}\}_i^E = \sum_{i=1}^N \left[\left(\int_V [\mathbf{N}]^T \{\Delta \mathbf{F}\} dV \right) + \left(\int_S [\mathbf{N}]^T \{\Delta \mathbf{T}\} dS \right) \right]_i \quad (4.23)$$

$$\{\mathbf{m}\}^T = \{111000\} \quad (4.24)$$

Using the principle of virtual work, the continuity Equation (4.3) can be written as

$$\int_V \left[\{\mathbf{v}\}^T \{\nabla(\Delta p_f)\} + \frac{\partial \varepsilon_v}{\partial t} \Delta p_f \right] dV - Q \Delta p_f = 0 \quad (4.25)$$

Substituting for $\{\mathbf{v}\}$ using Darcy's law given by Equation (4.4) gives

$$\int_V \left[-\{\nabla h\}^T [\mathbf{k}] \{\nabla(\Delta p_f)\} + \frac{\partial \varepsilon_v}{\partial t} \Delta p_f \right] dV = Q \Delta p_f \quad (4.26)$$

Noting that $\{\nabla h\} = \left(\frac{1}{\gamma_f} \right) \nabla p_f + \{\mathbf{i}_G\}$, and approximating $\frac{\partial \varepsilon_v}{\partial t}$ as $\frac{\Delta \varepsilon_v}{\Delta t}$, Equation (4.26)

can be written in finite element form as

$$[\mathbf{L}]^G T \left(\frac{\{\Delta \mathbf{d}\}_n^G}{\Delta t} \right) - [\Phi]^G \{\mathbf{p}_f\}_n^G = [\mathbf{n}]^G + Q \quad (4.27)$$

where:

$$[\Phi]^G = \sum_{i=1}^N [\Phi]_i^G = \sum_{i=1}^N \left(\int_V \frac{[\mathbf{E}]^T [\mathbf{k}] [\mathbf{E}]}{\gamma_f} dV \right)_i \quad (4.28)$$

$$[\mathbf{n}]^G = \sum_{i=1}^N [\mathbf{n}]_i^E = \sum_{i=1}^N \left(\int_V [\mathbf{E}]^T [\mathbf{k}] \{\mathbf{i}_G\} dV \right)_i \quad (4.29)$$

$$[\mathbf{E}] = \nabla [\mathbf{N}_p] \quad (4.30)$$

4.4.3 Solution procedure for coupled fluid flow and deformations

The solution of the consolidation problem requires that the soil behavior should include effects of the transient flow of the pore-water through the voids and the deformations of the soil skeleton. Therefore, a multiphase continuum formulation is required for examining deformable porous media. There are two common approaches for solving the governing coupled equations. One approach is to solve one set of equations first and then use these results as input for the solution of the second set of equations. The results obtained in the latter are resubstituted into the first set of equations to assess the changes in the solution. This process is continued until successive iterations produce results that are within a specified accuracy. This is referred to as a staggered approach to the solution of coupled systems of equations. The second approach is to solve the entire coupled system directly; this is the direct approach that is used in ABAQUS. The direct approach is used in ABAQUS because of the rapid convergence of the solution algorithm even for the case of highly nonlinear problems.

To solve Equations (4.20) and (4.27) a time marching process has to be adopted. In other words, the solution for $(\{\Delta \mathbf{d}\}_n^G, \{\mathbf{p}_f\}_n^G)$ at time $t_2 = t_1 + \Delta t$ can be obtained from the solution at time t_1 considering the following equation:

$$\int_{t_1}^{t_2} [\Phi]^G \{\mathbf{p}_f\}_n^G dt = [\Phi]^G \left[\beta^* \left(\{\mathbf{p}_f\}_n^G \right)_2 + (1 - \beta^*) \left(\{\mathbf{p}_f\}_n^G \right)_1 \right] \Delta t \quad (4.31)$$

where β^* is the parameter used for approximation in the pore fluid flow equation.

Substituting Equation (4.31) into (4.27) gives

$$[\mathbf{L}]^{GT} \{\Delta \mathbf{d}\}_n^G - \beta^* \Delta t [\Phi]^G \{\Delta \mathbf{p}_f\}_n^G = [\mathbf{n}]^G \Delta t + Q \Delta t + [\Phi]^G \left(\{p_f\}_n^G \right)_1 \Delta t \quad (4.32)$$

In order to ensure stability of the time marching process, it is necessary to choose $\beta^* \geq 0.5$ (see e.g. Selvadurai and Nguyen, 1995; Lewis and Schrefler, 1998). ABAQUS considers a fully implicit scheme ($\beta^* = 1$) to ensure the numerical stability of the analyses.

Equations (4.20) and (4.32) can be written in the following incremental form:

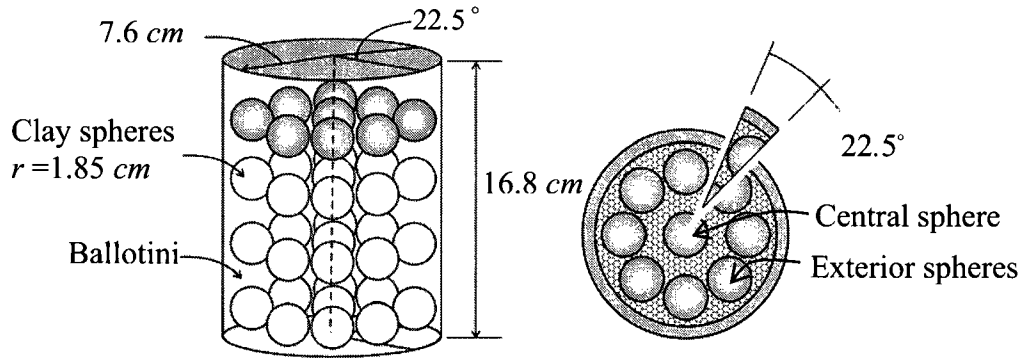
$$\begin{bmatrix} [\mathbf{K}]^G & [\mathbf{L}]^G \\ [\mathbf{L}]^{GT} & -\beta^* \Delta t [\Phi]^G \end{bmatrix} \begin{bmatrix} \{\Delta \mathbf{d}\}_n^G \\ \{\Delta \mathbf{p}_f\}_n^G \end{bmatrix} = \left\{ \left([\mathbf{n}]^G + Q + [\Phi]^G \left(\{\mathbf{p}_f\}_n^G \right) \right) \Delta t \right\} \quad (4.33)$$

These equations form the basis for the iterative solution of a time step in a coupled flow deformation solution in ABAQUS/Standard. These equations are non-symmetric due to a number of effects: changes in geometry, dependence of permeability on void ratio, changes in saturation in partially saturated cases, and inclusion of fluid gravity load terms in the pore pressure. ABAQUS/Standard uses the non-symmetric equation solver by default in all steady-state or partially saturated coupled analyses; in other cases it uses the symmetric solver by default. The porous media coupled analysis can provide solutions either in terms of total or of excess pore pressure. The accuracy of the solution scheme has been verified by the developers through comparison with known analytical solutions (ABAQUS/Standard, 2005).

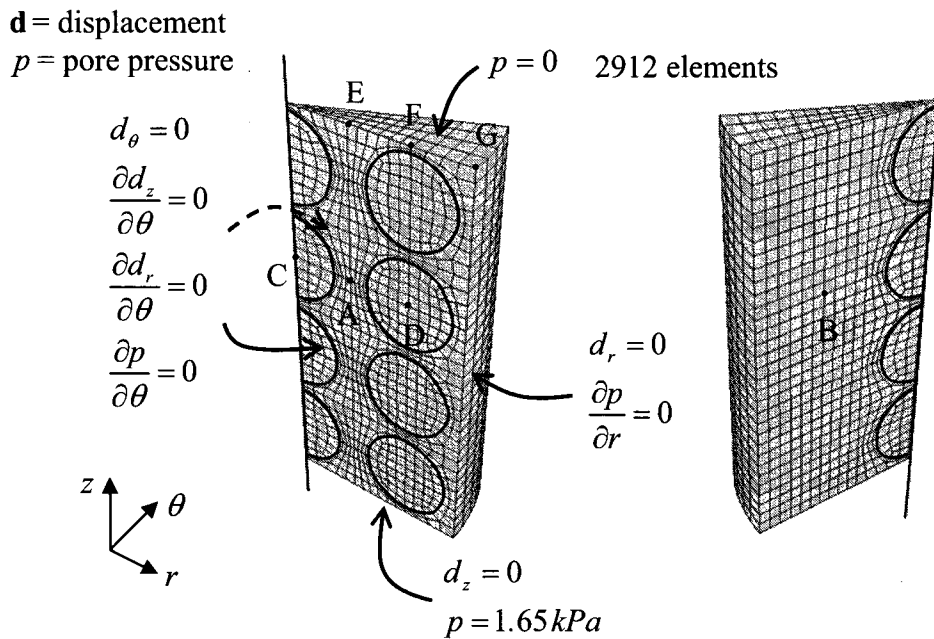
4.4.4 Computational modeling of the composite sample

The computational modeling of the oedometric compression of the clay spheres- ballotini composite specimen was conducted using the general-purpose finite element code ABAQUS/ Standard. The composite model that includes clay spheres enclosed by the ballotini region has a periodic symmetric arrangement; therefore, in order to reduce the computation time, a region with a sector angle of 22.5° was modeled with appropriate boundary conditions imposed on the displacement, traction and pore fluid pressure. The model could be easily discretized into brick elements. The finite element mesh discretization of the composite model used in this analysis is shown in Figure 4.6. In this study a 20-node brick element (C3D20RP) with a *quadratic variation* in the displacement and a *linear variation* in the pore pressure was selected, which employed a reduced integration scheme. The boundary conditions in the modeling, which were defined to represent both the symmetry and the oedometric conditions, are shown in Figure 4.6. The lateral boundaries were constrained horizontally with no provision for drainage; since drainage was provided through the geotextile layers and drainage vents, the upper and

lower surfaces of the specimens were assumed to be free draining. Furthermore, the pore pressures at the upper and lower surfaces were assigned at zero and 1.65 kPa, respectively, since during the experiments the water level in the container was maintained at the same level as the upper surface of the specimens.



(a) Schematic figure of the composite lumpy sample



(b) Mesh configuration and boundary conditions

Figure 4.6 Finite element models considered in the problem of consolidation of composite lumpy specimen

The composite model was subjected to a uniform axial stress, which was applied to the upper surface of the model. This stress was increased to the magnitudes of 81 *kPa* (initial load step), 149, 219, 273, 383 and 493 *kPa* in six successive loading steps. At each step, the stress increment was applied to the uppermost boundary within one second and maintained for a period of one day. Considering different constitutive characteristics of the constituent materials, the axial stress applied to the plunger resulted in a non-uniform contact stress between the plunger and upper surface of the models. Since the plunger is required to be infinitely rigid in comparison to the soil composite, the assumption of uniform oedometric settlement of the plunger is justified. This condition was modeled in ABAQUS by taking advantage of the “rigid body” constraint, which can be used as an interaction feature in the computations. Therefore, the uniform settlement of the surface can be obtained by constraining the nodes of the top surface to achieve an identical displacement in the axial direction. In other words, the uniform stress applied to the upper surface was converted to a non-uniform vertical stress, here referred to as contact stress, that induced uniform settlement at this surface.

The mechanical response of the soil composite considered in this study, under prescribed loading conditions, depends on the volume proportion of clay in relation to the granular (ballotini) region and the mechanical characteristics of the constituent materials. In order to achieve a better understanding of the problem, computational analysis was performed on a composite model, shown in Figure 4.6, by implementing the constitutive models developed in Chapters 2 and 3 for clay and ballotini materials. In the analysis, the initial physical state of the components was identified by defining the void ratio of the clay and ballotini equal to 0.63 and 0.612, respectively.

In coupled pore fluid flow and stress analysis, the dissipation of the fluid pressure, which is generated within the porous medium, results in the gradual transfer of the stress to the solid skeleton. Therefore, a time-dependent response takes place over a period of time that is required for the full dissipation of the excess pore pressures. Figure 4.7 depicts the variation of the pore fluid pressure in the first loading step at four points selected from different locations of the composite model (Figure 4.6). Results indicate that the pore fluid pressure at these points rises during the application of the axial load (the first second of the load step). The fluid pressures at points C and D, located at the centre of the central

and exterior clay spheres, increase to a magnitude higher than those computed for points A and B, located within the ballotini region. The results also indicate that the excess pore pressure generated within the ballotini medium dissipated within 10 seconds after the application of the load; however, the consolidation process in the clay parts was completed after approximately 2.5 hours, which is attributable to the lower hydraulic conductivity of the fine-grained clay lumps.

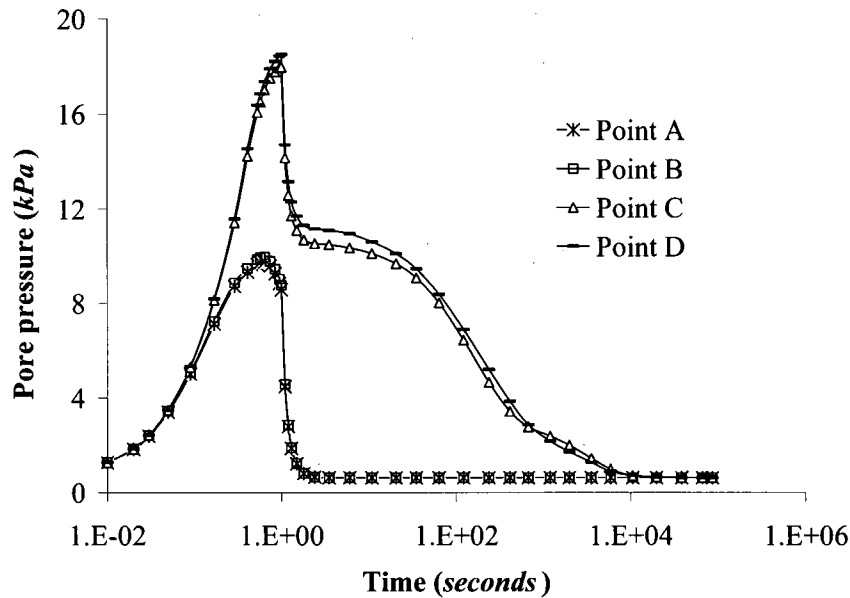


Figure 4.7 Pore fluid pressure change in different locations of composite model (first load step)

After the maximum axial load was applied at each load step, the load was maintained for a period of one day. During the early stage of this period, the dissipation of the excess pore pressure in ballotini resulted in a compression of the granular phase; therefore, the pore fluid pressure in clay spheres primarily decreased due to the stress relaxation encountered in the composite. This stress relaxation in the region that contains the clay spheres and ballotini can be verified by considering the variation of contact pressure computed at points E, F and G (Figure 4.6) during any load step. Figure 4.8 depicts the contact pressure change at points E, F and G located on the upper boundary of the model during the first load step. Results indicate that after the first second of the load increase, the vertical pressure applied to the composite columns gradually decreased due to the progress of consolidation in the clay spheres; this phenomenon resulted in a rise of

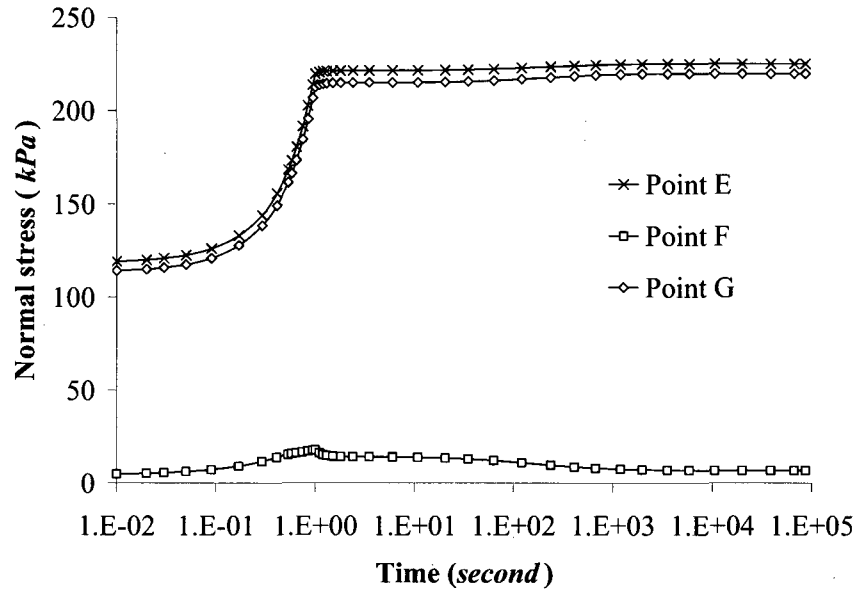


Figure 4.8 Variation of contact vertical stress in the composite model (first load step)

vertical stress in the ballotini column inside the specimens. Furthermore, no excess pore fluid pressure remained in the clay inclusions 10,000 seconds (2.78 hours) after the beginning of the load step; therefore, after this time period, the ultimate axial deformation of the composite soil has been achieved. The difference in contact stresses also indicates that a high portion of the load was carried by the ballotini column compared to the clay region. The contours of the axial σ_{zz} stress at the end of first load step, shown in Figure 4.9, illustrate the stress partitioning phenomenon that happens within the composite model. The maximum normal stress in the model occurred at the points located in the ballotini region between the exterior clay spheres. At the end of the first load step, for instance, the value of normal stress at point B is more than 300 times greater than that computed at points C and D, situated at the center of the fine-grained spheres.

The progressive axial deformation of the composite sample occurred as a result of the time-dependent consolidation process in the constituents. The normalized axial deformation of the composite model in the five consecutive load steps is presented in Figure 4.10 (U_t is the axial deformation at time t and U_∞ is the ultimate axial deformation at each load step). The computations show two different phases in the compression response of the composite; the first phase of the deformation occurred due to the dissipation of the fluid pressure trapped within the pores of the ballotini region, while the second phase of deformation was related to the pore fluid expelled from the

pores of the clay inclusions. The computational results indicate that at each load step 6% to 10% of the total settlement occurred during the second phase of axial deformation, corresponding to the consolidation process that took place in the clay spheres. At each load step, the axial deformation after 10,000 *seconds* is considered as the ultimate axial deformation U_∞ of the composite domain.

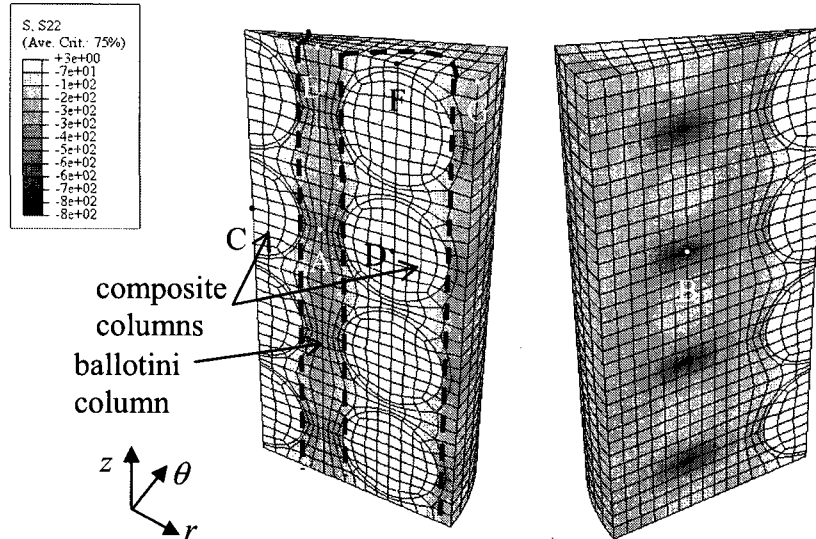


Fig. 4.9 Stress partitioning in composite sample- end of first load step

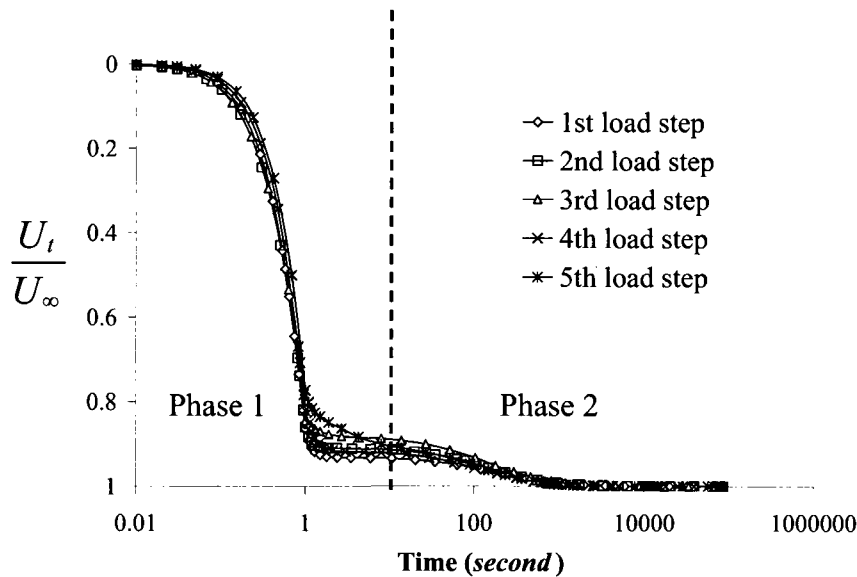


Figure 4.10 Axial deformation of the composite model subjected to oedometric compression test

4.5 Comparison between numerical predictions and experimental results

In this section, the mechanical behavior of the composite model described in the previous section is predicted using finite elements analysis. The comparison between the numerical predictions and experimental results will indicate the predictive capabilities of the methodology that can be used in further computational studies.

The computations were conducted on the finite element models shown in Figure 4.6. The constitutive models developed in Chapters 2 and 3 were implemented by taking into account the initial physical state of the materials, measured during the fabrication of the composite specimens. Figure 4.11 shows the comparison of the displacement-time responses between the computational predictions and the experimental results. The results presented include the axial deformation of the composite specimen subjected to an axial load that was increased in five successive load steps. It can be seen that, although the computational estimates slightly differ from the experimental results, it gives a reasonable prediction of the experimental trends of load-displacement response. During the first three load steps, the computed values slightly underestimated the experimental results for the axial deformation of the sample whereas a greater magnitude of settlement was predicted from the numerical simulation for the last two load steps. The maximum discrepancy between the predicted axial deformation and the experimental results, Δ ,

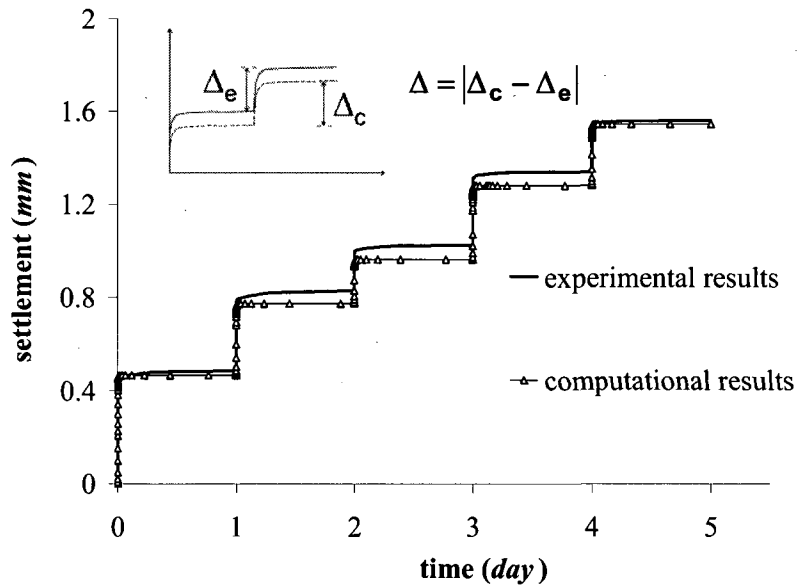


Figure 4.11 Axial compression of the composite sample in five successive load steps

occurred in the last load step, which is less than 3% of the total deformation of the sample. Furthermore, the final axial settlement, at the end of the last load step, predicted from the computations is in satisfactory agreement with the experimental result.

The computation also attempts to predict the rate of consolidation settlement of the composite samples. The simulations were conducted considering the hydraulic conductivities of silty clay and ballotini to be equal to the values estimated from the experiments ($k_{clay} = 2 \times 10^{-8} \text{ cm/s}$, $k_{ballotini} = 1.6 \times 10^{-3} \text{ cm/s}$). The computational estimates and experimental results for the settlement-time curves at different load steps are presented in Figure 4.12, for the composite sample. At each load step, the axial settlement is normalized using the settlement that occurred after a period of 10000 *sec*. Numerical estimates indicate that after this period, no excess pore pressure remains within the composites; therefore, the ultimate consolidation settlement was achieved. It can be seen that the computations provide an accurate prediction of the consolidation response during different loading steps, whereas the modeling slightly underestimates the axial deformations that take place in the second phase due to the consolidation of the clay spheres. The maximum discrepancy was computed in the last load step, in which the portion of axial deformation that occurred in the second phase was approximately 6% greater than that obtained from the computations. Furthermore, the computation gives a reasonable prediction of the rate of the consolidation process; the time required for the composite sample to exhibit 50% of the deformation in the second phase is approximately 2 *minutes*, which can be obtained from both experimental and computational results.

The experimental observations indicated that the time-dependent deformation of ballotini results in further axial settlement of the sample after the termination of the consolidation process. This phenomenon, also observed in the oedometric compression of the pure ballotini samples, is mainly attributed to the time-dependent deformation of ballotini due to the internal re-arrangement of the granular assembly. This time-dependent behavior has been observed in granular media, particularly when they are used in low density conditions in laboratory investigations (Murayama et al., 1984; Lade, 1994; Di Prisco and Imposimato, 1996; Kuwano and Jardine, 2002). As a result, in each load step, further axial deformation occurred in the specimen even after the termination of the consolidation process.

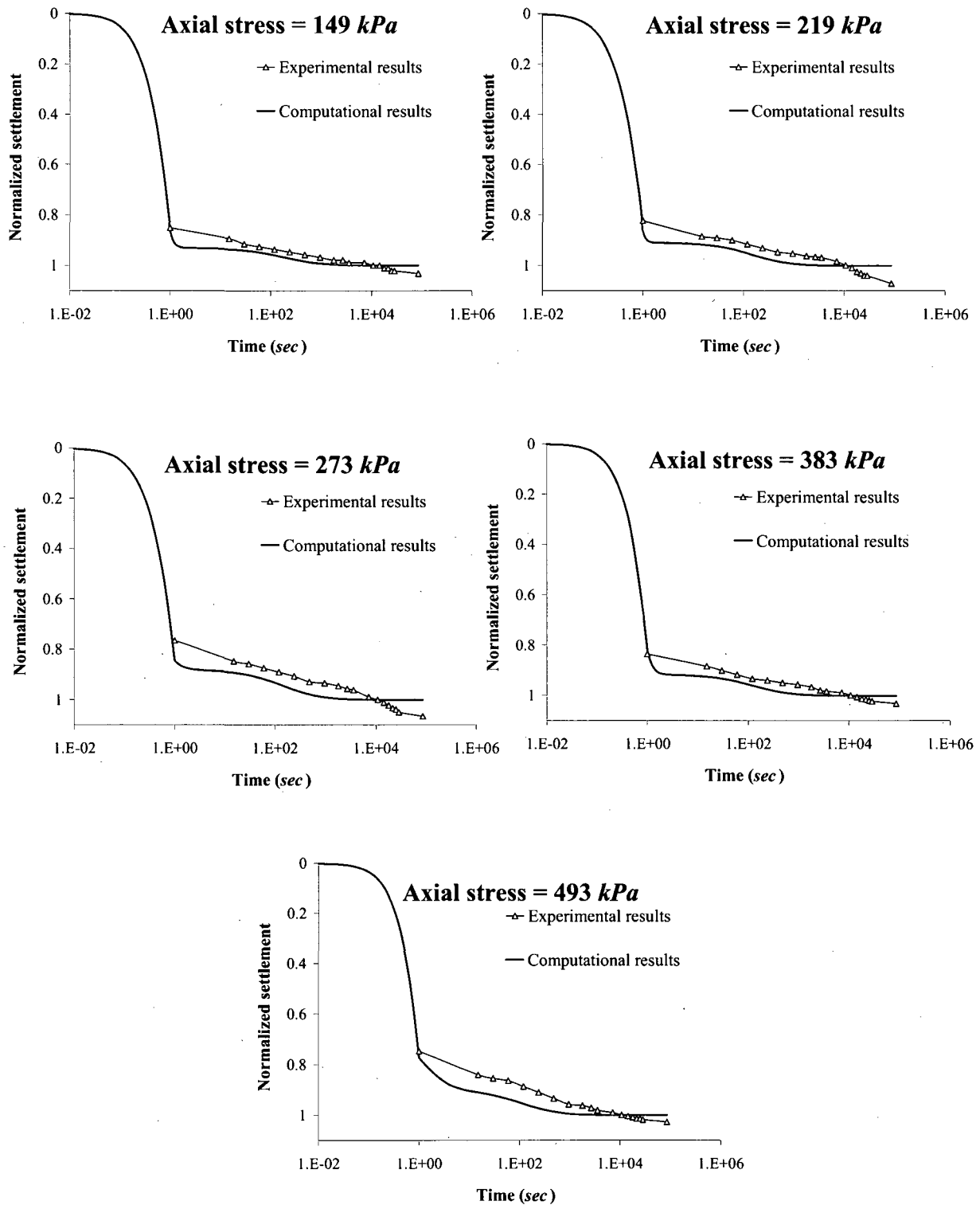


Figure 4.12 Consolidation curves of the composite sample subjected to the oedometric compression test

4.6 Summary remarks

In this chapter, the constitutive models that are specifically developed for modeling the mechanical behavior of reconstituted silty-clay and ballotini, as described in Chapters 2 and 3, have been implemented in the general purpose finite element code ABAQUS/Standard code. The finite element method is used to examine the mechanical response of a cylindrical composite specimen containing ballotini with 36 interspersed clay spheres placed at four levels within the sample. The experimental results showed that the presence of soft clay lumps results in higher consolidation settlement of the composite sample subjected to oedometric compression. Also, during each load step, two phases were observed in the axial deformation of the specimen; the first phase that occurred shortly after application of the load (<10 sec) corresponded to the “rapid consolidation” process in the ballotini region. This deformation phase was followed by a further compression that took place over a longer time period as a result of dissipation of excess fluid pressure generated within the clay regions. The results of the modeling show that the computations can accurately capture the experimental response in terms of the total deformation and also the portions of the axial deformation that occur in each consolidation phase. Furthermore, the simulations can provide a satisfactory trend for the rate of axial deformation at different load steps. The predictive capabilities of the methodology adopted here permit the study of further problems including bench-scale composite specimens. The computational scheme can be implemented to simulate large scale problems such as composite fills resulting from reclamation activities or soft clay layers that have been reinforced using stone columns.

CHAPTER 5

MECHANICAL BEHAVIOR OF A SOIL COMPOSITE: DISK-SHAPED CLAY INCLUSIONS EMBEDDED IN A GRANULAR REGION

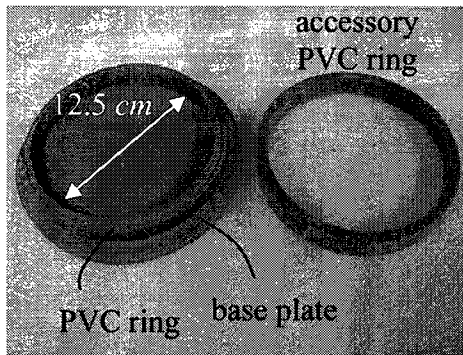
5.1 Introduction

A coarse-grained medium containing a regular array of disk-shaped clay inclusions is an idealized clay-granular medium arrangement that can be used to examine the mechanics of a soil composite region. The experimental research program described in this chapter uses the bench-scale oedometer test arrangement to examine the mechanical behavior of a composite specimen fabricated with different numbers of silty clay disks placed within the ballotini region. The research also develops a computational study that allows the incorporation of the constitutive models, developed respectively in Chapters 2 and 3 for the silty clay and the ballotini, to predict the oedometric response of the composite. The results of the oedometric compression test are also used to assess the influence of the volume proportion of the fine-grained region, in relation to the granular medium, on the mechanical response of the entire sample. The oedometer experiments also provide data that can be used to assess the predictive capabilities of the computational approach.

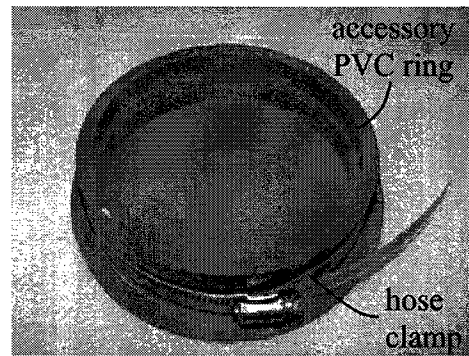
5.2 The test facility and sample preparation

The bench-scale test facility described in 3.2.4 was designed to induce overall oedometric compression to the composite samples fabricated within the cylindrical cell. The experiments were conducted on composite samples fabricated with different numbers of clay disks placed within the ballotini region. The reconstituted silty clay soil, with a moisture content near its liquid limit, was used to prepare the clay disks. A special device was fabricated to prepare the clay disks. A PVC ring of internal diameter of 12.5 *cm* and height of 1.94 *cm* was attached to a PVC base plate of thickness 1 *cm* and diameter 15.5 *cm* (Figure 5.1a). The close fit between the ring and the base plate prevented the

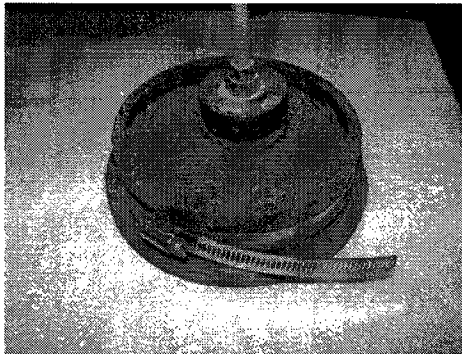
leakage of soil from the base. A second PVC ring (accessory ring), with the same dimensions as the first one, was mounted on the main ring using a hose clamp, which facilitates the molding process (Figure 5.1b). The silty clay paste was compacted in the mold up to a level higher than the height of the lower ring. To avoid trapping of air within the specimen during compaction, a plunger was used to lightly compact the soil paste inside the mold (Figure 5.1c). Next, the clamp was unfastened and the accessory ring was removed (Figure 5.1d). After removing the upper ring, the upper surface of the



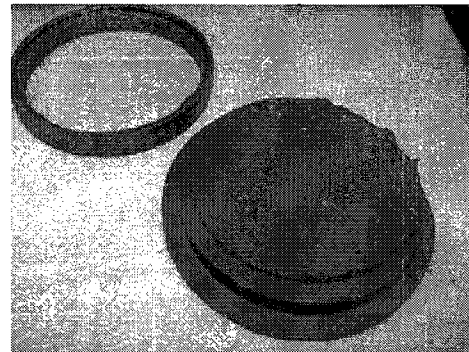
(a) The PVC mold-rings and the base plate



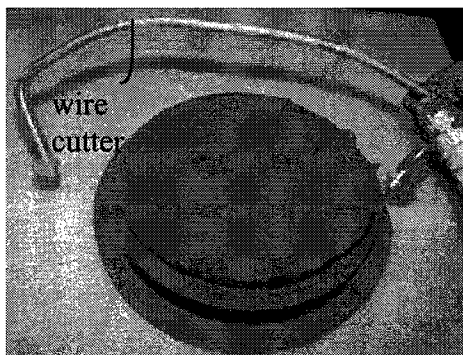
(b) Clamped PVC rings



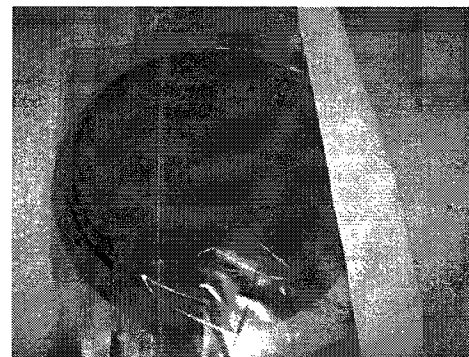
(c) Compacting clay paste with plunger



(d) Removing the accessory ring



(e) Trimming the clay disk using wire cutter



(f) Placing the molded clay in the sealed bag

Figure 5.1 Preparation of the silty clay disks

specimen was trimmed using a wire cutter (Figure 5.1e). The mold containing the specimen was then placed in a sealed bag (Figure 5.1f) and stored at the temperature of approximately -10°C . After a period of approximately one day, the PVC ring was dismantled from the base plate and detached from the frozen disks. The shape of the disks and their water content were maintained by re-freezing them in sealed bags prior to fabrication of the composite samples. The moisture contents determined from tests on additional frozen clay disks indicated that the specimens were at, approximately, the liquid limit of the silty clay.

The composite soil specimens prepared for the oedometric compression test consisted of silty clay disks placed within the ballotini region. The composite specimens were prepared in the cylindrical cell (internal diameter of 15.2 cm) of the bench-scale setup. The complete oedometric soil composite samples (approximate height 16.8 cm) contained either four, six or eight disks of clay with the volume fractions ($V_{\text{clay}}/V_{\text{total}}$) evaluated at 31%, 47% and 62.5%, respectively (Figure 5.2). The disks were placed equidistant with the central planes of the disks spaced 4.2 mm , 2.8 mm , and 2.1 mm , respectively in four-, six- and eight-disk samples, and the ballotini was dispersed and lightly compacted in layers to construct the soil composites; the weight of ballotini used in the specimens was measured in order to estimate the initial physical parameters of the granular phase of the composite. The samples were saturated with deaired water prior to application of the load, and the water level was maintained at the upper level of the samples for a period of two days. Computations indicate that a frozen clay disk will thaw completely within two

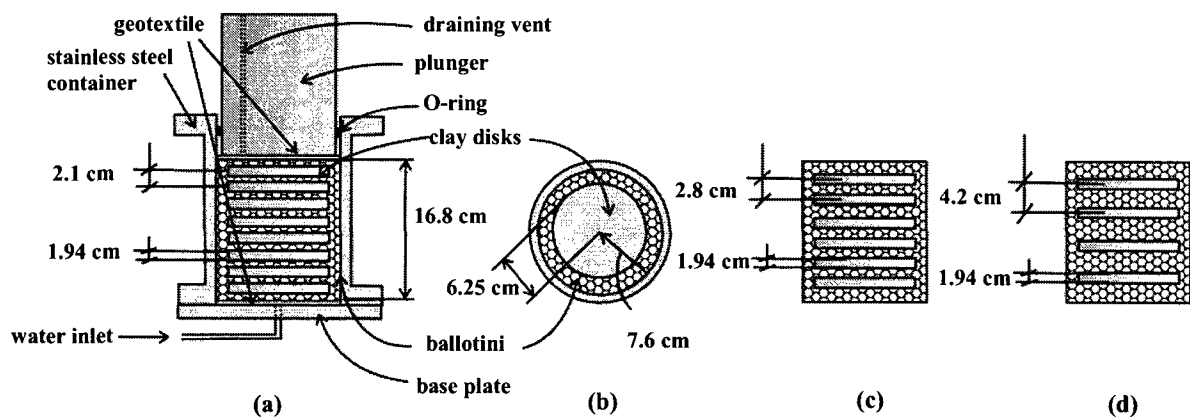


Figure 5.2 (a) Cross sectional view of the 8-disk composite sample (test-3) (b) Planar cross section (c) the 6-disk composite sample (d) the 4-disk composite sample

minutes; the volumetric heat capacity and thermal conductivity of the frozen clay are taken as $2.7 \times 10^6 \text{ J/m}^3 (\text{ }^\circ\text{C})$ and $0.6 \text{ W/mK } (\text{ }^\circ\text{C})$, respectively (see, e.g., Selvadurai et al., 1999). During the application of the axial load, proper drainage at the base of the sample and at its top was assured by placing two layers of geotextile at the upper and lower surfaces of the composite samples, which were connected to the draining vent and water container, respectively.

Oedometric consolidation in the bench-scale experiments is induced by the controlled application of static loads through a lever arm (Figure 3.9). A weight rack was designed to accommodate a maximum force of 2.67 kN , which could be increased in increments. The initial stress on the sample resulting from the weight of the lever arm, plunger, weight rack and other accessories connected to the lever arm was approximately 81 kPa . In subsequent loading sequences, the axial stress on the sample was increased to 149, 219, 273, 383 and 493 kPa by adding weights in five loading steps. To minimize the development of dynamic effects in the loading process, the load was applied gradually using a scissor jack installed in the loading frame. Each load step lasted for approximately 24 hours, after which no excess pore pressure was expected to remain in the system; the relevant time limit was arrived at through a computational modeling of the experimental configuration.

5.3 Experimental results

The axial deformation of the composite specimens forms the main test data that can be used in the calibration of the computational predictions. At each load step, the axial stress on the sample was increased, and the vertical movement of the plunger was continuously recorded through two LVDT transducers. The data acquired through the data acquisition system described in Chapter 3. Figure 5.3 shows a comparison of the time-dependent settlement response of the three composite samples compared with that of a pure ballotini specimen. The experimental results indicate that an increase in the volume proportion of clay results in a higher axial deformation of the composites; the axial settlement of the four-disk sample at the end of the final load step was approximately 2.8 times that of a pure ballotini sample. Furthermore, at the termination of the last load step, the eight-disk

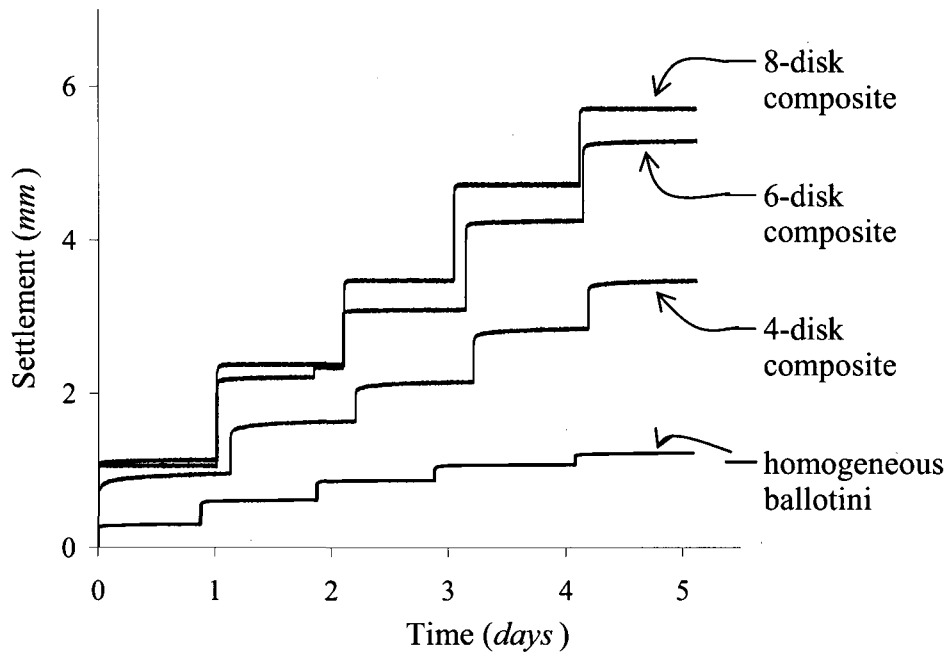


Figure 5.3 Axial settlement of the samples in five successive load steps

sample exhibits approximately 5 times more axial deformation than that experienced by the pure ballotini sample. The experimental results also show a progressive axial deformation at the end of each load step, which is mainly related to the time-dependent axial deformation of ballotini due to the internal re-arrangement of the granular assembly. Such time-dependent behavior observed in ballotini is discussed in the article by Ghiabi and Selvadurai (2008). Comparing the results of different tests, it was shown that this phenomenon diminished in the tests conducted on fabricated samples with a lower volume of ballotini; therefore, in the six-disk and eight-disk composites, an ultimate deformation state was observed at the end of the load steps.

During the axial loading of the soil composites, a mixture interface can develop at the boundary of two materials as a result of penetration of the soil grains into the soft clay. In this study, the development of this mixture interface was investigated by dissecting the composite samples at the termination of the tests. For this reason, the clay disks were extracted from the consolidation cell and were cut into smaller parts using a wire cutter. The observations indicated that there was no measurable penetration of the ballotini grains into the soft clay disks at the boundary of two materials. Figure 5.4 shows that a layer of ballotini beads stuck to the surface of the clay disks; however, this layer could be

easily removed from the surface of the clay. The issue of particle penetration and its influence on the consolidation response of the clay in terms of alteration of the fluid transport boundary conditions at the interface was recently investigated by Selvadurai (2008), using an idealized model of contact of disks at an interface. For both hexagonal and cubic arrangements of the contacting disks, the consolidation rate exhibits a marginal change but the total consolidation deformations are uninfluenced.

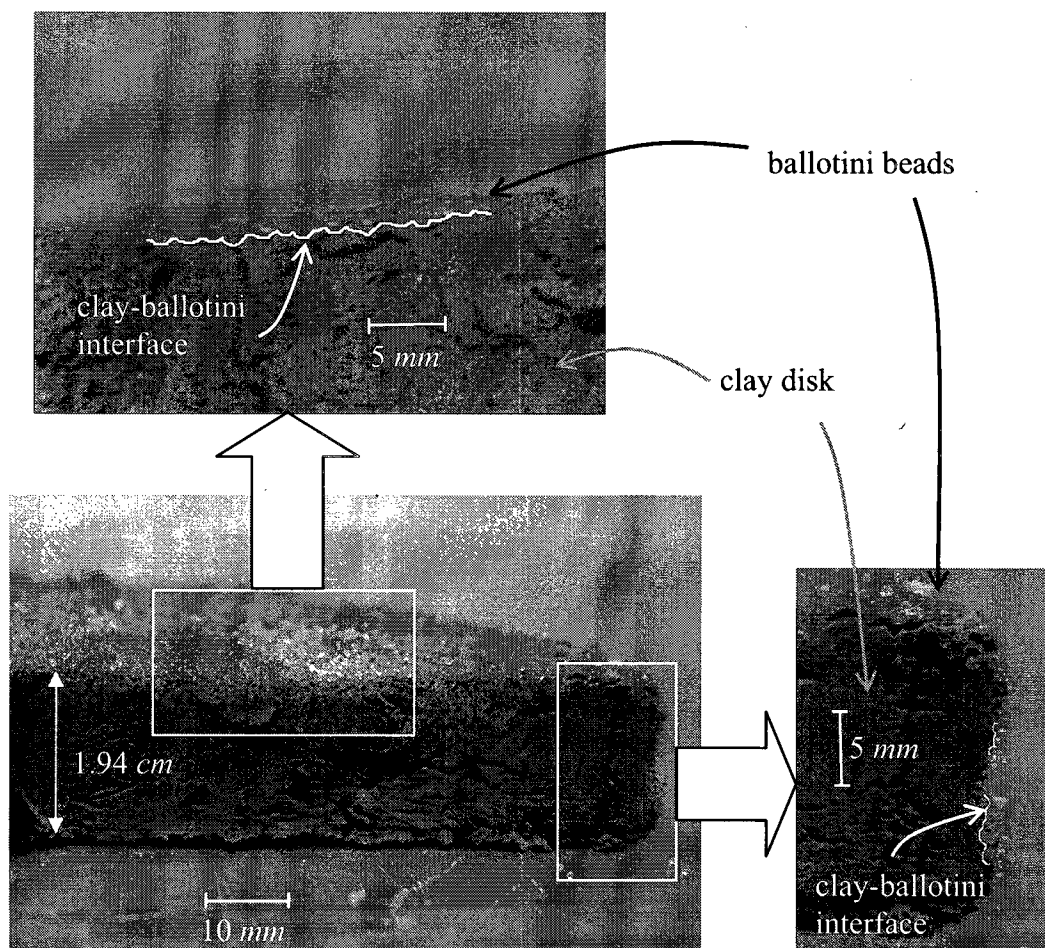


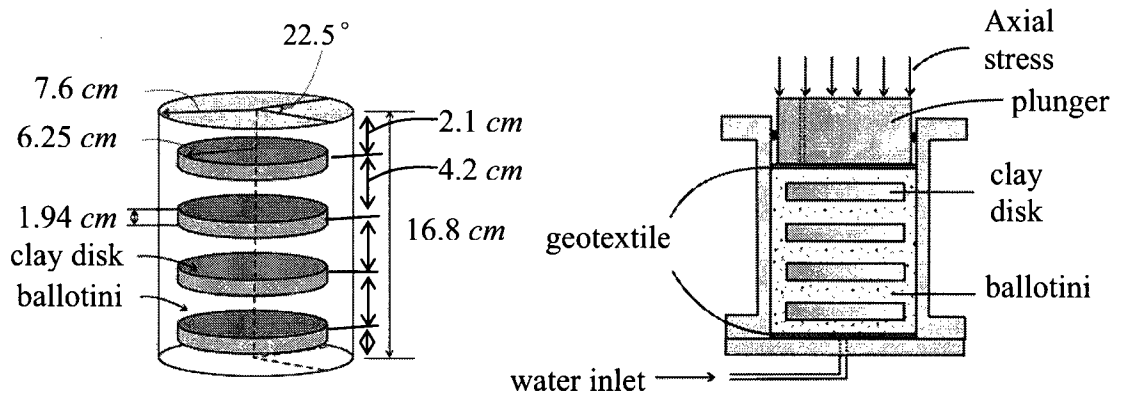
Figure 5.4 Dissecting the soil composite at the termination of the oedometer test

5.4 Computational implementations

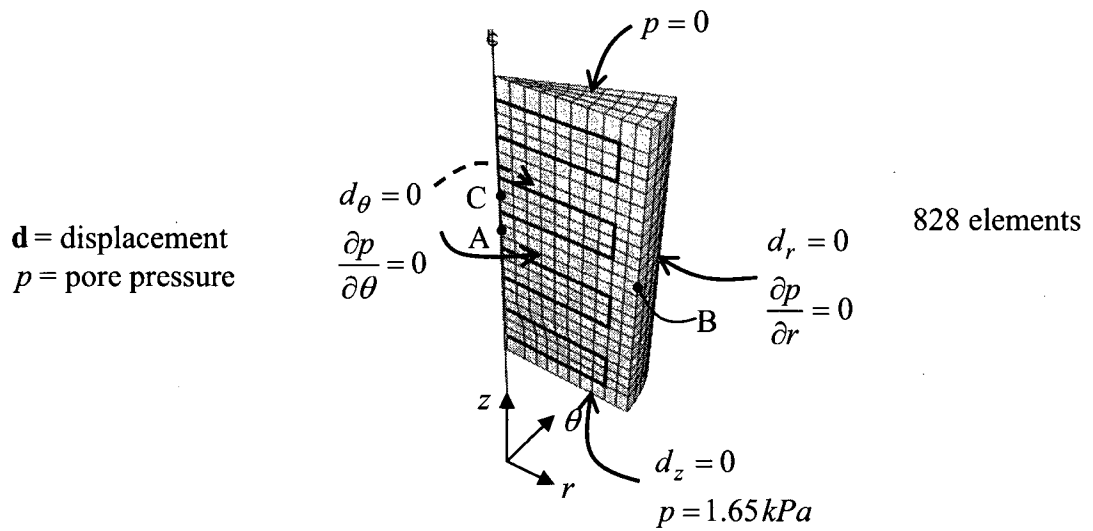
The computational modeling of the uniaxial compression of the composite samples was conducted using the general-purpose finite element code ABAQUS/Standard (2005). There are several computational features in ABAQUS/Standard that are relevant to the

computational modeling of the mechanical behavior of soil composites. These include the feature to model composite domains including two different materials, implementation of coupled pore fluid flow and stress analysis, and most importantly, the ability to implement the constitutive models derived in Chapters 2 and 3 for silty clay and ballotini. Complete descriptions of the implementations of these features are given in the user manual for ABAQUS/Standard (2005).

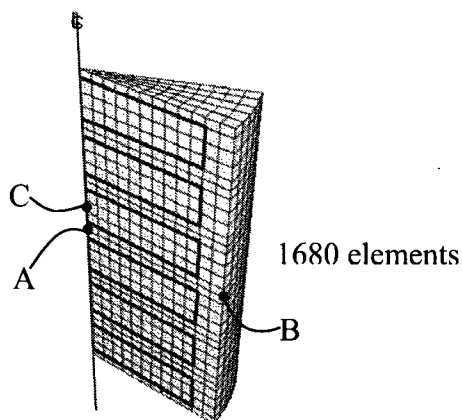
The problem of the oedometric compression of the composite samples, including clay disks placed within the ballotini region, is an axisymmetric problem whereas the UMAT subroutine used for ballotini was developed based on the three dimensional formulation to be used in a more general class of problems. Therefore, in order to reduce the computational time for modeling the composite region, only a sector region with an angle of 22.5° was modeled. This region could be easily discretized into brick elements. The finite element mesh discretizations of the composite domains used in this analysis are shown in Figure 5.5. In this study a 20-node brick element (C3D20RP) with quadratic variations in the displacement and linear variations in the pore pressure was selected, which employed a reduced integration scheme. The boundary conditions, which were defined to represent the oedometric condition, are shown in Figure 5.5. The lateral boundaries were constrained horizontally with no provision for drainage; since drainage was provided through the geotextile layers and drainage vents, the upper and lower surfaces of the specimens were assumed to be free draining. Furthermore, the pore pressure at the upper and lower surfaces was assigned as zero and 1.65 kPa , respectively, since during the experiments the water level in the container was maintained at the same level as the upper surface of the specimens.



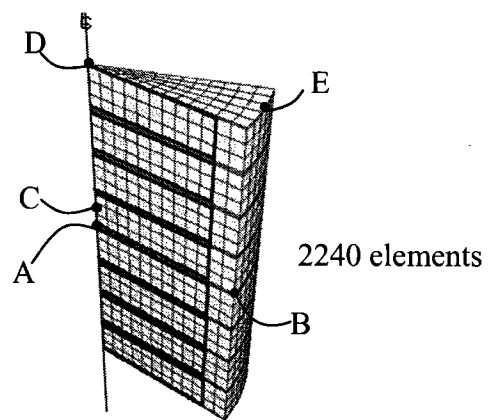
(a) Schematic view of the 4-disk composite sample



(b) Mesh configuration and boundary conditions (4-disk composite)



(c) Mesh configuration (6-disk composite)



(d) Mesh configuration (8-disk composite)

Figure 5.5 Finite element models considered in the modeling of the consolidation of composite soil specimens

The composite models were subjected to a uniform stress, applied to the upper surface of the rigid plunger, which increased from 81 *kPa* (initial load step) to 149, 219, 273, 383 and 493 *kPa* in subsequent loading steps. At each step, the pressure applied to the uppermost boundary was increased within one second and maintained for a period of approximately one day. Considering different constitutive characteristics of the constituent materials, the vertical pressure applied to the upper surface of the rigid plunger resulted in non-uniform contact stress between the plunger and the upper surface of the samples. This pressure resulted in a settlement that is assumed to be uniform due to the high stiffness of the plunger in comparison to the tested materials. This condition can be modeled in ABAQUS by taking advantage of the “rigid body” constraint, which can be used as an interaction feature in the computations. Therefore, the uniform settlement of the surface can be obtained by constraining the nodes of this surface to an identical displacement in the vertical direction. In other words, the uniform stress applied to the upper boundary was converted to a non-uniform vertical stress, here referred to as contact stress, that causes uniform settlement at this surface.

The mechanical response of the composite models considered in this study, under prescribed loading conditions, depends on the volume proportion of clay in relation to the granular region and the initial state of the constituent materials. In order to achieve better understanding of the problem, bench mark analyses were performed on three types of composites, shown in Figure 5.5, with identical physical and mechanical states of the constituents. The constitutive models developed in Chapters 2 and 3 for the clay and ballotini materials were implemented in this computational study. In these analyses the initial void ratios of the clay and ballotini were defined to be equal to 0.63 and 0.62, respectively. Figure 5.6 presents the axial deformation of three composite models subjected to an axial pressure increased over six loading steps. Computational results indicated that the ultimate axial deformation of the *six-disk* and *eight-disk* composite samples at the termination of the last loading step was 14% and 39% greater respectively than that in the *four-disk* specimen. This increase in axial deformation was attributed to the decrease in the load carrying capacity of the central core due to the higher volume fraction of soft clay in this region.

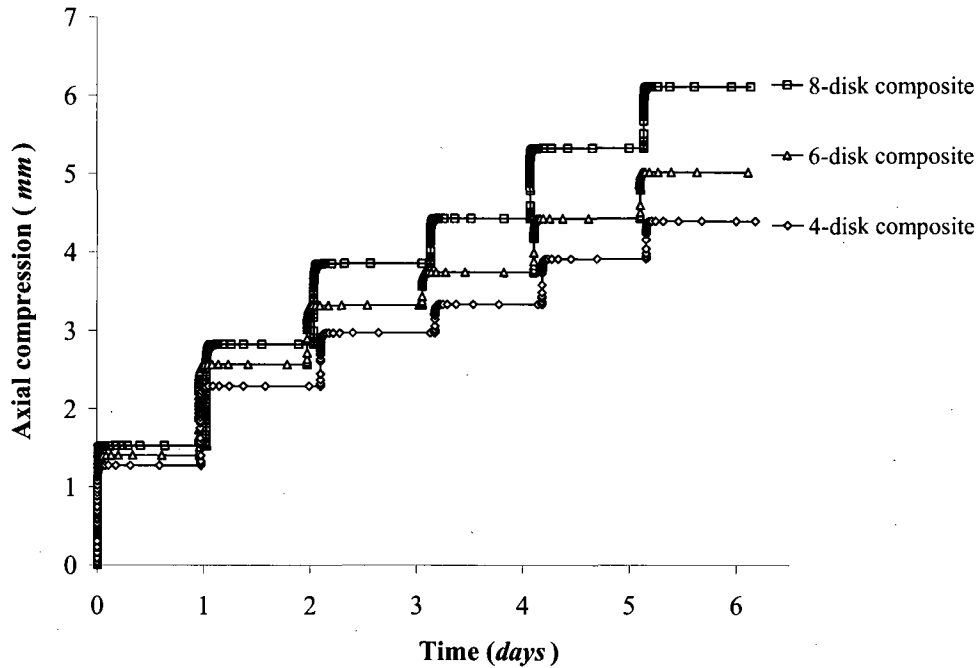
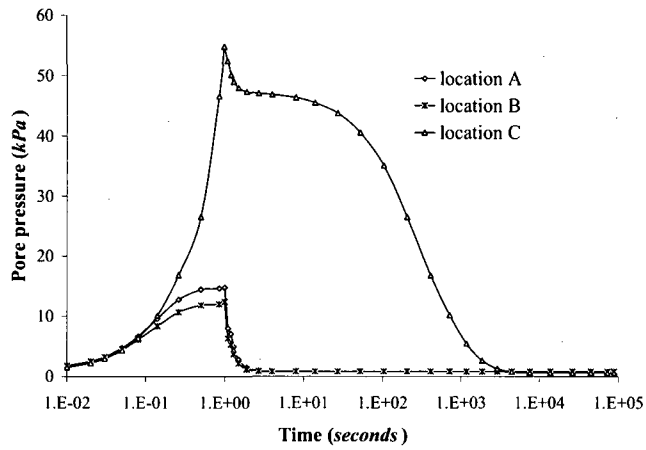
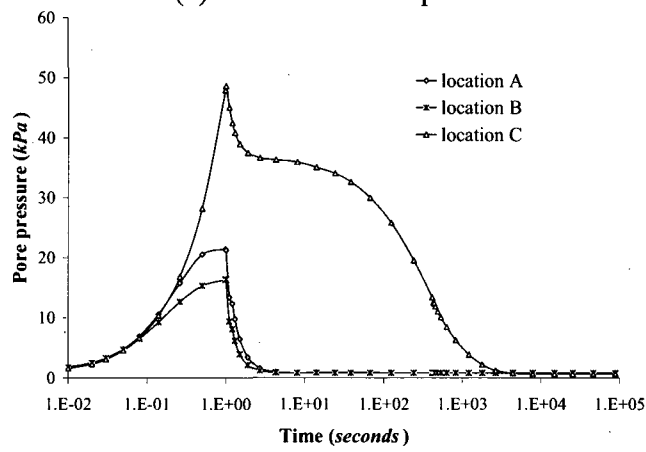


Figure 5.6 Axial compression of the composite samples in six successive load steps

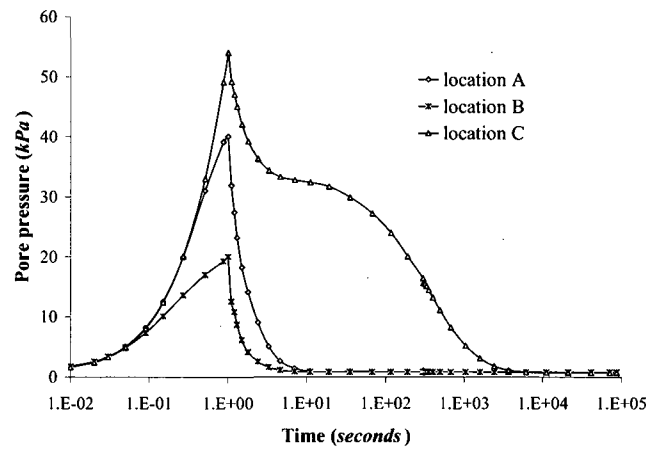
In coupled pore fluid flow and stress analysis, the dissipation of the fluid pressure, initially generated within the pores of a porous media, gives rise to a gradual transfer of the stress to the solid skeleton; this time-dependent response takes place over a time period that is required for full dissipation of the excess pore pressures. Figure 5.7 shows, for purposes of illustration, the variation of the pore fluid pressure in the last loading step for three points selected from different locations of the composite samples (Figure 5.5). Results indicate that the pore fluid pressure in these points rises during the application of the axial load (the first second of the load step). The fluid pressure at location C, located inside the clay disk, increases by a greater magnitude than that computed for locations A and B. As observed in the results of analyses, the fluid pressure at location A, located in the ballotini region between the clay disks, rises to a higher value as the number of clay disks in the specimen is increased. This could be attributed to the thinner ballotini layers between the clay inclusions that can impede the dissipation of the pore fluid from this region. The value of pore fluid pressure computed at location A of the four-disk composite is 27% of that at location C, whereas in eight-disk sample, this magnitude increases to 74% of fluid pressure computed at location C.



(a) 4- disk soil composite



(b) 6-disk soil composite



(c) 8-disk soil composite

Figure 5.7 Pore fluid pressure change in different locations of the soil composites

After the axial pressure was applied at each load step, the axial load was maintained for 24 hours. The variation of pore fluid pressure at locations A and B showed that no measurable excess pore pressure remained in the ballotini region 10 seconds after reaching the maximum axial load (Figure 5.7). Also, dissipation of the excess pore pressure in the ballotini resulted in compression of the ballotini layers between the clay disks. The pore fluid pressure in the clay region was therefore primarily decreased due to a stress relaxation encountered in the central core of the composites, which can be verified by considering the variation of contact stress computed at the upper surface of the sample during any load step. Figure 5.8 depicts the contact pressure change at the locations D and E (Figure 5.5d) of the eight-disk composite model during the fourth load step; here the vertical pressure applied to the central core gradually decreased, resulting in a rise of stress level within the outer annular part of the specimens. Furthermore, the excess pore fluid pressure generated within the clay regions was completely dissipated within 10,000 seconds after the start of the load step, at which time the ultimate axial deformation of the composite model was achieved.

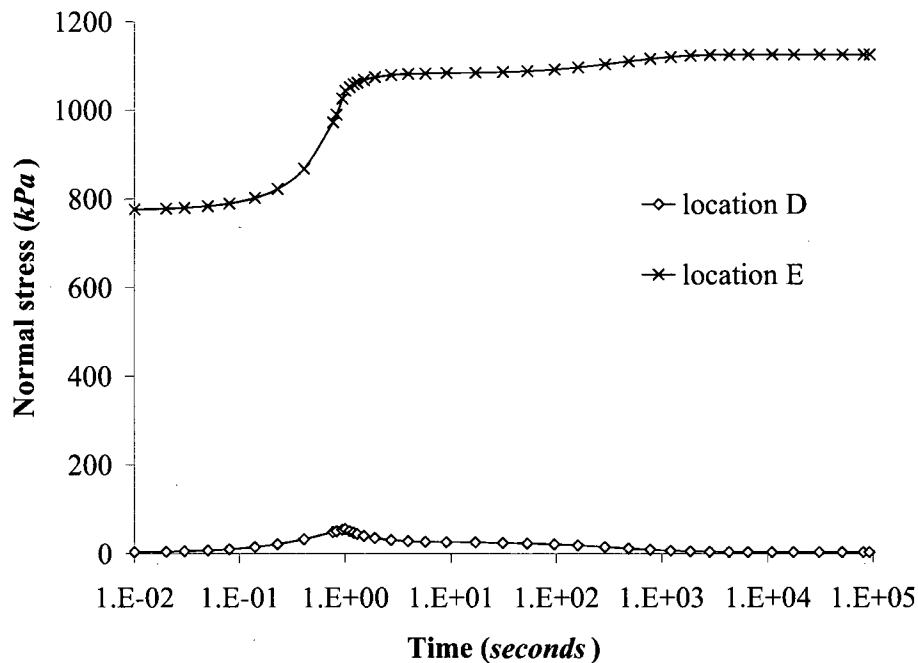
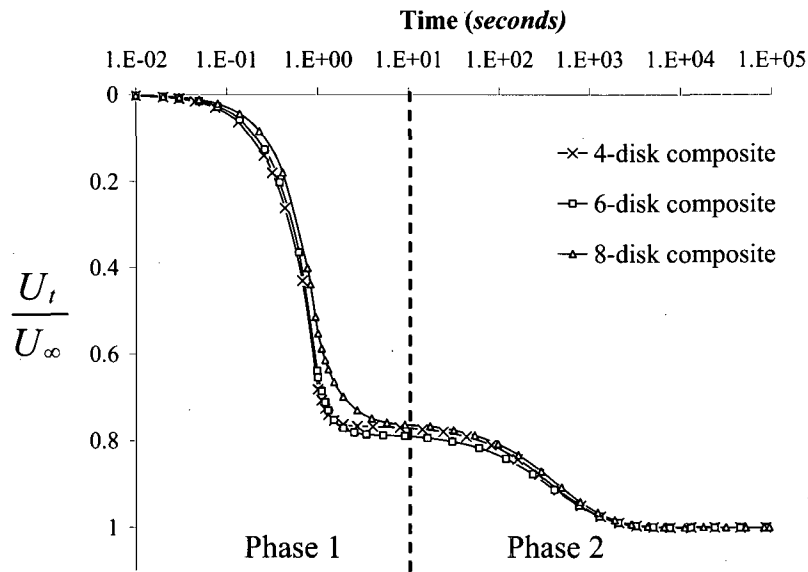


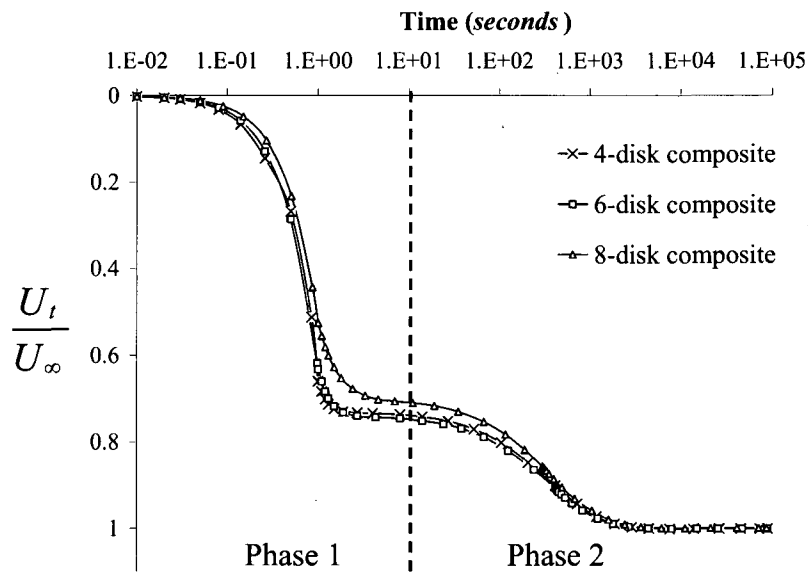
Figure 5.8 Variation of contact stress in the eight-disk composite model (fourth load step)

The progressive axial deformation of the soil composites occurred as a result of a time-dependent consolidation process in the constituents; the normalized axial deformation of the soil composites during the last two load steps, the fourth and fifth load steps respectively, is presented in Figure 5.9 (U_t is the axial deformation at time t and U_∞ is the ultimate axial deformation at each load step). The computations show two different phases in the axial deformation response of the composite; the first phase occurred due to dissipation of the fluid pressure trapped within the pores of the ballotini region. As observed in the results, the axial deformation of the eight-disk sample in this phase was slightly delayed in comparison to that for the other two composites. This difference is attributed to the delay in the dissipation of the pore pressure induced in the ballotini layers located between the clay regions of the eight-disk model. This fact can be verified by comparing the variation of pore fluid pressure at location A of the three composites, depicted in Figure 5.7. The second phase of deformation was related to the expulsion of the pore fluid from the pores of the clay inclusions. In addition, computational results indicate that at each load step 70% to 80% of the total axial deformation occurred during the first phase of the consolidation, which is referred to as the *initial settlement*.

Stress partitioning is another important factor that resulted in the different responses of the composite models. The computational estimates for the vertical contact stress at the upper surface of the three models, at the termination of the analyses, are presented in Figure 5.10. As observed in the contact stress distributions, a greater portion of the applied axial stress was carried by the circumferential region that consists of ballotini. The results also indicate that the contact stress over the central core decreased when the volume proportion of the clay region in relation to the ballotini phase was increased. The possible cause of this phenomenon could be attributed to the load carrying capacity of the central core that is reduced by increasing the volume of soft clay material in this region. As a result, in composite models that include a greater number of clay disks, the circumferential ballotini region was subjected to a higher stress level; therefore, higher axial deformation was obtained from the computations. In the stress partitioning phenomenon that occurred in the composite models, the equilibrium was preserved.



(a) Fourth load step



(b) Fifth load step

Figure 5.9 Axial deformation of the composite models subjected to an oedometric compression test

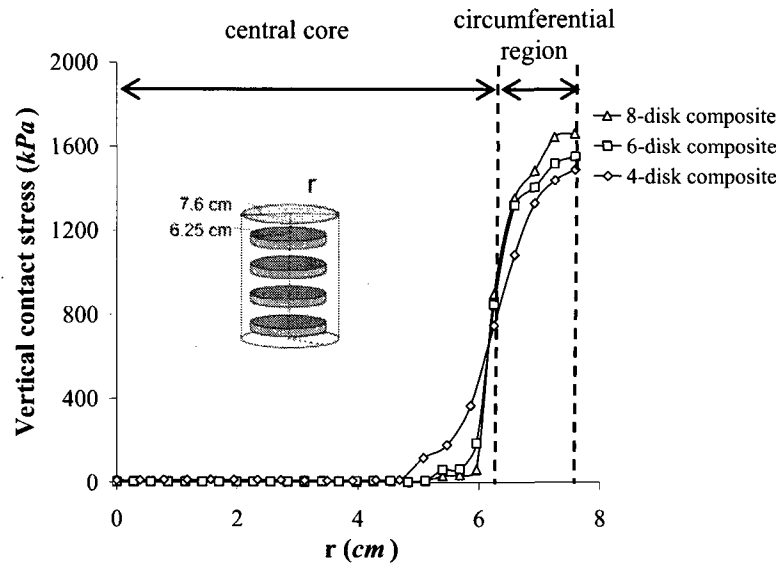


Figure 5.10 Contact stress distributions at the upper surface of the composites (at the termination of the last load step)

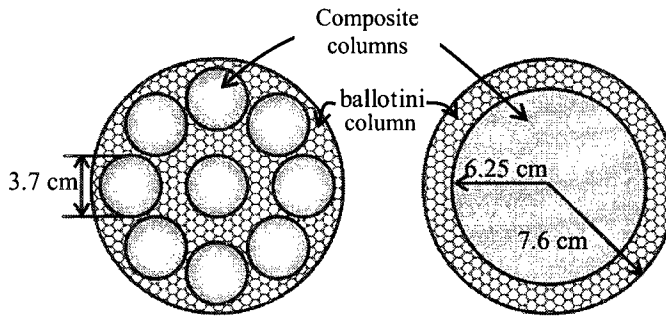
5.5 Dependency of the mechanical response on the shape and configuration of the clay inclusions

In the previous section, it was shown that the mechanical characteristics of the composite specimens depend on the volume proportion of the fine-grained inclusions in relation to the granular phase. In this section, two composite samples with identical volume fraction of clay, $V_{\text{clay}}/V_{\text{total}}$, were modeled in ABAQUS. The results of the simulation were used to indicate that the configuration of the soft lumps in the composites could give rise to different mechanical responses of the samples. The first model represents the composite sample discussed in Chapter 4 that includes 36 clay spheres placed in four layers within the ballotini region, whereas the second model corresponds to the four-disk specimen simulated in this chapter. The materials used in the composite models have identical physical properties and the same volume fraction of clay was considered in the models ($V_{\text{clay}}/V_{\text{total}} = 31\%$).

The computational analyses indicate that when the models are subjected to oedometric compression tests, the axial load is mainly sustained by granular columns that consist of ballotini. Therefore, larger ballotini columns in a composite sample results in a lower

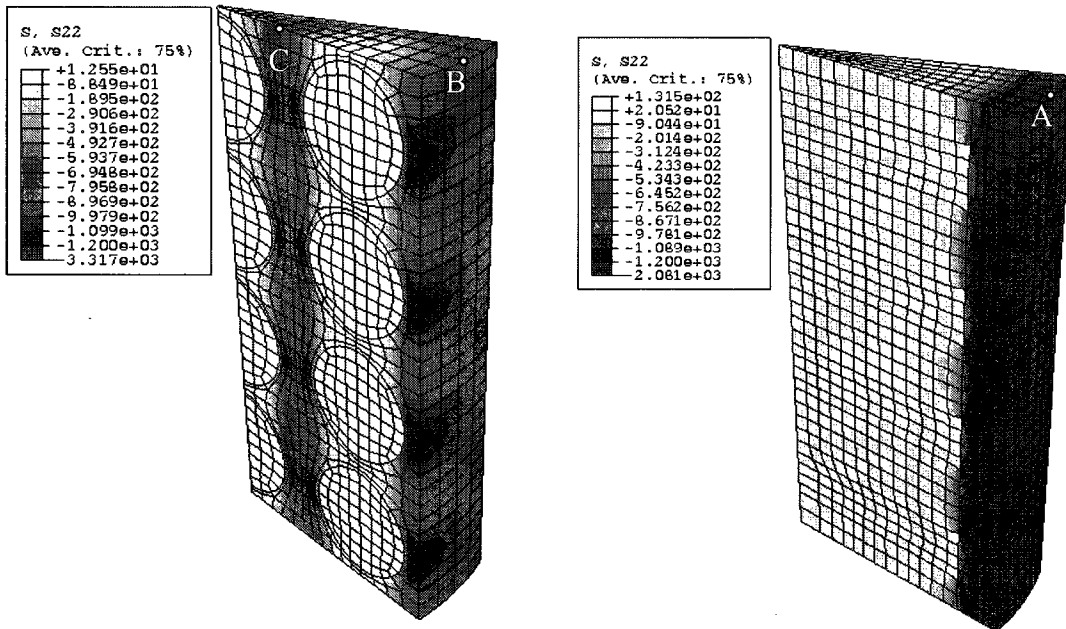
stress state in these columns and, as a result, lower compression is induced in the specimen. Figure 5.11a indicates that in the composite model with spherical inclusions (model-1), the size of the ballotini columns is 44% larger than that in the composite model with disk-shaped inclusions (model-2). As a result, a lower stress state is expected in the ballotini columns located inside model-1. Figure 5.11b illustrates the magnitude of normal stress in different parts of the models computed at the end of the last load step. This figure shows that a lower magnitude of normal stress is induced in model-1 as a result of the larger size of ballotini columns compared to that in model-2. To compare the results of the two simulations, three specific locations were selected on the upper boundaries of the composite models to examine the stress states in the ballotini columns (Figure 5.11b). The computations indicate that at different magnitudes of axial stress applied to the upper boundary, the magnitude of the normal stress at location A is 45% to 48% higher than that computed at locations B and C. The higher stress level in model-2, as compared to model-1, gives rise to a higher axial deformation of the model. As shown in Figure 5.12, at the end of the last load step, the model with spherical clay inclusions (model-1) shows an axial deformation of approximately 3.12 *mm*, which is 1.28 *mm* lower than that computed for the four-disk model (model-2).

The type and configuration of the clay inclusions can also alter the amount of settlement that takes place in the two different phases of the consolidation process. In order to investigate this phenomenon, a comparison was performed on the normalized consolidation settlement curves of the two composite models that occurred at different load steps (Figure 5.13). The computations indicate that, although both models have the same volume proportion of constituents, model-1 displays a higher percentage of settlement in the first consolidation phase, and this mainly corresponds to the progress of time-dependent deformation in the ballotini. The normalized consolidation curves indicate that in model-1, 6 to 10% of the axial deformation occurs in the second consolidation phase; this amount increases to 20% to 30% in model-2. Thus, the shape and distribution of the clay inclusions result in different stress distributions within the composite models while the variation of stress distribution gives rise to different magnitudes and rates of deformation.



Area of the composite column	96.7 cm ²	122.6 cm ²
Area of the ballotini column	84.7 cm ²	58.8 cm ²

(a) Planar cross section of the composite samples



(b) Normal stress distribution at the termination of the last load step

Figure 5.11 Computational modeling of the soil composites containing spherical and disk-shaped clay inclusions

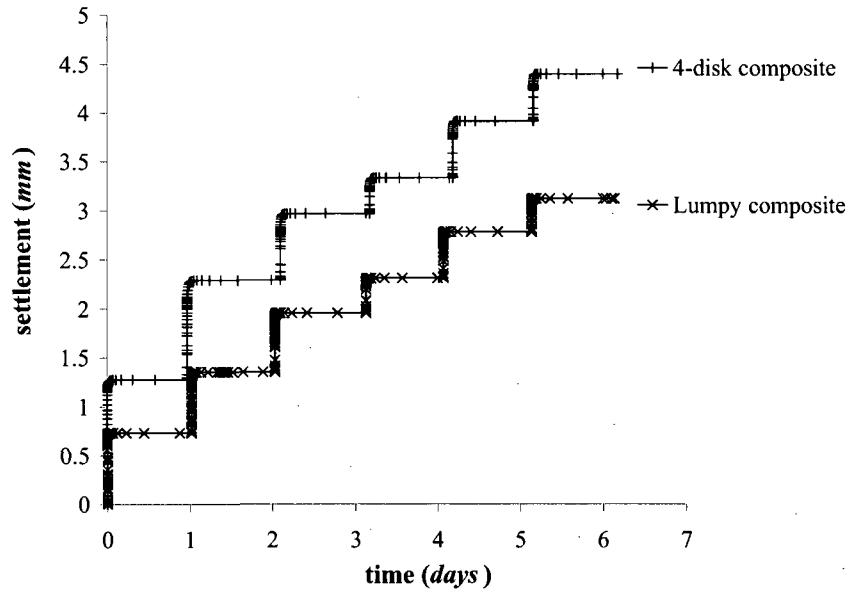


Figure 5.12 Axial deformation of the composite models during six successive load steps

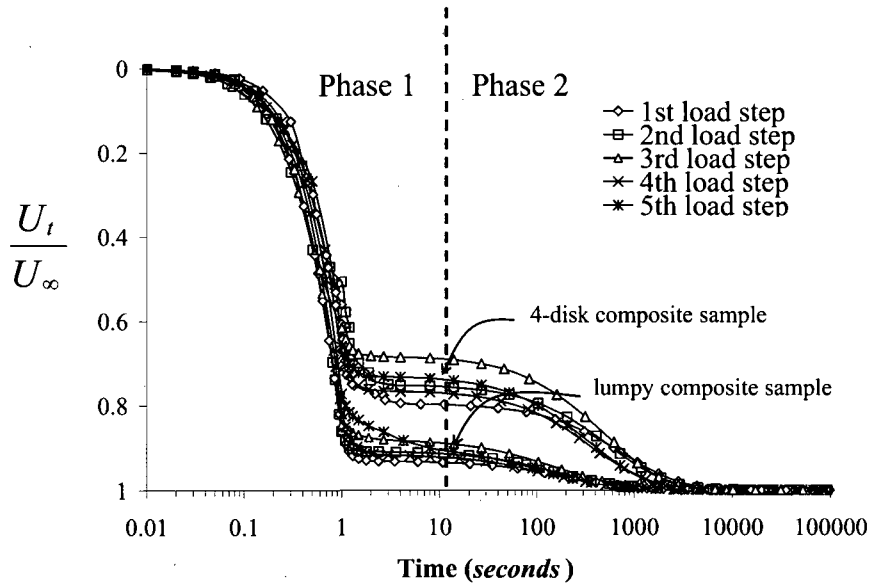


Figure 5.13 Axial deformation of the composite models subjected to an oedometric compression test

5.6 Comparison between numerical predictions and experimental results

In this section, the constitutive models, which were developed for modeling the mechanical behavior of the Montreal silty clay and ballotini, are implemented in the computational analyses of the soil composites. The comparison between the numerical predictions and experimental results will establish the predictive capabilities of the methodology that can be used in further computational studies of practical problems related to offshore land reclamation.

Computations were performed using the finite element models shown in Figure 5.5. The constitutive models and the initial physical state of the materials determined during the fabrication of the composite specimens were implemented in the analyses. Figure 5.14 shows the comparison of the displacement-time responses derived from the computations and the corresponding experimental results. For the purposes of comparison, results are presented for three soil composites (the four-disk, the six-disk, and the eight-disk configurations) subjected to an axial load that was increased during five consecutive load steps. It can be seen that the computational estimates predict, reasonably accurately, the *experimental trends* for the load-displacement response of the three composite specimens tested. The axial settlement of the composites at the end of the last load step, predicted from computations, is approximately 5% to 10% lower than the experimental responses.

The hydraulic conductivity of the silty clay was estimated using the consolidation curves obtained from conventional oedometer tests. The experimental results indicated that this parameter is dependent on the void ratio of the material; the hydraulic conductivity evaluated from the first load step, in which the void ratio of the specimen reduced from 0.63 to approximately 0.57, was estimated to be 7.2×10^{-8} cm/s, while it decreased to approximately 2×10^{-8} cm/s at a void ratio close to 0.46. Furthermore, in the central core of the composite specimens, that contained both soft silty clay disks and ballotini, a high proportion of the axial deformation of the composite column occurs in the clay disks, and not due to deformations in the separating ballotini, mainly attributed to the relative stiffness properties of these constituents. Although a higher deformation was obtained by incorporating more clay disks in the composite, increasing the number of disks in the core region results in lower compression of each disk due to the increase in the volume of

the soft soil. Therefore, lower compression of the clay inclusions gave rise to a higher void ratio and a correspondingly higher hydraulic conductivity of the material.

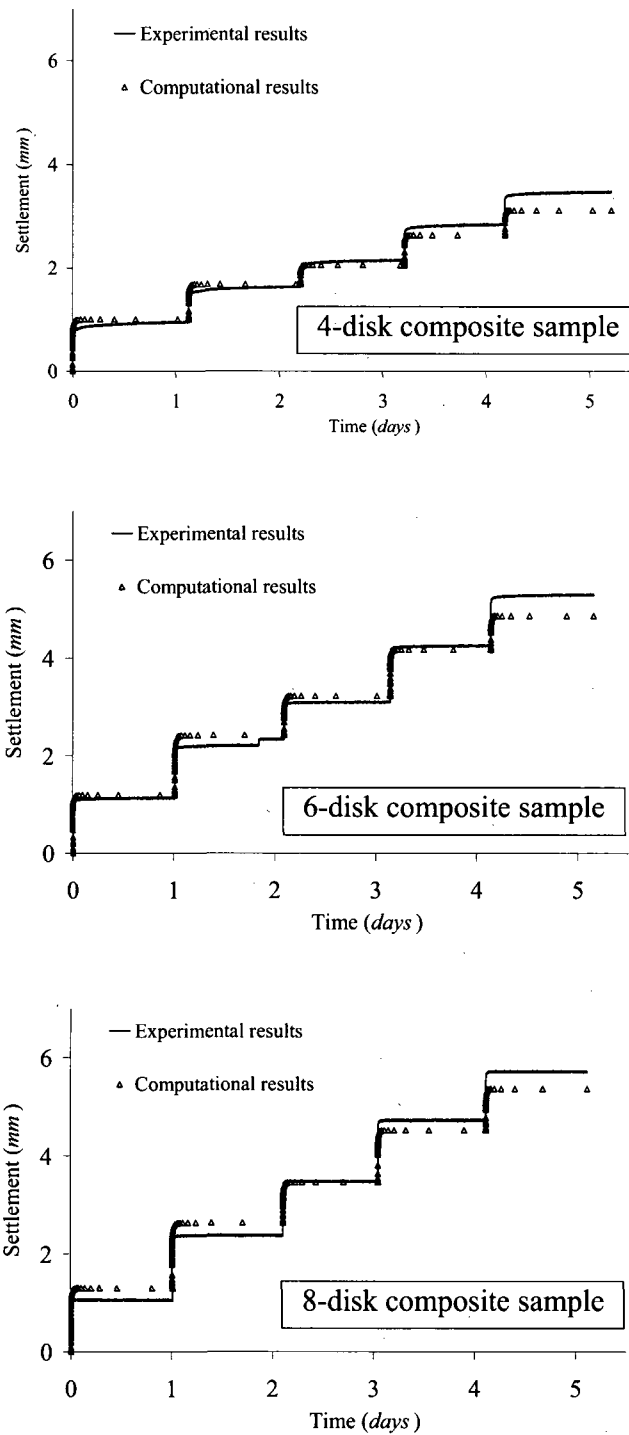


Figure 5.14 Axial deformation of the composite samples in five successive load steps

The computations attempt to predict the mechanical response of the composite samples by assigning two different values for the hydraulic conductivity. The lower value was selected, from the results of the oedometer tests, at $2 \times 10^{-8} \text{ cm/s}$ corresponding to a void ratio of 0.46. The hydraulic conductivity of the clay in the first load step of the oedometer test was estimated at $7.22 \times 10^{-8} \text{ cm/s}$ (Table 2.4). Due to the stress partitioning in the soil composites, the clay inclusions within the composite could be subjected to lower stress states, compared to that applied in the first load step of the oedometer test (normal stress of 12 kPa). The higher value for hydraulic conductivity was therefore chosen as $2 \times 10^{-7} \text{ cm/s}$ (10 times higher than the lower limit) which could be an estimate of the hydraulic conductivity when the clay has a void ratio higher than 0.57.

The computational estimates and experimental results for the settlement-time curves at different load steps are presented in Figures 5.15, 5.16 and 5.17 for four-disk, six-disk and eight-disk composite samples, respectively. Numerical estimates indicate that, after 10,000 *seconds*, no excess pore pressure remains within the composites, from which it could be concluded that the ultimate consolidation settlement of the composites was achieved. In the four-disk sample, the computations *overestimate* the settlement of the sample during the first two load steps (Figure 5.15 a,b); however, *reasonable predictions* were obtained for the consolidation curves during the last three load steps (Figure 5.15 c,d,e). It can be observed that, in the case of the four-disk composite, the computations performed with the value of $k_{clay} = 2 \times 10^{-8} \text{ cm/s}$ gave better predictions. Figure 5.16 compares the numerical results of the analysis performed on the six-disk model with the test data; the results indicate that the experimental results for the settlement curves approach the computational results when the higher hydraulic conductivity of the silty clay material is considered ($k_{clay} = 2 \times 10^{-7} \text{ cm/s}$). The computational and experimental results corresponding to the eight-disk composite are shown in Figure 5.17. It can be seen that the experimental results exhibit lower rates of consolidation during the first phase of the consolidation process. This phenomenon can be attributed to the slow dissipation of excess pore pressure generated in the ballotini layers located between the clay disks; in the eight-disk sample, the clay disks were placed approximately 1.6 mm apart, and it is likely that contact between the disks results in the entrapment of fluid within the thin

layers of ballotini. This results in a slower transfer of the load to the circumferential ballotini region and therefore a delay in the progress of the first phase of the consolidation process.

The experimental observations indicate that the time-dependent compression of ballotini results in further settlement of the sample after the termination of the consolidation process, a phenomenon that is more observable in the four-disk composite due to the higher volume proportion of ballotini. The reduction in the volume fraction of ballotini in the six-disk and eight-disk specimens results in negligible time-dependent axial deformation after the termination of the consolidation process.

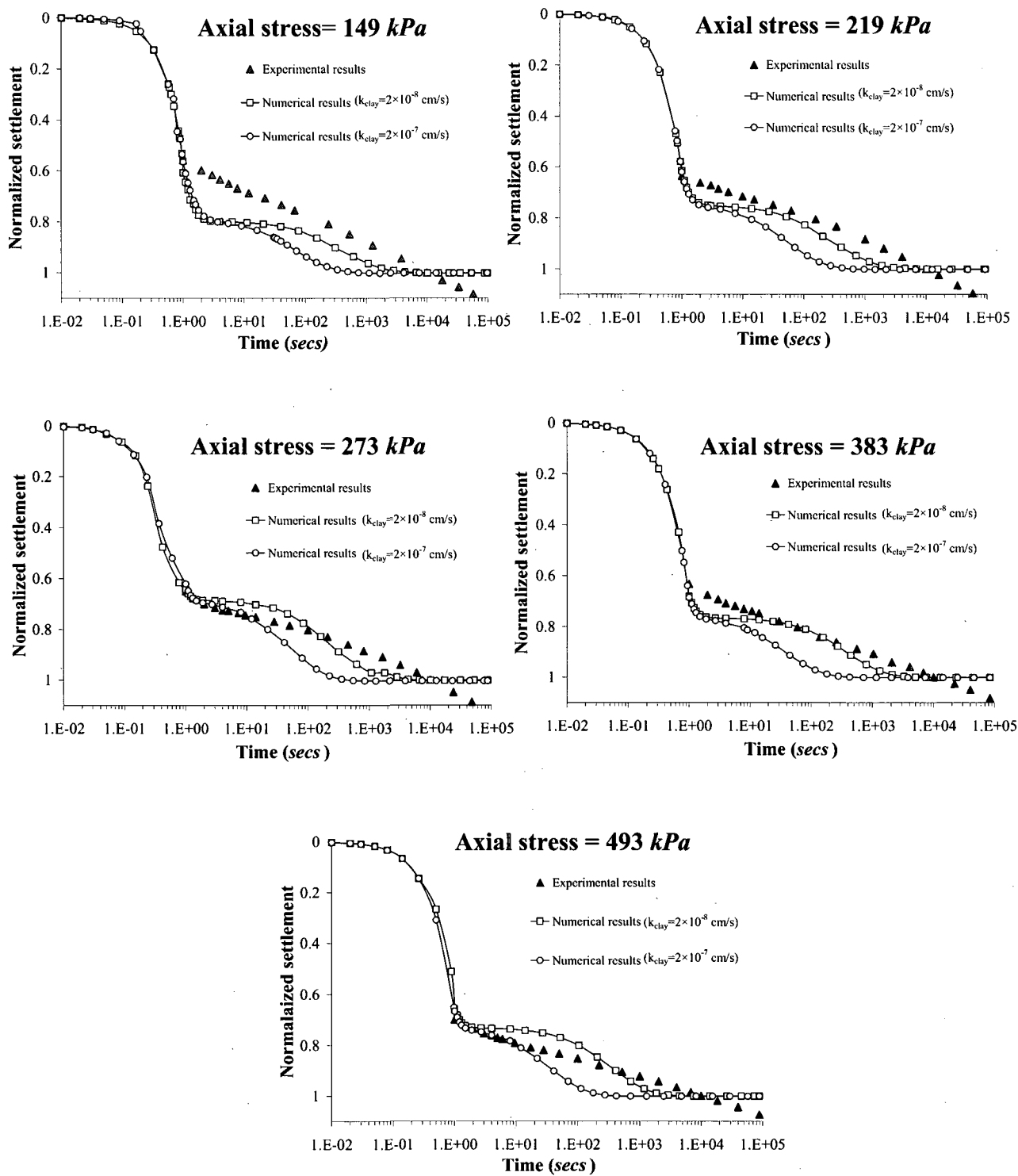


Figure 5.15 Consolidation curves of the four-disk composite sample subjected to an oedometric compression test

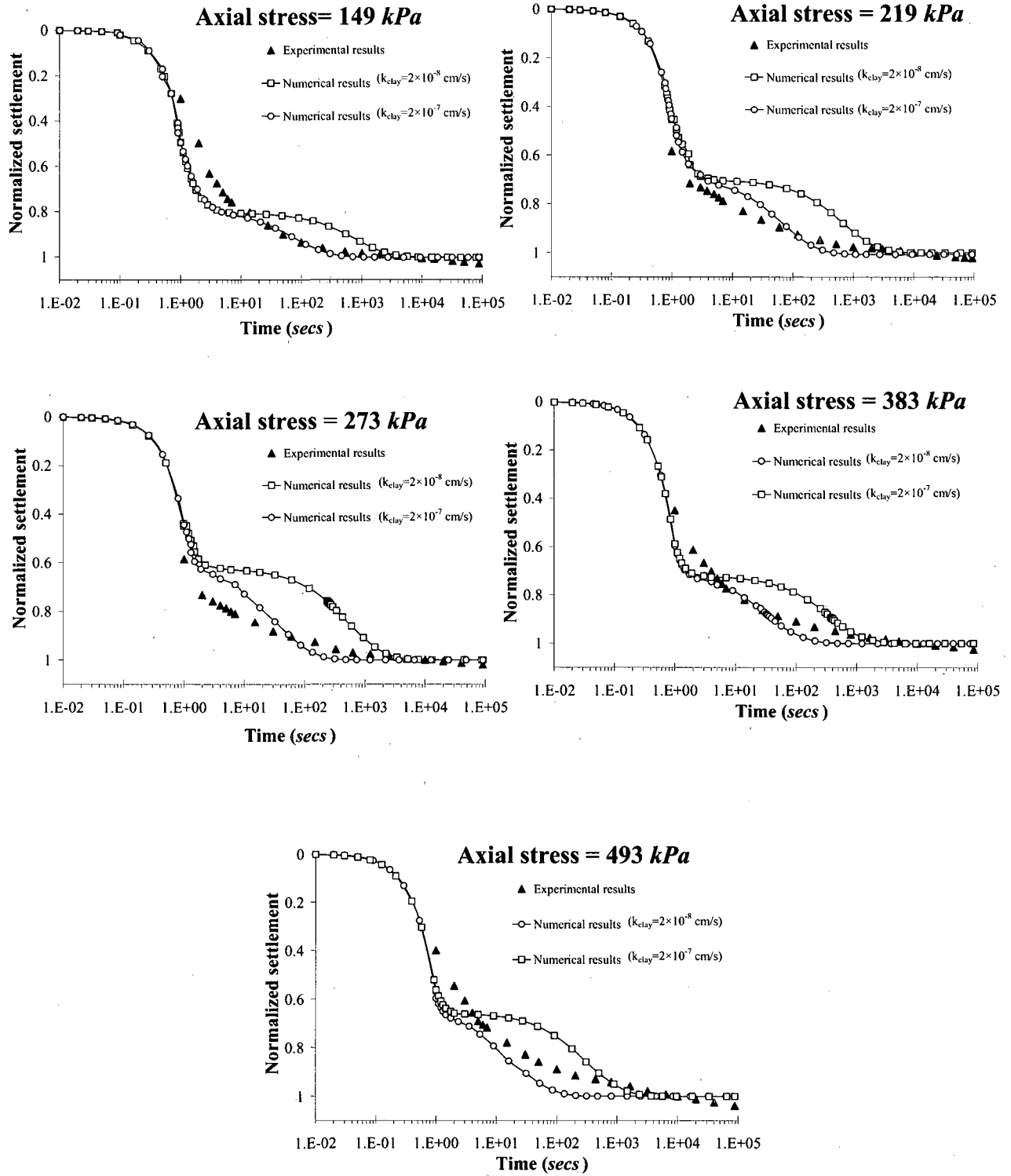


Figure 5.16 Consolidation curves of the six-disk composite sample subjected to an oedometric compression test

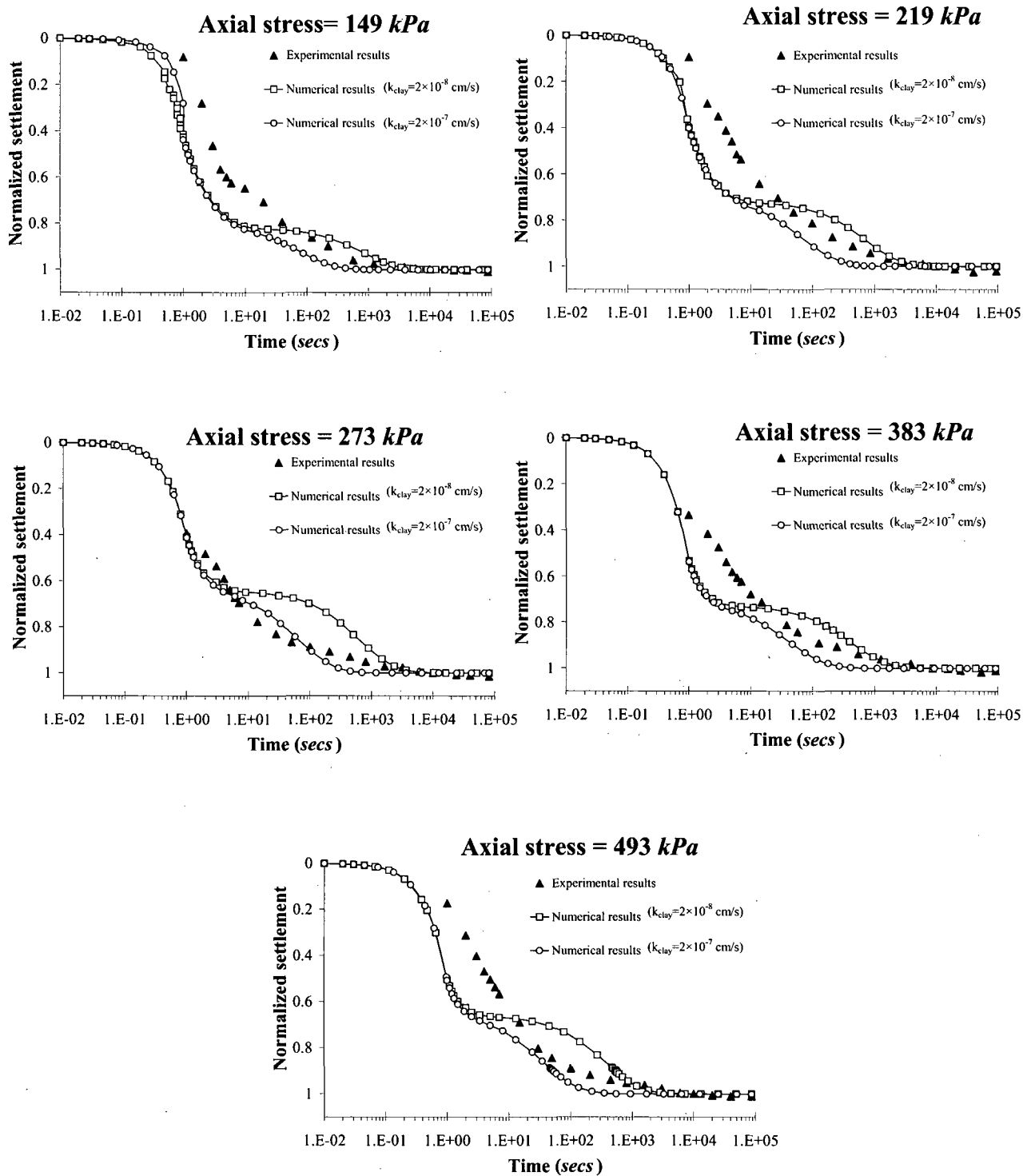


Figure 5.17 Consolidation curves of the eight-disk composite sample subjected to an oedometric compression test

5.7 Summary remarks

In this chapter, the bench-scale oedometric behavior of three types of composite samples was examined. The experimental research dealt with composite samples fabricated with different volume proportions of silty clay disks in relation to the ballotini. The bench-scale oedometer test provides a useful technique for assessing the mechanical characterization of a porous composite media including different volume proportions of fine-grained and coarse-grained constituents. The one-dimensional response also simulates the state of deformation in a land reclamation application where the thickness of the composite fill is much smaller than the area dimensions (Yang et al., 2002; Robinson et al., 2005). During each load step, two stages were observed in the time-dependent deformations of the specimens; the first phase occurred shortly after application of the load (<10 sec) mainly due to the progress of the consolidation process in the ballotini region. This deformation phase was followed by a further compression that took place over a longer time period as a result of the dissipation of excess fluid pressure generated within the pores of the fine-grained region. The constitutive models developed for the silty clay and ballotini were implemented in a computational code, and this was used to predict the mechanical response of the composites subjected to the oedometer compression test. The investigations show that the computations can establish the trends in the axial deformation of the composite specimens although the total displacement at the termination of the last load step is underestimated by 5% to 10%. Furthermore, the settlement-time curves predicted from the computational approach correlate well with the results of the experiments conducted on the three different composite specimens.

CHAPTER 6

MECHANICS OF A FLUID SATURATED COMPOSITE POROUS MEDIA SUBJECTED TO FOUNDATION LOAD

6.1 Introduction

The study of the interaction between a foundation and a supporting soil is a problem of continuing interests for both geotechnical and structural engineers. The estimation of the ultimate bearing capacity and the settlement of a foundation is necessary for serviceability and stability considerations. In several studies, the behavior of footings resting upon a homogeneous soil region has been investigated (Ueshita and Meyerhof, 1968; Poulos and Davis, 1974; Selvadurai, 1979, 2007; Davis and Selvadurai, 1996). It is recognized that the assumption of homogeneity cannot truly represent many soil profiles such as either naturally stratified non-homogeneous soil media or weak soil deposits that are reinforced to improve both their load carrying capacities and deformability characteristics.

Stratified soil deposits are non-homogeneous soils that have been formed naturally during different cycles of sedimentation associated with periodic changes in climatic conditions or cyclic shifting of tributaries on deltas (Tschebotarioff and Bayliss, 1948; Eden, 1955). Many sites with layered soil profiles have been investigated and analyzed (Hanzawa and Adachi, 1983; Cao et al., 2001). Other types of layered soil profiles are typically encountered in land reclamation activities; in clay-sand reclamation schemes the reclaimed land is constructed by spreading layers of coarse-grained soil between the layers of hydraulically placed soft clay. Several attempts have been made to investigate the behavior of footings resting upon a soil whose elastic stiffness varies with the depths of location. The related elasticity problem has been studied analytically by Gibson (1967), Gibson et al. (1971) and Brown and Gibson (1972, 1979) who considered the mechanical response of a loaded half-space and a finite layer where the stiffness

properties increase linearly with depth. Carrier and Christian (1973) and Boswell and Scott (1975) employed the finite element technique to investigate the elastic behavior of circular footings resting on a soil with linearly varying elastic modulus. In further studies, Rowe and Booker (1981a,b) used the finite layer method to examine the behavior of both strip and circular footings resting on a non-homogeneous soil profile, which included a deposit underlying a weathered crust. They concluded that the presence of a soil crust had a noticeable influence upon the settlement of a footing; the approximate approach that considered the soil to be a homogeneous deposit, resulted in $\pm 30\%$ errors in the estimation of the central settlement of the footing. Booker et al. (1985) developed a solution for the settlement response of a half-space whose elastic modulus increases as an exponential function of depth and subjected to surface load acting over a circular or strip footing. It was shown that the profiles of the surface settlement due to a load acting over the strip or circular regions (flexible and rigid) are highly dependent on the variation in the elastic modulus. A numerical solution presented by Tham et al. (1988) models the soil by combining the spline finite element and finite layer model; the soil is modeled by the finite layer method and the footing is represented by the double spline element. Analyzing the effects of the footing stiffness and different types of non-homogeneity on the behavior of foundations, these authors presented a series of influence charts that can be used by engineers to estimate the settlement of rigid and flexible footings resting on non-homogeneous soil layers. To investigate the behavior of sand beds containing an inter-stratified clay layer, Oda and Win (1990) conducted sets of experiments on bench-scale composite samples. It was observed that increasing the thickness of the clay layer and locating that closer to the surface result in lower failure load and higher settlement. Conte and Dente (1993) employed the stiffness method proposed for solving wave propagation problems to examine the plane strain response of a layered soil subjected to strip loads. They determined the settlement of a uniform soil deposit including a softer or stiffer layer placed at different depths within a uniform medium. It was shown that the inclusion of the soft layer significantly increases the amount of settlement, especially when the layer is located near the surface, whereas there is only a slight influence exerted by the presence of a stiff layer. In a further study Chandrashekhara and Antony (1996) investigated the interaction of a strip footing resting on a non-homogeneous half-plane

and a non-homogeneous elastic layer resting on a rigid stratum, using combined analytical and finite element methods. Their results showed that the variation in elastic modulus and the relative rigidity parameter of the footing to half-plane has a significant influence on the contact pressure distributions and the settlement profiles. In another study, Selvadurai (1996b) examined the axisymmetric problem of the indentation of a non-homogeneous elastic half-space by a smooth rigid indenter. The non-homogeneity in the linear elastic shear modulus was a bounded variation with depth (Selvadurai et al., 1986). The analysis of the problem was reduced to the solution of an integral equation, which was solved numerically. He showed that the load-settlement behavior of the footing is influenced by the spatial change and the ratio of the shear modulus at the surface to that at an infinite depth below the footing. The same model of elastic non-homogeneity was used by Vrettos (1998), for the development of simple algebraic expressions for estimating the elastic settlement and rotation of a rigid rectangular footing subjected to a vertical force and moments. Stark and Booker (1997) also developed a numerical scheme in which the surface displacement of both a homogeneous and a non-homogeneous half-space subjected to uniform traction on a rectangular shaped domain was calculated. In a further study performed by Doherty and Deeks (2003), a scaled boundary finite-element method is used to obtain semi-analytical stiffness coefficients for a rigid circular footing embedded in a non-homogeneous elastic half-space. The results of the investigation showed that there is an appreciable effect of the non-homogeneity on all stiffness coefficients; the greatest influences are for the vertical and moment load resultants as the displacement field extends deeper into the half-space where the elastic material has increasing stiffness. Maheshwary and Madhav (2006) considered the vertical displacement and stress distribution of strip footings resting on three-layered soil media with a thin, significantly stiffer layer, located between two comparatively soft layers. The solution of this problem, based on the finite difference method, revealed that the middle layer acted as a plate and redistributed the stress uniformly to the soft layer below. It was also shown that the magnitude of the surface settlement can be decreased by placing the stiff layer closer to the ground surface.

Stabilized composite fills are another type of non-homogeneous soil in which the load carrying capacity of soft deposits is improved by installing piles made of sand, gravels or stone; for this reason the procedure is also referred to as the use of stone columns, within soft soils (Hughes and Withers, 1974; Hughes et al., 1975). The analysis of settlement and the prediction of the ultimate bearing capacity are the main problems to be solved for this type of constructed fill. Madhav and Vitkar (1978) presented expressions based on upper bound theorem for the ultimate bearing capacity of strip footings resting on soft fills reinforced by granular trenches directly beneath the footing. Their parametric study indicated a substantial increase in the bearing capacity of a soil stabilized with a granular trench. Aboshi et al. (1979) observed in several field investigations that a soft clay subsoil stabilized by sand columns exhibited a higher bearing capacity and lower consolidation settlement, compared to an unstabilized soft clay subsoil. For a typical cylindrical pile-soil unit, Balaam and Booker (1981) proposed an analytical solution for the settlement of a rigid foundation based on the theory of elasticity. They also investigated the effect of the stiffness ratio of the pile to the soil on the magnitude and rate of settlement of the composite layers. These authors extended the solution to take into account confined yielding of the frictional column material and presented correction factors that can be applied to the elastic solution in order to estimate the settlement response of the stabilized composite layer (Balaam and Booker, 1985). In addition, Mitchell and Huber (1985) performed an axisymmetric finite element analysis of a stone column foundation in which the columns are modeled as cylindrical rings around a central column. Assuming undrained clay properties and drained properties for the sand columns, the settlements computed from finite element analysis were found to be in good agreement with the results obtained from individual field load tests. In a further study, the importance of the dilatancy of the material that constitutes the reinforcing columns was investigated by Poorooshasb and Madhav (1985). The homogenization approach was also employed in finite element analyses conducted by Schweiger and Pande (1986) to investigate the failure load and settlement of rafts resting on stone column-reinforced soft layers. They assumed that the effect of the stone columns is uniformly distributed over the stabilized region, whereas this assumption can be justified only when the dimension of the raft is considerably larger than the diameter and the spacing of the columns.

Canetta and Nova (1989) presented a method to derive the constitutive characteristics of the homogenized medium. In this method the equivalence was reached by satisfying the equilibrium and compatibility conditions at interfaces and by considering the work in the equivalent material to be equal to the sum of the work done in soil and reinforcing materials. Another homogenization technique was presented by Lee and Pande (1998) in which the elastoplastic constitutive behaviors were defined for both the stone column and reinforced soil base. For this purpose, they developed a new sub-iteration procedure within an implicit backward Euler integration scheme that satisfies the equilibrium and compatibility conditions. The scope of non-homogeneity in geomechanics applicable to both naturally occurring and constructed soils is extensive. Recent advances in experimental, computational and field studies can be found in the articles by (Aleynikov, 2000; Selvadurai, 2007).

6.2 Computational modeling of the composite lumpy fills

In this chapter, different composite lumpy fills are simulated in a computational modeling exercise to investigate the effect of various parameters on the mechanical characteristics of the composite fills. The primary area of application envisaged is in land reclamation activities involving dredged fills. To select proper dimensions for the composite fill and clay lumps dredged from the seabed, different features of the fills constructed in reclamation projects were examined.

The Logan Airport, opened in 1923 in Boston, has expanded over the years on the constructed fill consisting of 30 million m^3 of overconsolidated clay, formed with clay lumps (maximum diameter of 20 cm) that were hydraulically pumped to the site (Casagrande, 1949). In the Halmstad harbor, situated in South-Western Sweden, the reclamation project, which was started in 1974, deposited lumps of clay dredged from the seabed and dumped using bottom-opening barges. This dredged material mainly consisted of stiff silty clay blocks of up to 1 m^3 size. The height of the barge-dumped layer was about 3 m and was located 2 m below the sea level. Another layer, with a thickness of 3.4 m, was constructed from well-rounded lumps of clay with a diameter of

up to 30 cm extracted using a cutter suction dredger (Hartlen and Ingers, 1981). Leung et al. (2001) reported that during the construction of the New Container Terminal in Singapore, the clay parts dredged by a clam-shell grab typically consisted of lumps with an average volume of approximately 1 m^3 . In the construction of Punggol Timor Island, large dredged clay lumps of up to about 8 m^3 in volume were excavated using a clam-shell grab (Karthikeyan et al., 2004). These lumps were transported and dumped onto the seabed to form an island with a lumpy fill layer close to 8 m in thickness. During the transportation and dumping, the original large clay lumps may have been broken into lumps of various sizes ranging from 0.5 m to 2 m. A sand layer of 10 m thickness was used as a surcharge to accelerate the consolidation of this lumpy fill layer. Robinson et al. (2005) also indicated that in reclamation projects, dredging seabed clay using very large clam-shell grabs of sizes 10 m^3 to 24 m^3 often results in lumps in excess of 1 m^3 to 2 m^3 .

Size of the clay lumps and the depth of the composite model

Using information available on the dimensions of the lumpy fills in various reclamation projects, cube-shaped lumps of 1.5 m square in plane area and 1.4 m in height (volume= 3.15 m^3) were selected for the computational analyses. Observing the dimensions of the lumpy fills constructed in different reclamation projects, a composite layer with a depth of 5.6 m was considered in the computational modeling; this domain can enclose three composite lumpy layers separated by thin layers of a granular fill.

Lateral dimensions of the model

The lateral dimensions of the domain have to extend beyond the edge of the footing to eliminate the effect of the boundary interface on the numerical results. The computations attempt to determine the proper dimension of the domain so that the boundary interface condition does not contribute appreciably to the results (an error less than 5%). For this purpose, a homogeneous region with elasticity properties corresponding to that of ballotini in the loose state ($E = 27000\text{ kPa}$, $\nu = 0.3$) was chosen. The homogeneous granular medium is loaded by a 6 m square rigid footing placed on the surface of the fill. Due to the symmetrical configuration, only one-quarter of the domain need to be modeled. A uniform pressure of 1000 kPa was applied to the rigid footing for two

different types of boundary conditions considered for the outer boundaries: (i) a bonded condition in which the nodes on the boundary are restrained from moving in any direction, (ii) an unbonded condition corresponding to the case where nodes on the outer boundaries are only restrained from moving in the direction perpendicular to the boundary surface (Figure 6.1). Domains of different lateral extent were modeled keeping the depth the same (5.6 m), while the circumferential boundaries were successively located from a distance of 3 m (beside the edge of the footing) to 30 m away from the centre of the footing. The models are discretized into approximately 30,000 quadratic 10-node tetrahedron elements, with finer meshing incorporated in the region near the edge of the footing (Figure 6.1). The results indicate that in the unbonded case the maximum settlement occurs when the load is applied to a soil column with the same cross section as the footing (Figure 6.2). By increasing the size of the domain, the magnitude of settlement reduces as a result of the stress distribution that occurs in the homogeneous fill. For the *unbonded boundary*, the minimum settlement is obtained when the boundaries are located 4.5 m away from the center of the footing, while higher settlement is estimated when the width of the domain is increased. For the *bonded boundary* conditions, increasing the size of the fill in the lateral directions results in a constant increase in the settlement of the rigid footing. To reduce the computation costs, especially for more complicated analyses that incorporate time-dependent effects due to pore fluid pressure dissipation and non-linear responses that are associated with the skeleton response, a domain can be selected where the boundary interface condition does not appreciably influence the results. Figure 6.2 shows that by increasing the size of the domain from 30 m to 60 m results in an increase of less than 3% in the footing settlement. Therefore, in this numerical study, the size of the fill in both horizontal directions is set to 30 m with the vertical boundaries located 15 m away from the center of the footing.

d = displacement

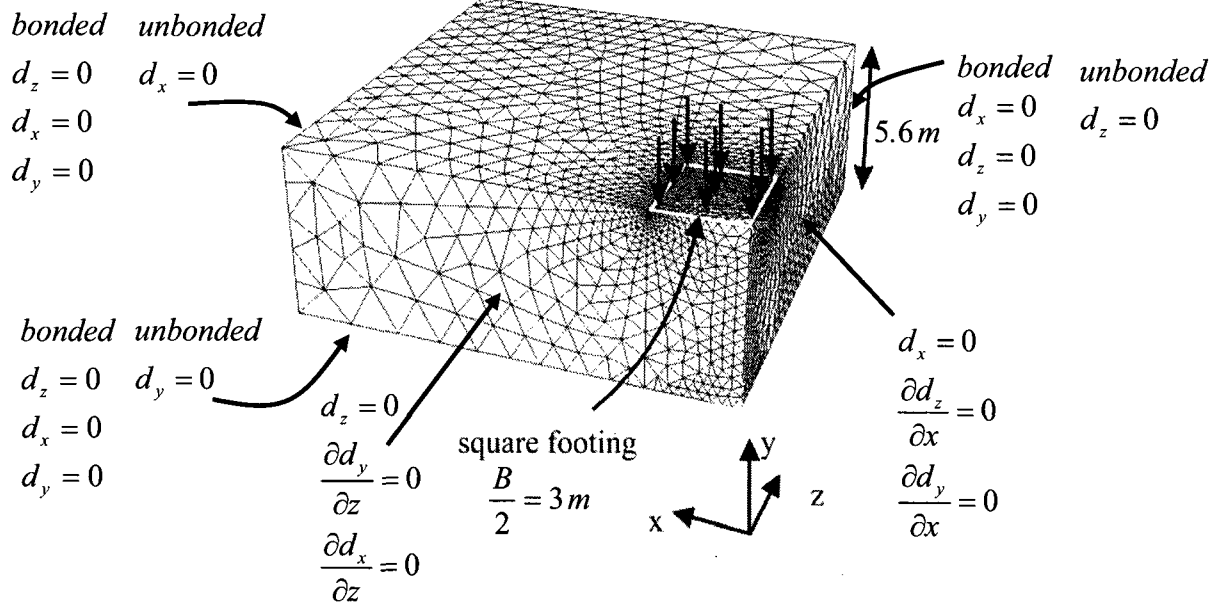


Figure 6.1 Typical discretized finite element model ($30 \times 30 \times 5.6\text{ m}$) used to determine the effect of the boundary interface

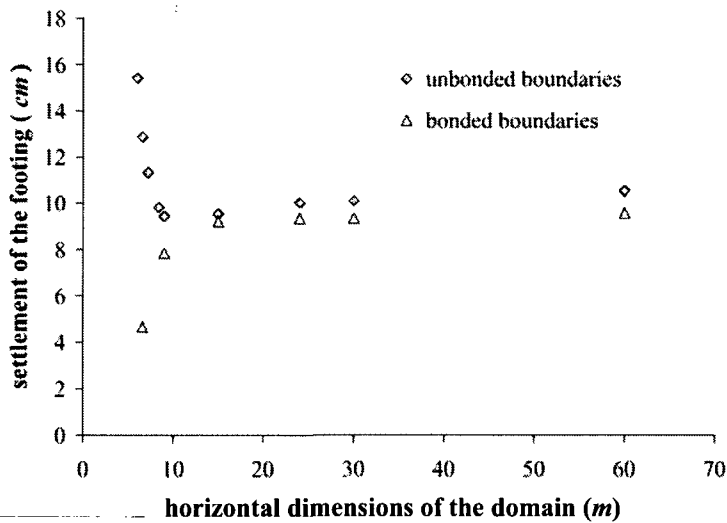


Figure 6.2 Settlement response of the footing for different sizes of the elastic domain

Composite lumpy fills modeled in the computational analyses

The composite lumpy fills consist of a granular region interspersed with cubes of fine-grained soil (referred to subsequently as lumps) with plan dimensions of $1.5\text{ m} \times 1.5\text{ m}$ and 1.4 m in height. The clay lumps were placed at different depths within the composite fill. In this modeling, different types of lumpy fills with various numbers of clay lumps were modeled using ABAQUS/Standard; the regions of the composite containing both ballotini (with the hypoelasto plastic constitutive model defined in Chapter 3 for ballotini) and clay material (with the Cam clay constitutive model defined in Chapter 2 for Montreal silty clay) were designated as *composite layers*. The composite fill can enclose three of the composite layers; each layer can contain different volume proportions of clay and ballotini. Figure 6.3 shows one composite layer that contains 25% volume proportion of the clay material ($V_{\text{clay}}/V_{\text{total}}$), the remainder being the ballotini phase. As the first part of the computational investigation, one composite layer was placed at three different levels within the composite fill. This arrangement is referred to as **one-layer** fills. The exact locations of the composite layer in the **one-layer** composite fills, denoted as **one-layer-B**, **one-layer-M**, and **one-layer-T**, are shown in Figure 6.4 a,b,c. The designations **B**, **M** and **T** refer respectively to the base, mid-section and top location of the composite layer within the composite fill. Furthermore, in **two-layer** and **three-layer** composite fills, respectively, two and three composite layers are modeled.

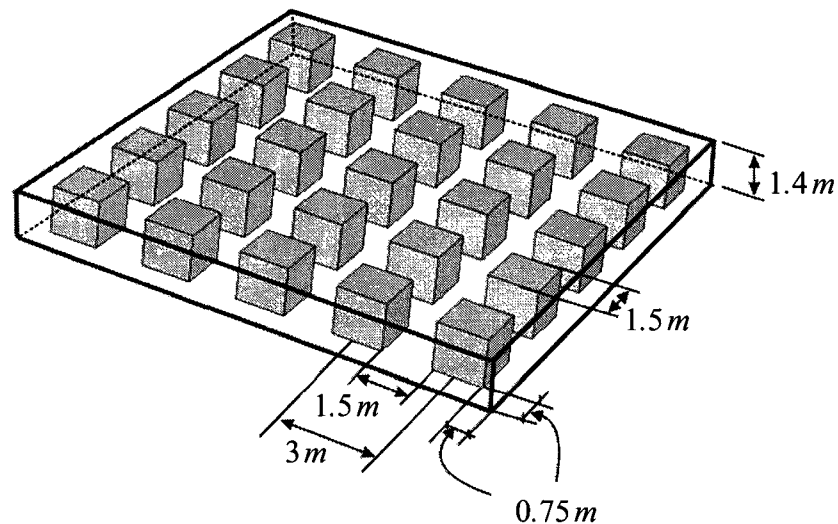


Figure 6.3 The composite layer with 25% volume fraction of clay

Figure 6.4 d,e shows the exact locations of the composite layers in the models: In the **two-layer** composite fill, the distance between two composite layers is 1.4 m, which is reduced to 35 cm in the **three-layer** fill.

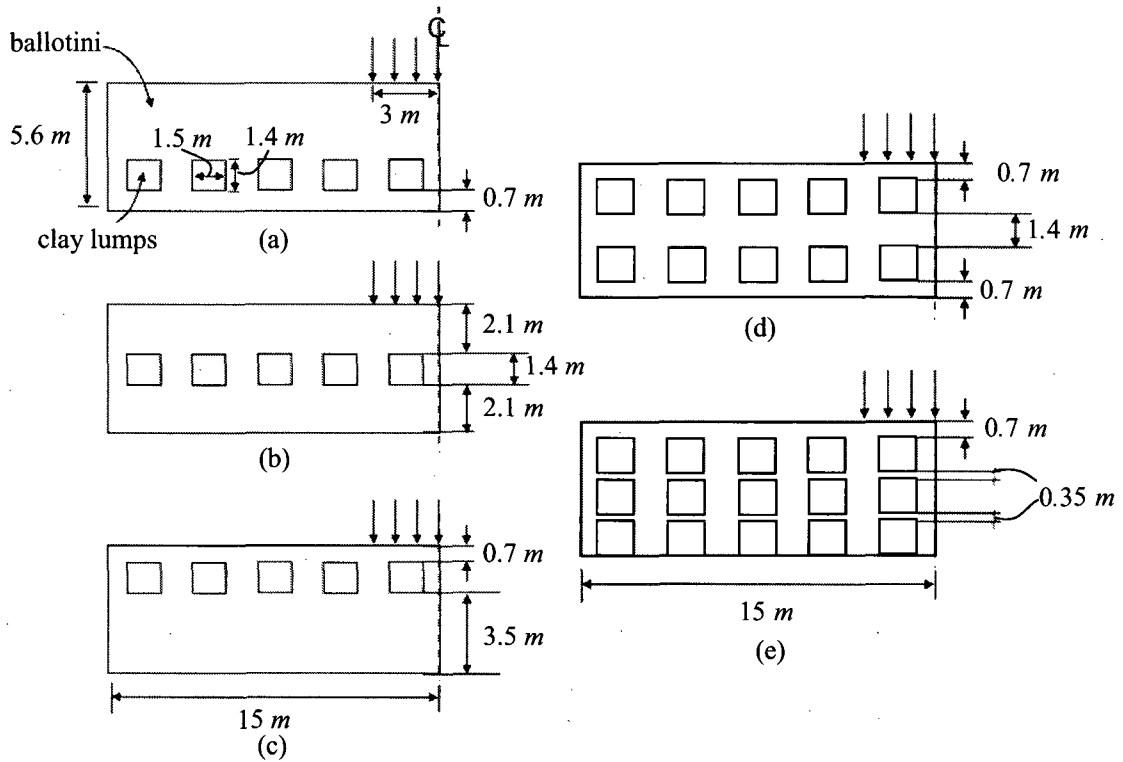


Figure 6.4 Locations of the composite layers in (a) one-layer-B (b) one-layer-M (c) one-layer-T (d) two-layer (e) three-layer composite fills

The observation made at the termination of the bench-scale experiments indicated that no noticeable penetration occurred in the interface of the soft lumps and ballotini region. Therefore, in the computational modeling of the problem, only the regions corresponding to reconstituted silty-clay and ballotini material were modeled and no special interface feature was incorporated. The interfaces between these regions were considered to be fully bonded and a complicated consideration of a contact analysis was avoided. Due to the symmetry in the horizontal plane, only one-quarter of the problem with proper boundary conditions was modeled. The displacement boundary conditions applicable to the domain are shown in Figure 6.5. Other boundary conditions required for modeling the coupled pore fluid diffusion and stress analysis relate to the pore pressure at the

boundaries. The only permeable boundary with zero excess pore pressure defined in the model is the upper surface of the fill including the base of the footing and all other boundaries are considered to be impermeable. The composite domains are discretized into 3200 (**one-layer** and **two-layer** composites) and 4400 (**three-layer** composite) 20-node brick elements with quadratic displacement and linear pore pressure formulations, using a mesh discretization of 0.7 m in the vertical direction and 0.75 m in the horizontal

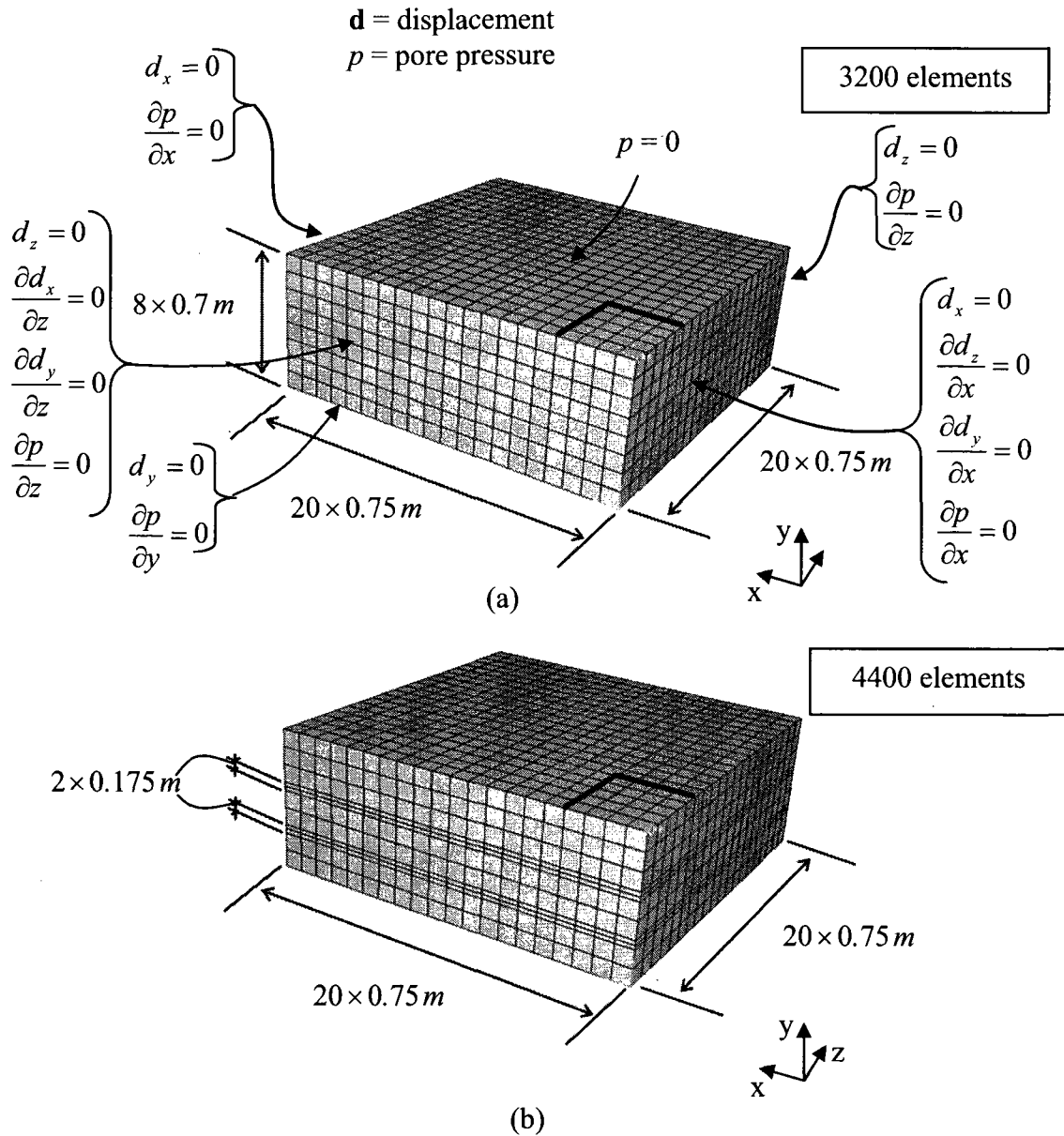


Figure 6.5 Mesh discretizations and boundary conditions in (a) one-layer (BMT) and two-layer (b) three-layer composite models

directions. The only exception is the **three-layer** composite model in which the regions between the composite layers are vertically divided in two layers of elements with a height of 0.175 m . The mesh discretization used in this study has the typical pattern implemented in several computational analyses of the composite models (Mitchell and Huber, 1985; Cheung et al., 1991; Callari and Federico, 2000). Using this meshing pattern, all the lumps are divided into 8 elements. The number of elements and finite element discretizations of the composite models are shown in Figure 6.5.

In most land reclamation projects, a layer of surcharge is used to accelerate the consolidation process of the lumpy fill layer. In the reclamation activities in Halmstad Harbor, Sweden, the 3 m depth lumpy fill was formed with barge-dumped clay lumps and was overlain by a surcharge layer with a thickness of 3.4 m formed from hydraulically placed clay lumps with a volume of approximately 0.02 m^3 in volume (Hartlen and Ingers, 1981). In the construction of Punggol Timor Island in Singapore, a 10 m thick sand layer was deposited on the lumpy region as a topping fill and also as a surcharge to accelerate the consolidation settlement of the layer (Karthikeyan et al., 2004). The surcharge stress and the self-weight of the deposited material are the loads that induce the initial state prior to the application of imposed structural loads, which in this simulation correspond to the rigid footing loading considered in the current modeling. The computational study examines the mechanical responses of the composite models subjected to different loading steps. The first loading step includes the self-weight and a surcharge pressure of 90 kPa (corresponding to a layer of sand 5 m thickness with a unit weight of 18 kN/m^3) gradually applied to the surface over a one day period. In the second loading step, a uniform pressure is applied to a square rigid footing of 6 m width placed on the surface of the region. This uniform pressure is increased to 1500 kPa over a period of 25 minutes (rate of 1 kPa/sec) and subsequently reduced to zero during the unloading step in 25 minutes . In the reloading step the pressure is increased to 1500 kPa over a 25 minute period, followed by the consolidation step, where the pressure on the footing is maintained at 1500 kPa to allow for expulsion of excess pore pressures generated mainly in the clay lumps and hydraulic transients that can occur in the ballotini region. The duration of this consolidation step is set equal to 200 days after which there is virtually no excess pore pressure in any constituent of the composite layer.

6.3 Computational results and discussion

The computational study was performed to predict the mechanical behavior of composite lumpy fills, described in Section 6.2. The fills are subjected to different loading–unloading steps applied for various periods of time; these loading-unloading cycles are considered to examine the irreversible deformations induced due to the plastic response of the constituent soils. The first part of the computations attempts to predict the mechanical response of **one-layer** fills where a composite layer is placed at different positions of the domain in relation to the surface. In the second part of the computational analysis, the **two-layer** and **three-layer** composites were simulated to examine the effect of volume proportion of clay on the mechanical behavior of the fills.

6.3.1 Composite fills with a composite layer placed at different positions

The computations are used to predict the settlement of the lumpy fills due to the *self-weight of the fill and the pressure from the surcharge* that is generally placed over the fills to induce preconsolidation. The results indicate that the presence of soft lumps within the granular fill contributes to greater surface settlements, with the maximum occurring in the area located over the clay lumps (Figure 6.6). In **one-layer-B** and **one-layer-M** fills, the profiles of the surface are almost identical, whereas the maximum settlement in **one-layer-T** fill shows an increase of approximately 28%. Therefore, the comparison of the settlement profiles indicates that there is no significant uneven settlement in **one-layer-B** and **one-layer-M** composites due to the location of the clay lumps, while greater variations in surface deflection were obtained in the **one-layer-T** fill due to the presence of soft clay lumps close to the surface.

The computations were extended to simulate the settlement of a $6m \times 6m$ rigid footing resting on the composite domains. The presence of a composite layer in the fill results in a 20% to 25% greater initial settlement compared to that of a homogeneous ballotini fill (Figure 6.7). The results also indicate that during a loading-unloading-reloading cycle, the initial settlement of **one-layer-B** and **one-layer-M** fills was about 21.5 cm while there was approximately 5% less settlement for the **one-layer-T** composite model.

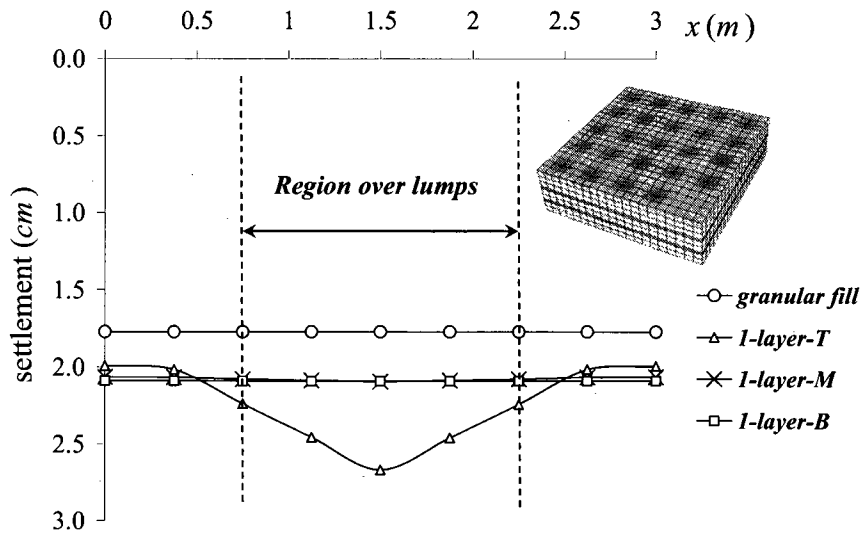


Figure 6.6 Surface settlement due to the self-weight and the surcharge pressure

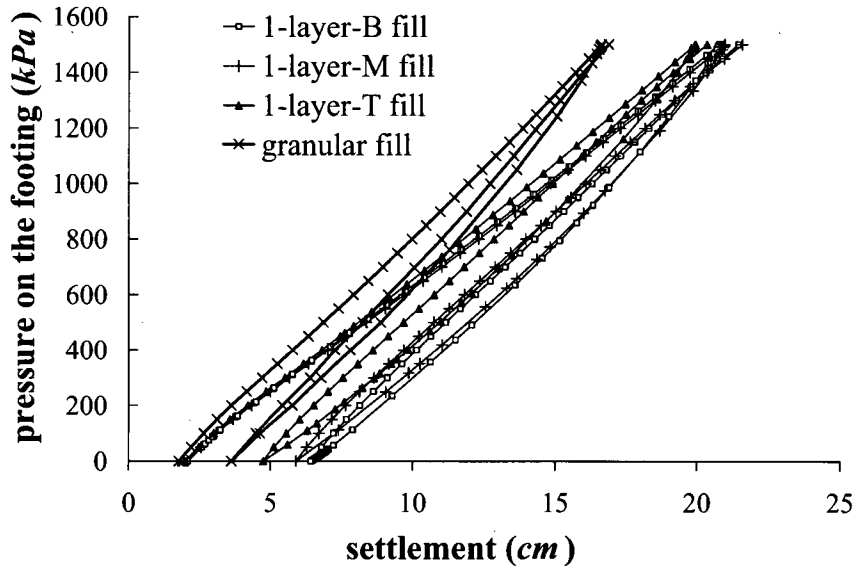


Figure 6.7 Load-settlement response of a rigid square footing resting on the surface of a granular layer containing a single soil composite layer

Self-weight effects, surcharge pressure and footing loads result in the generation of excess pore fluid pressure within the composite region, and the dissipation of this excess pore fluid pressure induces further settlement of the footing during the consolidation step

(200 days). The term “consolidation settlement” in this study refers to the settlement that occurs during the consolidation step, whereas a portion of consolidation settlement occurs during the loading and unloading-reloading steps. Figure 6.8 compares the consolidation settlement of the footing for the different **one-layer** models: The first phase of the consolidation settlement is complete within the first day and corresponds to the dissipation of the fluid pressure in the pores of the ballotini skeleton. This is followed by further settlement resulting from consolidation in the clay inclusions. The greatest settlement in this step is 3.3 mm occurring in the **one-layer-M** fill while the least occurs when the composite layer is located at the bottom of the fill (**one-layer-B**). It is important to note from these results that the maximum total settlement, including initial and consolidation settlement, is encountered when the composite soil layer is located at the midway location of the granular layer.

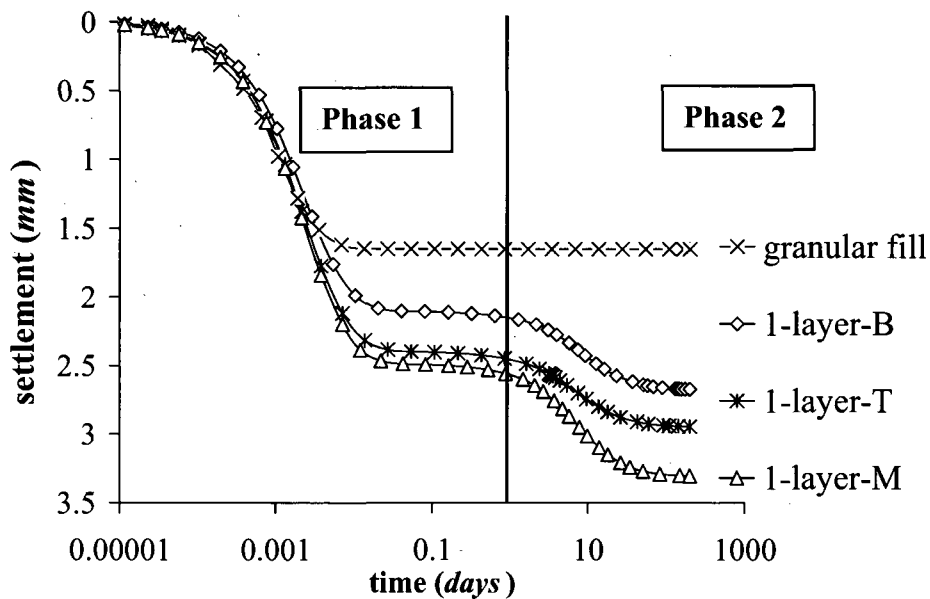


Figure 6.8 Consolidation settlement of a square rigid footing resting on a granular layer containing a single soil composite layer

6.3.2 Composite fills with different volume proportions of clay

The computations attempt to predict the behavior of the granular layers containing different volume fractions of clay. In this section, the results of the computational analyses conducted on **two-layer** and **three-layer** composite fills (Figure 6.4) are compared with the results obtained for **one-layer** fill. In the first step of the computational analyses, the composite models were subjected to the self-weight of the fill and the pressure of the surcharge that is generally placed over the fills. The computational results indicated that the presence of soft lumps within the granular fills results in higher settlements in the surface (Figure 6.9). The maximum surface settlement occurs in the region over the clay lumps. It is shown that in the **one-layer-B** composite fill, the maximum settlement is close to 2.1 *cm*, an increase of about 18% of that which occurred in the homogeneous fill. By increasing the number of lumps in **two-layer** and **three-layer** composite fills, the self-weight and surcharge pressure induce a settlement with the maximum value of about 70% and 80%, respectively, greater than that of the homogeneous granular fill. A comparison of the settlement profiles indicates that there is no significant, unevenness in the surface settlement in the **one-layer-B** composite due to

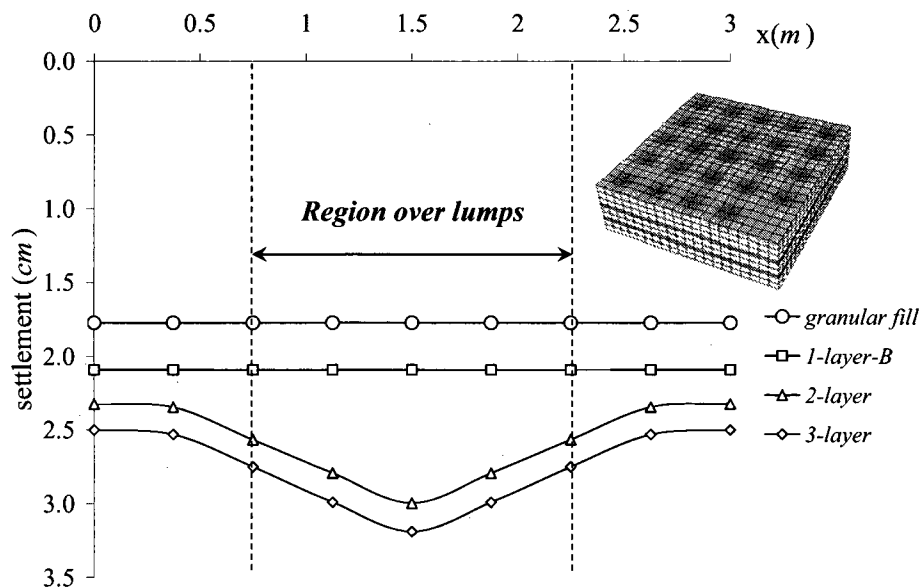
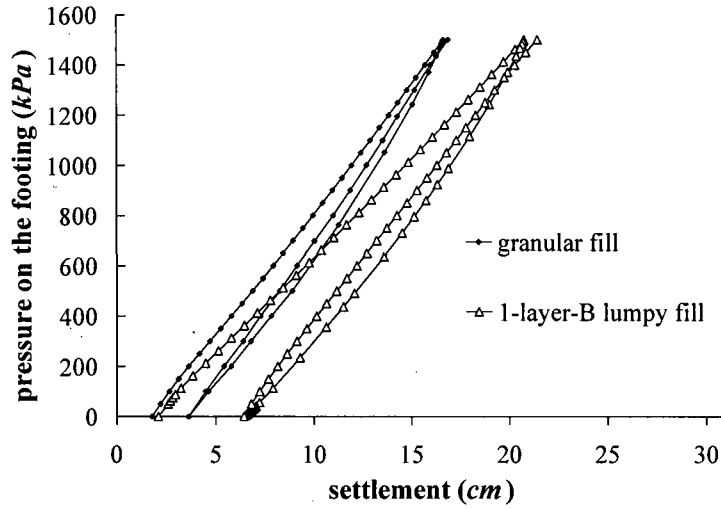


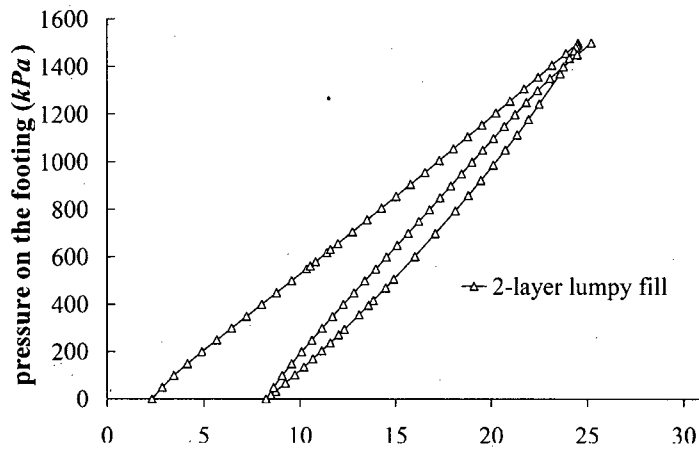
Figure 6.9 Surface settlement due to self-weight and the surcharge pressure

the location of the lumps, while greater variations in the surface deflection was obtained in **two-layer** and **three-layer** fills resulting from the presence of soft lumps closer to the surface.

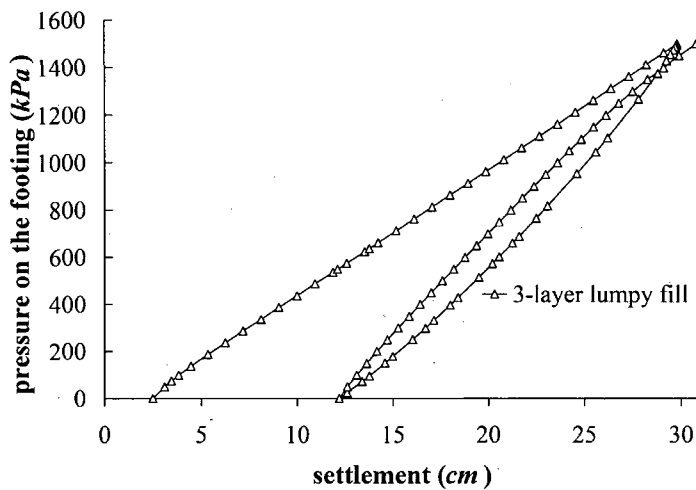
The computations also attempt to simulate the settlement of a 6 m square rigid footing on lumpy fills. The uniform pressure on the footing was increased to 1500 kPa in a period of 25 minutes. The unloading-reloading steps were also modeled in the composite fills to investigate the irreversible deformations that would occur due to the increased loading of the footing. After a complete unloading-reloading stage, the pressure on the footing is maintained for a period of 200 days to reach the ultimate deformation of the composite models. The computational estimates for the settlement of the footing at loading-unloading-reloading stages are presented in Figure 6.10 for different composite fills. Figure 6.10 a shows the settlement of the footing resting on a **one-layer-B** lumpy fill compared with the load-settlement curve estimated for the homogeneous granular fill. The footing on the **one-layer-B** fill settles 20.8 cm, which is approximately 25% higher than that occurring in homogeneous fill subjected to the same load. Figure 6.10 b,c also show that the settlement of the rigid footing increases with the increase in the number of composite layers within the lumpy fill. As a result, the footing placed on the **three-layer** lumpy fill, which contains three composite layers, displays the highest initial settlement, approximately twice that for the homogeneous fill. Figure 6.10 also shows the irreversible deformation after a complete loading-unloading cycle due to plastic deformation in both the clay lumps and granular filler: An increase in the number of lumps gives a higher irreversible settlement of the footing. At complete unloading, the **three-layer** lumpy fill had an irreversible displacement of 12.2 cm whereas the irreversible displacement in the **one-layer-B** fill was 6.4 cm.



(a) one-layer-B lumpy fill



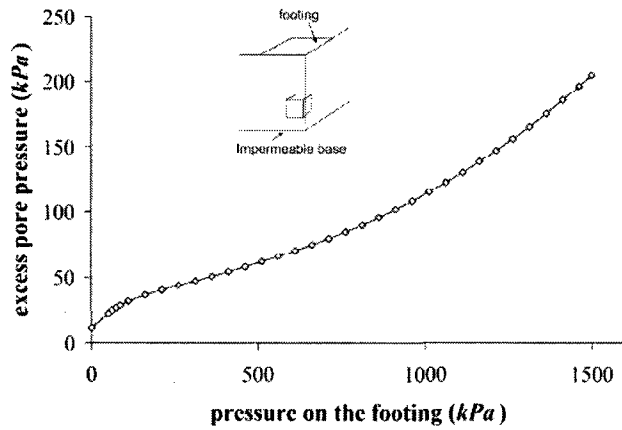
(b) two-layer lumpy fill



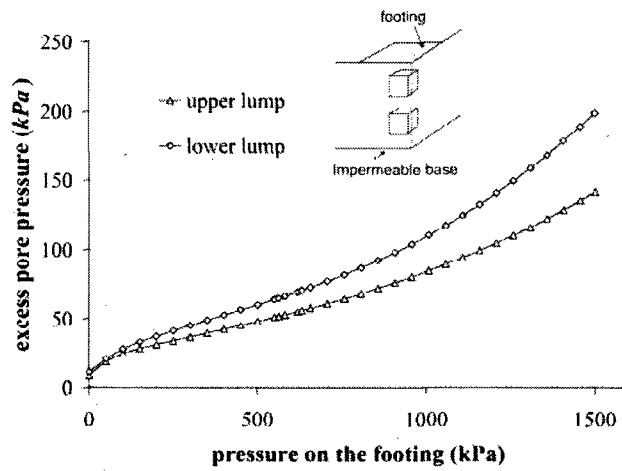
(c) three-layer lumpy fill

Figure 6.10 Load-settlement response of the rigid square footing resting on different types of composite soil layer

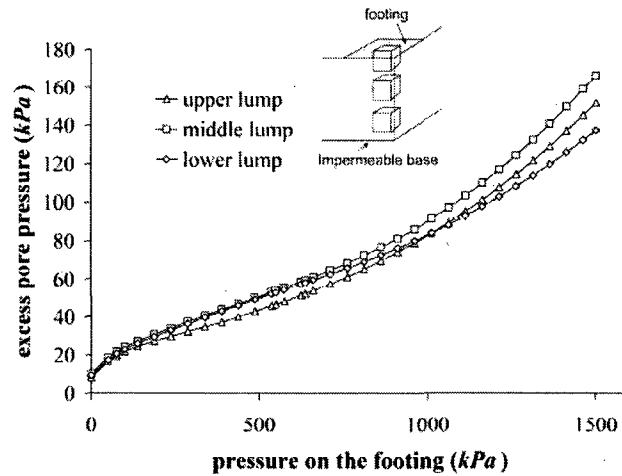
The excess pore pressure is generated in the porous geomaterials when the period of application of the loading is shorter than that needed for the complete dissipation of the induced pore pressure. In this simulation, the excess pore pressure was generated within the composites models during the different load steps. For three types of composite models, the computational results indicate that the maximum excess pore pressure at the end of the first loading step was less than the 12 *kPa* that occurs at the center of the clay lumps. During the application of pressure on the rigid square footing, the excess pore pressure increased within the composite sample with its maximum developed at the center of the lumps placed below the footing. Figure 6.11 shows the generation of excess pore pressure at the center of the lumps located under the footing while pressure is increased on the footing to a maximum value of 1500 *kPa*. In the **one-layer-B** composite, the maximum excess pore pressure was 205 *kPa*, occurring at the center of the clay lump beneath the footing. By increasing the number of composite layers, a lower volumetric strain was experienced by the lumps directly below the footing, resulting in lower pore pressure within the soft lumps: At the end of the second load step, the maximum excess pore pressure in the **three-layer** lumpy fill is 166 *kPa*, which is 23% lower than that induced in the **one-layer-B** composite model. In the next step, the complete unloading of the footing led to a decrease of the pore pressure and the development of negative pore pressure at different locations in the clay lumps. During the reloading step, the pore pressure in the lumps increased and exceeded the maximum value determined at the end of the second load step. This phenomenon can be attributed to the higher stiffness of the constituent materials in the reloading step compared to the initial loading due to the hypoelastic (for ballotini) and porous elasto-plastic (for clay) constitutive models used in the computations.



(a) one-layer-B composite fill



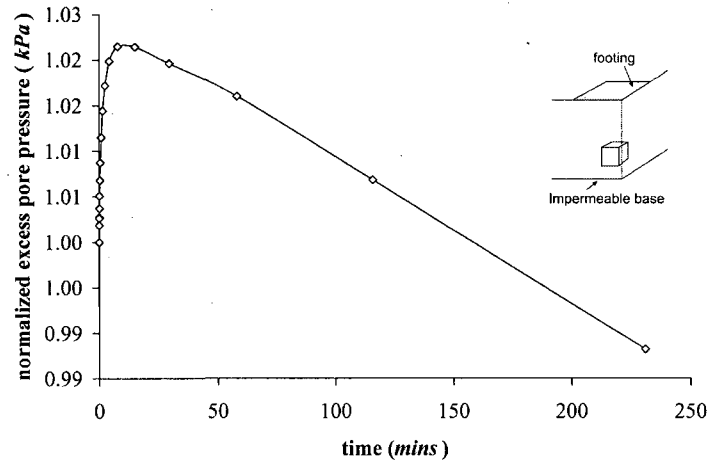
(b) two-layer composite fill



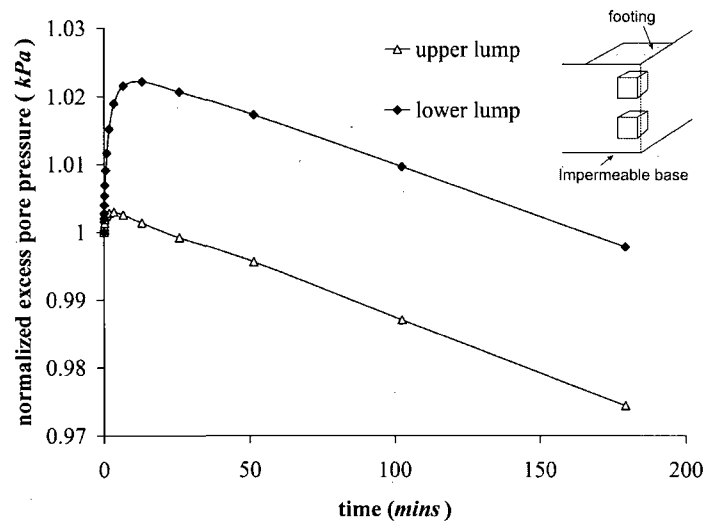
(c) three-layer composite fill

Figure 6.11 Excess pore pressure generation at the center of the clay lumps in different composite fills

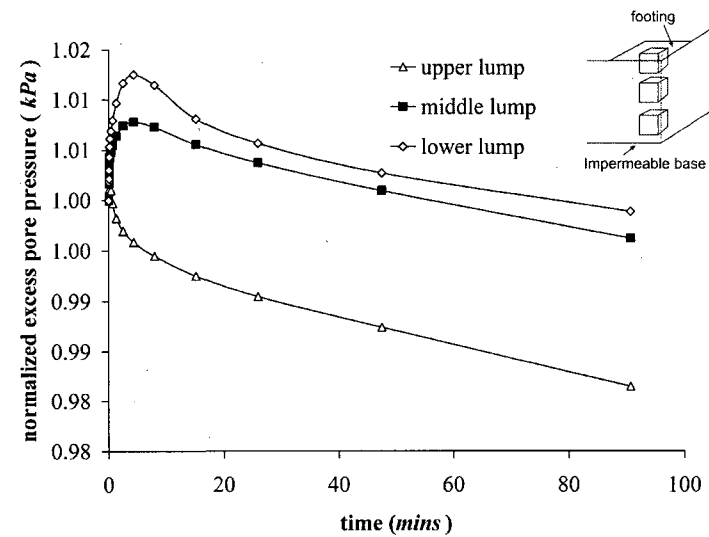
During the reloading step, the pressure on the footing was increased to the same value as prior to unloading (1500 *kPa*) and it was maintained for a period of 200 *days*. Computational results indicate that this period is sufficient to completely dissipate the excess pore pressure within the lumps, so that the final consolidation settlement of footing is reached. The variation of the pore pressure at the center of the lumps is normalized based on their initial value at the beginning of the 200-day consolidation step (Figure 6.12). The computations show an increase in the normalized pore pressure at the center of the lumps, at an early time, followed by a decay. This phenomenon, which is generally referred to as the Mandel-Cryer effect, was first observed by Mandel (1953) and confirmed by Cryer (1963). They observed that the analytical solutions obtained from Terzaghi's theory and from Biot's theory for pore pressure development at the center of a sphere subjected to all-around pressure can be considerably different: Biot's theory gives an initial increase of the pore pressure at the center of a poroelastic sphere, which is dependent on the mechanical properties of the poroelastic medium. Recently Selvadurai and Shirazi (2004) have also demonstrated the Mandel-Cryer effect by examining the stressing of a poroelastic media containing three-dimensional fluid inclusion. The existence of the Mandel-Cryer effect was also confirmed by the results of experiments conducted by Gibson et al. (1963) and Verruijt (1965). After an initial increase, the excess pore pressure generated at the center of the lumps decays at a rate corresponding to the diffusion equation (Figure 6.13). In all three composite models, the time for 50% and 90% dissipation of the pore pressure at the center of the lumps was estimated to be close to 3.5 *days* and 16 *days*, respectively, while the excess pore pressure in all points reduced to less than 1 *kPa* after 70 *days*.



(a)

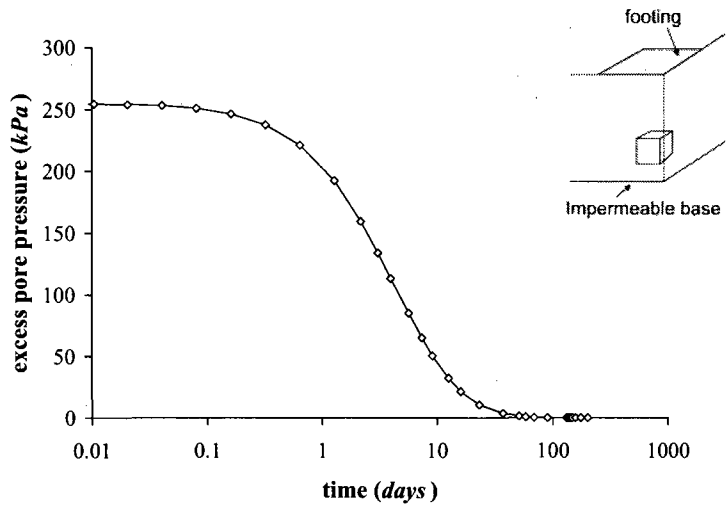


(b)

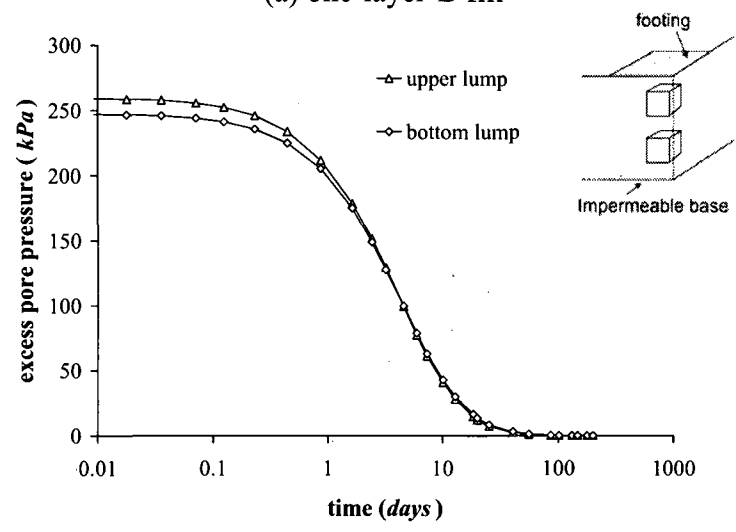


(c)

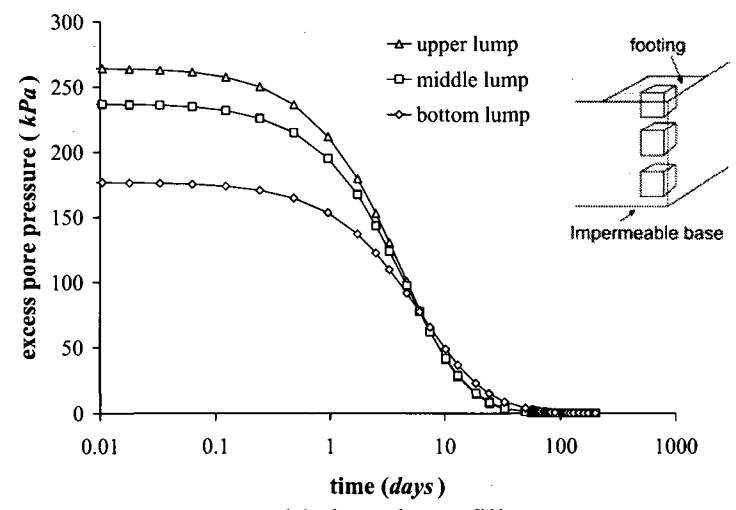
Figure 6.12 Mandel-Cryer effect – pore pressure increase at the beginning of the consolidation step



(a) one-layer-B fill



(b) two-layer fill



(c) three-layer fill

Figure 6.13 Dissipation of excess pore pressure generated at the center of the clay lumps due to the uniform normal stress of 1500 kPa applied to the rigid footing

The term “consolidation settlement” in this section refers to the settlement that occurs after maintaining the load on the footing at 1500 kPa, whereas a part of the consolidation settlement occurs during the loading and reloading steps. The degree of consolidation U presented in Figure 6.14 is defined as:

$$U = \frac{\Delta(t) - \Delta(0)}{\Delta(\infty) - \Delta(0)} \quad (6.1)$$

where $\Delta(0)$ is the vertical settlement of the footing at the beginning of the consolidation process and $\Delta(\infty)$ is the ultimate settlement obtained when the excess pore pressure in the models is negligible (in this study 200 days is regarded as the time for attainment of the ultimate consolidation settlement where all pore water pressures have been dissipated). Figure 6.14 presents two different phases in the settlement response of the composite fills. The first phase corresponds to the quick consolidation of the saturated ballotini region, a period of 1 day at the beginning of the consolidation step. The computational results indicate that the dissipation of the excess pore pressure generated within the clay lumps starts approximately 1 day after the beginning of the consolidation step (Figure 6.13). Therefore, the settlements that occur during the first day of the consolidation step are mainly attributed to the dissipation of the pore pressure developed inside the granular

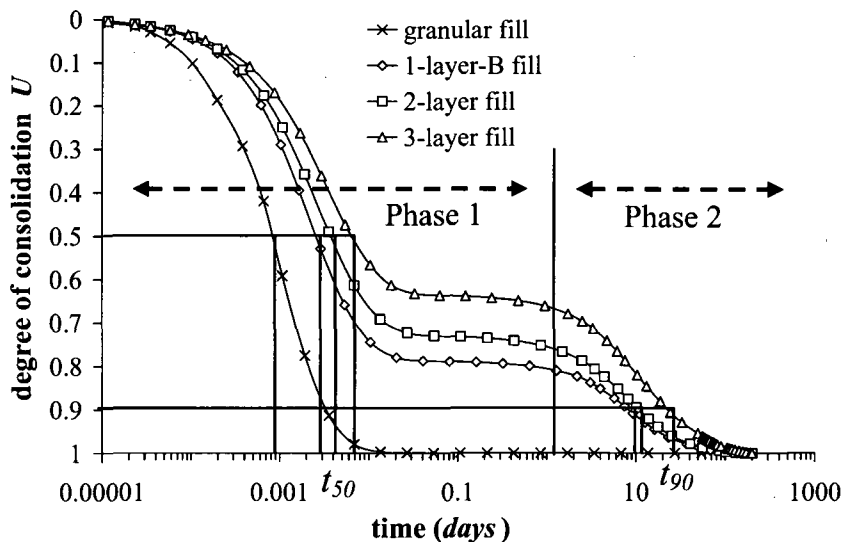


Figure 6.14 Numerical results for the degree of consolidation of composite lumpy fills settles under a square rigid footing

region. The high hydraulic conductivity of the coarse-grained soil results in a quick decay of the pore pressure developed in this region and causes 60% to 80% of the total settlements in the consolidation steps (phase 1). The next phase of the consolidation step (phase 2), which starts after approximately 1 *day*, is attributed to the consolidation process in the clay inclusions. In the homogeneous fill, there was no measurable settlement during phase 2 due to the absence of clay lumps in the model. By increasing the number of the lumps in the composite fill, the portion of settlement that occurs due to the consolidation of the clay lumps can be increased; in the **one-layer-B** fill this represents 21% of the settlement, which increases to 36% in the **three-layer** composite fill. The results also indicate that the consolidation settlement is delayed when the volume proportion of the clay lumps is increased; as a result, the time required for 50% and 90% consolidation, t_{50} and t_{90} , is approximately three times longer in the **three-layer** lumpy fill compared to that of the **one-layer-B** model. The consolidation settlement curves shown in Figure 6.15 also indicate that the increase in the volume proportion of soft lumps results in higher vertical displacement of the footing during the consolidation step; the ultimate consolidation settlement of the rigid footing in the **three-layer** fill (after 200 *days*) is approximately twice that of the **one-layer-B** fill.

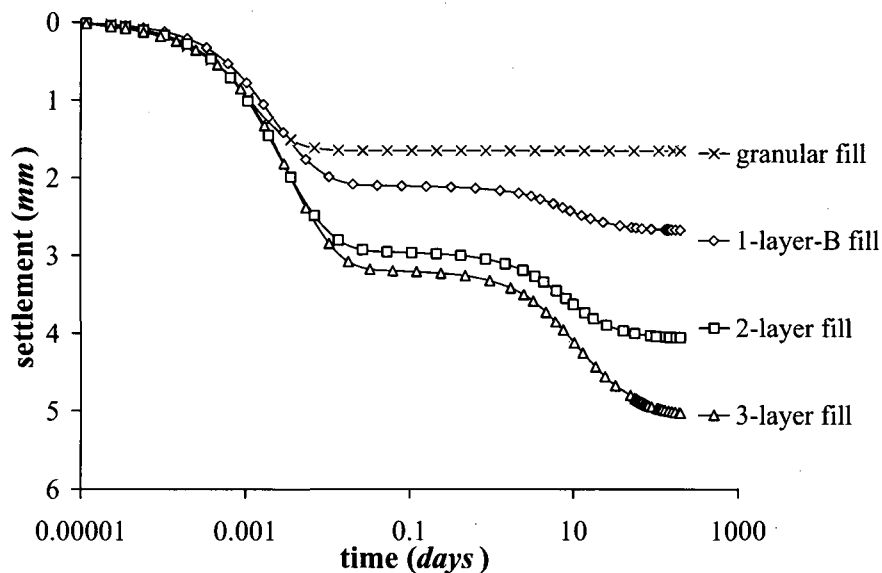


Figure 6.15 Time-dependent consolidation settlement of a square rigid footing resting on composite lumpy fills

In geotechnical problems dealing with the behavior of foundations, the evaluation of the contact pressures induced at the interface of the footing and soil mass is required for the design of the foundation rafts and also to assess the stress state within the soil region. Several efforts have been made to document the theoretical developments for determination of the contact stresses and the experimental evidence that deals with the measurement of contact stresses under different types of footings (Cummings, 1935; Schultze, 1961; Selvadurai, 1979). In this study, the distribution of the normal contact stress beneath a footing placed over a composite layer is investigated. Figure 6.16 illustrates the contact stress distribution along the diagonal of the square rigid footing, at the termination of the consolidation step, for homogeneous and the three types of soil composites. In the **one-layer-B** composite model, the contact pressure profile is only slightly different from that obtained computationally for the homogeneous layer; therefore, if the composite layer is placed near the base of the fill it does not significantly influence the contact stress distribution below the footing. In both the **two-layer** and the **three-layer** composite models, the lumps placed beneath the footing affect the distribution of the contact stress; the normal contact stress in the region above the clay lumps reduces whereas higher normal contact stresses are observed at the center of the square footing compared to that of the homogeneous and **one-layer-B** fills. In addition,

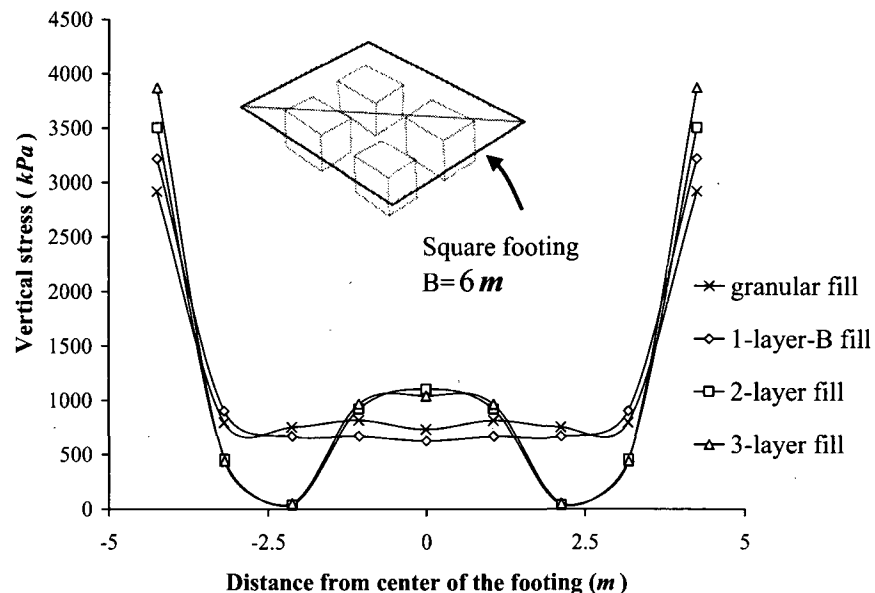


Figure 6.16 Normal contact stress profile along the diagonal of the square footing

an increase in the number of composite layers results in a higher maximum contact stress occurring at the edge of the footing.

The constitutive model implemented in the computational code for ballotini is the hypoelastic perfectly-plastic model, developed in Chapter 3, where the stiffness of the material increases during volumetric compression. To investigate the effect of hypoelasticity on the mechanical response of the composite fills, computations were also carried out to include the case where an elastic perfectly-plastic model is considered for ballotini. In this case, the modulus of elasticity is considered to be constant, ($E = 27000 \text{ kPa}$) and corresponds to ballotini in loose condition (void ratio > 0.605). Figure 6.17 shows the load-displacement response of the footing when the two different constitutive models for ballotini are considered, the elastic perfectly-plastic and the hypoelastic perfectly-plastic. For purposes of comparison, results are presented for loading-unloading-reloading steps for **one-layer-B** and **three-layer** composite fills. The implementation of the elastic perfectly-plastic constitutive model results in a 14.5% and 11% increase in the settlement of the footing in the **one-layer-B** and the **three-layer** fills, respectively. This fact indicates that the influence of ballotini on the mechanical response of the composite fill decreases as the volume proportion of clay increases within the fill.

Another important factor in the constitutive behavior of granular materials is the presence of dilatancy, quantified by the dilatancy angle ψ . Several studies have been conducted to examine the effects of non-associativity in plasticity on the magnitude of the deformation and bearing capacity of soil deposits located under different types of loading (Zienkiewicz et al., 1975; Mizuno and Chen, 1983; Bolton, 1986; Yin et al., 2001; Erickson and Drescher, 2002). These computations attempt to investigate the effect of dilatancy on the settlement response of the footing considering different values of the dilation angle; the dilation angle mainly used in analyses is equal to 22° , which is obtained from the results of the CD triaxial compression test (Figure 3.6). Other analyses were performed by considering the nondilatant behavior ($\psi = 0$) and associativity in flow rule, in which the dilation angle is assumed to be equal to the friction angle ($\psi = \phi$). Figure 6.18 depicts the results of computations carried out to account for the effects of

flow rule on the mechanical response of the **one-layer-B** composite fill. The results indicate that when the associative flow rule is adopted for the ballotini part of the composite, the footing settles 12% less than the case with the non-associative flow rule ($\psi = 22^\circ$), whereas for a non-dilatant soil 47% more settlement is predicted.

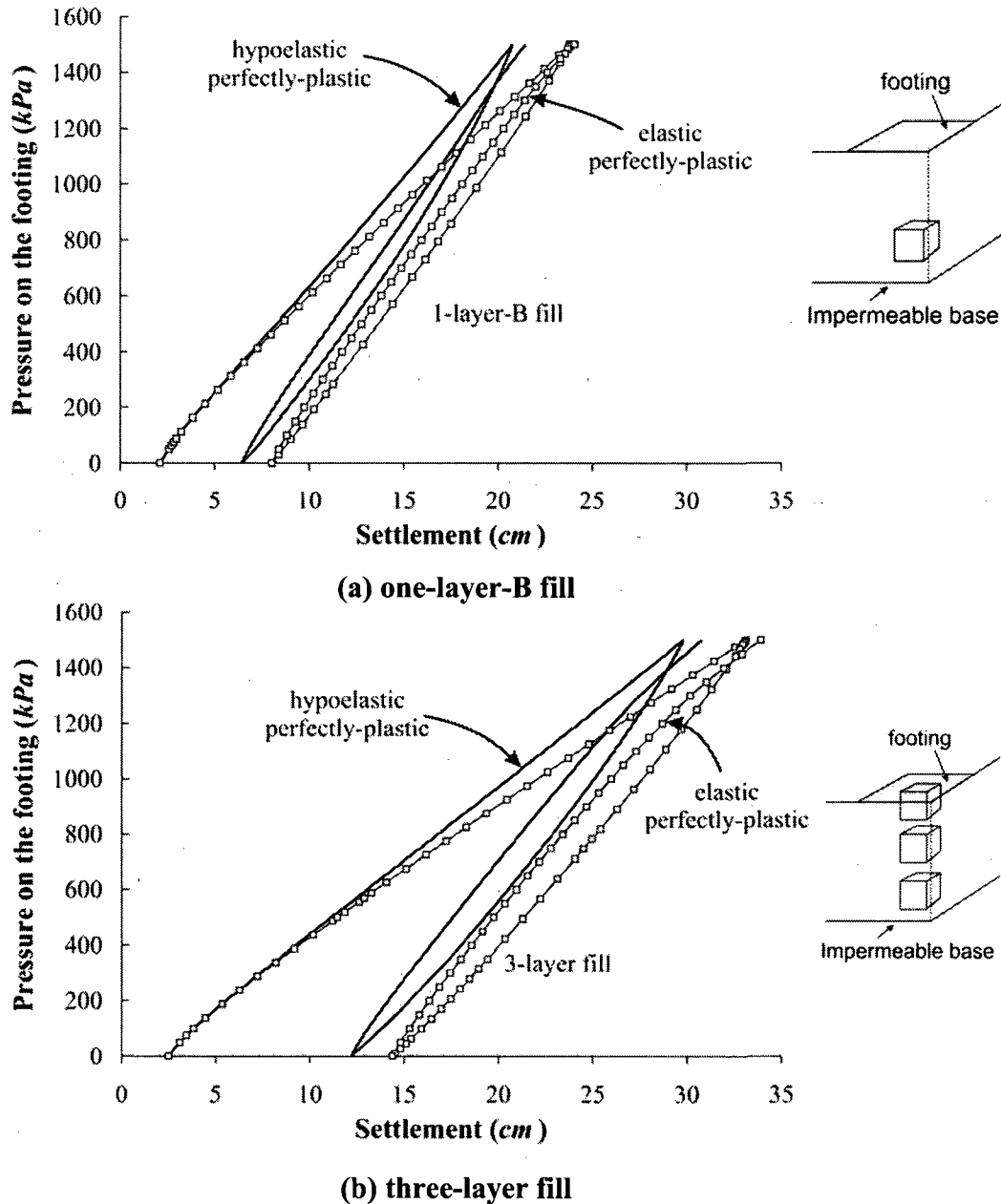


Figure 6.17 Load-displacement response of the footing for different constitutive models for ballotini

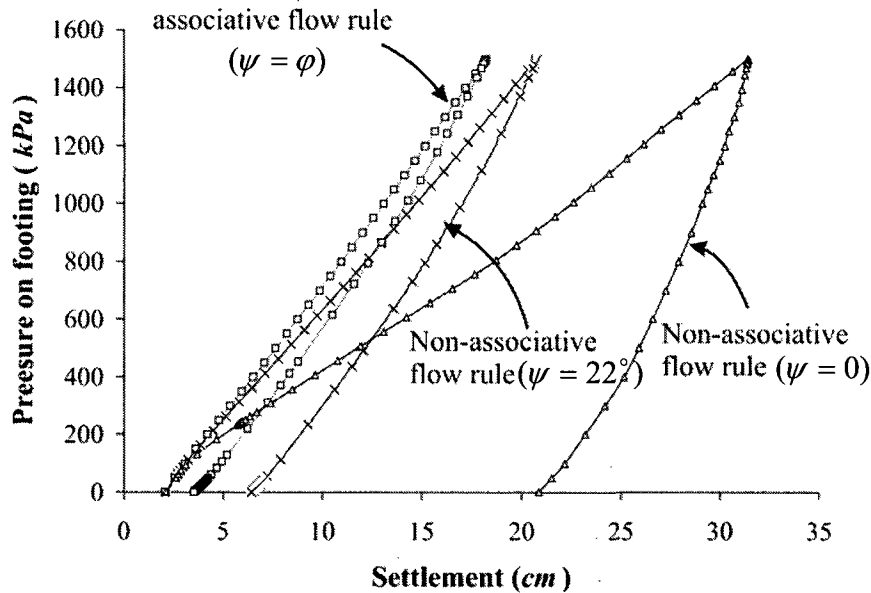


Figure 6.18 Settlement response of the footing for different flow rules in the constitutive model of ballotini (one-layer-B)

6.4 Composite fills with densely packed clay lumps

The composite layer used in the previous section to model the composite lumpy fills contained a 25% volume fraction of lumps arranged in a square grid pattern (Figure 6.3). In order to investigate the influence of volume fraction and the arrangement of clay lumps on the mechanical behavior of composite fills, a **dense composite layer**, containing 50% by volume of lumps arranged in a dense packing was considered (Figure 6.19). Two composite models were assembled, each with three dense composite layers located at the same depths defined previously for the **three-layer** fill (Figure 6.4); the configuration of the dense composite models are shown in Figure 6.20, with either a cubical (**three-layer-D1**) or a hexagonal (**three-layer-D2**) packing. In the cubical packing (**three-layer-D1**) the lumps in the three dense composite layers are located directly above each other, whereas in the hexagonal packing (**three-layer-D2**) the middle composite layer is offset. Thus, in **three-layer-D2** fill, the lumps in the middle composite layer are only overlain and underlain by ballotini. A mesh discretization identical to that shown in Figure 6.5 b for the **three-layer** model is used for the new dense clay fraction soil composites. Other details of the simulations, such as boundary conditions and loading specifications, are identical to those implemented in the previous simulations.

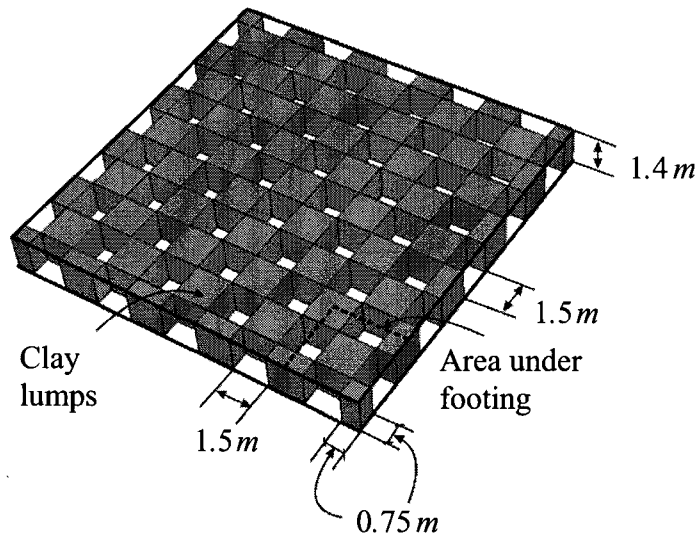
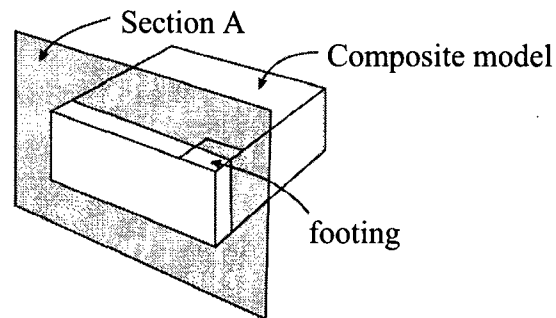
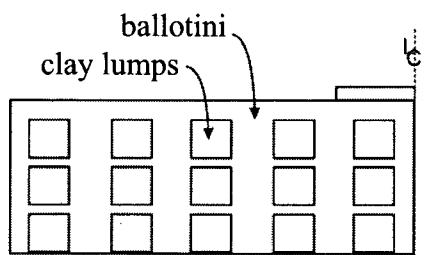


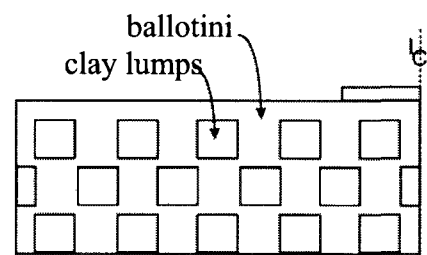
Figure 6.19 The composite layer with 50% volume fraction of clay (dense composite layer)



(a) location of section A in the composite model



(b) section A in cubical packing (three-layer-D1)



(c) section A in hexagonal packing (three-layer-D2)

Figure 6.20 Configurations of the composite fills with densely packed clay lumps

Figure 6.21 presents a comparison of the surface settlement profiles for the **three-layer** composite fills (**three-layer**, **three-layer-D1** and **three-layer-D2**) due to the self-weight and a uniform surcharge pressure, with maximum initial surface settlement occurring in the area over the lumps of the top composite layer. The results indicate that increasing the volume proportion of soft clay in the fill results in higher surface settlement. In the **three-layer-D1** fill, the maximum settlement is 5.1 *cm*, which is approximately 1.6 times that of **three-layer** composite fill. The maximum surface settlement computed in **three-layer-D2** fill is, however, 7.4 *cm*; this value is approximately 2.3 times that of **three-layer** fill. Therefore, computational results indicate that a lower surface settlement is obtained due to self-weight and surcharge pressure when the lumps are packed in a hexagonal form.

Figure 6.22 shows the settlement responses of the footing placed on three different composite layers and subjected to uniform pressure up to a maximum of 1500 *kPa*. The initial settlement of the footing in dense packing composite layers is approximately 120% greater than that estimated for the **three-layer** composite fill, and can be attributed to the higher volume of clay present in the dense composite layer. During the loading step, the computations estimate the same magnitude of footing settlement for both the cubic and

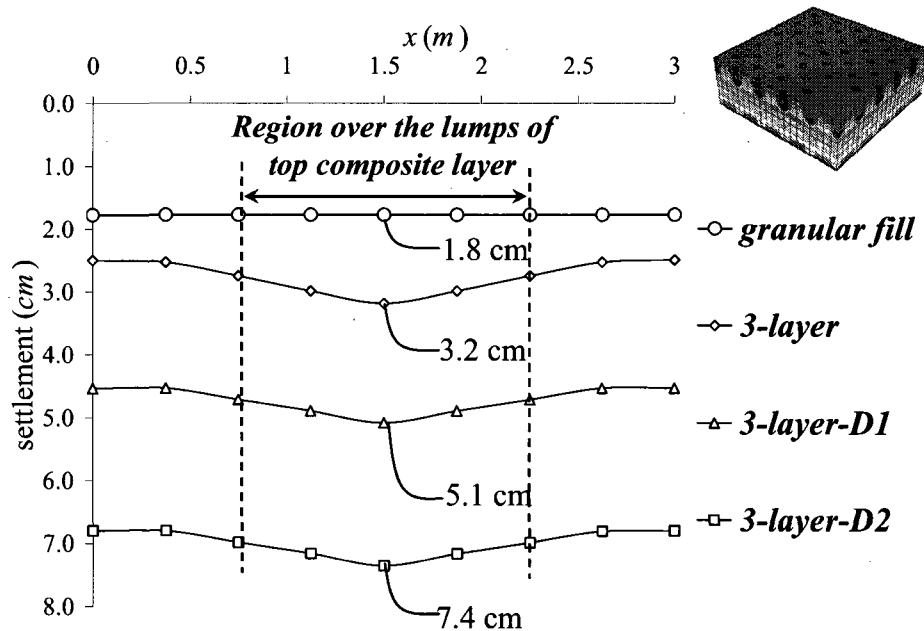


Figure 6.21 Profile of the surface settlement due to the application of self-weight and surcharge load

the hexagonal dense packing configurations; therefore, the difference in settlement predicted during the initial load steps remains relatively unchanged until the termination of the loading step. After complete unloading, however, a 40.8 *cm* irreversible settlement is induced in the **three-layer-D1** fill, which is 4.4 *cm* lower than that for **three-layer-D2** fill.

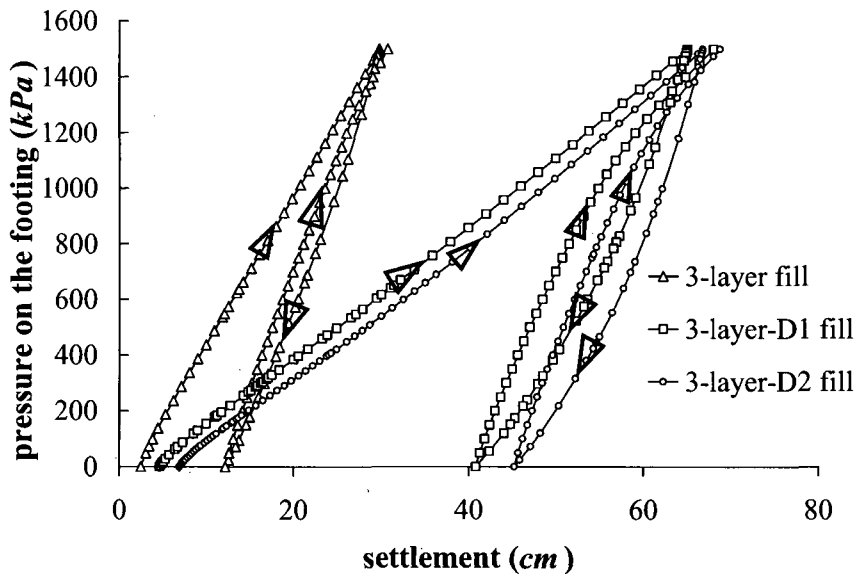


Figure 6.22 Load-settlement response of the rigid square footing resting on different types of three-layer lumpy fills

The settlement of the footing continues during the 200-day consolidation step due to the dissipation of the excess pore fluid pressure generated in the composite fills. The results indicate that the consolidation settlement of the footing in the **three-layer-D1** and **three-layer-D2** composite fills is 33.6 *mm* and 28.6 *mm*, respectively, which is approximately 6 times greater than that computationally estimated for the **three-layer** fill (Figure 6.23). It was also observed that in densely packed fills a higher portion of the consolidation settlement occurs in phase 2 due to the consolidation of the fine-grained lumps. Figure 6.24 indicates that in densely packed lumpy fills, only 25% of the consolidation settlement takes place in the first phase compared to 65% in loosely packed layers. As a result, the time required for 50% consolidation to occur in the densely packed fills increases to about 2.4 *days* compared to the 9 *minutes* estimated for **three-layer** fill.

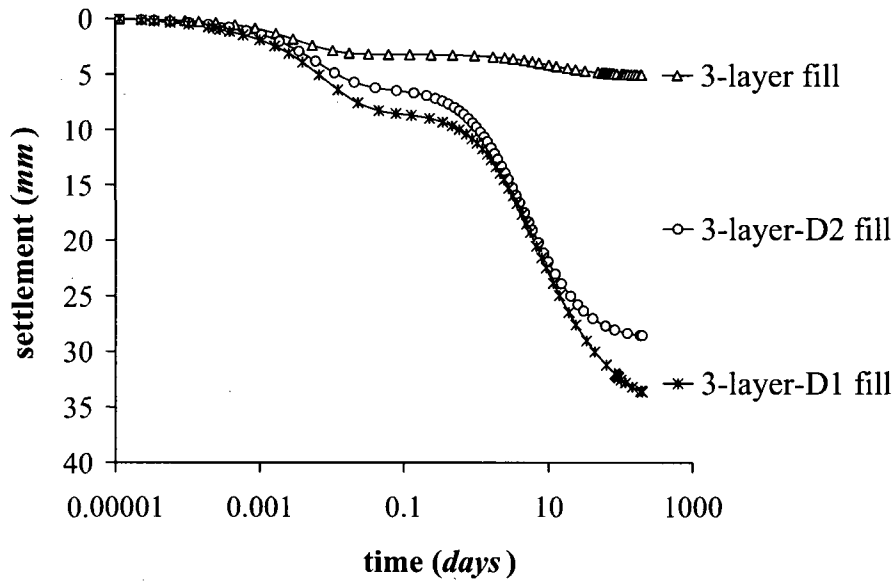


Figure 6.23 Consolidation settlement of a square rigid footing resting on composite lumpy fills

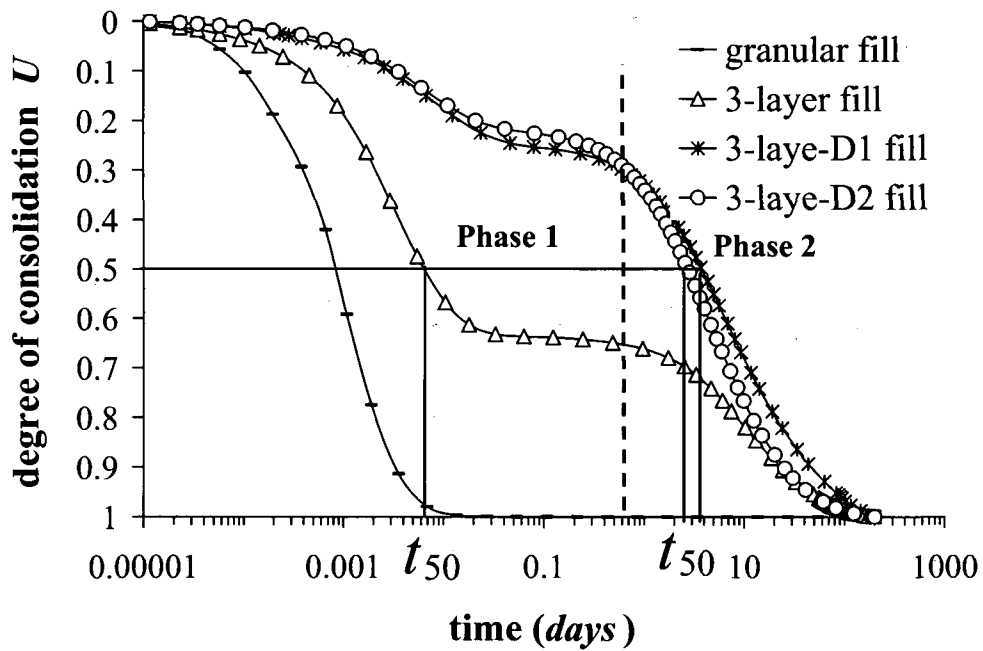


Figure 6.24 Degree of consolidation for 3-layer lumpy fills subjected to a footing load

6.5 Summary remarks

In this chapter, the mechanical behavior of the composite soil layer consisting of clay lumps distributed in a granular material and subjected sequentially to self-weight, surcharge pressure and footing load, were computationally analyzed. The composite models contain different volume fractions of clay placed in the shape of cuboidal regions within the granular medium. The computational results indicate that a higher volume proportion of clay lumps results in a greater initial settlement due to the self-weight, surcharge pressure and the pressure applied to the footing. It was also shown that for the same volume fraction of clay, a hexagonal packing leads to greater initial settlement compared to that for a cubical packing under self-weight and surcharge loads. Furthermore, increasing the volume proportion of the lumps gives rise to a higher initial settlement of the rigid footing. The results also indicated that in composite fills containing higher volume fraction of ballotini (loosely packed lumpy fills), higher percentage of the settlement of the rigid footing occurs in the first phase associated with the dissipation of pore fluid pressure within the granular region. However, an opposite result was obtained for densely packed lumpy layers: higher portion of the settlement occurs in the second phase, corresponding to the consolidation of the clay lumps, and the consolidation process is delayed in densely packed models when compared to the loosely packed fills. In terms of the constitutive behavior adopted for the granular region (ballotini), the results indicate that the consideration of an associative flow rule, results in an under estimation in the amount of footing settlement. On the other hand, higher settlement is predicted when the initial elastic stiffness is used instead of the hypoelastic model implemented in the computations. The profiles of contact stress distribution beneath the foundation also show that, compared to the homogeneous granular fills, lower normal contact stress is induced in the area located directly above the lumps, whereas the contact stress increases in other parts of the interface area between the footing and soil layer.

CHAPTER 7

CONCLUSIONS AND RECOMMENDATIONS

7.1 Summary and Conclusions

Land reclamation efforts have become a major part of geotechnical engineering activities and include various national projects particularly in small coastal territories. The reclamation projects have been undertaken to modify the coastlines and to construct new land needed to expand commercial and industrial activities as well as to provide the growing population with more residential and recreational facilities. Early land reclamation activities, dating back to the beginning of the twentieth century, used materials extracted from the hills and inland borrow-pit areas. Due to environmental regulations, these materials have become scarce resources; therefore dredged marine soils have become the preferred source of materials for use in reclamation activities. The resources of sand and gravel are now limited in many coastal regions, whereas several reclamation sites are surrounded only soft clay deposits. The use of these soft soils to construct the reclaimed fills is therefore regarded as a plausible solution for providing a fill material for land reclamation works which can significantly reduce the cost of such projects.

A common technique used in the construction of reclaimed fills involves placing dredged clay lumps directly on top of other layers. The *New Container Terminal* in Singapore has recently been constructed on one of the reclaimed land formed by placing large dredged lumps extracted from the seabed. The built-up fills contain a large volume of inter-lump voids that may not close completely, even after application of the surcharge load, and may lead to significant short and long term settlement when structures are constructed on these fills. These reclaimed lumpy fills, therefore, experience substantial compression purely due to the reduction of the void space, quite apart from the consolidation of the

clay lumps themselves, rendering this fill technique ineffective and unreliable unless account is taken of the large compression associated with the reduction in the inter-lump voids.

This research proposes a practical method for the construction of lumpy clay fills in which the void space between the lumps (inter-lump voids) is filled with a granular filler material. To date, many attempts have been made to examine the behavior of different types of composite soils, such as natural or constructed layered subsoils or soft soil deposits stabilized using stone columns. However, the composite lumpy fill, constructed using clay lumps in conjunction with an interspersed granular fill, is a soil composite with different mechanical characteristics from that of a typical lumpy fill. There are several factors contributing to the mechanical responses of this type of composite medium including the deformability characteristics and the hydraulic conductivities of each constituent. The major emphasis of this research, therefore, relates to the class of soil composites that could be encountered in land reclamation practices and contains dredged clay lumps embedded within a granular fill. The presence of this granular filler material can improve the mechanical characteristics of the fills, under self-weight and structural loads, by reducing the initial settlement induced due to the closure of inter-lump voids. Furthermore, a composite fill achieves consolidation within a shorter period, since the presence of the filler material in the composite acts as a porous medium that reduces the drainage path, which increases the rate of consolidation, compared to a homogeneous clay fill whose inter-lump voids can close up during the initial stages of the loading.

In this research, reconstituted silty clay obtained from a site in Montreal and ballotini, consisting of glass beads, were used to respectively represent the fine-grained phase and granular filler part of a composite in the experimental investigations. The moisture content of the reconstituted silty clay material was close to its Liquid Limit; the consistency of such a soft clay used in this investigation required adopting an appropriate technique to prepare the samples for different tests. In Chapter 2, the results of experiments conducted on the reconstituted Montreal silty clay were used to develop a plausible constitutive model, based on *Critical State Concepts*, which incorporates both the stiffness and strength characteristics of the material. The mechanical characteristics of

ballotini, which represented the coarse-grained phase of the composite in this experimental investigation, were examined in different tests (Chapter 3). The results of the experiments indicated that, in a loose state, ballotini exhibits low stiffness properties, whereas the stiffness of the material increases at higher densities; this is mainly attributed to the compression and subsequent densification of the material due to the sliding and rolling of the particles. The development of a constitutive model to characterize the nonlinear elastic and irreversible plastic behavior observed in the experiments was approached through the consideration of an elastic-perfectly plastic model that was modified to account for the *nonlinear elastic behavior* of the material; this is a novel development of the research. The ABAQUS code was used in the computational modeling and a UMAT material subroutine was developed for specifically modeling the nonlinear behavior of the ballotini. This UMAT subroutine is capable of incorporating the nonlinear elastic-perfectly plastic response by considering a non-associative flow rule that governs the evolution of plastic deformations. The effects of nonlinearity in elasticity and type of flow rule in plasticity on the overall response of the composite models were also examined in the computations.

Experimental research work is important when modeling the mechanical response of a composite soil, both from the point of view of examining the capabilities of the computational scheme and for the verification of the constitutive models developed for the constituents. This study includes an experimental program that examined the oedometric mechanical behavior of a composite specimen fabricated with a number of silty clay spheres placed within a granular ballotini region and tested in a bench-scale setup (Chapter 4). The experimental results showed that the presence of soft clay lumps ($V_{\text{clay}}/V_{\text{total}} = 31\%$) in the composite sample resulted in a 27% higher axial settlement than that which occurred in an identical sample consisting entirely of homogeneous ballotini specimen. Also, during each load step, two phases were observed in the axial deformation of the specimen; the first phase, occurring shortly after application of the load (<10 sec), corresponded to the “rapid consolidation” process in the ballotini region. This deformation phase was followed by a further consolidation that took place over a longer period as a result of the dissipation of excess fluid pressure generated within the

clay regions. Furthermore, the constitutive models specifically developed for modeling the mechanical behavior of reconstituted silty-clay and ballotini were implemented in the general purpose finite element code, ABAQUS/Standard, to predict the oedometric compression of the cylindrical composite sample. A comparison between the experimental test data and the computational results established the predictive capabilities of the methodology adopted for the computational modeling.

A coarse-grained medium containing a regular array of disk-shaped clay inclusions, described in Chapter 5, is another idealized clay-granular medium arrangement used to further examine the mechanics of the soil composite regions. The experimental research dealt with composite samples that contained either four, six or eight disks of clay with the volume fractions ($V_{\text{clay}}/V_{\text{total}}$) evaluated at 31%, 47% and 62.5%, respectively. The experimental results indicated that an increase in the volume proportion of clay resulted in a higher axial deformation of the composites; the axial settlement of the four-disk sample at the end of the final load step was approximately 2.8 times that of a pure ballotini sample. Furthermore, the six-disk and eight-disk samples exhibited approximately 4.4 and 5 times more axial deformation than that experienced by the pure ballotini sample.

The shape and configuration of the clay inclusions are other important factors that could affect the mechanical response of the composite media. This fact was verified by comparing the results of the oedometric compression tests conducted on composite samples with identical volume fractions but with clay inclusions of different shapes (the composites containing 36 spherical and four disk-shaped clay parts). The experimental results indicated that the four-disk composite sample exhibited more axial deformation compared to that observed for the composite containing spherical clay inclusions. The computational analyses of the composite samples indicated that the shape and distribution of the clay inclusions results in different stress distributions within the composite models while the variation of stress distribution gives rise to different magnitudes and rates of deformation.

The experimental results and their computational arrangements presented in Chapters 4 and 5 indicated that the computational scheme gives reasonable correlation with the mechanical responses of the soil composites obtained from the experiments. The computational scheme was therefore used to analyze the behavior of idealized composite lumpy fills. Different soil composites were simulated in a computational modeling exercise to investigate the effect of various parameters on the mechanical characteristics of the composite lumpy fills consisting of a granular region interspersed with cube-shaped clay regions. Due to the coupled nature of the poroelasto-plasticity problem, the composite nature of the models and the influence of complex geometries associated with the problem, solutions can be obtained only through a computational procedure. The soil composites considered in the modeling exercise were subjected to the self-weight, the surcharge pressure and the load applied from a rigid footing. The main features of the computational modeling of the composite lumpy fills, discussed in Chapter 6, and related computational results can be summarized as follows:

- In the first part of the computational investigation, a **one-layer** composite fill was modeled in which one composite layer was placed at three different levels within the granular fill. Different **one-layer** composite fills, denoted as **one-layer-B**, **one-layer-M**, and **one-layer-T**, corresponded to the locations of the composite layer: the base, mid-section and top of the composite layer, respectively. During the application of the self-weight and surcharge load, the profiles of the surface deflection were almost identical for **one-layer-B** and **one-layer-M** fills, whereas the maximum settlement in **one-layer-T** fill showed an increase of approximately 28%. A comparison of the settlement profiles also indicated that there was no significant uneven settlement in **one-layer-B** and **one-layer-M** composites due to the location of the clay lumps. As a result, the substantial unevenness in the surface settlement of the fill observed in the **one-layer-T** fill was associated with the presence of soft clay lumps close to the surface. This uneven settlement, which can limit the engineering application of any reclaimed fills, can be avoided by placing clay lumps at a depth from the surface of the fill.

- The computations were extended to simulate the settlement of a $6m \times 6m$ rigid footing resting on **one-layer** composite domains. The results indicated that the presence of a composite layer in the fill results in a 20% to 25% greater settlement compared to that of a homogeneous ballotini fill. It is also important to note from these results that the maximum total settlement of the rigid footing was observed when the composite soil layer was located at the mid-depth of the granular fill.
- A higher volume proportion of clay lumps in the soil composite resulted in a greater settlement due to the self-weight, surcharge pressure and the pressure applied to the footing. This fact, which was also observed in the experiments, was investigated through computational modeling of the composite lumpy fills. The computations attempted to predict the behavior of the granular layers containing two layers (**two-layer** fill) and three layers (**three-layer** fill) of composite lumpy layers. The results indicated that, by increasing the number of lumps in the **two-layer** and the **three-layer** fills, the self-weight and surcharge pressure induce a settlement with the maximum value of about 43% and 52%, respectively, greater than that of the **one-layer-B** composite fill. Furthermore, the settlement of the rigid footing computed for the **three-layer** fill was approximately 22% and 43% greater than that obtained, respectively, for the **two-layer** and the **one-layer-B** fills. It was also shown that an increase in the number of lumps gives a higher irreversible settlement at the complete unloading of the footing load: the **three-layer** lumpy fill had an irreversible displacement of 12.2 *cm*, approximately twice that experienced by the **one-layer-B** fill.
- The constitutive model implemented in the computational code for ballotini is the nonlinear elastic-perfectly plastic model, developed in Chapter 3, where the stiffness of the material increases during volumetric compression. In order to investigate the effect of nonlinear elasticity of ballotini on the mechanical response of the composite fills, computations were also carried out to include the case where an elastic-perfectly plastic model is considered for ballotini, corresponding to the mechanics of the material in a loose condition (void ratio > 0.605). It was shown that the implementation of the elastic-perfectly

plastic constitutive model for ballotini overestimated the settlement of the footing by 14.5% and 11% in the **one-layer-B** and the **three-layer** fills, respectively. Another important factor considered in developing a constitutive model for ballotini was the non-associative flow rule that governs the incremental plastic deformations of the material. The computations indicated that when the *associative flow rule* is adopted for the ballotini portion of the **one-layer-B** composite, the footing settles 12% less than the case with the *non-associative flow rule*, whereas considering a *non-dilatant* behavior for ballotini overestimated the settlement by 47%.

- In order to investigate the influence of volume fraction and the arrangement of clay lumps on the mechanical behavior of composite fills, densely packed composite fills (**three-layer-D1** and **three-layer-D2**) enclosing three **dense composite layers** were modeled. The **dense composite layers** contained 50% volume fraction of lumps arranged in a densely packed configuration. It was observed that the settlement of the rigid footing in dense packing composite layers was approximately 120% greater than that estimated for the **three-layer** composite fill, and can be attributed to the higher volume of clay enclosed in the dense composite layer. The computations also indicated that in the loosely packed **three-layer** fill, approximately 35% of the consolidation settlement occurred in the second phase, corresponding to the consolidation of the fine-grained lumps; however, this portion increased to about 80%, for the densely packed composite fills. As a result, the time required for 50% and 99% consolidation to occur in the densely packed fills (**three-layer-D1** and **three-layer-D2**) increased to about 2.4 *days* and 165 *days* , respectively, compared to the 9 *minutes* and 120 *days* estimated for **three-layer** fill.

7.2 Recommendations for future work

In the preceding sections, the main achievements of this study have been summarized. A computational scheme, validated with experimental results, was used to investigate the effect of different factors on the mechanical characteristics of composite lumpy fills

consisting of a granular region interspersed with clay inclusions. In the ensuing, possible extensions are suggested for both the experimental and computational parts of this research:

- As discussed previously in the literature review of this research, there are only a limited number of experimental observations on the behavior of composite soil samples, and these mainly deal with the mechanical response of layered soils or stone column reinforced soil composites. However, a granular soil layer containing clay inclusions is another class of soil composites that can be constructed during reclamation activities. The experimental investigations in this study included testing such composite samples under bench-scale oedometric compression tests. The one-dimensional response can simulate the state of deformation in a land reclamation application where the thickness of the composite fill is much smaller than the area dimensions and the layer is subjected to uniformly distributed loads such as self-weight or surcharge stress. The experimental study can be extended to evaluate the response of the bench-scale or large-scale composite samples subjected to a plate load. The results obtained from the lab-scale experiment can be considered to evaluate the response of various reclaimed composite fills subjected to different localized loadings, such as foundation loads.
- During the application of the loads on the soil composites, a mixture interface can develop at the boundary of the two materials as a result of penetration of the granular soil particles into the clay inclusions. In the experiments conducted in this study, there was no measurable penetration of the ballotini grains into the soft clay disks, merely a layer of ballotini beads that had adhered to the surface of the disks. However, when a composite is fabricated from clay inclusions with a higher water content or subjected to higher stress levels, a mixture phase can be formed as a result of penetration of grains into the soft clay. This mixture interface, which exhibits different deformability and hydraulic conductivity characteristics, can change the overall response of the soil composites. The current research can be extended to the experimental evaluation of composite samples whose fine-grained phase is reconstituted at a very low consistency.

Results derived from such experiments could be used to calibrate a computational scheme for predicting the behavior of such composite fills subjected to different loading conditions.

- The swelling of the clay lumps, due to suction, occurs when the dredged clay lumps are subjected to a stress level after being consolidated under higher stress states (Robinson et al., 2004). In lumpy fills, which contain no filler material, the all-round drainage of the lumps with free lateral boundaries results in a gradual increase in the water content of the lumps; therefore higher deformability is obtained in swollen clay inclusions. The softened clay lumps therefore deform easily during the application of the load. In composite fills that contain a granular filler, the existence of the filler around the lumps could constrain the free swelling of the lumps as a result of the contact stresses induced at the interface of the two regions. The magnitude of the contact stress and the extent of the swelling process are, therefore, related to the stiffness characteristics of both materials. Computational analyses can be performed to account for the swelling of the overconsolidated lumps and its influence on the mechanical characteristics of the composite fills.
- The soil composites analyzed in this thesis were idealized lumpy fills whose inter-lump voids are filled with a granular filler. When the filler is placed or deposited on a constructed lumpy layer, due to the cohesionless nature of the filler, it can fill the inter-lump voids that exist within the lumpy fills. However, to minimize the volume of inter-lump voids within the composite layer that are not filled with granular filler soil, different practical reclamation methods have to be investigated. This could result in producing different practical guidelines for use in reclamation activities in order to construct fills that are closer to the idealized intact composite samples simulated in this study.
- The computational methodologies could be further used to examine a case study that involves an actual reclamation exercise where the efficiency and relevance of the computational approach can be further tested.

References

- AASHTO (1996) Standard Specification for Highway Bridges, *American Association of State Highway and Transportation Officials*, **no. 16**.
- ABAQUS/Standard (2005) *A General-Purpose Finite Element Program, Version 6.5*, Hibbitt, Karlsson & Sorensen Inc., Providence, RI, USA.
- Abid, M. M. and Pyrah, I. C. (1990) Consolidation behaviour of finely laminated clays, *Computers and Geotechnics*, **10(4)**, pp. 307-323.
- Aboshi, H., Ichimoto, E., Enoki, M. and Harada, K. (1979) The "Compozer"- A method to improve characteristics of soft clays by inclusion of large diameter sand columns, *Proceedings of International Conference on Soil Reinforcement*, Paris, pp. 211-216.
- Aleynikov, S. M. (2000) *Boundary Element Method in Contact Problems for Elastic Spatial and Nonhomogeneous Bases*, Publishing House of Civil Engineering University Association, Moscow, p. 754.
- Alramahi, B. A. and Alshibli, K. A. (2006) Particle-to-particle interaction during shearing of granular materials, *Proceedings of the 10th Biennial International Conference on Engineering, Construction, and Operations in Challenging Environments*, League City/ Houston, TX, ASCE, pp. 1-8.
- Anon. (1985) Building new land for industrial development, *World Dredging & Marine Construction*, **21(9)**, pp. 12-19.
- Anon. (2004) Investment grows at middle east airports, *Jane's Airport Review*, **May Issue**, pp. 15-17.
- Anon. (2005a) IHC dredgers involved in dredging 'THE WORLD' in Dubai, *Ports and Dredging*, **164**, pp. 16-20.
- Anon. (2005b) A new world from scratch, *Dredging and Port Construction*, **July Issue**, pp. 20-22.
- Aoki, T., Tan, C. P., Cox, R. H. T. and Bamford, W. E. (1996) Measurement of the undrained pore pressure response of a shale in triaxial tests, *Proceedings of the 11th Conference on Engineering Mechanics*, Fort Lauderdale, FL, ASCE, **2**, pp. 1086-1089.
- Arulrajah, A., Nikraz, H. and Bo, M. W. (2004) Field instrumentation assessment of offshore land reclamation works, *International Journal of Offshore and Polar Engineering*, **14(4)**, pp. 315-320.
- ASCE (1994) *Settlement analysis, technical engineering and design guides adapted from the U.S. Army Corps of Engineers*, American Society of Civil Engineers, **no. 9**.
- ASTM (1999) D4767-88, Test method for consolidated undrained triaxial compression test on cohesive soils, *American Society for Testing and Materials*.
- ASTM (2000) D4318-05 Standard Test Methods for Liquid Limit, Plastic Limit, and Plasticity Index of Soils, *American Society for Testing and Materials*.

- Auriault, J.-L., Geindreau, C., Royer, P., Bloch, J.-F., Boutin, C. and Lewandowska, J. (eds.) (2002) *Poromechanics II. Proceedings of the 2th Biot Conference on Poromechanics*, A.A. Balkema, Rotterdam/Brookfield, p. 955.
- Balaam, N. P. and Booker, J. R. (1981) Analysis of rigid rafts supported by granular piles, *International Journal for Numerical and Analytical Methods in Geomechanics*, **5(4)**, pp. 379-403.
- Balaam, N. P. and Booker, J. R. (1985) Effect of stone column yield on settlement of rigid foundations in stabilized clay, *International Journal for Numerical and Analytical Methods in Geomechanics*, **9(4)**, pp. 331-351.
- Balaam, N. P. and Poulos, H. G. (1983) The behaviour of foundations supported by clays stabilized by stone columns, *Proceedings of the 8th European Conference on Soil Mechanics and Foundation Engineering*, Helsinki, **1**, pp. 199-204.
- Baldi, G., Hight, D. W. and Thomas, G. E. (1988) A re-evaluation of conventional triaxial test methods. *Advanced Triaxial Testing of Soil and Rock*, R. T. Donaghe, R. C. Chaney, and M. L. Silver, eds., ASTM, Philadelphia, pp. 219-263.
- Barber, E. S. (1945) Discussion of 'Simultaneous Consolidation of Contiguous Layers of Unlike Compressible Soils' by H. Gray', *Trans. ASCE*, **110**, pp. 1345-1349.
- Bardet, J. P. (1997) *Experimental Soil Mechanics*, Prentice Hall, Upper Saddle River, New Jersey, p. 583.
- Barksdale, R. D. and Bachus, R. C. (1983) *Design and Construction of Stone Columns*, U. S. Department of Transportation- Federal Highway Administration, Washington, D. C., p. 210.
- Barron, R. A. (1948) Consolidation of fine-grained soils by drain wells, *Transactions of American Society of Civil Engineers*, **113**, pp. 718-742.
- Barron, R. A., Lane, K. S., Keene, P. and Kjellman, W. (2002) Consolidation of fine-grained soils by drain wells, *Geotechnical Special Publication*, **n 118**, pp. 324-360.
- Baumann, V. and Bauer, G. E. A. (1974) The performance of foundations on various soils stabilized by the vibro-compaction method, *Canadian Geotechnical Journal*, **11(4)**, pp. 509-530.
- Been, K., Jefferies, M. G. and Hachey, J. (1991) Critical state of sands, *Geotechnique*, **41(3)**, pp. 365-381.
- Belviso, R., Ciampoli, S., Cotecchia, V. and Fedecrico, A. (1985) Use of the cone penetrometer to determine consistency limits, *Ground Engineering*, **18(5)**, pp. 21-22.
- Berre, T. (1985) Suggested international code for soil engineering practice for triaxial compression tests, *Norwegian Geotechnical Institute*, **Internal report 56103-30**.
- Bishop, A. W. and Henkel, D. J. (1962) *The Measurement of Soil Properties in the Triaxial Test*, Edward Arnold, London, p. 228.
- Bjerrum, L. and Simons, N. E. (1960) Comparison of shear strength characteristics of normally consolidated clays, *ASCE Research Conference on the Shear Strength of the Cohesive Soils*, Boulder, pp. 711-726.

- Bo, M. W., Bawajee, R. and Chao, V. (2001) Reclamation using dredged materials, *Proceedings of the International Conference on Port and Maritime R&D and Technology*, Singapore, **1**, pp. 455-461.
- Bolton, M. D. (1986) Strength and dilatancy of sands, *Geotechnique*, **36(1)**, pp. 65-78.
- Booker, J. R., Balaam, N. P. and Davis, E. H. (1985) Behaviour of an elastic non-homogeneous half-space. part II - circular and strip footings, *International Journal for Numerical and Analytical Methods in Geomechanics*, **9(4)**, pp. 369-381.
- Booker, J. R. and Small, J. C. (1987) Method of computing the consolidation behaviour of layered soils using direct numerical inversion of Laplace transforms, *International Journal for Numerical and Analytical Methods in Geomechanics*, **11(4)**, pp. 363-380.
- Borgesson, L. (1981) Shear strength of inorganic silty soils, *Proceedings of the International Conference on Soil Mechanics and Foundation Engineering*, Stockholm, A. A. Balkema, Rotterdam, **1**, pp. 567-572.
- Borja, R. I. (1991) Cam-clay plasticity, part II: implicit integration of constitutive equation based on a nonlinear elastic stress predictor, *Computer Methods in Applied Mechanics and Engineering*, **88**, pp. 225-240.
- Borja, R. I. and Lee, S. R. (1990) Cam-clay plasticity, part I: implicit integration of elastoplastic constitutive relations, *Computer Methods in Applied Mechanics and Engineering*, **78**, pp. 49-72.
- Boswell, L. F. and Scott, C. R. (1975) A flexible circular plate on a heterogeneous elastic half-space: influence coefficients for contact stress and settlements, *Geotechnique*, **25(3)**, pp. 604-609.
- Bourgeois, E., Corfdir, A. and Dormieux, L. (1997) Double time scale analysis of the consolidation of a two-strata poroelastic layer with high permeability contrast, *Transport in Porous Media*, **29(1)**, pp. 15-26.
- Brandon, T. L., Rose, A. T. and Duncan, J. M. (2006) Drained and undrained strength interpretation for low-plasticity silts, *Journal of Geotechnical and Geoenvironmental Engineering*, **132(2)**, pp. 250-257.
- British Standards Institution (1990) BS 1377 Methods of test for soils for civil engineering purposes. Part 2: Classification tests, *London: BSI*.
- Britto, A. M. and Gunn, M. J. (1987) *Critical State Soil Mechanics via Finite Elements*, Ellis Horwood, Chichester, p. 734.
- Brown, P. J. and Huxley, M. A. (1996) The cone factor for a cone, *Ground Engineering*, **29(10)**, pp. 34-36.
- Brown, P. T. and Gibson, R. E. (1972) Surface settlement of a deep elastic stratum whose modulus increases linearly with depth, *Canadian Geotechnical Journal*, **9(4)**, pp. 467-476.
- Brown, P. T. and Gibson, R. E. (1979) Surface settlement of a finite elastic layer whose modulus increases linearly with depth, *International Journal for Numerical and Analytical Methods in Geomechanics*, **3(1)**, pp. 37-47.

- Callari, C. and Federico, F. (2000) FEM validation of a double porosity elastic model for consolidation of structurally complex clayey soils, *International Journal for Numerical and Analytical Methods in Geomechanics*, **24(4)**, pp. 367-402.
- CAN/BNQ (1986) Soils- determination of liquid limit by the Swedish fall cone penetrometer method and determination of plastic limit - CAN/BNQ 2501-092-M-86, *Canadian Standards Association and Bureau de normalization du Quebec, Rexdale*.
- Canetta, G. and Nova, R. (1989) A numerical method for the analysis of ground improved by columnar inclusions, *Computers and Geotechnics*, **7(1)**, pp. 99-114.
- Cao, L. F., Chang, M. F., Teh, C. I. and Na, Y. M. (2001) Back-calculation of consolidation parameters from field measurements at a reclamation site, *Canadian Geotechnical Journal*, **38(4)**, pp. 755-769.
- Carrier, W. D. and Christian, J. T. (1973) Rigid circular plate resting on a non-homogeneous elastic half space, *Geotechnique*, **23(1)**, pp. 67-84.
- Casagrande, A. (1949) Soil mechanics in design and construction of Logan Airport, *Boston Society of Civil Engineers*, **36(2)**, pp. 192-221.
- Casagrande, A. and Fadum, R. E. (1940) Notes on soil testing for engineering purposes, *Harvard University- Graduate School of Engineering- Publications soil mechanics series*, **n. 268**.
- Chan, D. H. and Law, K. T. (eds.) (2006) *Soft Soil Engineering: Proceedings of the Fourth International Conference on Soft Soil Engineering*, Taylor & Francis, p. 804.
- Chandrashekhara, K. and Antony, S. J. (1996) Interaction analysis of strip footing resting on a non-homogeneous elastic medium, *Computers and Structures*, **60(1)**, pp. 79-86.
- Chang, M.-F., Yu, G., Na, Y.-M. and Choa, V. (2006) Evaluation of relative density profiles of sand fill at a reclaimed site, *Canadian Geotechnical Journal*, **43(9)**, pp. 903-914.
- Chen, W. F. and Mizuno, E. (1990) *Nonlinear Analysis in Soil Mechanics*, Elsevier, Amsterdam, p. 672.
- Cheung, Y. K., Lee, P. K. K. and Xie, K. H. (1991) Some remarks on two and three-dimensional consolidation analysis of sand-drained ground, *Computers and Geotechnics*, **12(1)**, pp. 73-87.
- Cheung, Y. K. and Tham, L. G. (1983) Numerical solutions for Biot's consolidation of layered soil, *Journal of Engineering Mechanics*, **109(3)**, pp. 669-679.
- Chiou, Y. J. and Chi, S. Y. (1993) On consolidation of layered soils, *Proceedings of the International Conference on Boundary Element Methods*, Worcester, MA, Computational Mechanics Publ, Southampton, Engl, pp. 443-458.
- Chiou, Y. J. and Chi, S. Y. (1994) Boundary element analysis of Biot consolidation in layered elastic soils, *International Journal for Numerical and Analytical Methods in Geomechanics*, **18(6)**, pp. 377-396.
- Choa, V. (1994) Application of the observational method to hydraulic fill reclamation projects, *Geotechnique*, **44(4)**, pp. 735-745.

- Christian, J. T. and Desai, C. S. (1977) Constitutive laws for geologic media. *Numerical Methods in Geotechnical Engineering- Chapter 2*, C. S. Desai and J. T. Christian, eds., McGraw Hill, New York, pp. 65-115.
- Chung, S. G., Kim, G. J., Kim, M. S. and Ryu, C. K. (2007) Undrained shear strength from field vane test on Busan clay, *Marine Georesources and Geotechnology*, **25(3-4)**, pp. 167-179.
- Collins, I. F. (2005) Elastic/plastic models for soils and sands, *International Journal of Mechanical Sciences*, **47(4-5)**, pp. 493-508.
- Conte, E. and Dente, G. (1993) Settlement analysis of layered soil systems by stiffness method, *Journal of Geotechnical Engineering*, **119(4)**, pp. 780-785.
- Coussy, O. (1995) *Mechanics of Porous Media*, John Wiley, New York, p. 454.
- Crawford, C. B. (1968) Quick clays of Eastern Canada, *Engineering Geology*, **2(4)**, pp. 239-265.
- Cryer, C. W. (1963) A comparison of the three-dimensional consolidation theories of Biot and Terzaghi, *Quarterly Journal of Mechanics and Applied Mathematics*, **16**, pp. 401-412.
- Cummings, A. E. (1935) Distribution of stresses under a foundation, *Transactions of American Society of Civil Engineers*, **100**, pp. 1072-1083.
- Davis, E. H. and Raymond, G. P. (1965) Non-linear theory of consolidation, *Geotechnique*, **15(2)**, pp. 161-173.
- Davis, R. O. and Selvadurai, A. P. S. (1996) *Elasticity and Geomechanics*, Cambridge University Press, Cambridge, UK, p. 256.
- Davis, R. O. and Selvadurai, A. P. S. (2002) *Plasticity and Geomechanics*, Cambridge University Press, Cambridge, UK, p. 299.
- Day, R. W. (1999) *Geotechnical and Foundation Engineering: Design and Construction*, McGraw-Hill, New York, p. 1500.
- Day, R. W. (2001) *Soil Testing Manual: Procedures, Classification Data, and Sampling Practices*, McGraw-Hill, New York, p. 644.
- Desai, C. S. and Saxena, S. K. (1977) Consolidation analysis of layered anisotropic foundations, *International Journal for Numerical and Analytical Methods in Geomechanics*, **1(1)**, pp. 5-23.
- Desai, C. S. and Siriwardane, H. J. (1984) *Constitutive Laws for Engineering Materials, with Emphasis on Geologic Materials*, Prentice Hall Inc., Englewood Cliffs, New Jersey, p. 468.
- Di Prisco, C. and Imposimato, S. (1996) Time dependent mechanical behaviour of loose sands, *Mechanics of Cohesive-Frictional Materials*, **1(1)**, pp. 45-73.
- Doherty, J. P. and Deeks, A. J. (2003) Elastic response of circular footings embedded in a non-homogeneous half-space, *Geotechnique*, **53(8)**, pp. 703-714.

- Du-Plat-Taylor, F. M. (1931) *Reclamation of Land From Sea*, Richard R. Smith Inc., New York, p. 153.
- Eden, W. J. (1955) Laboratory study of varved clay from Steep Rock Lake, Ontario, *American Journal of Science*, **253(11)**, pp. 659-674.
- Eden, W. J. and Crawford, C. B. (1957) Geotechnical properties of Leda clay in the Ottawa area, *Proceedings of the 4th International Conference on Soil Mechanics and Foundations Engineering*, London, **1**, pp. 22-27.
- Eden, W. J. and Law, K. T. (1980) Comparison of undrained shear strength results obtained by different test methods in soft clays, *Canadian Geotechnical Journal*, **17(3)**, pp. 369-381.
- Erickson, H. L. and Drescher, A. (2002) Bearing capacity of circular footings, *Journal of Geotechnical and Geoenvironmental Engineering*, **128(1)**, pp. 38-43.
- Feda, J. (2002) Notes on the effect of grain crushing on the granular soil behaviour, *Engineering Geology*, **63(1-2)**, pp. 93-98.
- Fodil, A., Aloulou, W. and Hicher, P. Y. (1997) Viscoplastic behaviour of soft clay, *Geotechnique*, **47(3)**, pp. 581-591.
- Fukushima, S. and Tatsuoka, F. (1984) Strength and deformation characteristics of saturated sand at extremely low pressures, *Soils and Foundations*, **24(4)**, pp. 30-48.
- Ghiabi, H. and Selvadurai, A. P. S. (2008). The time-dependent mechanical behaviour of a granular medium used in laboratory investigations, *International Journal of Geomechanics*, (accepted).
- Gibson, R. E. (1967) Some results concerning displacements and stresses in non-homogeneous elastic half-space, *Geotechnique*, **17(1)**, pp. 58-67.
- Gibson, R. E. (1974) The analytical method in soil mechanics, *Geotechnique*, **24(2)**, pp. 115-140.
- Gibson, R. E., Brown, P. T. and Andrews, K. R. F. (1971) Some results concerning displacements in a non-homogeneous elastic layer, *Zeitschrift fuer Angewandte Mathematik und Physik*, **22(5)**, pp. 855-864.
- Gibson, R. E., England, G. L. and Hussey, M. J. L. (1967) Theory of one-dimensional consolidation of saturated clays, *Geotechnique*, **17(3)**, pp. 261-273.
- Gibson, R. E., Knight, K. and Taylor, P. W. (1963) A critical experiment to examine theories of three-dimensional consolidation, *Proceedings of the European Conference on Soil Mechanics and Foundation Engineering*, Wiesbaden, **1**, pp. 69-76.
- Glaser, R., Haberzettl, P. and Walsh, R. P. D. (1991) Land reclamation in Singapore, Hong-Kong, and Macau, *GeoJournal*, **24(4)**, pp. 365-373.
- Goldscheider, M. and Scherzinger, T. H. (1991) Laboratory tests on the soft clayey soil of an old city, *Proceedings of the International Conference on Soil Mechanics and Foundation Engineering*, Florence, **1**, pp. 101-106.
- Goughnour, R. R. and Bayuk, A. A. (1979) Analysis of stone column-soil matrix interaction under vertical load, *Colloq Int sur le Renf des Sols, Terre Armees et Autres Tech*,

- Paris, Fr, Assoc Amicale des Ing Anc Eleves de L'Ec Natl des Ponts et Chaussees, **1**, pp. 271-277.
- Gray, H. (1945) Simultaneous consolidation of contiguous layers of unlike compressible soils, *Transactions of American Society of Civil Engineers*, **71(6)**, pp. 954-958.
- Greenwood, D. A. (1970) Mechanical improvement of soils below ground surface, *Proceedings of the conference on ground engineering*, London, pp. 11-22.
- Greenwood, D. A. and Kirsch, K. (1983) Specialist ground treatment by vibratory and dynamic methods, *Proceedings of the International Conference on Advances in Piling and Ground Treatment for Foundations*, London, Thomas Telford Ltd., London, pp. 17-45.
- Griffith, A. (2006) Dubai: Where the sun is hot, and the buildings are tall, *Building Engineer*, **81(7)**, pp. 34-35.
- Hansbo, S. (1957) A new approach to the determination of the shear strength of clay by fall-cone test, *Royal Swedish Geotechnical Institute*, **Vol.14**, pp. 1-48.
- Hansbo, S. (1979) Consolidation of clay by band-shaped prefabricated drains, *Ground Engineering*, **12(5)**, pp. 16-18.
- Hansbo, S. (1981) Consolidation of fine-grained soils by prefabricated drains, *Proceedings of the 10th International Conference on Soil Mechanics and Foundation Engineering*, Stockholm, Swed, A. A. Balkema, Rotterdam, **3**, pp. 677-682.
- Hansbo, S., Jamiolkowski, M. and Kok, L. (1981) Consolidation by vertical drains, *Geotechnique*, **31(1)**, pp. 45-66.
- Hanzawa, H. and Adachi, K. (1983) Overconsolidation of alluvial clays, *Soils and Foundations*, **23(4)**, pp. 106-118.
- Hanzawa, H., Matsuda, E. and Makoto, H. (1980) Evaluation of sample quality of sandy soil obtained by the modified Bishop sampler, *Soils and Foundations*, **20(3)**, pp. 17-32.
- Hartlen, J. and Ingers, C. (1981) Land reclamation using fine-grained dredged material, *Proceedings of the International Conference on Soil Mechanics and Foundation Engineering*, Stockholm, Swed, A. A. Balkema, Rotterdam, **1**, pp. 145-148.
- Head, K. H. (1994) *Soil Laboratory Testing*, Pentech Press, London, p. 416.
- Helwick, S. J., Jr. and Bryant, W. R. (1977) Geology and geotechnical characteristics of sediments in east bay area, Mississippi delta, *Marine Geotechnology*, **2**, pp. 161-175.
- Henkel, D. J. and Gilbert, G. D. (1952) The effect of rubber membrane on the measured triaxial compression strength of clay samples, *Geotechnique*, **3(1)**, pp. 20-29.
- Hill, J. M. and Selvadurai, A. P. S. (2005) Mathematics and mechanics of granular materials, *Journal of Engineering Mathematics*, **53(1-3)**, pp. 1-9.
- Holtz, R. D. and Kovacs, W. D. (1981) *An Introduction to Geotechnical Engineering*, Prentice-Hall Inc., Englewood Cliffs, New Jersey, p. 733.
- Horne, M. R. (1965) The consolidation of a stratified soil with vertical and horizontal drainage, *International Journal of Mechanical Sciences*, **6**, pp. 187-197.

- Houlsby, G. T. (1982) Theoretical analysis of the fall cone test, *Geotechnique*, **32(2)**, pp. 111-118.
- Hughes, J. M. O. and Withers, N. J. (1974) Reinforcing of soft cohesive soils with stone columns, *Ground Engineering*, **7(3)**, pp. 42-49.
- Hughes, J. M. O., Withers, N. J. and Greenwood, D. A. (1975) Field trial of the reinforcing effect of a stone column in soil, *Geotechnique*, **25(1)**, pp. 31-44.
- Jin, H., Bernspang, L., Larsson, R. and Wiberg, N. E. (1989) Mesh generation and mesh refinement procedures for computational plasticity, *Proceedings of the 2nd International Conference on Computational Plasticity, Models, Software and Applications*, Barcelona, Spain, pp. 347-357.
- Karlsson, R. (1961) Suggested improvements in the liquid limit test- with reference to flow properties of remoulded clays, *Proceedings of the 5th International Conference on Soil Mechanics and Foundation Engineering*, Paris, **1**, pp. 171-184.
- Karlsson, R. (1977) Consistency limits, a manual for the performance of and interpretation of laboratory investigations, *Swedish Council for Building Research*, **Part 6**.
- Karthikeyan, M., Dasari, G. R. and Tan, T.-S. (2004) In situ characterization of land reclaimed using big clay lumps, *Canadian Geotechnical Journal*, **41(2)**, pp. 242-256.
- Katagiri, M. and Imai, G. (1994) A new in-laboratory method to make homogeneous clayey samples and their mechanical properties, *Soils and Foundations*, **34(2)**, pp. 87-93.
- Katayama, T. (1991) Meeting the challenge to the soft ground- the Tokyo International Airport offshore expansion project, *Proceedings of Geo-Coast 91*, Yokohama, pp. 954-967.
- Kenney, T. C. (1959) Discussion of "Geotechnical properties of glacial lake clays" by T.H. Wu., *ASCE Journal of the Geotechnical Engineering Division*, **85(SM3)**, pp. 67-79.
- Khan, M. A. and Garga, V. K. (1991) Undrained shear strength of a clay crust using field vane, *Proceedings of the 44th Canadian Geotechnical Conference*, Calgary, Alberta, Canadian Geotechnical Society, **1**, pp. 3-10.
- Kietkajornkul, C. and Vasinvarthana, V. (1989) Influence of different vane types on undrained strength of soft Bangkok clay, *Soils and Foundations*, **29(2)**, pp. 146-152.
- Kim, Y. T. and Lee, S. R. (1997) An equivalent model and back-analysis technique for modelling in situ consolidation behavior of drainage-installed soft deposits, *Computers and Geotechnics*, **20(2)**, pp. 125-142.
- Kjellman, W. (1948) Discussion: "Consolidation of fine-grained soils by drain wells" by R.A. Barron, *Transactions of American Society of Civil Engineers*, **113**, pp. 748-751.
- Kuerbis, R. H. and Yoginder, P. V. (1990) Corrections for membrane strength in the triaxial test, *Geotechnical Testing Journal*, **13(4)**, pp. 361-369.
- Kumar, G. V. and Wood, D. M. (1999) Fall cone and compression tests on clay-gravel mixtures, *Geotechnique*, **49(6)**, pp. 727-739.
- Kutter, B. L. and Sathialingam, N. (1992) Elastic-viscoplastic modelling of the rate-dependent behaviour of clays, *Geotechnique*, **42(3)**, pp. 427-441.

- Kuwano, R. and Jardine, R. J. (2002) On measuring creep behaviour in granular materials through triaxial testing, *Canadian Geotechnical Journal*, **39(5)**, pp. 1061-1074.
- Ladd, C. C., Foott, R., Ishihara, K., Schlosser, F. and Poulos, H. G. (1977) Stress-deformation and strength characteristics- State-of-the-art report, *Proceedings of the 9th International Conference on Soil Mechanics and Foundation Engineering*, Tokyo, **2**, pp. 421-494.
- Lade, P. V. (1994) Creep effects on static and cyclic instability of granular soils, *Journal of Geotechnical Engineering*, **120(2)**, pp. 404-419.
- Lade, P. V. (2005) Overview of constitutive models for soils, *Proceedings of Soil Constitutive Models - Evaluation, Selection, and Calibration*, Austin, TX, American Society of Civil Engineers, pp. 2493-2526.
- Lade, P. V., Yamamuro, J. A. and Bopp, P. A. (1996) Significance of particle crushing in granular materials, *Journal of Geotechnical Engineering*, **122(4)**, pp. 309-316.
- Lam, W. K. and Tatsuoka, F. (1986) The strength surface of sand, *Proceedings of Japanese Symposium on Soil Mechanics and Foundation Engineering*, **1**, pp. 315-318.
- Lambe, T. W. and Whitman, R. V. (1969) *Soil Mechanics*, Wiley, New York, p. 553.
- Law, K. T. (1979) Triaxial-vane tests on a soft marine clay, *Canadian Geotechnical Journal*, **16(1)**, pp. 11-18.
- Lee, C. F., Lau, C. K., Ng, C. W. W., Kwong, A. K. L., Pang, P. L. R., Yin, J.-H. and Yue, Z. Q. (eds.) (2001) *Soft Soil Engineering: Proceedings of the 3rd International Conference on Soft Soil Engineering*, Swets & Zeitlinger, p. 720.
- Lee, J. S. and Pande, G. N. (1998) Analysis of stone-column reinforced foundations, *International Journal for Numerical and Analytical Methods in Geomechanics*, **22(12)**, pp. 1001-1020.
- Lee, K. M., Shen, C. K., Leung, D. H. K. and Mitchell, J. K. (1999) Effects of placement method on geotechnical behavior of hydraulic fill sands, *Journal of Geotechnical and Geoenvironmental Engineering*, **125(10)**, pp. 832-846.
- Lee, P. K. K., Xie, K. H. and Cheung, Y. K. (1992) Study on one-dimensional consolidation of layered systems, *International Journal for Numerical and Analytical Methods in Geomechanics*, **16(11)**, pp. 815-831.
- Lee, S. L., Inoue, T. and Tan, T. S. (1994) Study of sand penetration in clay slurry, *Proceedings of the Symposium on Prediction Versus Performance in Geotechnical Engineering*, Bangkok, Thailand, A.A. Balkema, pp. 55-64.
- Lee, S. L., Karunaratne, G. P., Lo, K. W., Yong, K. Y. and Chao, V. (1985) Developments of soft ground engineering in Singapore, *Proceedings of the 11th International Conference on Soil Mechanics and Foundation Engineering*, San Francisco, pp. 1661-1666.
- Lee, S. L., Karunaratne, G. P., Yong, K. Y. and Ganeshan, V. (1987) Layered clay-sand scheme of land reclamation, *Journal of Geotechnical Engineering*, **113(9)**, pp. 984-995.

- Leung, C. F., Lau, A. H., Wong, J. C. and Karunaratne, G. P. (1996) Centrifuge model tests of dredged material, *Proceedings of the 2nd International Conference on Soft Soil Engineering*, **1**, pp. 401-406.
- Leung, C. F., Wang, J. C., Manivanann, R. and Tan, S. A. (2001) Experimental evaluation of consolidation behavior of stiff clay lumps in reclamation fill, *Geotechnical Testing Journal*, **24(2)**, pp. 145-156.
- Lewis, R. W. and Schrefler, B. A. (1998) *The Finite Element Method in the Static and Dynamic Deformation and Consolidation of Porous Media*, J. Wiley & Sons, New York, p. 492.
- Li, C.-C. and Jeng, C.-J. (1997) Mechanical characteristics of flat shaped hydraulic fill sand, *Proceedings of the National Science Council, Republic of China, Part A: Physical Science and Engineering*, National Science Council, Taipei, Taiwan, **21**, pp. 113-125.
- Li, X., Chu, X. and Feng, Y. T. (2005) A discrete particle model and numerical modeling of the failure modes of granular materials, *Engineering Computations: International Journal for Computer-Aided Engineering*, **22(8)**, pp. 894-920.
- Long, M. and Menkiti, C. O. (2007) Geotechnical properties of Dublin boulder clay, *Geotechnique*, **57(7)**, pp. 595-611.
- Lui, P. C. and Tan, T. S. (2001) Building integrated large-scale urban infrastructures: singapore's experience, *Journal of Urban Technology*, **8(1)**, pp. 49-68.
- Madhav, M. R. and Vitkar, P. P. (1978) Strip footing on weak clay stabilized with a granular trench or pile, *Canadian Geotechnical Journal*, **15(4)**, pp. 605-609.
- Maheshwari, P. and Madhav, M. R. (2006) Analysis of a rigid footing lying on three-layered soil using the finite difference method, *Geotechnical and Geological Engineering*, **24(4)**, pp. 851-869.
- Mandel, J. (1953) Consolidation of soils, mathematical study, *Geotechnique*, **3(7)**, pp. 287-299.
- Matsuo, M. and Shogaki, T. (1988) Effects of plasticity and sample disturbance on statistical properties of undrained shear strength, *Soils and Foundations*, **28(2)**, pp. 14-24.
- Mikasa, M. (1963) Consolidation of non-homogeneous ground, *Proceedings of Autumn Annual Convention of Japan Society of SMFE*.
- Mikasa, M. (1965) Consolidation of soft clay- new consolidation theory and its application, *Civil Engineering in Japan*, **4**, pp. 21-26.
- Mitchell, J. K. (1976) *Fundamentals of Soil Behavior*, John Wiley & Sons Inc., New York, p. 422.
- Mitchell, J. K. (1981) Soil Improvement: State-of-the-Art, *Proceedings of the 10th International Conference on Soil Mechanics and Foundation Engineering*, Stockholm, **4**, pp. 509-565.
- Mitchell, J. K. and Huber, T. R. (1985) Performance of a stone column foundation, *Journal of Geotechnical Engineering*, **111(2)**, pp. 205-223.

- Mizuno, E. and Chen, W. F. (1983) Cap models for clay strata to footing loads, *Computers and Structures*, **17(4)**, pp. 511-528.
- Modaresi, H. and Aubert, P. (1996) Diffuse element-finite element technique for transient coupled analysis, *International Journal for Numerical Methods in Engineering*, **39(22)**, pp. 3809-3838.
- Moh, Z. C. (1988) Geotechnical engineering in Southeast Asia. Past, present and future, *Geotechnical Engineering*, **19(1)**, pp. 1-72.
- Muir Wood, D. (1990) *Soil Behaviour and Critical State Soil Mechanics*, Cambridge University Press, Cambridge, p. 486.
- Munfakh, G. A., Abramson, L. W., Barksdale, R. D. and Juran, I. (1987) In-situ ground reinforcement: Soil nailing, *Soil Improvement - A Ten Year Update ASCE Geotechnical Publication*, pp. 1-17.
- Murakami, A., Kawabata, H. and Aoyama, S. (2001) EFGM analysis for saturated soil. *Computer Methods and Advances in Geomechanics*, C. S. Desai et al., ed., Tucson, Arizona, pp. 153-156.
- Murayama, S., Michihiro, K. and Sakagami, T. (1984) Creep characteristics of sands, *Soils and Foundations*, **24(2)**, pp. 1-15.
- Murthy, V. N. S. (2003) *Geotechnical Engineering Principles and Practices of Soil Mechanics and Foundation Engineering*, Marcel Dekker Inc., New York, p. 1029.
- Nagaraj, T. and Murthy, B. R. S. (1985) Prediction of the preconsolidation pressure and recompression index of soils, *Geotechnical Testing Journal*, **8(4)**, pp. 199-202.
- Nakata, Y., Hyodo, M., Hyde, A. F. L., Kato, Y. and Murata, H. (2001) Microscopic particle crushing of sand subjected to high pressure one-dimensional compression, *Soils and Foundations*, **41**, pp. 69-82.
- Nayak, G. C. and Zienkiewicz, O. C. (1972) Elasto-plastic stress analysis. A generalization for various constitutive relations including strain softening, *International Journal for Numerical Methods in Engineering*, **5(1)**, pp. 113-135.
- Newson, T. A., Davies, M. C. R. and Bondok, A. R. A. (1997) Selecting the rate of loading for drained stress path triaxial tests, *Geotechnique*, **47(5)**, pp. 1063-1067.
- Nogami, T. and Li, M. (2002) Consolidation of system of clay and thin sand layers, *Soils and Foundations*, **42(4)**, pp. 1-11.
- Nogami, T. and Li, M. (2003) Consolidation of clay with a system of vertical and horizontal drains, *Journal of Geotechnical and Geoenvironmental Engineering*, **129(9)**, pp. 838-848.
- Nogami, T., Wang, W. and Li, M. (2001) Consolidation of lumpy clay fills, *Proceedings of the Inaugural International Conference on Port and Maritime R&D and Technology*, pp. 483-489.
- Nogami, T., Wang, W. and Wang, J. G. (2004) Numerical method for consolidation analysis of lumpy clay fillings with meshless method, *Soils and Foundations*, **44(1)**, pp. 125-142.

- Oda, M. and Win, S. (1990) Ultimate bearing capacity tests on sand with clay layer, *Journal of Geotechnical Engineering*, **116(12)**, pp. 1902-1907.
- Palmeira, E. M. and Gardoni, M. G. (2002) Drainage and filtration properties of non-woven geotextiles under confinement using different experimental techniques, *Geotextiles and Geomembranes*, **20(2)**, pp. 97-115.
- Pande, G. N., Lee, J. S. and Pietruszczak, S. (1993) Homogenisation techniques for strain localisation and interface analysis, *Proceedings of the 2nd Asian-Pacific Conference on Computational Mechanics*, Sydney, Aust, A.A. Balkema, pp. 411-418.
- Pestana, J. M. and Whittle, A. J. (1995) Compression model for cohesionless soils, *Geotechnique*, **45(4)**, pp. 611-631.
- Poorooshasb, H. B. and Madhav, M. R. (1985) Application of rigid plastic dilatancy model for prediction of granular pile settlement, *Proceedings of the 4th International Conference on Numerical Methods in Geomechanics*, Nagoya, Japon, A. A. Balkema, Rotterdam, Neth, **4**, pp. 1805-1808.
- Potts, D. M. and Zdravkovic, L. (1999) *Finite Element Analysis in Geotechnical Engineering*, Thomas Telford Ltd., London, p. 460.
- Poulos, H. G. (1972) Load settlement predictions for piles and piers, *Journal of the Soil Mechanics and Foundation Division, ASCE*, **98**, pp. 879-897.
- Poulos, H. G. and Davis, E. H. (1974) *Elastic Solutions for Soil and Rock Mechanics*, John Wiley & Sons, Inc, New York, p. 424.
- Priebe, H. J. (1976) Abschätzung des setzungsverhaltens eines durch Stopfverdichtung verbesserten Baugrundes, *Die Bautechnik*, **53**, pp. 160-162.
- Pui, S. K. (1987) 100 years of foreshore reclamation in Singapore, *Proceedings of the 20th Coastal Engineering Conference*, Taipei, Taiwan, ASCE, New York, **3**, pp. 2631-2636.
- Pyrah, I. C. (1996) One-dimensional consolidation of layered soils, *Geotechnique*, **46(3)**, pp. 555-560.
- Quigley, R. M., Sethi, A. J., Boonsinsuk, P., Sheeran, D. E. and Yong, R. N. (1985) Geologic control on soil composition and properties, Lake Ojibway clay plain, Matagami, Quebec, *Canadian Geotechnical Journal*, **22(4)**, pp. 491-500.
- Reina, P. (2006) Palm-shaped islands symbolize Dubai's new wealth, *Engineering News-Record*, **257(18)**, pp. 36-37.
- Robinson, R. G., Dasari, G. R. and Tan, T. S. (2004) Three-dimensional swelling of clay lumps, *Geotechnique*, **54(1)**, pp. 29-39.
- Robinson, R. G., Tan, T. S., Dasari, G. R., Leung, C. F. and Vijayakumar, A. (2005) Experimental study of the behavior of a lumpy fill of soft clay, *International Journal of Geomechanics*, **5(2)**, pp. 125-137.
- Roscoe, K. B. and Burland, J. B. (1968) On the generalized stress-strain behavior of 'wet' clay. *Engineering Plasticity*, J. Heyman and F. A. Leckie, eds., Cambridge University Press, pp. 535-608.

- Roscoe, K. H., Schofield, A. N. and Thurairajah, A. (1963) Yielding of clays in states wetter than critical, *Geotechnique*, **13(3)**, pp. 211-240.
- Roscoe, K. H., Schofield, A. N. and Wroth, C. P. (1958) On yielding of soils, *Geotechnique*, **8**, pp. 22-53.
- Rowe, P. W. (1962) The stress dilatancy relation for static equilibrium of an assembly of particles in contact, *Proceedings of the Royal Society, Series A*, **269**, pp. 500-527.
- Rowe, P. W. (1972) The relevance of soil fabric to site investigation practice, *Geotechnique*, **22(2)**, pp. 195-300.
- Rowe, R. K. and Booker, J. R. (1981a) Behaviour of footings resting on a non-homogeneous soil mass with a crust - 1. strip footings, *Canadian Geotechnical Journal*, **18(2)**, pp. 250-264.
- Rowe, R. K. and Booker, J. R. (1981b) Behaviour of footings resting on a non-homogeneous soil mass with a crust - 2. circular footings, *Canadian Geotechnical Journal*, **18(2)**, pp. 265-279.
- Sadiku, S. (1991) Analytical and computational studies on the consolidation of multilayered soils, *Engineering Computations*, **8(2)**, pp. 181-188.
- Sampson, L. R. and Netterberg, F. (1985) The cone penetration index: A simple new soil index to replace the plasticity index, *Proceedings of the 11th International Conference on Soil Mechanics and Foundation Engineering*, San Francisco, **2**, pp. 1041-1048.
- Sanchez, J. M. and Sagaseta, C. (1981) Undrained behavior of soft clays in triaxial tests, *Proceedings of the International Conference on Soil Mechanics and Foundation Engineering*, Brighton, **1**, pp. 771-774.
- Sanchez, J. M., Sagaseta, C. and Ballester, F. (1979) Influence of stress history on undrained behaviour of soft clays, *Proceedings of the 7th European Conference on Soil Mechanics and Foundation Engineering*, **1**, pp. 257-261.
- Sasaki, S., Nakamura, Y. and Tokuhira, T. (1987) Long-term goals of Osaka port improvement project, *Proceedings of the 5th Symposium on Coastal and Ocean Management*, Seattle, WA, ASCE, New York, **1**, pp. 267-274.
- Saxena, S. K., Desai, C. S. and Vir, J. (1976) Consolidation settlement of a layered subsurface, *American Society of Mechanical Engineers, Applied Mechanics Division, AMD*, **2**, pp. 1082-1088.
- Schiffman, R. L. and Gibson, R. E. (1964) Consolidation of nonhomogeneous clay layers, *Journal of the Soil Mechanics and Foundations Division, ASCE*, **90(SM5, Part 1)**, pp. 1-30.
- Schiffman, R. L. and Stein, J. R. (1969). PROGRS-I, A computer program to calculate the progress of ground settlement, *Computing Center- University of Colorado*, Boulder, No. 69-9.
- Schiffman, R. L. and Stein, J. R. (1970) One-dimensional consolidation of layered systems, *Proceedings of the American Society of Civil Engineers*, **96(SM4)**, pp. 1499-1504.

- Schofield, A. N. and Wroth, C. P. (1968) *Critical State Soil Mechanics*, McGraw Hill, London, p. 310.
- Schultze, E. (1961) Distribution of stress beneath a rigid foundation, *Proceedings of the 5th International Conference on Soil Mechanics and Foundation Engineering*, Paris, **1**, pp. 807-813.
- Schweiger, H. F. and Pande, G. N. (1986) Numerical analysis of stone column supported foundations, *Computers and Geotechnics*, **2**, pp. 347-372.
- Selvadurai, A. P. S. (1979) *Elastic Analysis of Soil Foundation Interaction: Developments in Geotechnical Engineering*, Elsevier, Amsterdam, p. 543.
- Selvadurai, A. P. S. (eds.) (1996a) *Mechanics of Poroelastic Media*, Kluwer Academic Publ., Dordrecht, The Netherlands, p. 302.
- Selvadurai, A. P. S. (1996b) Settlement of a rigid circular foundation resting on a half-space exhibiting a near surface elastic non-homogeneity, *International Journal for Numerical and Analytical Methods in Geomechanics*, **20(5)**, pp. 351-364.
- Selvadurai, A. P. S. (2000) *Partial Differential Equations in Mechanics Vol. 1: Fundamentals, Laplace's Equation, the Diffusion Equation, the Wave Equation*, Springer Verlag, Berlin, p. 595.
- Selvadurai, A. P. S. (2007) The analytical method in geomechanics, *Applied Mechanics Reviews*, **60(3)**, pp. 87-106.
- Selvadurai, A. P. S. (2008) Interface porosity and the Dirichlet/Neumann pore fluid pressure boundary conditions in poroelasticity, *Transport in Porous Media*, **71(2)**, pp. 161-172.
- Selvadurai, A. P. S., Bauer, G. E. and Nicholas, T. J. (1980) Screw plate testing of a soft clay, *Canadian Geotechnical Journal*, **17(4)**, pp. 465-472.
- Selvadurai, A. P. S., Hu, J. and Konuk, I. (1999) Computational modelling of frost heave induced soil-pipeline interaction. I. modelling of frost heave, *Cold Regions Science and Technology*, **29(3)**, pp. 215-228.
- Selvadurai, A. P. S. and Nguyen, T. S. (1995) Computational modelling of isothermal consolidation of fractured porous media, *Computers and Geotechnics*, **17(1)**, pp. 39-73.
- Selvadurai, A. P. S. and Nicholas, T. J. (1979) A theoretical assessment of the screw plate test, *Proceedings of the 3rd International Conference on Numerical Methods in Geomechanics*, Aachen, Germany, **3**, pp. 1245-1252.
- Selvadurai, A. P. S. and Shirazi, A. (2004) Mandel-Cryer effects in fluid inclusions in damage-susceptible poroelastic geologic media, *Computers and Geotechnics*, **31(4)**, pp. 285-300.
- Selvadurai, A. P. S., Singh, B. M. and Vrbik, J. (1986) Reissner-Sagoci problem for a non-homogeneous elastic solid, *Journal of Elasticity*, **16(4)**, pp. 383-391.
- Sheahan, T. C. and DeGroot, D. J. (1997) Laboratory determination of coastal sediment mechanical properties, *Marine Georesources and Geotechnology*, **15(3)**, pp. 231-252.

- Shintani, N. (1991) Land reclamation work for Yanai Thermal Power Plant- soil improvements in ultra-soft ground, *Civil Engineering in Japan*, **30**, pp. 104-122.
- Simo, J. C. and Hughes, T. J. R. (1998) *Computational Inelasticity (Interdisciplinary Applied Mathematics)*, Springer, New York, p. 392.
- Siriwardane, H. J. and Desai, C. S. (1983) Computational procedures for non-linear three-dimensional analysis with some advanced constitutive laws, *International Journal for Numerical and Analytical Methods in Geomechanics*, **7(2)**, pp. 143-171.
- Sivrikaya, O. and Togrol, E. (2006) Determination of undrained strength of fine-grained soils by means of SPT and its application in Turkey, *Engineering Geology*, **86(1)**, pp. 52-69.
- Skempton, A. W. (1944) Note on the compressibility of clays, *Quarterly Journal of the Geological Society of London*, **100(1)**, pp. 119-135.
- Skempton, A. W. (1953) The colloidal activity of clays, *Proceedings of the 3rd International Conference on Soil Mechanics and Foundation Engineering*, Zurich, pp. 57-61.
- Skempton, A. W. and Northey, R. D. (1952) The sensitivity of clays, *Geotechnique*, **3(1)**, pp. 30-53.
- Sladen, J. A. and Hewitt, K. J. (1989) Influence of placement method on the in situ density of hydraulic sand fills, *Canadian Geotechnical Journal*, **26(3)**, pp. 453-466.
- So, C. L. (1986) Reclamation and its impact on current flows in Hong Kong - 1, *Dock & Harbour Authority*, **67(783)**, pp. 117-122.
- Sridharan, A. and Nagaraj, T. S. (1962) One-dimensional consolidation of layered soils, *Journal of the Institution of Engineers (India)*, **42(11, Part CI 6)**, pp. 616-625.
- Stark, R. F. and Booker, J. R. (1997) Surface displacements of a non-homogeneous elastic half-space subjected to uniform surface tractions. Part II: loading on rectangular shaped areas, *International Journal for Numerical and Analytical Methods in Geomechanics*, **21(6)**, pp. 379-395.
- Takada, N. and Mikasa, M. (1984) Consolidation of multi-layered clay, *Proceedings of a Symposium held in conjunction with the ASCE Convention*, San Francisco, CA, ASCE, New York, pp. 216-228.
- Tan, S.-A., Karunaratne, G. P. and Muhammad, N. (1994a) Sand penetration into clay slurry through jute interlayer, *Soils and Foundations*, **34(2)**, pp. 19-25.
- Tan, S.-A., Liang, K.-M., Yong, K.-Y. and Lee, S.-L. (1992) Drainage efficiency of sand layer in layered clay-sand reclamation, *Journal of Geotechnical Engineering*, **118(2)**, pp. 209-228.
- Tan, S.-A., Muhammad, N. and Karunaratne, G. P. (1994b) Forming a thin sand seam on a clay slurry with the aid of a jute geotextile, *Geotextiles and Geomembranes*, **13(3)**, pp. 147-163.
- Tan, T. S., Leung, C. F. and Yong, K. Y. (2000) Coastal reclamation projects in Singapore, *Proceedings of the International Symposium on Coastal Geotechnical Engineering in Practice*, **2**, pp. 119-125.

- Tanaka, H. (1994) Consolidation of ground reclaimed by inhomogeneous clay, *Proceedings of the Conference on Vertical and Horizontal Deformations of Foundations and Embankments*, College Station, TX, Publ by ASCE, New York, **2**, pp. 1262-1273.
- Tatsuoka, F. (1987) Discussion- Strength and dilatancy of sands, *Geotechnique*, **37(2)**, pp. 219-226.
- Taylor, D. W. (1942) Research on the consolidation of clays, *Department of Civil and Sanitary Engineering, MIT*, **no.82**.
- Taylor, D. W. (1948) *Fundamentals of Soil Mechanics*, Wiley, New York, p. 700.
- Terzaghi, K. (1923) Die berechnung des durchlassigkeitsziffer des tones aus dem verlauf der hydrodynamischen Spannungserscheinungen, *Akademie der Wissenschaften in Wien, Sitzungsberichte, Mathematisch-Naturewissenschaftlichen Klasse*, **132**, pp. 125-138.
- Terzaghi, K. (1940) Sampling, testing and averaging, *Proceedings of the Purdue Conference on Soil Mechanics and Its Applications*, West Lafayette, pp. 151-160.
- Terzaghi, K. (1943) *Theoretical Soil Mechanics*, John Wiley and Sons, New York, p. 528.
- Terzaghi, K. and Peck, R. B. (1948) *Soil Mechanics in Engineering Practice*, John Wiley & Sons. Inc., New York, p. 566.
- Tham, L. G., Man, K. F. and Cheung, Y. K. (1988) Analysis of footing resting on non-homogeneous soil by double spline element, *Computers and Geotechnics*, **5(4)**, pp. 249-268.
- Thorburn, S. (1968) Soil stabilization employing surface and depth vibrators, *Structural Engineer*, **36(10)**, pp. 309-316.
- True, D. G. (1971) Determination of engineering properties of ocean-bottom soils by in-situ testing- sampling and laboratory testing, *International Symposium on Engineering Properties of Sea Floor Soils and their Geophysical Identification*, Seattle, UNESCO, pp. 11-25.
- Tschebotarioff, G. P. and Bayliss, J. R. (1948) The determination of shearing strength of varved clays and their sensitivity to remoulding, *Proceedings of the 2nd International Conference on Soil Mechanics and Foundation Engineering*, Rotterdam, Netherlands, pp. 203-207.
- U.S.Navy (1971) *Soil Mechanics, Foundations, and Earth Structures, Department of the Navy, Naval Facilities Engineering Commands, Design Manual DM-7*.
- Ueshita, K. and Meyerhof, G. G. (1968) Surface displacement of elastic layer under uniformly distributed loads, *National Research Council- Highway Research Record*, **no. 228**, pp. 1-10.
- Urzua, A. and Christian, J. T. (2002) Limits on a common approximation for layered consolidation analysis, *Journal of Geotechnical and Geoenvironmental Engineering*, **128(12)**, pp. 1043-1045.
- USDA (1975) *Agriculture Handbook, United States Department of Agriculture, No. 436*.
- Uygar, E. and Doven, A. G. (2006) Monotonic and cyclic oedometer tests on sand at high stress levels, *Granular Matter*, **8(1)**, pp. 19-26.

- Vermeer, P. A. and de Borst, R. (1984) Non-associated plasticity for soils, concrete and rock, *Heron*, **29(3)**, pp. 1-62.
- Verruijt, A. (1965) Discussion, *Proceedings of the 6th International Conference on Soil Mechanics and Foundation Engineering*, Montreal, **3**, pp. 401-402.
- Vrettos, C. (1998) Elastic settlement and rotation of rectangular footings on nonhomogeneous soil, *Geotechnique*, **48(5)**, pp. 703-707.
- Wang, J. G., Leung, C. F. and Chow, Y. K. (1997) Consolidation analysis of lumpy fills using a homogenization method, *Proceedings of International Conference on Computer Methods and Advances in Geomechanics*, Wuhan, China, pp. 1075-1080.
- Wang, J. G., Leung, C. F. and Ichikawa, Y. (2002a) A simplified homogenisation method for composite soils, *Computers and Geotechnics*, **29(6)**, pp. 477-500.
- Wang, J. G. and Liu, G. R. (2002) A point interpolation meshless method based on radial basis functions, *International Journal for Numerical Methods in Engineering*, **54(11)**, pp. 1623-1648.
- Wang, J. G., Liu, G. R. and Lin, P. (2002b) Numerical analysis of Biot's consolidation process by radial point interpolation method, *International Journal of Solids and Structures*, **39(6)**, pp. 1557-1573.
- Wang, X., Wang, L. B. and Xu, L. M. (2004) Formulation of the return mapping algorithm for elastoplastic soil models, *Computers and Geotechnics*, **31**, pp. 315-338.
- Ward, W. H., Marsland, A. and Samuels, S. G. (1965) Properties of London clay at Ashford common shaft- In-situ and undrained strength tests, *Geotechnique*, **15(4)**, pp. 321-344.
- Wasti, Y. (1987) Liquid and plastic limits as determined from the fall cone and the Casagrande methods, *Geotechnical Testing Journal*, **10(1)**, pp. 26-30.
- Weatherill, N. P. (1996) A review of mesh generation, *Proceedings of the 3rd International Conference in Computational Structure Technology Advances in Finite Element Technology*, Budapest, Hungary, pp. 1-10.
- Wedage, A. M. P., Morgenstern, N. R. and Chan, D. H. (1998) Strain rate dependent constitutive model for clays at residual strength, *Canadian Geotechnical Journal*, **35(2)**, pp. 364-374.
- Whitman, R. V. (1970) Hydraulic fills to support structural loads, *Journal of the Soil Mechanics and Foundations Division, ASCE*, **96(SM1)**, pp. 23-47.
- Wong, J. C. (1997) Model Studies of Lumpy Fill, *Master Thesis, National University of Singapore*.
- Wong, P. P. (1985) Artificial coastlines: the example of Singapore, *Zeitschrift für Geomorphologie N.F.*, **57**, pp. 175-192.
- Wood, D. M. (1985) Some fall-cone tests, *Geotechnique*, **35(1)**, pp. 64-68.
- Wu, T. H. (1976) *Soil Mechanics*, Allyn and Bacon Inc., Boston, p. 440.

- Xie, K.-H., Xie, X.-Y. and Gao, X. (1999) Theory of one-dimensional consolidation of two-layered soil with partially drained boundaries, *Computers and Geotechnics*, **24(4)**, pp. 265-278.
- Xie, K. H., Xie, X. Y. and Jiang, W. (2002) A study on one-dimensional nonlinear consolidation of double-layered soil, *Computers and Geotechnics*, **29(2)**, pp. 151-168.
- Yamaguchi, H., Ohira, Y., Kogure, K. and Mori, S. (1985) Undrained shear characteristics of normally consolidated peat under triaxial compression and extension conditions, *Soils and Foundations*, **25(3)**, pp. 1-18.
- Yamamuro, J. A. and Kaliakin, V. N. (eds.) (2005) *Soil Constitutive Models - Evaluation, Selection, and Calibration*, American Society of Civil Engineers, Austin, TX, p. 502.
- Yang, H. and Huang, M. (1970) Consolidation-time relationship for layered clays, *Proceedings of the American Society of Civil Engineers*, **96(SM1)**, pp. 371-375.
- Yang, L. A. and Tan, T. S. (2005) One-dimensional consolidation of lumpy clay with non-linear properties, *Geotechnique*, **55(3)**, pp. 227-235.
- Yang, L. A., Tan, T. S., Tan, S. A. and Leung, C. F. (2002) One-dimensional self-weight consolidation of a lumpy clay fill, *Geotechnique*, **52(10)**, pp. 713-725.
- Yilmaz, I. and Erzin, Y. (2004) On the reliability of SPT-N value as an indication of consistency of clayey soils, *Electronic Journal of Geotechnical Engineering*, **9F**, pp. 1-5.
- Yin, J. H. (2002) Stress-strain strength characteristics of a marine soil with different clay contents, *Geotechnical Testing Journal*, **25(4)**, pp. 459-462.
- Yin, J. H., Wang, Y. J. and Selvadurai, A. P. S. (2001) Influence of nonassociativity on the bearing capacity of a strip footing, *Journal of Geotechnical and Geoenvironmental Engineering*, **127(11)**, pp. 985-990.
- Zhu, G. and Yin, J.-H. (1999) Finite element analysis of consolidation of layered clay soils using an elastic visco-plastic model, *International Journal for Numerical and Analytical Methods in Geomechanics*, **23(4)**, pp. 355-374.
- Zienkiewicz, O. C., Humpheson, C. and Lewis, R. W. (1975) Associated and non-associated visco-plasticity and plasticity in soil mechanics, *Geotechnique*, **25(4)**, pp. 671-689.
- Zienkiewicz, O. C., Valliappan, S. and King, I. P. (1969) Elasto-plastic solutions of engineering problems 'initial stress', finite element approach, *International Journal for Numerical Methods in Engineering*, **1(1)**, pp. 75-100.
- Zreik, D. A., Ladd, C. C. and Germaine, J. T. (1995) New fall cone device for measuring the undrained strength of very weak cohesive soils, *Geotechnical Testing Journal*, **18(4)**, pp. 472-482.